Forward genetic analysis of Toll-like receptor induced necroptosis and RIP1 kinase driven inflammation in wild-derived mice

A dissertation

submitted by

Stephen Schworer

In partial fulfillment of the requirements
for the degree of

Doctor of Philosophy

in

Immunology

TUFTS UNIVERSITY

Sackler School of Graduate Biomedical Sciences

May 2016

Adviser: Alexander Poltorak

ABSTRACT

The innate immune system, including the Toll-like receptor family, recognizes invading pathogens and activates the immune response through the induction of cytokines and other antimicrobial factors. The outcomes of TLR ligation and signaling extend beyond activation of gene expression to include programmed cell death. When virus-encoded caspase inhibitors block caspase activity or when caspase expression in tissues is low, cells activate a necrotic cell death pathway through RIP1 and RIP3 known as necroptosis. In addition to established signaling pathways to trigger necroptosis such as TNF-R1, TLRs activate necroptosis when caspases are inhibited.

Peritoneal macrophages from the wild-derived mouse strain MOLF are resistant to necroptosis when compared with the classical inbred strain C57BL/6. Forward genetic analysis using an N2 backcross panel identified two loci in which harboring a MOLF allele conferred resistance to TLR-induced necroptosis. One locus exhibited differential regulation of CYLD, a deubiquitinase that cleaves K63 and linear polyubiquitin chains from RIP1 and is known to promote necroptosis downstream of TNF-R1. CYLD was shown here to promote necroptosis driven by TRIF-dependent TLRs in the absence of TNF-R1. In MOLF peritoneal macrophages, TLR stimulation reduced *Cyld* mRNA expression and diminished protein levels. Decreased recruitment of RNA polymerase II to a promoter proximal site in MOLF *Cyld* suggested that a defect in promoter pausing or elongation may underlie CYLD downregulation. With low levels of CYLD, MOLF peritoneal macrophages are resistant to TLR-induced necroptosis when compared to B6, which express higher levels of CYLD.

RIP1 kinase activity can also contribute to activation of gene transcription and cytokine production in the absence of caspase activity. While a scaffolding role for RIP1 is well documented for TNF-R1 and TRIF-mediated signaling pathways, RIP1 kinase activity augmented the induction of TNF and IFNβ after TLR4 ligation when caspases were inhibited by the pan-caspase inhibitor ZVAD. MOLF macrophages generated more cytokine mRNA through the RIP1 kinase dependent pathway than B6. MOLF but not B6 macrophages activated p38 in a RIP1 kinase-dependent manner through a mechanism involving IRAK2 and the activation of this arm of the MAPK pathway likely contributed to the more robust response of MOLF macrophages.

ACKNOWLEDGEMENTS

My past six years at Tufts University have been filled with influence from the classrooms of medical school to the bench top of the Poltorak lab. Countless people have contributed to my growth as a person, a scientist, and a future physician. I'll do my best to express my appreciation for everyone here, but all of the guidance I have received, whether I realize it now or not, has helped me to expand my mind and will be invaluable as I continue in my training.

Sasha has been an outstanding mentor and research adviser to me over the past four years. What stands out about Sasha is his energy for research – part of which is exemplified by his tireless passion for 'finding the gene.' This characteristic is perhaps best illustrated by the fact that many of our most insightful exchanges have occurred between the hours of 11 pm and 1 am over email or over Skype with a nine-hour time difference between Boston and Russia. However, most importantly, Sasha is an impeccable teacher in person, both in laboratory skills and how to observe and think critically about a result. I came into Sasha's lab only with undergraduate research experience, and through his efforts I've made significant growth as a scientist. He walked me step-by-step through molecular cloning at the bench, and we shared many hours priming hundreds mice and collecting cells for the many, many mapping panels. I am truly happy and grateful that I've been able to study with Sasha and look forward to our continued relationship as we both move ahead in our respective careers.

Work in the laboratory would not be the same without fellow students to share in triumph and disappointment. During my years with Sasha, the laboratory has grown and seen high quality students come and go. The current members of the lab each bring

incredible enthusiasm. Irina Smirnova is a constant in the lab and I've enjoyed sharing a lab bay with her for the past four years. She is critical for the day-to-day functions in the lab and helped me to get through difficult cloning and huge sequencing tasks. Daniel Ram and Guy Surpris both are incredibly knowledgeable and eager to discuss the work of the lab and other aspects of science and policy. Caitlin Liu, Joe Sarhan, and Bridget Larking have all made the lab an even more vibrant place – from the joyous outbursts of Caitlin to commiserating (or at times celebrating) with Joe as a fellow MDPhD student to Bridget's thoughtful insights and dinner parties. I also want to acknowledge Jay Conner, Berri Jacque, and particularly Annie Park Moseman, previous students in the lab who helped to get me started and, in the case of Annie, continued to be a positive influence on my time at Tufts. One of the most exciting parts of being a member of Sasha's lab is the opportunity to meet and collaborate with numerous scientists within and outside of Tufts. I greatly appreciate the insight from Kate Fitzgerald and Jon Kagan and the outstanding help with the manuscript from Ananda Roy as well as the hands on teaching I received from Andy Camilli, Trent Fowler, and Alexei Degterev.

The model of see one, do one, teach one is as applicable in the laboratory as in medical education (albeit we often skip the 'see one' step in bench research). I was fortunate to be able to mentor numerous rotation and summer students during my time in the Poltorak laboratory. They challenged me at times and often illuminated traits in which I was lacking. It was also a pleasure to see many of them grow in their time in the Poltorak lab and especially beyond. So, thank you to Chari Cortez, Maria RePass, John Yoon, Andrew Lutz, Peregrine Rothman-Ostrow, and Nishadh Sutaria for helping me to begin my career as an educator. I also want to express gratitude for the work of Sasha's

lab members at Petrozavodsk State University, particularly Maria Churova, Uliana Bagina, and Irina Kurbatova work their expeditious work on genotyping the BMDM panels. It was also a pleasure to meet them as well as Sergei and Vladimir when they visited Boston.

The guidance and mentorship of Tufts MSTP and the Immunology graduate program has been essential for me to develop as a young scientist. Naomi Rosenberg played an instrumental part in finding me two great labs in which to rotate and to guide me into Sasha's laboratory for my PhD research. My first rotation with Philip Tsichlis and Christos Tsatsanis was also a pivotal point in my training. To be honest, I had never heard of a TLR before spending time studying Akt isoforms in LPS tolerance during my first summer in Boston and I am thankful to Christos for getting me involved with such an interesting topic and for his support and encouragement at the beginning of my time at Tufts.

The wealth of other students, post-docs, and other researchers at the small community of Tufts Immunology and Microbiology has been an outstanding resource for learning new techniques, being exposed to medically relevant pathogens, and receiving research and career advice. I want to first thank my committee members Peter Brodeur, Stephen Bunnell, and Miguel Stadecker for putting in the time to guide my research during committee meetings and for being available outside of our scheduled meeting times for advice on my thesis work and my future career. I appreciate Michelle Kelliher for taking the time to be my outside examiner and lend her expertise on RIP1 to this work. Collaborations with Andy Camilli and his post-docs Chelsea Witte-Garcia and Mara Shainheit have been a great pleasure for me. My work with Alexei Degterev and his

students Malek Najjar and Danish Saleh has been a rewarding experience as well. I am also greatly appreciative of the many discussions of what lies ahead in my career and how best to get there with Steve Bunnell and Maria-Cristina Seminario.

Finally, I am happy to say I've been on this journey with great companions. My MSTP classmates, Adam Skibinski, Laura Wong, and Vallent Lee (who all are headed back to medical school this year with me) and Immunology graduate school classmates Guy Surpris, Michelle Paczosa, Elizabeth DeRiso, and Ben Umiker have grown alongside of me during the past six years. Outside of Tufts my family has been a great influence on me in perhaps a rare way. My parents are both scientists and have provided emotional support and scientific support over the past four years – both of which I greatly appreciate. My sister Emily has also challenged my scientific prowess with the occasional phone call for help to explain an old Nature paper for undergraduate seminar classes. And last but not least, my wife Katie, who has been my partner since the early years of medical school and has been supportive the whole way through – even if I failed to spark her interest in bench research or cell death signaling.

TABLE OF CONTENTS

ABSTRACT……... ii
ACKNOWLEDGEMENTS……... iv
TABLE OF CONTENTS…… viii
LIST OF TABLES…….. x
LIST OF FIGURES……... xi
ABBREVIATIONS……. xiii
CHAPTER 1: INTRODUCTION……... 2
The inflammatory response……..…….. 2
Toll-like receptor signaling…… 9
Functions of cylindromatosis protein – CYLD…… 20
Molecular mechanisms of RIP1 in cell death and inflammatory signaling……. 28
Necroptosis – Pathophysiology…… 42
Experimental approach: Forward genetic analysis in wild-derived mice…… 49
Summary and thesis goals…… 54
CHAPTER 2: MATERIALS AND METHODS…….. 56
CHAPTER 3: TOLL-LIKE RECEPTORS ACTIVATE NECROPTOSIS IN C57BL/6 MACROPHAGES……..…. 64
Caspase inhibition leads to RIP1 kinase-dependent cell death in macrophages stimulated with TLR agonists……... 65
TLR-induced necroptosis has a differential requirement for TNF-R1 based on MyD88 or TRIF adapter usage…… 68
CHAPTER 4: GENETIC DIVERSITY OF WILD-DERIVED STRAINS CONTRIBUTES TO DIFFERENTIAL SUSCEPTIBILITY TO TLR-INDUCED NECROPTOSIS…… 71
Macrophage susceptibility to TLR-induced necroptosis varies based on mouse genetic background…… 72
Forward genetic analysis of TLR-induced necroptosis in N2 peritoneal macrophages links to resistance alleles on MOLF Chromosomes 1 and 8…….. 75
MOLF BMDMs are resistant to necroptosis activated by low doses of LPS…….. 82
CHAPTER 5: CYLD DOWN-REGULATION CONFERS PROTECTION FROM NECROPTOSIS IN MOLF PERITONEAL MACROPHAGES……. 86
CYLD promotes TLR-induced necroptosis in macrophages……... 87
TLR stimulation causes acute down-regulation of CYLD in MOLF peritoneal macrophages…… 90
MOLF *Cyld* promoter has a single CA deletion with no detectable functional impact…….. 95
Transcriptional regulation of the *Cyld* locus may be altered in MOLF by differences in RNA polymerase II pausing, stalling or elongation……... 98
CYLD expression and susceptibility to necroptosis are restored in MOLF BMDM.100
CHAPTER 6: RIP1 KINASE-DEPENDENT CYTOKINE PRODUCTION…… 105
Necrostatin-1 treatment does not impact pro-inflammatory cytokine production in macrophages with activate caspases……... 105
RIP1 kinase activity contributes to cytokine production in *Casp8*$^{-/-}$*Ripk3*$^{-/-}$ macrophages……..……. 107

ZVAD treatment leads to a RIP1 kinase-dependent increase in TNF and IFNβ, which is augmented in MOLF over B6……. 109
MOLF RIP1 kinase response requires p38 activity whereas both mouse strains require TAK1……... 111
ZVAD induces sustained RIP1 kinase dependent MAPK activation that is hyper-activated in MOLF…….. 113
IRAK2 knockdown reduces MOLF TNF production but has a minor impact on p38 phosphorylation……... 115
CHAPTER 7: FORWARD GENETIC ANALYSIS OF TLR SIGNALING IN BMDM……... 119
A locus on Chromosome 10 contributes to high IL-6 production in MOLF BMDM…… 120
Low production of CXCL1 in MOLF BMDM maps to a locus on Chromosome 13…….. 124
CHAPTER 8: DISCUSSION…….…. 129
MOLF resistance to necroptosis: Work beyond macrophages…….. 129
A novel mechanism of *Cyld* regulation……. 135
A role for RIP1 kinase activity in pro-inflammatory cytokine production…… 138
Use of ZVAD and Nec-1 in the BMDM model system……. 140
Necroptosis: relevance to human disease……...……....141
APPENDIX 1…….. 145
APPENDIX 2…….. 150
APPENDIX 3…….. 152
APPENDIX 4…….. 154
APPENDIX 5…….. 157
REFERENCES……... 159

LIST OF TABLES

APPENDIX 1: List of candidate genes on Chromosome 1 ……... 145
APPENDIX 2: List of candidate genes on Chromosome 14 ……..… 150
APPENDIX 3: List of candidate genes on Chromosome 18 ……. 152
APPENDIX 4: List of candidate genes on Chromosome 10 ……. 154
APPENDIX 5: List of candidate genes on Chromosome 13 ……. 157

LIST OF FIGURES

Figure 1. TLR ligands and adapter proteins…… 10
Figure 2. TLR4 signaling cascade to activate pro-inflammatory cytokines and type I interferon……...…… 15
Figure 3. CYLD domain structure…… 27
Figure 4. TNF-R1 signaling triggers NF-κB, apoptosis, or necroptosis based on presence or absence of regulatory proteins…….…….. 33
Figure 5. Caspase inhibition results RIP1 kinase-dependent cell death in macrophages stimulated with TLR agonists……..…….. 66
Figure 6. TLR-induced necroptosis has a differential requirement for TNF-R1 based on MyD88 or TRIF adapter usage…… 69
Figure 7. Susceptibility to TLR-induced necroptosis varies based on mouse genetic background…….. 73
Figure 8. Forward genetic analysis of IMQ-induced necroptosis maps resistance to loci on Chromosome 1 and Chromosome 8…… 76
Figure 9. Resistance to necroptosis in MOLF peritoneal macrophages is linked to *Cyld*…….. 78
Figure 10. Resistance to necroptosis in MOLF peritoneal macrophages is linked to a locus on Chromosome 1…… 81
Figure 11. MOLF BMDM are resistant to low dose LPS-induced necroptosis and linkage analysis of this trait suggests four linked loci……. 83
Figure 12. CYLD promotes TLR-induced necroptosis……..... 89
Figure 13. CYLD is down-regulated by TLR stimulation in MOLF peritoneal macrophages.…… 92
Figure 14. MOLF *Cyld* promoter has a single CA-deletion but no functional impact is detected.……. 96
Figure 15. Reduced RNA Pol II recruitment to *Cyld* promoter-proximal region in MOLF.…….…….…. 99
Figure 16. CYLD expression and susceptibility to necroptosis are restored in MOLF BMDM…… 102
Figure 17. Schematic of the impact of CYLD regulation on pro-survival and necroptotic signaling ……..…… 104
Figure 18. Necrostatin-1 treatment does not affect cytokine production in BMDM..… 106
Figure 19. RIP1 kinase activity contributes to cytokine production in *Casp8*$^{-/-}$*Ripk3*$^{-/-}$ macrophages…….. 108
Figure 20. ZVAD treatment induces RIP1 kinase-dependent cytokine and type I interferon production to a greater degree in MOLF than B6…….. 110
Figure 21. Chemical inhibition of p38 reduces RIP1 kinase-dependent cytokine production in MOLF BMDM while TAK1 inhibition prevents RIP1 kinase-dependent cytokine production in B6 and MOLF…….. 112
Figure 22. ZVAD treatment induces RIP1 kinase-dependent MAPK phosphorylation, which is hyperactivated in MOLF…….…. 114
Figure 23. IRAK2 knockdown substantially reduces MOLF TNF production but has a modest effect on p38 phosphorylation……... 116

Figure 24. Proposed model for B6 and MOLF RIP1 kinase dependent pro-inflammatory signaling cascade……... 118
Figure 25. MOLF BMDM hyper-IL-6 production in response to TLR2 and TLR7 agonists……. 121
Figure 26. High IL-6 production by MOLF BMDM in response to LTA or CpG stimulation is linked to a region on Chromosome 10……. 123
Figure 27. MOLF BMDM produce low levels of CXCL1 in response to multiple TLR agonists……... 125
Figure 28. Low production of CXCL1 in MOLF BMDM is linked to a 10 Mb region on Chromosome 13…….. 127

ABBREVIATIONS

ARE - adenine and uridine-rich element
Bcl - B cell lymphoma
CAP-GLY - cytoskeletal-associated protein-glycine
cGAS - cyclic GMP-AMP synthase
cM - centimorgan
COX - cyclooxygenase
CYLD - Cylindromatosis protein
DAI - DNA-dependent activator of IFN- regulatory factors
DAMP - Damage-associated molecular pattern
DMSO - Dimethyl sulfoxide
DUB - deubiquitinase
ENU - N-ethyl-N-nitrosourea
ERK - extracellular related kinases
FADD - Fas-Associated protein with Death Domain
FLIP - FLICE-like inhibitory protein
GFP - Green fluorescent protein
HECT - homologous to the E6AP carboxyl terminus
HMGB1 - High-mobility group box 1
IAP - Inhibitor of apoptosis protein
IDO - indoleamine 2,3-dioxygenase
IFN - Interferon
IKK - IκBα kinase
IL - Interleukin
IRAK - Interleukin-1 receptor-associated kinase
IRF - Interferon regulatory factor
IRI - Ischemia reperfusion injury
JNK - c-Jun NH2-terminal kinases
LOD - Logarithm of odds
LPS - Lipopolysaccharide
LTA - Lipoteichoic acid
MAPK - Mitogen activated protein kinase
MCMV - Mouse cytomegalovirus
MDA5 - Melanoma differentiation-associated protein 5
MLKL - Mixed lineage kinase domain-like
Nec-1 - Necrostatin-1
NEMO - NF-κB essential modifier
NLR - Nod-like receptor
OTU - Ovarian tumour proteases
PAMP - Pathogen associated molecular pattern
PBMC - Peripheral blood monocytic cells
PRR - Pattern recognition receptor
QTL - Quantitative trait locus
RANK - Receptor Activator of Nuclear Factor κ B
RHIM - RIP homotypic interaction motif

RIG-I - retinoic acid-inducible gene 1
RING - Really interesting new gene
RIP - Receptor interacting protein
RLR - Retinoid acid-inducible gene-I-like receptor
SMAC - Second Mitochondria-Derived Activator Of Caspase
TAB - TAK-1 binding protein
TAK1 - Transforming growth factor activated kinase-1
TBK1 - TANK-binding kinase 1
TIR - Toll/interleukin-1 receptor homology
TIRAP - Toll-interleukin 1 receptor (TIR) domain containing adaptor protein
TLR - Toll-like receptor
TNF - Tumor necrosis factor
TRAF - TNF receptor associated factor
TRAM - TRIF-related adaptor molecule
TRIF - TIR-domain-containing adapter-inducing-interferon-β
USP - Ubiquitin-specific protease
VV - vaccinia virus
ZVAD - Benzyloxycarbonyl-val-ala-asp (OMe) fluoromethylketone

Forward genetic analysis of Toll-like receptor induced necroptosis and RIP1 kinase driven inflammation in wild-derived mice

CHAPTER 1: INTRODUCTION

Diverse outcomes can occur when cells are activated through innate immune receptors such as Toll-like receptors (TLR) or death receptors. A pro-inflammatory and pro-survival program appears to be the 'default' for TLRs and TNF-receptor 1 (TNF-R1) in contrast to the pro-death effects of other death receptors such as FAS. However, various pathophysiological states including ischemia, trauma, and infection may alter how cells respond in comparison to healthy cells. Thus, appropriate *in vitro* systems to study how these pathological signaling pathways are regulated may be useful tools to demonstrate important signaling components in a given pathway and identify meaningful pharmacological targets for disease processes. One common aspect of pathology and normal physiology is the signaling pathways that activate response to stress that manifests as the inflammatory response.

The inflammatory response

Inflammation

When a noxious stimulus damages a tissue, the inflammatory response delivers blood plasma and leukocytes to the region to fight infection and promote tissue repair (1). The first century Roman encyclopedian Cornelius Celsus recorded the four cardinal signs of inflammation, *rubor et tumor cum calore et dolore* (redness and swelling with heat and pain) (2). The idea that inflammation and disease were caused by an imbalance of 'humors' in the body became popular over the next one hundred years and persistent for centuries (3). Not until the 19th century, when Rudolf Virchow added a fifth cardinal sign, *functio laesa* (disturbance of function), did the notion of disease causation substantially

evolve (2, 3). Virchow's contribution to cellular pathology and microscopy along with the development of germ theory by Louis Pasteur shifted the understanding of what underlies inflammation from the idea of internal humors to the external source that is microbial infection. In addition to his role in the development of germ theory, Pasteur also recognized the essential function for the host internal milieu to maintain equilibrium in the setting of an inflammatory response. The modern understanding is that inflammation consists of inducers that activate sensors found on tissue resident cells leading to production and release of a spectrum of mediators that specifically impact target tissues (2).

Inducers of inflammation arise from microbes, non-infectious irritants, and host molecules exposed after cell death (1, 4, 5). Microbes activate inflammation through recognition by pathogen recognition receptors (PRR), which sense common components found on pathogenic and commensal microbes, or through action of virulence factors from pathogenic invaders. Non-infectious irritants include crystals, toxins, chemicals, and minerals that stimulate tissue damage or inflammatory cell recruitment following activation of inflammasomes. Finally, host cell death caused by mechanical trauma, ischemia, or programmed host cell death leads to 'de-sequestration' of intracellular proteins such as HMGB1, ATP, and uric acid. These so-called damage-associated molecular patterns (DAMPs) activate the inflammatory cascade (6). Toll-like receptors (TLR) and other innate immune sensors recognize these various molecules (1). Sentinel cells such as tissue resident macrophages and mast cells express these receptors and are essential for the induction of a rapid, effective inflammatory response (5).

Activation of macrophages and mast cells causes production of inflammatory molecules and degranulation causing release of pre-formed mediators which act on host tissues to generate the cardinal signs of inflammation (1, 5). The vasoactive amines serotonin and histamine released from mast cell granules cause immediate changes to the vasculature causing vasodilation (redness and heat) and an increase in vascular permeability (swelling). Both mast cells and macrophages produce eicosanoid lipid mediators, cytokines, chemokines, and proteolytic enzymes. Eicosanoids are generated from arachidonic acid, an unsaturated fatty acid generated from plasma membrane phospholipids through the activity of phospholipase A_2. Cyclooxygenases (COX-1 and COX-2) synthesize prostaglandins and thromboxane while lipoxygenases generate leukotrienes and lipoxins. These lipid mediators exert diverse effects on a broad range of tissues during an inflammatory response including vasodilation, bronchoconstriction, and fever based on their target tissue.

Inflammatory cytokines such as TNF, IL-1, and IL-6 activate the endothelium, recruit lymphocytes, and induce acute phase proteins from the liver. Activation of the endothelium causes up-regulation of adhesion molecules on the endothelial surface, recruitment of lymphocytes, and further activation of macrophages (7). These activated macrophages produce proteases such as matrix metalloproteases to cleave the extracellular matrix and activate serum factor cascades. Decades of research have established the cytokine-based theory of disease (3). Immune system-generated cytokines cause the signs, symptoms, and damaging effects of certain conditions. For example, TNF injection alone is sufficient to induce shock in mouse models. Utilization of this information for disease treatment has resulted in the common use of anti-TNF treatments

to treat conditions such as rheumatoid arthritis, Crohn's disease, and psoriatic arthritis, among others (8).

Cell death and inflammation

Cell death can function as a primitive host defense system: the host cell dies before an infecting bacterium, virus, or parasite can replicate, kill the infected cell, and spread disease to adjacent cells within a host (9). Unlike the sequence of events during infection, where a pathogen interacts with innate receptors to cause inflammation, the specific functions of host cell death in inflammation are less clear (10). Although proposed in the context of the adaptive immune response and tolerance to normal self, the danger model can be easily applied to this concept of stress-induced production of pro-inflammatory mediators that lead to activation of the immune system (10, 11). Signals produced by dying cells are termed DAMPs. In normal cells, DAMPs are sequestered within the intracellular compartment. Only during cell death or other cell stress scenarios are these molecules exposed. There are two types of DAMPs: those that perform nonimmune functions in living cells (ATP, HMGB1, uric acid), and alarmins, which have cytokine-like functions (IL-33, IL-1α) (6).

Interestingly, both the context of cell death and the morphological attributes of a cell death program play important roles in determining the inflammatory sequelae (9). The classical view that apoptosis is anti-inflammatory and necrosis is pro-inflammatory does not hold true in all settings. Apoptosis can be highly immunogenic and lead to cross-presentation of apoptotic components to DCs while necrotic cell death can lack the high immunogenicity found in this type of apoptotic response. However, under most

circumstances apoptosis is an anti-inflammatory cell death mechanism as it prevents the release of DAMPs and causes inactivation of pro-inflammatory molecules by caspase activation (6). Overall, the inflammatory response to a dying cell is determined by which cell dies, how it dies, where it dies, which phagocyte eats it, and if antigens from it are presented by dendritic cells and recognized by lymphocytes (9).

Innate immune receptors and inflammation and the importance of TLR4

Bacterial toxins and infection-driven cell death cause inflammation during infection. The primary drivers of the inflammatory response are components of the pathogen that activate specific receptors (12). These innate immune receptors are expressed on professional innate immune cells (hematopoietic lineage) such as macrophages, dendritic cells, and neutrophils and on non-professional cells such as epithelium, endothelium, and fibroblasts (13). There are four main classes of innate immune receptors: Toll-like receptors C-type lectin receptors, which are transmembrane receptors, and retinoic acid-inducible gene-I-like receptors (RLR) and NOD-like receptors (NLR), which are expressed in the cytoplasm. Activation of these receptors leads to expression of pro-inflammatory cytokines, chemokines, type I interferon, and antimicrobial proteins. Additionally, members of the NLR family activate inflammasomes to cleave IL-1β and IL-18 into biologically active forms and to drive cell death by pyroptosis (14). Together, gene expression changes, inflammasome activation, and pyroptosis drive the inflammatory response to infection, helping to clear the infection if properly controlled but contributing to pathology without proper negative regulation.

Some pathogen-associated molecules are sensed in multiple compartments by different innate immune receptors (13). Well-described examples include sensing of DNA by cytoplasmic cGAS and endolysosomal TLR9 and RNA by cytoplasmic/mitochondrial MDA5 and RIG-I and TLR3, TLR7, and TLR8 in the endolysosomal compartment (13, 15). Interestingly, LPS sensing also occurs in multiple compartments. In addition to sensing by TLR4 (discussed in detail below), a novel cytoplasmic LPS sensor that activates the non-canonical caspase-11 inflammasome to drive pyroptosis rather than to induce gene expression changes (16, 17). It is possible that this activation of this receptor may underlie lethality in mice injected with LPS. Although the scope of innate immune receptors continues to widen to include activation of multiple receptors by one molecule in different compartments, the prototypical receptor remains to be TLR4, which leads to gene expression changes to activate the inflammatory response driven by bacterial infection.

Years following the development of germ theory, in addition to Robert Koch's demonstration of the transmission of disease by microbes, Richard Pfeiffer discovered an additional means by which bacteria damages the host (18). A heat-stable toxin found on *Vibrio cholerae* was lethal upon injection even when bacteria were killed. This toxin was termed 'endotoxin', and later found to be lipopolysaccharide (LPS) expressed on the outer leaflet of the outer membrane in Gram-negative bacteria. The largely protein-free LPS structure consists of lipids and carbohydrates in three main components: 1) variable O antigen, 2) core oligosaccharide, and 3) lipid A, the molecule with immunostimulatory properties (19). The capacity for purified LPS to induce a damaging inflammatory response was demonstrated in 1965 with the use of mouse models (18). Two mouse

strains (C3H/HeJ and C57BL/10ScCR) lack responses to LPS injection. F1 hybrids of these mice also do not respond to LPS, demonstrating that each strain has an allelic defect in same region of the genome, termed the *Lps* locus. Characterization of these mouse strains demonstrated that a genetic component in the *Lps* locus underlies the ability for the host to respond to LPS *in vivo*. The innate immune system was brought the forefront of immunological research when Charles Janeway proposed that innate immune receptors were instrumental in the development of an appropriate adaptive immune response (20).

Discovery of the identify of the LPS receptor using positional cloning revealed the defect in the *Lps* locus is caused by mutations in *Tlr4*, a single nucleotide polymorphism in C3H/HeJ and a deletion in C57BL/10ScCR (21). TLR4 is a homolog of *Drosophila melanogaster* Toll, which had recently been found to contribute anti-fungal defense in flies in addition to its known role in dorsoventral patterning (22). Critical work showed that human TLR4 also contained a Toll/IL1-R domain found in *Drosophila* Toll that can drive NF-κB when artificially ligated (23). Importantly, positional cloning and forward genetic analysis were essential to demonstrate that TLR4 was indeed the receptor for LPS (21). Attempts in reconstitution systems *in vitro* were unsuccessful likely because of the need for the co-receptor MD-2 to form a functional LPS-TLR4 signaling complex (19). Though MD-2 lacks a transmembrane domain and intracellular region, its deletion phenocopies TLR4 deletion and structural analysis has revealed that MD-2 functions as a co-receptor for LPS with TLR4 (24). Through all of these efforts, the importance of TLRs in pathogen recognition was established and illustrated the critical role for innate immune receptors to drive the inflammatory response during infection.

Toll-like receptor signaling

TLRs and their ligands

TLRs are single-pass type I transmembrane receptors responsible for innate immune sensing of microbe-derived molecules at the plasma membrane and endolysosome (25). The TLR structure contains N-terminal leucine-rich repeats that bind to ligands directly or with a co-receptor, a transmembrane domain, and a cytoplasmic Toll/IL-1R homology (TIR) domain to recruit downstream signaling molecules (13, 24). Homo- or hetero-dimers of TLRs assemble as an M-shaped structure with N-terminal ends facing away from the other molecule in the dimer and C-terminal ends converging to bring TIR domains into proximity to activate signaling. Thirteen paralogs of TLRs are expressed between mice and humans (TLR1-10 in human, TLR1-9 and 11-13 in mouse) and each TLR recognizes a distinct structure (often referred to as pathogen-associated molecular patterns or PAMPs) (Figure 1).

The localization of TLRs dictates the molecules with which they come into contact (13). TLRs are localized to either the plasma membrane or the endolysosome. A notable exception is TLR4, which can signal from both compartments, first from the plasma membrane and from the endosome following CD14-mediated endocytosis (26). As described above, two TLR4-MD2 heterodimer complexes form a symmetric homodimer to recognize LPS (13). Other plasma membrane-associated TLRs include TLR2, which forms heterodimers with TLR1 or TLR6, and TLR5. Heterodimers involving TLR2 recognize bacterial lipoproteins including lipoteichoic acid from Gram-positive *Staphylococcus aureus*. TLR1/2 heterodimers recognize diacyl lipoproteins and

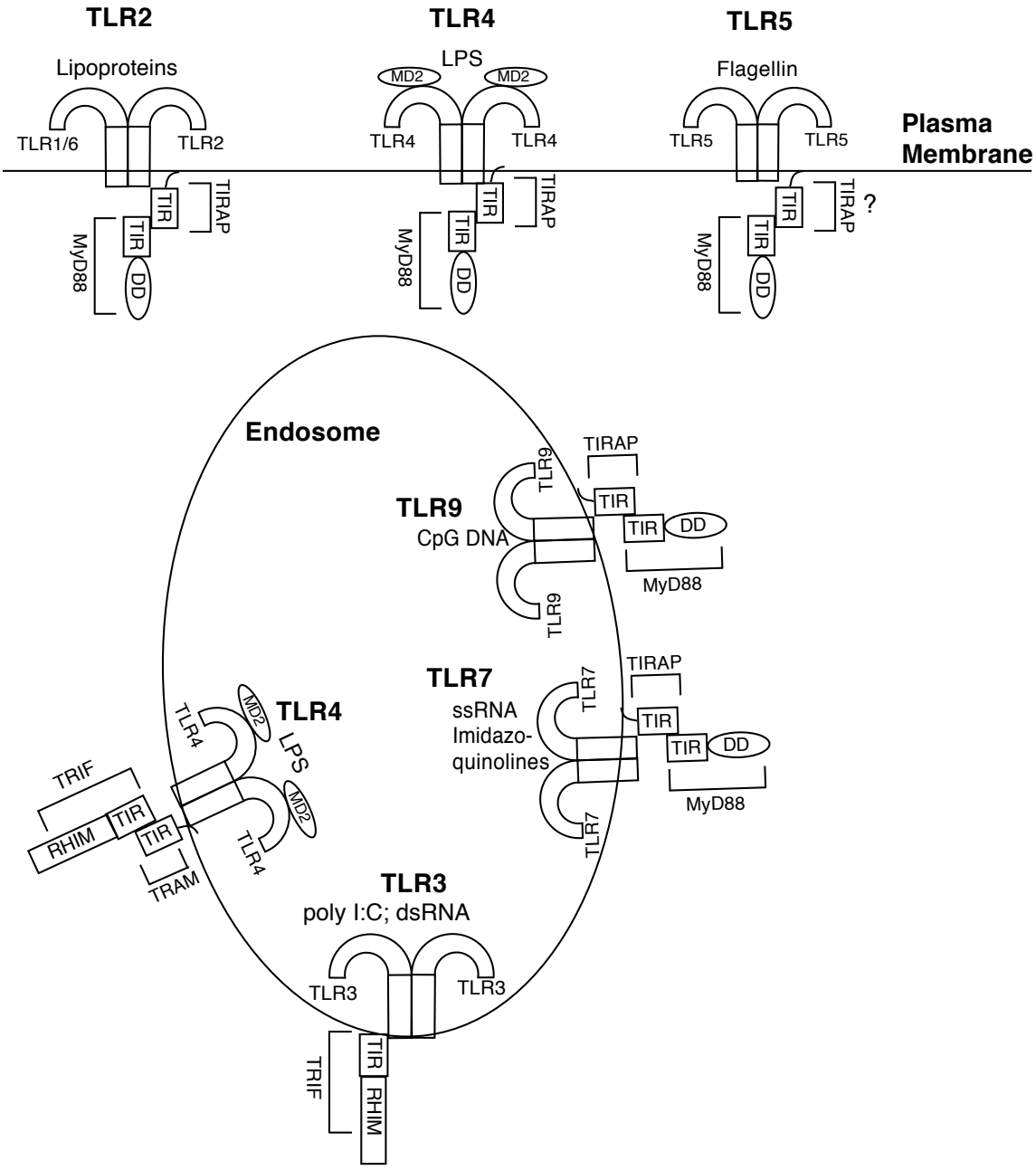

Figure 1. **TLR ligands and adapter proteins.** TLRs form homo- or heterodimers to bind their indicated agonists. TLR2, TLR4, and TLR5 are localized to the plasma membrane and signal using the TIRAP-MyD88 adapter proteins. TLR2 can form heterodimers with TLR1 or TLR6. TLR3, TLR4, TLR7, and TLR9 are localized to the endosome. TLR7 and TLR9 use the TIRAP-MyD88 adapter proteins whereas TLR3 and TLR4 use TRIF. TLR4 but not TLR3 requires the adapter protein TRAM for functional signaling.

TLR2/6 heterodimers bind triacyl lipoproteins. TLR5 is also localized to the plasma membrane and binds to flagellin.

Endolysosomal TLRs function in the acidified endolysosome and detect nucleic acids. Trafficking of these TLRs occurs through the activity of Unc93B, which translocates TLRs from the ER to the endolysosome (27). TLR3 detects virus-derived double-stranded RNA and its synthetic analog polyinosinic polycytodylic acid (poly I:C) (28). Single-stranded RNA and imidazoquinoline purine analogs are recognized by TLR7 and TLR8 (29). Interestingly, these TLRs can discriminate between the natural RNA ligand and imidazoquinolines by recognition site on the TLR7 and TLR8 ectodomains (30). TLR9 recognizes unmethylated CpG DNA often found in bacterial and viral genomes (27). Finally, in mice TLR11 and TLR2 are involved in the recognition of profiling derived from *Toxoplasma gondii* infection (31).

TIRAP and the Myddosome

Following TLR ligation, the TIR domain of the activated TLR forms homotypic interactions with a TIR domain-containing adapter which recruits kinases leading to the activation of the E3 ubiquitin ligase TRAF6 and activation of NF-κB and MAPK (32). In addition to their localization, the recruitment of MyD88 or TRIF TIR domain-containing adapter proteins and their downstream constituents govern the function of TLRs. MyD88-deficiency in macrophages leads to a loss of signaling activation from TLRs 2,5,7,8, and 9 with no detectable difference in NF-κB signaling from TLR3 and a delayed TLR4-driven response (32, 33). These MyD88-dependent TLRs share this adapter protein with signaling from IL-1R (23). Additionally, the sorting adapter TIRAP (TIR domain

containing adapter protein, also known as MAL) is used to bridge the receptor-MyD88 interface in signaling from MyD88-dependent TLR but not IL-1R (34–36). Previous work described TIRAP only to be important for TLR2 and TLR4 (34) and exclusively as a sorting adapter to recruit MyD88 to phosphatidylinositol 4,5-bisphosphatate (PIP2) at the plasma membrane (37). However, activating cells with natural TLR ligands revealed that TIRAP is required as an adapter for efficient signaling and formation of the myddosome for TLR9 in addition to TLR2 and TLR4 (35). Furthermore, promiscuous phosphatidylinositol lipid binding by TIRAP allows it to function as a MyD88 recruiting adapter at the plasma membrane and in the endolysosome (Figure 1).

Signaling downstream of MyD88 is accomplished by the assembly of a higher-order signaling complex termed the myddosome (38). Through homotypic interactions MyD88 recruits the death domain-containing serine threonine interleukin-1 receptor associated kinases (IRAK)-4 and IRAK1 or IRAK2 (39, 40). A crystal structure of the myddosome revealed the formation of a helical oligomer with hierarchical assembly of six MyD88 molecules followed by four IRAK4 molecules and finally four IRAK2 or IRAK1 molecules (38). The myddosome brings the IRAK kinase domains into proximity to promote phosphorylation and activation. Signaling from TLRs, unlike that of receptor tyrosine kinases, lacks receptor proximal enzymatic activity (41). These receptors use an alternative approach to signaling activation that includes higher order assembly and spatial clustering to increase the local concentration of kinases and promote signaling through proximity-driven activation. The activation of IRAK1 and IRAK2 may possess a sequential activation in which IRAK1 is responsible for early NF-κB activity while IRAK2 drives late NF-κB responses (42). However, work in wild-derived mouse

macrophages and human cells places IRAK2 as a critical mediator for the early MAPK and NF-κB response (43, 44). IRAKs then activate the E3 ubiquitin ligase TRAF6, which promotes its own lysine 63-linked polyubiquitination to recruit TAB2/3 and NEMO through ubiquitin binding domains, which activate TAK1 and NF-κB, respectively (45). In summary, MyD88-dependent TLRs utilize TIRAP to recruit MyD88 to the TLR, followed by formation of the higher-order myddosome complex including IRAKs leading to activation of NF-κB and MAPK through TRAF6 (Figure 2).

TRIF-dependent TLR signaling

Myd88$^{-/-}$ macrophages are not devoid in all NF-κB activation downstream of TLR4 and the loss of MyD88 has no impact on LPS-driven type I interferon responses (46, 47). TRIF (TIR-domain-containing adapter-inducing-interferon-β) is responsible for all signaling from TLR3 and for all interferon-β from TLR4 as well as a portion of the NF-κB response. TRIF, like MyD88, uses a sorting adapter (TRAM; TRIF-related adapter molecule) for recruitment to TLR4 but not TLR3 (48–50). Through homotypic interactions between the RHIM (RIP homotypic interaction motif) domains in each protein, TRIF-dependent TLR3 signaling to NF-κB uses receptor interacting protein-1 (RIP1) rather than IRAKs to connect to TRAF6 (51).

Type I interferon induction in macrophages only occurs through TRIF-mediated signaling and thus only occurs downstream of TLR3 and TLR4 (45). CD14-mediated endocytosis is required for TLR4-mediated interferon production (26, 49, 52), while TLR3 does not have this requirement as it localizes to the endolysosome. Activation of the TLR leads to TRIF recruitment followed by activation of TRAF3, which only

localizes to endosomal compartments (49, 53, 54). TRAF3 subsequently recruits the IKK-related kinases, TBK1 and IKKε, which activate IRF3 to promote IFN transcriptional activation (Figure 2). Currently, no myddosome-like structure has been elucidated for TRIF-mediated interferon production (i.e. TRIF-TRAF3-TBK1 axis) or NF-κB response (i.e. the RHIM-containing TRIF-RIP1) though TRAFs have been proposed to have the capacity to form higher-ordered structures (55). However, other RHIM containing complexes (DAI-RIP3, RIP1-RIP3) form higher order structures with amyloid characteristics (56). It would be interesting to determine whether the TRIF containing structures downstream of TLR3 and TLR4 form similar structures as the myddosome or as the RIP1 necrosome amyloid complex. Because the signaling properties of TLRs in general tend toward the use of higher-order signaling complexes, it is likely that TRIF-dependent signaling shares many properties with the myddosome (41).

Activation of the NF-κB pathway

The NF-κB transcription factor family is defined by a highly conserved DNA binding/dimerization domain, the Rel homology domain (57). These transcription factors form dimers and bind to 9-10 base pair κB sites in promoters or enhancers of genes (58). Within the transcription factor family there are two sub-families, Rel, comprised of c-Rel, RelB, and RelA (p65), and NF-κB, which contains p105 and p100. Rel family members contain a C-terminal transactivating domain, allowing them to drive transcription after binding DNA, while in the NF-κB subfamily C-terminal ankyrin domains inhibit translocation into the nucleus until limited proteolysis occurs (57). Limited proteolysis

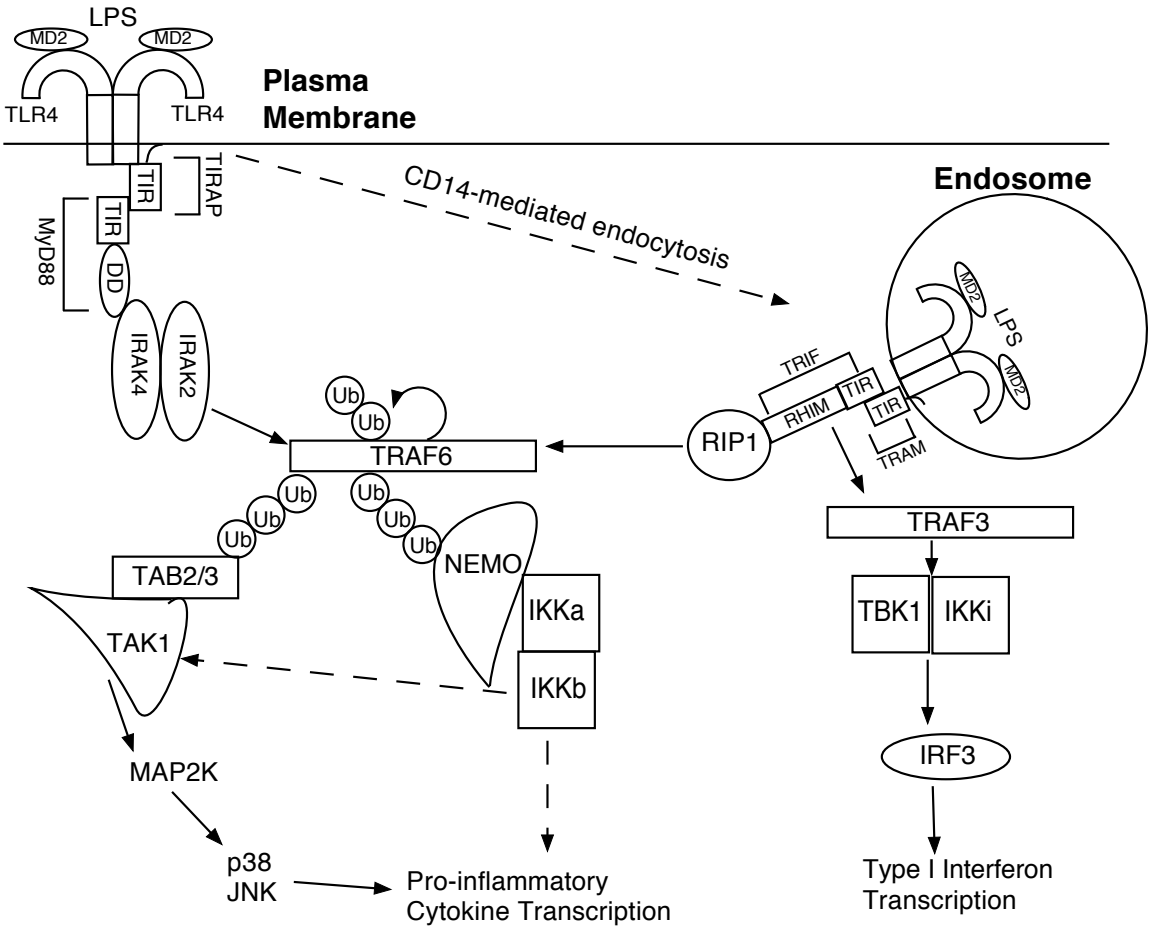

Figure 2. **TLR4 signaling cascade to activate pro-inflammatory cytokines and type I interferon.** TLR4-MD2 binds to LPS at the plasma membrane and recruited to TIRAP-containing lipid rafts. TIRAP recruits MyD88 leading to Myddosome formation with IRAK4 and IRAK2 (or IRAK1). Subsequent activation of TRAF6 and auto-ubiquitination leads to recruitment of TAK1 and NEMO through ubiquitin binding domains. TAK1 acts as a MAP3K leading to MAPK activation while NEMO recruits the IKK complex leading to IκBα degradation and translocation of p65 into the nucleus. Both of these events lead to pro-inflammatory cytokine production. Additionally, TLR4 is endocytosed in a CD14-dependent manner, leading to recruitment of TRAM-TRIF at the endosome. TRIF signaling recruits RIP1 to feed into the TRAF6 pathway and activate TRAF3. Type I interferon production is activated following activation of the IKK-related kinases TBK1 and IKKi (also called IKKε) that phosphorylate and lead to dimerization and nuclear translocation of IRF3.

causes p105 to form p50 and p100 becomes p52. However, neither p50 or p52 contain transactivation domains, necessitating their binding to molecules that contain a transactivation domain in the form of heterodimers containing Rel proteins or homodimers of p50 which can bind to IκB family members such as Bc13, which contain a transactivation domain (57, 58).

TLR signaling results in a strong activation of p65/p50 heterodimers (58). The activity of this complex is negatively regulated sequestration in the cytosol by IκBα, which obstructs the p65 nuclear localization sequence. Other IκB family members function by different mechanisms such as allowing nuclear-cytoplasmic shuttling without permitting DNA binding. Activation of NF-κB occurs when IκBα is degraded, exposing the nuclear localization sequence and subsequent DNA binding and transactivation by p65/p50. Degradation of IκBα occurs following phosphorylation by the IKK (IκBα kinase) complex, which begins a cascade leading to IκBα lysine 48-linked polyubiquitination and degradation by the 26S proteasome (57). The IKK complex is comprised of IKKα, IKKβ, and NEMO (NF-κB essential modifier) (59). Notably, canonical p65/p50 heterodimers are activated primarily by IKKα/β heterodimers, though IKKβ is necessary and sufficient, while noncanonical phosphorylation of p100 is driven by IKKα homodimers. Finally, NF-κB generates a negative feedback loop to control its activity by acting as a transcription factor to promote expression of IκBα (55).

Mitogen activated protein kinase (MAPK) activation by TLRs

MAPK signaling is activated by numerous stimuli including hormones, growth factors, cytokines, TGF-β, and pathogen recognition receptors (60). The three tiered

signaling module of MAP3K, MAP2K, and MAPK sequential activation is a property of MAPK. Serine threonine phosphorylation by MAP3K activates the dual-specificity kinase activity of MAP2K to phosphorylate tyrosine and threonine residues on MAPK. The specificity of activation of a particular MAPK by MAP2K is generated by docking domains on MAPK (61). The most well-studied MAPK family members activated during TLR signaling are extracellular related kinases (ERK1/2), c-Jun NH2-terminal kinases (JNK1-3), and p38α/β (60). Activation of these kinases downstream of TLR ligation leads to phosphorylation of other protein kinases or activation transcription factors to contribute to changes in gene expression and mRNA stability that influences cytokine production, antimicrobial transcription, and other macrophage activation properties important for the innate immune response (60, 61). Though other mechanisms of activation exist, the canonical mechanism for MAP2K activation of MAPK involves MEK1/2 phosphorylation of ERK, MKK4/7 phosphorylation of JNK, and MKK3/6 phosphorylation of p38. Additionally, the activation of MAP2K by MAP3K is increasingly complex (61). Though some recent supports suggest otherwise, TAK1 kinase is the best-documented activator of p38 and JNK and also has a role in ERK activation. TAK1 is activated following binding of TAB2/3 to polyubiquitinated TRAF6, which leads to phosphorylation of MAP2K as previously mentioned for p38 and JNK activation. In addition, TAK1 activates the IKK complex, causing p105 degradation and release of Tpl2 from an inactivating complex, which promotes ERK activation to drive cytokine production. Together the activity of MAPK and NF-κB leads to transcription and subsequent release of pro-inflammatory cytokines.

Transcriptional and post-transcriptional regulation of cytokine production

Innate immune cells produce a rapid and robust transcriptional response. Signal transduction through MAPK or IKK-mediated pathways generates a physiological response caused by gene induction, which occurs following modulation of subcellular localization, promoter recruitment, and transcriptional activation of various transcription factors (62). Transcription factors bind DNA in a sequence-specific manner and their activities are regulated by many coregulatory proteins and chromatin-associated proteins (63). For example, the maximal induction of *Tnf* mRNA requires that two overlapping *cis*-acting DNA elements (Sp1/Erg-1 and CRE/NFκB) to recruit a number of different transcription factors including NF-κB, EGR-1, ELK-1, ATF-2, and AP-1 (64). Each of these transcription factors is activated through events triggered by MAPK phosphorylation of their upstream kinases or induction of nuclear translocation such as in the case of NF-κB. Following transcription factor activation and recruitment to promoter and enhancer regions through sequence-specific DNA binding, these transcription factors synergize to recruit transcriptional machinery including RNA polymerase II to the core promoter and transcription start site (65).

Temporal regulation leads to biologically significant activation of different sets of genes. Primary response genes do not require new translation. Primary response genes including *Fos* and *Jun*, do not require nucleosome remodeling while other primary response genes do require SWI/SNF-mediated remodeling of nucleosomes. Following transcription of some cytokines, chemokines, and transcription factors by primary response genes, genes that require new translation, secondary response genes, are transcribed.

Recent studies have illuminated additional levels of transcriptional regulation within the group of primary response genes. Though sharing κB binding site sequences, some genes recruit NF-κB rapidly following activation and its nuclear entry while others take substantially longer (66). One reason for this difference is the intrinsic control of chromatin structure associated with whether a given promoter is a CpG-island promoter such as *Fos* and *Jun*, which do not require SWI/SNF-mediated remodeling and are associated with high levels of RNA Pol II and active H3K4me3 chromatin marks, or low-CpG promoters, found in tightly regulated genes such as *Il12b*, *Il6*, and *Nos2* that demonstrate low RNA Pol II recruitment and require SWI/SNF nucleosome remodeling for transcription to occur (65).

Post-transcriptional mRNA regulation can occur through action on nuclear export, cytoplasmic localization, translation initiation, and mRNA decay (67). Many cytokines and chemokines are regulated by mRNA decay mediated through adenine and uridine rich elements (ARE) in the 3' UTR. AREs consist of pentamers (AUUUA), nonamers (UUAUUUAUU), and AU-rich clusters containing pentamers and nonamers. Proteins containing domains that bind to AREs affect translation efficiency or drive mRNA decay. For example, p38 MAPK-activated kinase 2 (MK2) phosphorylates and inactivates tristetraprolin (TTP), a protein that binds to and destabilizes ARE-containing mRNA transcripts. Following MK2-mediated inactivation of TTP, certain cytokine mRNAs such as *Tnf* are stabilized. Together, gene transcription, induced transcription silencing or decay, and the intrinsic stability of a transcript govern the magnitude and temporal nature of a cytokine response (68).

Functions of cylindromatosis protein - CYLD

Ubiquitination and deubiquitination

Ubiquitination involves covalent binding of the C-terminus of the 76 amino acid ubiquitin molecule to a substrate or to another ubiquitin molecule (known as polyubiquitination) (69). Ubiquitination can occur in monomers or through multiple additions of single ubiquitin monomers to create polyubiquitination chains. Polyubiquitination links the C-terminus of one ubiquitin to the ε-amino group on one of the seven internal lysine residues in the second ubiquitin molecule (K6, K11, K27, K29, K33, K48, or K63) or to the N-terminus methionine (M1 or linear ubiquitination). Three steps are required for this process: 1) activation of ubiquitin by E1, 2) coupling of activated ubiquitin to an E2 ubiquitin conjugating enzyme, and 3) transfer of ubiquitin to its substrate by an E3 ligase. E3 ligases can be HECT domain-containing, to which ubiquitin is transferred from E2 to the E3 prior to ligation to its substrate, or RING domain-containing, which act as a scaffold for direct ubiquitin transfer from E2 to the substrate (70). Within the human genome there are two E1s, at least 38 E2s, and more than 600 E3 ligases (69, 71, 72). Like phosphorylation, ubiquitin modifications are reversible and can target proteins for degradation by the proteasome (K48 polyubiquitination) or alter their structure in a way to serve nonproteolytic functions such as trafficking and activation of signaling proteins (71, 73).

Cleavage and removal of the ubiquitin modification is accomplished by deubiquitinases (DUBs) (71). Approximately 80 DUBs are encoded by the human genome and are separated into five families based on structural domains: ubiquitin C-terminal hydrolases, ubiquitin-specific proteases (USP), ovarian tumor proteases (OTU),

Josephins, and JAMMs. The USP family is the largest group, made up of over 50 proteins including CYLD. The second largest group is the OTUs, which contains A20, DUBA, and Cezanne (73). DUBs are recruited to ubiquitinated substrates through ubiquitin-binding domains contained within the DUB itself or through the use of adapter proteins that contain ubiquitin-binding domains. As is true with E3 ligases, enzymatic action of DUBs is specific, both to the protein substrate that is being deubiquitinated and to the type of ubiquitin chain that is being hydrolyzed (73, 74). Substrate specificity is achieved through specific protein-protein interactions governed by protein interaction domains within the substrate and the DUB, intrinsic preference of each DUB for a particular di-ubiquitin linkage (as K63 and M1 linkages have distinct structures from K48 linkages), and differential expression and subcellular localization. As an example, A20 and CYLD share common substrates such as RIP1 but serve different functions in the NF-κB pathway (69, 71). A20 functions as a negative regulator of NF-κB and an anti-apoptotic molecule by cleaving K63-linked ubiquitin from RIP1 with its OTU domain followed by ligating K48-linked chains to target RIP1 to the proteasome (71, 75). CYLD negatively regulates NF-κB and promotes cell death by cleaving K63- and M1-linked ubiquitin chains from RIP1 leading to its interaction with the pro-death 'complex II' to drive apoptosis and necroptosis (see below) (72, 76). This differential function is governed by differences between A20 and CYLD in expression (A20 requires up-regulation, CYLD is basally expressed), adapter protein usage for binding to a given substrate, and intrinsic properties of the DUB itself (71).

CYLD – a tumor suppressor gene

The function of CYLD as a tumor suppressor gene was first appreciated in familial cylindromatosis (77). Now included in the spectrum of Brooke-Spiegler Syndrome, familial cylindromatosis and multiple familial trichoepitheliomas are autosomal dominant conditions characterized by multiple skin appendage tumors (78, 79). In these conditions, tumors of sweat glands (cylindromas and spiradenomas) and/or hair follicles (trichoepitheliomas) develop. Tumor development begins in the second and third decade of life and the vast majority of tumor growth occurs in the head and neck region (77). Severe overgrowth of cylindromas on the scalp resulting in a confluent tumor mass that has the potential for ulceration and infection is referred to as the 'turban tumor syndrome.' Mutations in *CYLD* are present in the majority of familial cylindromas and many sporadic cylindromas. Of the 51 documented *CYLD* mutations, 86% lead to truncated proteins or nonsense-mediated RNA decay while the remaining 7 mutations are within the USP domain (78, 79). In addition to its role in familial skin appendage tumor syndromes, loss of heterozygosity or decreased protein expression is documented in many cancers including multiple myeloma, hepatocellular carcinoma, melanoma, basal cell carcinoma, and uterine cervix carcinoma (80, 81).

CYLD – domain structure and function

Following the identification of *CYLD* as the gene underlying familial cylindromatosis, thorough investigation into its mechanism of action revealed that NF-κB is negatively regulated by the DUB activity of CYLD (82–84). CYLD interacts with NEMO, TRAF2, and TRAF6 to remove ubiquitin modifications from these proteins. The

domain structure of CYLD contains three cytoskeletal-associated protein-glycine conserved (CAP-GLY) domains (80, 81). The first two CAP-GLY domains associate with microtubules and contribute to cell migration. The third CAP-GLY domain is proline-rich and folds into an SH3-like structure. NEMO interacts with CYLD within the third CAP-GLY domain. The USP ubiquitin hydrolase domain is located at the C-terminus of the protein (Figure 3).

Cyld$^{-/-}$ mice – diversity of phenotypes

In 2006, three groups generated CYLD knockout mice to further explore the function of this protein (85–87). These three models generated some controversy over the roles of CYLD in different cell types, specifically due to the inconsistency of the presence or absence of phenotypes in between the groups. Interestingly, despite phenotype in CYLD-deficient humans, none of the CYLD-deficient mice developed spontaneous tumors (79). All three models were designed to create nonsense-mediated degradation of CYLD protein, which was confirmed by western blot in each study. Massoumi and Fassler generated a *Cyld* knockout mouse by deleting exon 4 of CYLD and backcrossing five generations to C57BL/6 (87). The *Cyld$^{-/-}$* demonstrated heightened susceptibility to UV- and chemical-induced keratinocyte tumorigenesis through increasing the proliferative capacity of these cells rather than decreasing susceptibility to apoptosis. The loss of CYLD led to increased NF-κB activation by Bcl3-p50/p52 heterodimers. CYLD removes K63- polyubiquitin chains from Bcl3, leading to its nuclear export. Without CYLD, cells retained Bcl3 in the nucleus where it formed heterodimers with p50 or p52 to activate transcription of cyclin D1. Overall, this model

demonstrates a tumor suppressor function CYLD through negative regulation of Bcl3-mediated NF-κB activation.

Zhang and Jain created a CYLD knockout mouse with a deletion of exons 2 and 3 on a C57BL/6-albino background (86). CYLD deficiency increases susceptibility to DSS-induced colitis in this model. In vitro experiments demonstrated that CYLD knockout macrophages stimulated with TLR2, TLR4, or CD40 agonists had increased activation of JNK and NF-κB, in agreement with the initial characterization of CYLD functions (82–84). However, TNF stimulation did not show any change in the activation of these pathways when compared to wild-type macrophages. Additionally, while CYLD deficient macrophages stimulated with TNF show increased ubiquitination of TRAF2 compared to wild-type macrophages, there was no change in RIP1 ubiquitination between the wild-type and CYLD-deficient macrophages.

The Sun group generated a CYLD deficient mouse by deleting exons 1 and 2 of CYLD (85). Macrophages from this mouse did not show the changes in MAPK or NF-κB pathways that were observed in the mouse created by Zhang and Jain. However, the Sun *Cyld*$^{-/-}$ mouse generated revealed numerous phenotypes not seen in either of the aforementioned knockout mice. These mice showed defects in T cell development from double positive to single positive stages due to a defect in Lck recruitment to ZAP70 (85) and peripheral T cells with constitutively activated TAK1 accumulated in the liver and colon (88). Male *Cyld*-deficient mice were infertile due to a defect in apoptosis in testicular germ cells (89). Resistance to apoptosis was caused by increased RIP1 ubiquitination and increased production of anti-apoptotic proteins through NF-κB. CYLD knockout mice were also prone to osteoporosis due to increased osteoclast-genesis

signaled by RANK/RANK-L (90). Finally, *Cyld*$^{-/-}$ dendritic cells showed constitutive activation of anti-viral mediators IKKε and TBK1 (91).

CYLD in cell death

As mentioned above, CYLD cleaves K63- and M1-ubiquitin from RIP1 to negatively regulate NF-κB (69, 84). The CYLD-deficient cells accumulate polyubiquitinated RIP1 and these proteins physically interact, though the interaction domains and whether an adapter protein is required for their interaction is not known (71, 89, 92). CYLD-deficiency leads to constitutive NF-κB activation in certain conditions (89, 93), however, CYLD also promotes the formation of pro-apoptotic and pro-necroptotic complexes (76, 92). In TNF-mediated apoptosis and necroptosis, some studies have demonstrated a requirement for RIP1 deubiquitination for the transition between the pro-survival TNF-R1 complex to the pro-death caspase-8/FADD or RIP1/RIP3 containing complex for apoptosis and necroptosis, respectively. However, there is still a question as to whether this deubiquitination event is required for the formation of the pro-death complex (94). Taken together, CYLD promotes cell death through inhibiting NF-κB in certain conditions and cell types and directly promotes the formation of a pro-death signaling complex by acting on RIP1 in TNF-R1 signaling.

Regulators of Cyld expression and function

Not surprisingly given its established function as a tumor suppressor gene and its promoter of cell death, *Cyld* is under multiple levels of regulation (80, 81). Epigenetic, transcriptional, and post-translational regulation of CYLD is documented in normal cells

and cancers. However, many of the observations documented appear to be cell type and/or agonist-specific (90).

CYLD up-regulation by NF-κB is triggered by TNF, IL-1, *H. influenza* and RANK-L stimulation (90, 95). In a p38 MAPK dependent fashion, serum stimulation activation serum response factor to increase CYLD expression in MEFs (96). Activation of SWI/SNF subunit BAF57 also promotes CYLD expression (97). Down-regulation of CYLD is documented primarily in the context of cancer cells. In T-ALL, the Notch-dependent transcription factor *Hes1* represses CYLD expression (98) while in CLL, LEF1, a Wnt-dependent transcription factor, suppresses CYLD levels (99). Hedgehog signaling in basal cell carcinoma and melanoma down-modulates CYLD through activation of GLI1 and Snail (100, 101). MicroRNAs miR-181b-1 and miR-19 down-regulate CYLD as well, also contributing to tumorigenesis (102, 103). Finally, activation of human 293EBNA cells infected with Sendai virus and stimulated with TNF causes a stimulus-dependent down-regulation of CYLD, though the mechanism is unclear (104).

An attempt to generate a novel CYLD knockout mouse lacking exon 7 led to the discovery of CYLD regulation by alternative splicing (105). Without exon 7, rather than leading to a missense mutation from splicing of exon 6 to exon 8 as was expected, CYLD preferentially splices exon 6 to exon 9, generating the $CYLD^{ex7/8}$ isoform, which lacks NEMO and TRAF binding motifs (Figure 3). Additionally, this isoform is co-expressed with the full-length isoform in lymphoid tissues of wild-type mice. In mice expressing only $CYLD^{ex7/8}$ an increase in B cell survival leads to significant lymphadenopathy, however the effects of this isoform alongside the full-length isoform are not known. In

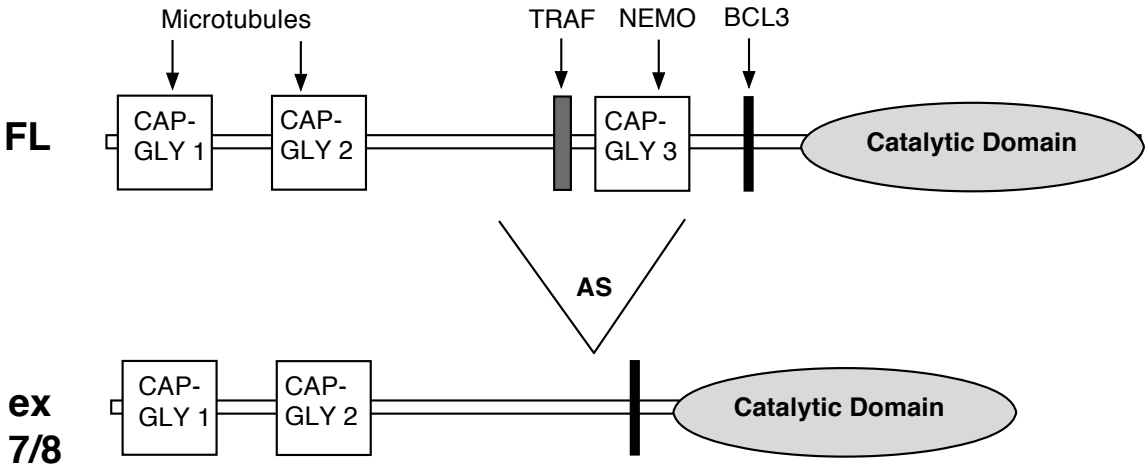

Figure 3. **CYLD domain structure.** Full-length (FL) CYLD contains three CAP-GLY domains with a NEMO binding site in the third CAP-GLY, a TRAF binding site, a Bcl3 binding site, and a catalytic USP domain. Alternative splicing (AS) generates the $CYLD^{ex7/8}$ splice variant that lacks the TRAF binding site and third CAP-GLY domain that contains the NEMO interaction site but retains the Bcl3 interaction motif. The binding site for RIP1 has not been mapped. Graphic adapted from Sun (2010) *Cell Death Differ* (80) and Hovelmeyer (2007) *J Exp Med* (105).

humans, alternative splicing occurs in the non-coding exon 3 and the 9-nucleotide exon 7 but the functions of each have yet to be examined (80).

Post-translational modification by phosphorylation and proteasomal degradation occurs to negatively regulate CYLD function. Phosphorylation of a seven serine residue cluster by IKK in a NEMO-dependent fashion led to decreased DUB activity on TRAF2 to permit signaling (106). This phosphorylation event occurred followed cell stimulation. In an independent study, IKKε-mediated CYLD phosphorylation decreases DUB activity (107). Furthermore, this phosphorylation even was required for IKKε driven cell transformation. In addition to phosphorylation, one report identifies that HPV E6 protein causes polyubiquitination and proteasomal degradation of CYLD to allow for an increase in NF-κB activity (108).

Molecular mechanisms of RIP1 in cell death and inflammatory signaling

Cell death modalities

Cell death was initially described through observation of morphological features that characterized apoptosis or necrosis (109, 110). Apoptosis, long held as the only programmed cell death mechanism, involves nuclear and cytoplasmic condensation, reducing in cytoplasmic and nuclear volume (pyknosis), nuclear fragmentation, and blebbing of the plasma membrane. In contrast, necrosis is characterized by cytoplasmic and organelle swelling followed by plasma membrane rupture and release of cellular contents. Necrosis was classically described as accidental cell death induced by noxious stimuli or trauma. The presence or absence of certain events such as release of cellular contents has critical impact on the subsequent response to dying cells. However, as the

biochemical characterization of cell death has developed, it is now well accepted that distinct signaling mechanisms may generate similar morphology, and the study of these mechanisms is imperative for a full description of a given cell death pathway (111). The best characterized of these signaling mechanisms are apoptosis, pyroptosis, and necroptosis.

Apoptosis is cell death induced by activation of caspases, cysteine proteases that cleave many cellular proteins, and disruption of the mitochondrial outer membrane potential (MOMP) (112). Caspases are separated into initiator caspases activated by induced proximity (caspase-2, -8, -9, and -10) and executioner caspases activated by cleavage (caspase-3, -6, and -7). The extrinsic apoptosis pathway is activated through plasma membrane receptors of the death receptor family including FAS and TNF-R1 (111, 113). Ligation of a death receptor ligand leads to the formation of a multi-protein complex (discussed in detail below) that activates caspase-8. In 'type-I' cells, such as lymphocytes, caspase-8 directly activates caspase-3. However, in 'type-II' cells, such as hepatocytes, caspase-8 activates the BH3-only protein BID that localizes to the mitochondria, initiating a series of events leading to release of cytochrome C, activation of caspase-9, and activation of caspase-3. Intrinsic apoptosis is activated by a variety of intracellular stresses such as DNA damage, oxidative stress, and ER stress, which lead to activation of BH3-only proteins (including BID, BIM, and BAD) (114). BH3-only proteins disrupt the anti-apoptotic activity of Bcl-2 allowing for the formation of the mitochondrial pore by the pro-apoptotic proteins BAX and BAK. Opening of this pore release cytochrome C, leading to the formation of the apoptosome around APAF,

recruitment of the initiator caspase-9, and cleavage of caspase-3 followed by cleavage of caspase substrates and cell death.

Multiple distinct cellular signaling mechanisms appear to activate necrotic cell death. Discussion is ongoing as to whether these disparate triggers and mechanisms should be grouped as pathways of regulated necrosis (115) or separated into distinct cell death mechanisms identified by specific signaling components (111). Necroptosis was the first described mechanism of regulated necrotic cell death (discussed in detail below) (116). Pyroptosis, a caspase-1 or caspase-11 dependent cell death mechanism, is associated with release of IL-1β and IL-18 along with cellular contents (117). Largely studied in the context of intracellular bacteria infection of macrophages, pyroptosis is induced through formation of the canonical inflammasome that forms a large oligomeric structure to recruit caspase-1 into proximity (118, 119), similar to initiator caspases. This inflammasome activates caspase-1, which causes cell death by an unknown mechanism while cleaving IL-1β and IL-18 into biologically activate forms. Caspase-11 activation (non-canonical inflammasome) is less well characterized, but appears to be downstream of bacteria that escape the phagolysosome or vacuole into the cytosol (120, 121). Importantly, caspase-11 appears to be activated by cytoplasmic LPS through an as-yet unidentified sensor, resulting in pyroptosis without cleaving IL-1β and IL-18 (16, 17).

RIP1 – a critical molecule for pro-inflammatory and cell death signaling

Extrinsic apoptosis and necroptosis are activated through death receptor-mediated signaling cascades including TNF-R1. RIP1 regulation by ubiquitination, cleavage, and kinase activity plays an important role in dictating whether TNF-R1 ligation causes pro-

inflammatory signaling, apoptosis, or necroptosis (69). RIP kinases are a family of serine/threonine kinases with a conserved kinase domain (RIP1-7) that are best characterized as mediators of stress responses to activate NF-κB, MAPK, apoptosis, and necrosis (122). The non-kinase domains of RIP kinases dictate the pathways with which they interact. RIP1 contains a C-terminal death domain and an intermediate domain containing a RIP homology interaction motif (RHIM), both capable of homotypic interactions. RIP3 lacks a death domain but also contains a RHIM domain.

In addition to interactions by homotypic domain binding, RIP1 recruits binding partners following its modification by non-degradative ubiquitination and is itself targeted for degradation by ubiquitination (123). RIP1 is modified by addition of M1, K11, K48, and K63 polyubiquitin chains. K48 ubiquitination targets a protein for proteasomal degradation while the other forms of ubiquitination act in a similar fashion to phosphorylation, modifying the structure of a protein and prompting interaction with proteins that contain ubiquitin-binding domains. The importance of RIP1 ubiquitination in dictating its interaction partners and its capacity to influence signaling outcomes is best described for TNF-R1 signaling (69). Trimeric TNF binds and activates TNF-R1 causing recruitment of TRADD (TNF receptor associated death domain). A homotypic death domain interaction recruits RIP1 to TRADD and RIP1 subsequently recruits the RING domain-containing E3 ligases TRAF2/5 and cIAP1/2. K63-linked polyubiquitination of RIP1 follows and leads to recruitment of NEMO, TAB2/3, and LUBAC through their ubiquitin binding domains. The kinase activity of RIP1 is completely dispensable for this process (124). NEMO recruits IKKα/β leading to NF-κB activation and TAB2/3 recruit TAK1, which activates IKKα/β and MAPK (Figure 4). LUBAC (linear ubiquitin

activation complex) is comprised of HOIL, HOIP, and SHARPIN and ligates M1-linked polyubiquitin chains to RIP1 and NEMO and functions to stabilize the interactions described above (125, 126). This membrane-associated complex, known as 'complex I', acts as a pro-survival signal by promoting transcription of the anti-apoptotic proteins A20, c-FLIP$_L$, and cIAPs while also preventing interaction with pro-death molecules such as FADD (Fas-associated death domain) and capsase-8 (127).

If these anti-apoptotic signals are suppressed or the activity of deubiquitinases (DUB) removes ubiquitin chains, the TNF-R1 complex transitions to a pro-death signaling complex known as 'complex II' (Figure 4). Complex II is localized to the cytoplasm and contains RIP1, FADD, and caspase-8 (and caspase-10 in humans) (76, 128, 129). Multiple DUBs are implicated in removal of ubiquitin chains from RIP1 (69) but Cylindromatosis protein (CYLD) is a major RIP1 DUB (92), specifically cleaving K63- and M1-linked polyubiquitin chains (130). Complex II then activates apoptosis or necroptosis based on the activity of caspase-8, expression of RIP3, and differential expression of FLIP isoforms (69, 131).

In addition to its role in TNF-R1 signaling, RIP1 acts in other death receptor signaling pathways and in TLR signaling. RIP1 interacts with the TLR3 and TLR4 adapter TRIF through a RHIM homotypic interaction and permits signaling to NF-κB but not IRF3 (51, 132). RIP1 ubiquitination in TLR signaling is mediated by Peli1 rather than cIAP1/2 and TRAF2 in TNF-R1 (133). In contrast to TNF-R1 signaling complexes I and II, it appears that death signaling from TLR3 occurs in the receptor-proximal complex, as TRIF recruits RIP1 with FADD and caspase-8 and/or RIP3 to activate apoptosis or

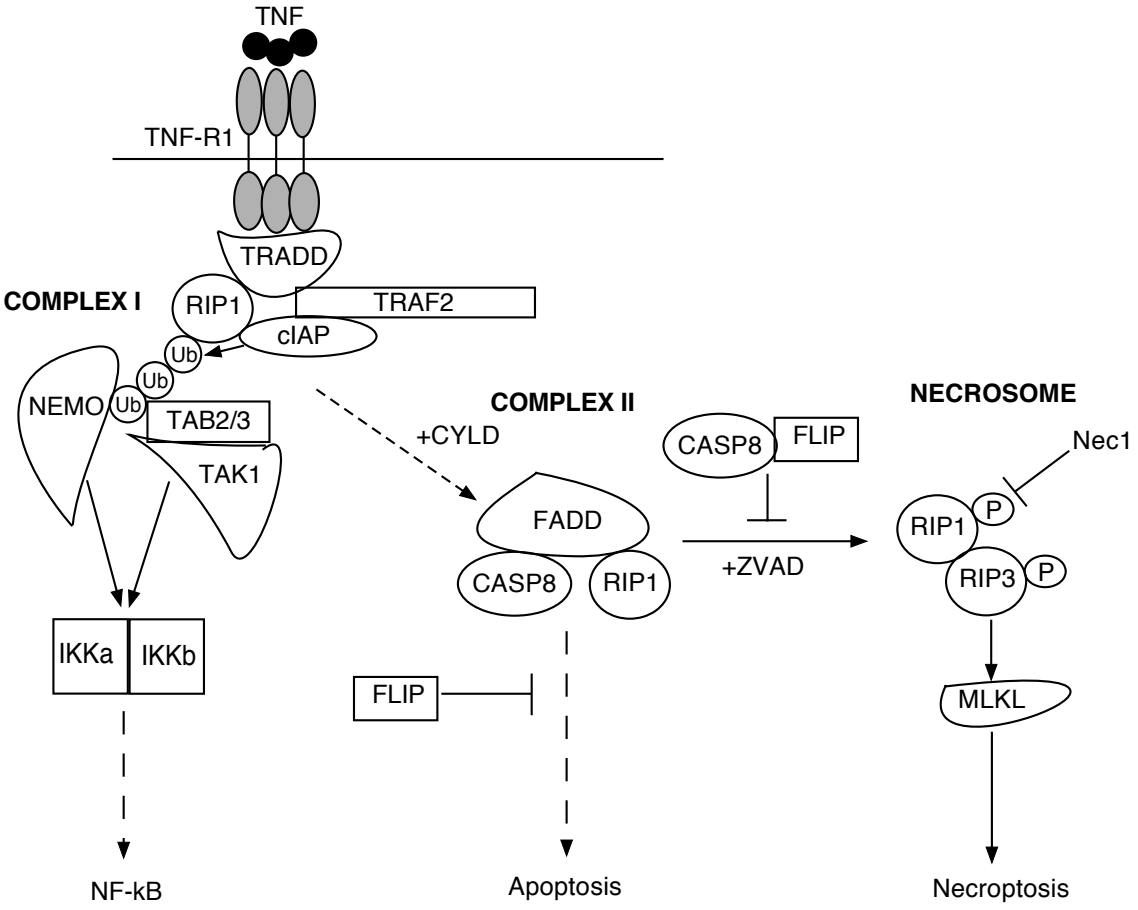

Figure 4. **TNF-R1 signaling triggers NF-κB, apoptosis, or necroptosis based on presence or absence of regulatory proteins.** TNF receptor ligation causes trimers of TNF-R1. Following recruitment of TRADD, TRAF2 and cIAP1/2 act to add K63 polyubiquitin chains to RIP1. Ubiquitin binding domains from TAB2/3, NEMO, and LUBAC (not shown) recruit these molecules to the complex (complex I) and together activate NFκB and MAPK. The activity of the deubiquitinase CYLD removes K63 and linear ubiquitin chains from RIP1 and forms a cytoplasmic complex containing RIP1, FADD, and caspase-8 (complex II). This complex can activate apoptosis if FLIP is not present. When FLIP is expressed at low levels and caspase-8 is inhibited and expressed at a low level, the necrosome forms. The necrosome consists of RIP1 and RIP3, both of which require their kinase activity to drive necroptosis through MLKL (necrosome). The RIP1 kinase inhibitor prevents necroptosis through disrupting the activity of this complex. Graphic adopted from multiple excellent reviews (128, 134, 135).

necroptosis (136, 137). However, whether deubiquitination of RIP1 is necessary in TLR-mediated cell death is not clear.

Molecular components of necroptosis

As discussed above, cell death with a necrotic morphology can be induced through specific cellular signaling mechanisms and is not restricted to accidental cell death (116). Seminal works in L929 fibroblasts established that TNF-R1 (138) and FAS (139) activation cause cell death with a necrotic morphology when caspases are inhibited, in contrast to the apoptotic morphology without caspase inhibition. In T cells, caspase inhibition causes cell death morphology to switch from apoptotic to necrotic in FAS, TRAIL, and TNF-R1-mediated signaling (140, 141). This necrotic cell death requires FADD and RIP1 (140). Intriguingly, both the death domain and the kinase domain of RIP1 are required for necrotic cell death. Caspase-8 in a complex with cellular FLICE-like inhibitory protein (c-FLIP, referred to as FLIP here) directly cleaves RIP1 to negatively regulate this form of cell death (142–144), hence why the inhibition of caspases promotes necrotic cell death. The terms "programmed necrosis" and "necroptosis" were coined to describe this RIP1 kinase activity-dependent necrotic cell death process activated by death receptor signaling during caspase inhibition (142, 145). The tools to study this form of cell death grew when Necrostatin-1 (Nec-1), a chemical inhibitor of caspase independent TNF-mediated cell death was described (145) and was demonstrated to inhibit RIP1 kinase activity, as measured by capacity for RIP1 to auto-phosphorylate (146). Furthermore, the first broad siRNA screen for components of the

necroptosis signaling network identified 25 genes uniquely required for necroptosis (and not apoptosis) (147), establishing this cell death mechanism as a distinct entity.

In death receptor-mediated necroptosis, RIP1 activates a second member of the RIP kinase family, RIP3 (148–150). RIP3, like RIP1, is a serine/threonine kinase that contains a RHIM domain but RIP3 lacks a death domain. Expression of RIP3 varies between cell lines and tissues and both expression and kinase activity are required for necroptosis (149, 151). Importantly, the kinase activity and oligomerization of RIP3 are necessary and sufficient to cause necroptosis and RIP1 appears to act as a 'seed' for RIP3 oligomers (152–154). When RIP1 and RIP3 are activated, a functional amyloid signaling complex is formed through kinase-dependent interactions between the RHIM domains of these two molecules (56). Prior to interaction with RIP3, RIP1 is recruited to a FADD-caspase-8-FLIP-containing "necrosome" or "Ripoptosome" complex (136, 155, 156). This complex can form following activation of TNF-R1 (157), TLR3 or TLR4 (136, 137), and inhibitor of apoptosis protein (IAP) depletion by genotoxic stress (155). Following necrosome formation, multiple factors including caspase-8 activity, FLIP expression, predominance of the short or long isoforms of FLIP, and RIP3 expression determine whether cells will undergo apoptosis or necroptosis (158).

While RIP1 and RIP3 are important activators of necroptosis, the execution of necrotic cell death is mediated by mixed lineage kinase domain-like (MLKL) (159, 160) through a mechanism of action that is now coming into focus. While some studies identify a mitochondrial pathway involving the mitochondrial phosphatase PGAM5 as an executer of necroptosis (161), more recent analysis identifies a non-mitochondrial process as causing necroptosis (162) that does not require PGAM5 (163). MLKL is a

pseudokinase that binds ATP but does not require this step for its activity (163). Phosphorylation by RIP3 causes a conformational change in MLKL which leads to oligomerization of its N-terminal coiled-coil domain (163–165). Whereas RIP1 and RIP3 are implicated in cellular processes beyond necroptosis, MLKL is currently identified as a necroptosis-specific protein (123, 151, 163).While multiple reports establish that MLKL oligomers localize to the plasma membrane, the next step is less certain with three current models proposed. The first involved tetramers of MLKL allowing sodium influx from the plasma membrane through an unidentified channel (166). In a similar model, a second group demonstrated that MLKL trimers localize to the plasma membrane and cause calcium influx through transient receptor potential M7 (TRPM7) (167). Finally, two recent reports propose an alternative model by which MLKL localizes to membranes through charge-mediated interactions with the phosphatidylinositol phosphates (165, 168). After translocation to the plasma membrane, MLKL oligomers insert into the membrane and form a pore that disrupts plasma membrane integrity.

Chemical inhibitors used to study necroptosis

Since the observation that necrosis occurs following death receptor ligation during caspase inhibition, chemical inhibitors of caspases have become a mainstay of necrosis research (116, 138). Caspases are cysteine proteases, existing in cells as inactive zymogens, that are activate as dimers (169). These enzymes cleave after the P1 residue of their substrates and strong preference for aspartate at this residue (170). Some viruses express proteins that act as caspase inhibitors, presumably as a mechanism to subvert apoptotic clearance (171). In the study of necrosis, synthetic inhibitors are often used,

including the pan-caspase inhibitor Benzyloxycarbonyl-val-ala-asp (OMe) fluoromethylketone (z-VAD-FMK; abbreviated throughout this document as ZVAD) (170). ZVAD is a trimer peptide inhibitor (Val-Ala-Asp) that acts as a pseudosubstrate for caspases. Upon binding, an irreversible inhibition occurs through binding of the caspase activate site cysteine to FMK to form a thiomethyl ketone. Though these molecules are quite specific and widely used, there is noted cross-reactivity with similar other cysteine proteases such as cathepsins B and H (172).

As mentioned above, the RIP1 kinase inhibitor Necrostatin-1 is a highly specific inhibitor of RIP1 kinase activity (173, 174) and an important tool for the study of necroptosis. It was identified in a screen for compounds that inhibit cell death caused by TNF with ZVAD a human monocytic cell line U937 (145) and was shown to target RIP1 by the capacity to inhibit RIP1 auto-phosphorylation (146). While the atomic structures of RIP1 and RIP3 are not yet characterized, the kinase domain of RIP1 contains an N-lobe and a C-lobe with the activation loop located between the two (175). Nec-1 acts as a noncompetitive allosteric inhibitor through binding between the N- and C- lobes, compromising the activation loop by locking RIP1 into an inactive conformation. Inhibition of RIP1 does not occur through interaction with the ATP binding pocket and no nucleotide is found in this pocket when Nec-1 is present. A recent report documented that the structure of Nec-1 is identical to methyl-thiohydantoin-tryptophan (MTH-Trp), an inhibitor of indoleamine 2,3-dioxygenase (IDO), the rate-limiting enzyme in tryptophan catabolism (176). IDO has noted roles in antibacterial defense, immunomodulation, and neuroprotection, making necessary the confirmation of any

studies performed with the original Nec-1. Fortunately, a more potent and more bioavailable variant of Nec-1 (Nec-1s or 7-CL-O-Nec-1) does not target IDO (145, 176).

Control of embryonic development by RIP1, RIP3, and Caspase-8

In addition to functioning in death receptor and pattern recognition receptor signaling in response to inflammation and pathogen encounter in adult tissues, RIP1, RIP3, and the capsase-8/FADD/FLIP complex are in active interplay during mouse embryonic development. Mice deficient in caspase-8 (*Casp8*), *Fadd*, or FLIP (*Cflar*) do not survive beyond embryonic day 11.5 (E11.5, however this number has been reported between 10.5-12.5 by various groups) (177–180). These embryos display abnormal yolk sac vascularization, cardiac developmental impairment, and hyperemia in the abdominal region of the embryo. Using tissue-specific *Casp8*$^{-/-}$ mice, a *Tie1*-Cre-driven *Casp8* deletion closely resembled the phenotype in global *Casp8*-knockout mice, identifying the endothelium as the most critical tissue for this phenotype (181). Notably, excessive apoptosis was not apparent in these embryos (180). In contrast, *Ripk1*-null mice on a mixed C57BL/6-129S1 background develop normally and are born at Mendelian frequencies, however, these mice develop substantial apoptosis in lymphoid and adipose tissues and experience failure to thrive by postnatal day 1-3 (P1-3) (182). Additionally, *Ripk1*$^{-/-}$ mice backcrossed onto a C57BL/6 background show spontaneous inflammation beginning *in utero* and death follows minutes after birth caused by respiratory failure (183). Generalized edema, cyanosis, necrotic liver and thymus, massive apoptosis in the lung, liver, and intestine, and epidermal hyperplasia suggestive of massive necrosis in the skin comprised the broad pathological findings. Crossing *Ripk1*$^{-/-}$ with *Myd88*$^{-/-}$, *Ripk3*$^{-/-}$,

or *Mlkl*$^{-/-}$ suppresses inflammation in these mice, suggesting a mechanism involving necroptosis-mediated DAMP release (IL-1α and IL-33 in this case) to drive MyD88-dependent signaling to generate the substantial inflammatory response. Even when the spontaneous inflammation is reduced, Caspase-8-dependent intestinal apoptosis and failure to thrive develops at P4. Whereas *Ripk1*$^{-/-}$ on either genetic background demonstrate perinatal lethality, mice with genetic deletion of other necroptosis-associated proteins, RIP3 or MLKL, develop normally into adulthood (163, 184, 185).

Mechanisms underlying embryonic lethality in *Casp8*, *Fadd,* and *Cflar* deficient mice were recently revealed using knockout crossings. In contrast to *Casp8*$^{-/-}$ or *Fadd*$^{-/-}$ mice, *Ripk3*$^{-/-}$*Casp8*$^{-/-}$ and *Ripk3*$^{-/-}$*Fadd*$^{-/-}$ double-knockout mice are born at normal Mendelian ratios and survive into adulthood (144, 157, 186). While hematopoietic development in young mice is normal, double-knockout mice develop B220^{+}CD3^{+} double-negative T lymphocyte accumulation in secondary lymphoid organs similar to autoimmune lymphoproliferative syndrome in *lpr/lpr* or *gld/gld* mice (187). Thus, embryonic lethality mediated by the absence of *Casp8* or *Fadd* is executed through RIP3-mediated necrosis (144, 186), which is triggered through TNF-R1 (188). Additionally, *Ripk1*$^{-/-}$ rescues the *in utero* lethality caused by *Casp8*- or *Fadd*-deficiency, though these double-knockout mice only survive until P1-4, revealing that RIP1 also contributes to embryonic death but that neither Caspase-8 or FADD deficiency is sufficient to protect from *Ripk1*$^{-/-}$ perinatal lethality (188, 189). Interestingly, *Cflar*$^{-/-}$ mice are only rescued from embryonic lethality when crossed with *Ripk3*$^{-/-}$ and *Fadd*$^{-/-}$ double knockout animals (157). Because FLIP negatively regulates apoptosis and necroptosis, the triple-knockout

is necessary to prevent activation of both of these cell death pathways and allow normal development.

Efforts to use knockout crossing to rescue *Ripk1*$^{-/-}$ perinatal lethality have identified that in addition to its role in driving necroptosis activated by TNF-R1, RIP1 acts as a critical negative regulator of both apoptosis and necroptosis (183, 188, 190). While *Ripk1*$^{-/-}$*Ripk3*$^{-/-}$ and *Ripk1*$^{-/-}$*Casp8*$^{-/-}$ die in the perinatal period from TNF-R1-driven apoptosis or TRIF- or IFNAR-driven necroptosis, respectively, *Ripk1*$^{-/-}$*Ripk3*$^{-/-}$*Casp8*$^{-/-}$ triple-knockout mice survive into adulthood, albeit with an ALPS-like lymphoid compartment, suggesting that RIP1 acts as a "gatekeeper" from aberrant apoptosis and necroptosis. Interestingly, two different kinase-dead knock-in mice, *Ripk1*^{D45A} and *Ripk1*^{D138N} are fully viable, revealing that expression of RIP1 even without kinase activity curtails apoptosis and necroptosis that cause perinatal death (151, 190). Furthermore, *Ripk1*^{D45A} fibroblasts are no longer hyper-sensitive to TNF-R1-mediated cell death, which supports a role for RIP1 scaffold activity in preventing hyper-sensitivity to cell death (190). Together these knockout intercross studies utilize regulated events during embryogenesis and perinatal life to illuminate the complex network of regulation that exists within the necrosome.

RIP1 kinase activity in cytokine transcription and inflammasome activation

Although the kinase activity of RIP1 does not affect on gene transcription or cytokine production *in vitro* when caspases are active (124), its role in these processes *in vivo* and in conditions in which caspases are inhibited are just beginning to be explored. In cell lines, ZVAD treatment induces low levels of RIP1 kinase dependent TNF

transcription (191, 192). These studies do not comment on whether this transcription is dependent on RIP3 or MLKL. However, cIAP1 inhibits RIP1 kinase dependent TNF production while the scaffold EDD, JNK, and Akt1/2 may be involved in promoting it. In a more physiological setting for pro-inflammatory cytokine production, cIAP depletion with Smac-mimetics or cIAP1/2 gene deletion induces TNF production in BMDM that is dependent on RIP1 kinase activity and RIP3 but not MLKL (193). Recent studies using the aforementioned RIP1 kinase-dead knock-in mice reinforce the findings that *in vitro* stimulation with TNF does not require RIP1 kinase activity for normal activation of NF-κB, MAPK, and cytokine expression (151, 194). When stimulated with TNF and ZVAD, $RIP1^{K45A}$ expressing macrophages showed a considerable decrease in CXCL1 mRNA and protein expression, suggesting that when caspases are inhibited RIP1 kinase activity contributes to gene activation (194).

Whether RIP1 kinase activity contributes to cytokine production *in vivo* is not yet clear. While $RIP1^{K138N}$ and $RIP1^{K45A}$ are resistant to TNF-induced death (151, 194), there was no impact on cytokine production in $RIP1^{K138N}$ (151), and the effect of $RIP1^{K45A}$ on cytokine production has not yet been published. However, $RIP1^{K45A}$ are protected from *cpdm* inflammatory dermatitis caused by *Sharpin* deficiency, though it is likely this phenotype is driven by excessive cell death rather than elevated cytokine transcription. These studies also do not rule out a role for RIP1 kinase activity through receptors other than TNF-R1. *Ripk1*$^{-/-}$*Ripk3*$^{-/-}$*Casp8*$^{-/-}$ triple knockout mice produce lower amounts of IL-6, CXCL1, and RANTES in response to LPS injection when compared to wild-type, *Ripk3*$^{-/-}$, or *Ripk3*$^{-/-}$*Casp8*$^{-/-}$ mice (188). This study does not distinguish between the

adapter function or kinase activity of RIP1 but leaves open the possibility that RIP1 kinase activity in drives cytokine production in response to LPS.

The release of IL-1β is regulated by proteolytic cleavage by caspase-1 following activation of inflammasomes in addition to transcriptional up-regulation (195). Inflammasome activation in most cell types requires two signals: a priming signal and an inflammasome activation signal. In *Casp8*$^{-/-}$ dendritic cells, LPS stimulation alone is sufficient to produce cleaved IL-1β through the NLRP3 inflammasome in a RIP1 kinase-, RIP3-, and MLKL-dependent fashion (196). An independent study identified that LPS stimulation with cIAP inhibition is sufficient to produce cleaved IL-1β in a RIP3- and MLKL-dependent manner (197). IL-1β cleavage occurs via caspase-1 in the NLRP3 inflammasome and caspase-8 in a non-canonical inflammasome. Finally, a recent report demonstrated that IL-1β release in response to *Yersinia pestis* infection was abrogated by RIP1 kinase inhibition using a novel inhibitor GSK'963 (198). While these studies demonstrate a role for RIP kinases in the regulation of inflammasome activation, the physiological context in which this type of RIP1 activation occurs is still under active investigation.

Necroptosis – Pathophysiology

Initial reports of necroptosis focused extensive on molecular characterization of this cell death process in widely used transformed cell lines, usually downstream of TNF-R1 signaling (116). As the components of this cell death process come into focus, research is shifting to understand how necroptosis contributes to physiology and the pathophysiology of various diseases (199). This list of pathological conditions has

expanded substantially in recent years due to the development of *Ripk3*$^{-/-}$ and *Mlkl*$^{-/-}$ mouse models, which develop normally but are deficient in necroptosis. RIP3 dependent necroptosis is implicated in a wide range of pathologies including viral and bacterial infections, systemic inflammation, atherosclerosis, traumatic brain injury, drug-induced liver injury, necrotizing pancreatitis, inflammatory bowel disease, and ischemia-reperfusion injury.

Viral infection – the evolutionary reason for necroptosis?

The spread of viruses relies on the fate of infected cells. Efficient viral clearance by the host immune system prevents cell-cell and host transmission. Thus, viruses have evolved mechanisms to evade host cell death and permit their own spread (200). Accordingly, host systems co-evolved new clearance mechanisms (201). This scenario has played out in host cell death pathways and virus encoded proteins to block them. Interestingly, this interplay is largely a characteristic of DNA viruses (202). Intrinsic apoptosis is the most ancient cell death pathway. Supposedly to prevent activation of this pathway, herpesviruses, poxviruses, and adenoviruses each evolved Bcl2 family member-like proteins. The extrinsic apoptosis pathway involving caspase-8 may have evolved to activate apoptosis in the presence of virus-encoded Bcl2 mimics. Subsequently, viruses evolved caspase-8 inhibitors and viral FLIPs to block caspase activation (200). These include baculovirus, adenovirus, poxviruses (cowpox and vaccinia), gamma-herpesviruses, and cytomegalovirus. Vaccinia virus blocks caspase activation by synthesizing the serpin B13R (148). Innate defenses against vaccinia require signaling

through TNF-R1. Interestingly, RIP3-deficient mice are susceptible to VV infection, implying that necroptosis is required for host defense to certain viruses.

Finally, RIP3-dependent necrosis in the host may have evolved as a final backup mechanism to combat viral infection. Viral FLIPs in molluscum contagiosum, Kaposi's sarcoma-associated herpesvirus, and equine herpesvirus have the capacity to bock apoptosis and necroptosis. Interestingly, cytomegaloviruses evolved novel viral inhibitors of RIP activation (vIRA) to prevent necroptosis and allow productive infection (203). Mouse cytomegalovirus (MCMV) synthesizes M45, which contains a RHIM domain. Expression of this protein is necessary and sufficient to suppress MCMV-induced RIP3-dependent, RIP1-independent necroptosis. Because RIP1 is not required for necrosis induced by MCMV, search for the trigger of this cell death revealed that the RHIM-containing cytosolic DNA sensor DAI activates RIP3 (204). Interestingly, human CMV also blocks necroptosis but through a different mechanism (202).

Though it is not formally proven that necroptosis evolved specifically to prevent virus-driven pathology, multiple groups propose that this form of cell death occurs as a last resort during infection (205, 206). The host accepts the damage that will be induced by the release of cell death associated molecules such as IL-33 and HMGB1 and triggers necroptosis (6, 205). While there still is no evidence for a role of necroptosis in normal physiology, a number of pathogenic processes require necroptosis – RIP1 kinase activity, RIP3, and/or MLKL activation.

Bacterial infection

Recent reports identify necroptosis as a cell death mechanism that can promote or restrict certain bacterial infections. *Salmonella* Typhimurium infection induces type I interferon response that is detrimental to host defense (207). IFNAR is activated and induces cell death through a RIP1 kinase and RIP3 dependent mechanism, killing macrophages that are important for *Salmonella* control (207, 208). As mentioned above, *Yersinia pestis* also employs necroptosis for host defense (198). RIP1 kinase activity, RIP3, and caspase-8 contribute to inflammasome-mediated caspase-1 activation required for host defense. Interestingly, other bacteria activate necroptosis that damages the host. *Clostridium perfringens* infection causes hemorrhagic enteritis through its β-toxin (209). Infection of cells with this bacterium leads to cell death with a necrotic morphology that was inhibited by Necrostatin-1. Finally, infection with *Mycobacterium tuberculosis* in a zebrafish macrophage model has revealed a role for RIP1 and RIP3 mediated necroptosis in the release of live bacteria into the permissive growth environment of the extracellular medium, promoting infection spread (210).

TNF injection and cecal ligation and puncture – mouse models of septic shock

TNF injection and cecal ligation and puncture are widely used methods for inducing conditions that attempt to model human septic shock (211, 212). In the TNF injection model, removal of necroptosis-associated proteins is protective. Mice deficient in RIP3 (213, 214) and RIP1 kinase-dead knock-in mice (D161N and K45A) (151, 194) do not succumb to TNF-induced shock. Necrostatin-1 injection has produced conflicting results, however (213, 214). A proposed, though unconfirmed, model posits that early

activation of cytokines by TNF signaling then activate necroptosis to release DAMPs cause pathology in this disease model (213). Investigation of necroptosis in the cecal ligation and puncture polymicrobial sepsis model has revealed conflicting results. While one group demonstrated that RIP3-deficient mice demonstrate improved pathology scores than wild-type mice (213), another group in RIP3 could not repeat this result in *Ripk3*$^{-/-}$ mice and also saw no effect in *Mlkl*$^{-/-}$ (185). These differences may be explained by the extent of cecal ligation accomplished by different groups, which is user-dependent and known to be variable (211).

Necroptosis in tissues

It is not clear whether necrotic morphology is genetically regulated in some or all circumstances. Additionally, the specific molecular pathway driving genetically regulated necrosis cannot be identified without empiric testing (205). Pathologically, tissue necrosis is classified as coagulative, colliquative (or liquefactive), fibrinoid, or caseating. Examples of RIP1 kinase dependent and/or RIP3 dependent necroptosis exist within each pathological category except for caseating necrosis, and whether the signaling machinery that drives this necroptosis can be pharmacologically manipulated to prevent tissue damage is under active investigation.

Coagulative necrosis is exemplified by ischemic solid organs such as the spleen, kidney, and heart (205). Ischemia-reperfusion injury (IRI) is the best-characterized disease process for investigation of necroptotic contributions to this type of necrosis. IRI develops following hypoxic tissue damage when blood reperfusion occurs, exposing the tissue to oxidative stress and a pro-inflammatory cytokine milieu (215). Cerebral, renal,

myocardial, and retinal tissues are predisposed to IRI due to the anatomy of their blood supply, and IRI also occurs during procedures such as organ transplantation and cardiothoracic surgery (216). Cellular damage during IRI is predominantly necrosis (217) accompanied by the release of cell death associated proteins such as HMGB1 and IL-33 causing activation of the innate immune system (6, 215). Necrostatin-1 treatment prior to reperfusion is profoundly beneficial in cerebral, myocardial, and renal IRI models (145, 218, 219). Interestingly, necrotic damage in renal IRI is not activated by TNF-R1 or TNF-R2, suggesting that a full understanding of other means to activate necroptosis (TLRs, other death receptors, and intracellular receptors) is imperative (199, 219). Further investigation in renal allograft transplant, a clinically important scenario for IRI, revealed that RIP3-deficient donor kidneys demonstrated less necrotic damage than their wild-type counterparts (199, 220).

Colliquative (liquefactive) necrosis occurs in fatty tissues such as the brain and pancreas. Acute necrotizing pancreatitis presents a difficult clinical scenario due to the lack of specific therapies (205). Mouse models using ceruletide-driven acute pancreatitis demonstrated that RIP3 (149, 150) and MLKL (185) are required for tissue damage, suggesting an underlying genetic mechanism for this preclinical model that could be applied to at least a subset of patients if properly targeted (199).

Fibrinoid necrosis is characterized by collagen deposition, as found in atherosclerotic plaques. Notably, atherosclerosis development in LDLR- or APOE-deficient mice was reduced by the loss of RIP3 and was conferred by the bone marrow compartment (221).

Spontaneous intestinal inflammation

In addition to the in utero lethality discussed above, tissue specific deletion of caspase-8 or FADD causes spontaneous inflammation (222–225). When caspase-8 or FADD is specifically deleted in intestinal epithelial cells, a phenotype that resembles human inflammatory bowel disease arises. Crossing these mice to *Ripk3*$^{-/-}$ or a catalytically inactive CYLD transgenic mouse protected mice from spontaneous colitis, implicating necroptosis as the underlying trigger or the means to amplify this response (223). Results from these studies were extended to clinical specimens to draw a connection between these molecular studies of necroptosis and human pathology. In inflamed tissue from Crohn's disease and ulcerative colitis patients, RIP3 and MLKL protein levels were increased while caspase-8 levels were diminished (222, 226). While these studies do not establish causality, they support the current models in which necroptosis may be a therapeutic target for inflammatory bowel disease.

Therapeutic perspectives

While the evolution of necroptosis may have been driven by the host response to viral infection, broad study of disease processes involving necrotic tissue reveals that RIP1 kinase activity, RIP3, and MLKL contribute to disease and damage that may be treatable. Currently, RIP1 kinase inhibitors are more thoroughly studied small molecule inhibitors in preclinical disease models (174, 194) but specific inhibitors of RIP3 and MLKL have also been identified (137, 159). RIP1 may be a suboptimal therapeutic target because of the functions of its kinase activity outside of necroptosis (227). However, RIP1 kinase-dead knock-in mice are viable and develop normally, similar to RIP3- and

MLKL-deficient mice and both RIP3 and MLKL may also be involved in non-necroptotic responses as investigation into their functions continues.

Experimental approach: Forward genetic analysis in wild-derived mice

The forward genetic approach

Though separated by substantial evolutionary distance, the mouse has proven to be an essential model of human physiology and disease processes. Mice and humans display 99% homology between genes and over 75% of genes are orthologous, meaning they have shared ancestry, are intact, and non-duplicated (228). Additionally, 90% of the human/mouse genomes are syntenic. Inbred mouse models are essential tools for biological research because of the capability to reproduce experiments on an identical genetic background. The process of inbreeding currently used mouse lines began over 100 years ago in work by Clarence Little that generated the widely used DBA, C57BL/6, C3H, and BALB/c strains from 'fancy mice' (229).

The study of genes in inbred mice is performed by reverse or forward genetic approaches (228). Reverse genetics involves using a hypothesis-driven approach to interrogate the function of a known gene through altering its the sequence or expression, often through generation of knockout mice. Alternatively, forward genetics approaches a biological question from the perspective of an observed phenotype rather than a hypothesis (230). The molecular explanation of phenotype is then pursued by positional cloning (230, 231). Two main approaches are used in forward genetic analysis, ENU mutagenesis and QTL mapping. ENU (N-ethyl-N-nitrosourea) is an alkylating agent applied to spermatogonia prior to breeding that induces point mutations at an

approximate frequency of one mutation per 1-2 Mb of genomic DNA. Most often, ENU mutagenesis causes A to T or A to G mutations and most phenotypes are conferred as monogenic traits (232). Interestingly, the documented ENU mutations are more often structural changes in the coding sequence of genes rather than *cis*-acting mutations that affect gene expression (228). One of the major advantages of ENU mutagenesis is the high rate of monogenic traits induced by this trait. However, with the benefit comes the caveat of the large numbers of mice required for positional cloning. However, next generation sequencing may reduce the time and number of mice required for successful mapping using ENU mutagenesis. The second approach to forward genetic analysis, QTL (quantitative trait locus) analysis, relies on genetic differences that cause a measurable change in phenotype, often between two strains of mice (232). Unlike ENU mutagenesis, the degree of nucleotide polymorphisms between mouse strains lends itself to the study of complex, polygenic traits rather than monogenic ones. Also unlike ENU mutagenesis, the genetic lesion underlying many QTLs is a SNP outside of a coding region, causing changes in gene expression levels (228, 232, 233). The QTL approach is useful to identify gene interactions underlying complex traits. However, because of the complexity of most traits studied using QTL, identification of a single causative gene can be a challenge.

The design of a QTL-based forward genetic approach involves appropriate breeding, phenotyping, genotyping, and statistical analysis (234). First, two appropriate inbred strains are selected for breeding. Because a substantial degree of identify exists in classical inbred strains due to their derivation from a common ancestor, the great genetic diversity of evolutionary distinct inbred mouse strains is now being exploited for

exploration of QTLs (discussed below). Next, F1 hybrids of the two parental mouse strains are bred based on the devised breeding strategy to generate meioses: either a cross to one parental strain to generate an N2 backcross or to another F1 mouse to generate an F2 intercross. These mice are then tested for a given phenotype and genotyped across the genome. Genotyping can be accomplished using SNP genotyping, restriction fragment length polymorphism, or microsatellite markers. Often map units or 'centimorgans' are used to define distances in forward genetic analysis. A centimorgan (cM) is defined as the distance between which there is a one percent chance of recombination a chromosomal crossover event in one generation. This unit of measurement, along with more standard base pair measurements, is used when defining linked intervals. Finally, marker regression analysis is performed to determine the correlation between genotype at phenotype at a given locus. 'Linkage' between genotype and phenotype is presented as a logarithm of odds (LOD) score, which represents the log base 10 likelihood ratio that genotype and phenotype are correlated (232, 234). LOD scores greater than three are highly suggestive of linkage and greater than four represent near certainty of linkage of a phenotype to a given locus. A region of interest is defined by a marker with higher linkage proximal to one marker and distal to another, separated by recombination events. The identification of the molecular basis of a QTL involves narrowing the linked area with additional recombination events and potentially generating congenic mice to isolate the QTL from potential interacting genes within the parental genome. Although not always possible, replacement of one allele with another is the most stringent test to demonstrate the causality of a QTL (231).

Wild-derived mice

One approach to QTL analysis involved the use of natural genetic polymorphism to generate novel and interesting testable phenotypes. Because commonly used classical inbred strains contain a substantial degree of identity, the so-called 'wild-derived' inbred mice, which contain natural genetic polymorphism created by differences in subspecific and geographical origins, offer a useful model for forward genetic analysis (229, 235). The ancestry of classical inbred strains is comprised of four *Mus musculus* subspecies from diverse geographical origins: *M.m. domesticus* (Western Europe, North Africa), *M.m. musculus* (spanning North Asia), *M.m. castaneus* (Southeast Asia), and *M.m. molossinus* (Japan), a hybrid between *musculus* and *castaneus* (236–238). Two approaches of subspecific contribution analysis identify that a majority of the genome of classical inbred strains such as C57BL/6 is derived from the *M. m. domesticus* subspecies, calculated at 68% in one study and 94% in the second while *M. m. castaneus* and *musculus* contribute less than 10% (236, 237). Although interspecific recombination also exists in wild-derived mice (such as MOLF/Ei), the contribution of *M. m. domesticus* is significantly lower, calculated at 11% of the genome (239). In MOLF/Ei mice, *M. m. castaneus* comprises 15% of the genome and *M. m. musculus* makes up 74%. This comparison clearly demonstrates the evolutionary divergence that wild-derived mice contain relative to classical inbred strains.

In general, wild-derived mice are more resistant to infectious agents than classical inbred strains (235). Though not firmly supported by experimental evidence, this claim hypothesizes than critical alleles for host defense have been lost or replaced with hypomorphic versions in laboratory mice due to a lack of selective pressure. Multiple

groups use the *M. m. molossinus* representative MOLF/Ei (MOLF) strain of wild-derived inbred mice as a model to investigate host defense, including the Malo laboratory studies of *Salmonella enterica* Typhimurium and the Poltorak laboratory examination of innate immune responses. Contrary to the previously stated hypothesis, MOLF are highly susceptible to *Salmonella* Typhimurium infection *in vivo*. This trait has been mapped to three QTL, two in which the MOLF allele is protective and one where it promotes susceptibility (240, 241).

In the Poltorak laboratory, forward genetic analysis of macrophages elicited from MOLF mice have revealed novel pathways in TLR signaling, some of which more closely resemble human signaling than classical inbred mouse models. The study of a high IL-6 response to the TLR2 agonist LTA identified a gene-gene interaction regulating cytokine production in MOLF macrophages (43, 242). *Irak1bp1* is expressed in MOLF macrophages and human PBMC but not in B6 macrophages. This protein acts as a negative regulator of IL-6 production through promoting the formation of p50/p50 homodimers during TLR2 signaling (243). The second gene, *Irak2*, conferred the high production of IL-6 observed in parental strains. Mouse *Irak2* transcribes four isoforms, including an inhibitory isoform IRAK2c while humans express only a single pro-inflammatory isoform (244). The expression of this inhibitory isoform has created a signaling network in B6 where IRAK2 contributes only to late signaling events downstream of TLRs (42). In MOLF macrophages, the IRAK2c promoter is mutated, reducing its expression, and permitting IRAK2 to contribute to early activation of p38 and NF-κB (43). Notably, study of IRAK2 in human PBMC reveals that human IRAK2

also impacts early signaling events (44), demonstrating that the MOLF model may be a more accurate approximation of the human signaling network.

Summary and thesis goals

Activation of Toll-like receptors on macrophages contributes to the sterile and antimicrobial inflammatory response and the activation of adaptive immunity. Though many essential elements of the TLR signaling cascade to activate pro-inflammatory gene expression are well characterized, their roles to activate other cellular outcomes, including caspase independent necroptotic cell death are just now coming to light. The work described in this thesis begins to address some open questions related to mechanisms of TLR-induced necroptosis and the role of RIP1 kinase activity in TLR-driven cytokine production. Despite the molecular mechanisms underlying TNF-R1-mediated necroptosis are well described, the components and regulators this signaling pathway downstream of diverse receptors, including TLRs, may differ. Furthermore, although it is well established that RIP1 kinase activity does not affect cytokine production *in vitro* under standard experimental conditions, *in vivo* models suggest that in addition to its role in necroptosis, RIP1 kinase activity positively contributes to pro-inflammatory cytokine production. Work with collaborators has shown that cytokine production driven by low doses of LPS is significantly reduced by Nec-1.

In its essence, this work aims to use the genetic diversity of wild-derived strains to identify novel regulators of TLR signaling, specifically related to RIP1 kinase activity in promoting cell death and pro-inflammatory cytokine production. The central hypothesis is that the differences in pro-inflammatory cytokine release and susceptibility

to cell death between wild-derived mice and the classical inbred strain C57BL/6J has a genetic basis, and that forward genetic analysis will reveal novel mechanisms of TLR signaling regulation. After identifying MOLF peritoneal macrophages as resistant to TLR-induced necroptosis, an unbiased forward genetic approach was used to uncover genes that confer this resistance. Because RIP1-mediated signaling toward cell death different between wild-derived and classical inbred strains, this signaling pathway was assessed with regard to additional outputs, such as pro-inflammatory cytokine production. An *in vitro* system for the study of RIP1 kinase-dependent cytokine production was developed and the importance of known aspects of TLR signaling were assessed followed by an unbiased mapping approach to identify any novel mediators in this pathway. Finally, genetic analysis revealed multiple QTLs for cytokine production downstream of MyD88-dependent TLRs in MOLF macrophages. Low CXCL1 was documented and mapped to a single QTL and high IL-6 production was revisited in an alternative cell type to identify linkage to additional TLR signaling regulators.

CHAPTER 2: MATERIALS AND METHODS

Mice and isolation of primary cells

C57BL/6, MOLF/ Ei, SPRET/Ei, CZECHII, PWD, PWK, CAST, CASA, MSM, WSB, PERA, SJL, BALB/c, LP, KK, SEA, SWR, CBA, C3H/HeJ, TNFR1$^{-/-}$ (C57BL/6-Tnfrsf1a^{tm1Imx}), IL1R1$^{-/-}$ (B6.129S7- Il1r1^{tm1Imx}), and NOD2$^{-/-}$ (B6.129S1-Nod2^{tm1Flv}) mouse strains were obtained from The Jackson Laboratory. Mice were housed in a pathogen-free facility at Tufts University School of Medicine. All experiments with mice were performed in accordance within regulations and with the approval of the Tufts University Institutional Animal Care and Use Committee. Peritoneal macrophages were isolated from 6- to 12-week-old mice. Mice were injected with 1 ml of 3% thioglycollate, and cells were collected by peritoneal lavage with cold PBS. Cells were resuspended, plated, and stimulated 4 h after plating in DMEM supplemented with 10% FBS (Atlas Biologicals or Atlanta Biologicals), 1% Pen- Strep (Invitrogen) at 37 °C in 5% CO_2 . Bone marrow cells were isolated by washing femurs with cold RPMI medium. Cells were centrifuged for 10 min at 1000 rpm. Cell pellets were resuspended in BMDM differentiating medium (RPMI medium with L-glutamine, 20% FBS, 28% L-cell conditioned medium, and 1% Pen-Strep) and cultured for 7–8 days at 37 °C in 5% CO_2 to mature to macrophages (245).

Cell lines

HEK293 and L929 cells were obtained from Dr. R. Isberg (Tufts University) and grown in DMEM, supplemented with 10%FBS and 1% Pen-Strep or RPMI medium with 10% FBS and 1% Pen-Strep, respectively. Immortalized *Ripk1*$^{-/-}$ fetal liver-derived macrophages, immortalized *Ripk3*$^{-/-}$ *and Casp8*$^{-/-}$*Ripk3*$^{-/-}$ BMDM were obtained from Dr.

K. Fitzgerald (University of Massachusetts) and grown in DMEM, 10% FBS, and 1% Pen-Strep. RAW264.7 macrophages were obtained from the ATCC and cultured in DMEM, 10% FBS, and 1% Pen-Strep.

Reagents

Salmonella minnesota Re595 and R5 LPS was purchased from Enzo Biochem Inc. Poly I:C-LMW, Imiquimod (R837), CL-097, and lipoteichoic acid (purified from *Staphylococcus aureus*) were purchased from Invivogen. CpG oligodeoxynucleotides were synthesized by Integrated DNA Technologies. Z-VAD(OMe)-FMK was purchased from Bachem (catalog no. N-1560) for cell death assays or APExBio (catalog no. A1902) for cytokine assays. Necrostatin-1 was purchased from Sigma. SM164 was obtained from Dr. A. Degterev (Tufts University). GAPDH, phopsho-p38, phospho-ERK, phospho-JNK, phospho-TBK1, total ERK antibodies purchased from Cell Signaling Technology. CYLD antibody (clone E10) was purchased from Santa Cruz Biotechnology.

Genetic mapping and analysis

Peritoneal macrophages were elicited as described above from N2 or F2 mice. Genomic DNA was isolated from all mouse tails using a DirectPCR (Viagen) or DNeasy blood and tissue kit (Qiagen). Genome-wide genotyping was performed by PCR of known microsatellite markers per chromosome using primers obtained from Jackson Laboratories Mouse Genome Informatics. Genotyping PCR reactions were performed using JumpStart Red Taq (Sigma), and PCR products were electrophoresed on 3.5% agarose gels. Quantitative trait locus analysis was performed using QTXb or j/QTL software.

DNA sequencing

Genomic DNA or cDNA was amplified using Phusion high-fidelity DNA polymerase (New England BioLabs). PCR products were electrophoresed on a 1.2% agarose gel and extracted using a QIAquick gel extraction kit (Qiagen). DNA was sequenced from gene-specific primers using an ABI 3130XL DNA sequencer at the Tufts University Core Facility.

Luciferase assay

CYLD promoter was cloned into PGL4.76 luciferase vector and stably transfected into RAW 264.7 cells followed by hygromycin selection. After stimulation, renilla luciferase was read with a luciferase reporter system (Promega).

ELISA

Peritoneal macrophages or BMDM were plated in 96-well plates at a density of $1x10^5$ cells/well. After stimulation, protein concentrations measured from cell-free supernatants using ELISA kits purchased from R&D Systems (catalog nos. DY410, TNF; DY406, IL-6,). IFNβ measured using a protocol obtained from S. Vogel, using mouse IFN-B Santa Cruz sc-57201 as capture antibody, Polyclonal rabbit anti-mouse IFN-B 32400-1 RnD Systems as detection antibody, and Goat anti-rabbit-HRP #7074, Cell Signaling Technology as secondary antibody.

Cell viability assay

Peritoneal macrophages were plated in 96-well plates at a density of $5x10^4$ cells/well. Cell viability was measured 18 hours post-stimulation using a CellTiter-Glo luminescence ATP viability assay (Promega), and data were presented as a percentage of the signal from treated cells to cells in medium with vehicle (DMSO).

RNA preparation and analysis

Cells were lysed with TRIzol (Invitrogen) or TriPure (Roche) isolation reagent, and RNA was extracted according to the instructions of the manufacturer. For 5' rapid amplification of cDNA ends, mRNA was extracted and amplified using the GeneRacer kit (Invitrogen) according to the protocol of the manufacturer. A gene-specific primer within CYLD was used for initial RNA priming (CACAGTGTCCAGGGCAGAACTAAAAGCA), GGCCCTGGATGCCTTTCTTCTTT CCA and TTAGGTGGAGTATTTTCTTCTACTAC primers were used to amplify CYLD mRNA species in combination with forward primers amplifying from the RNA oligo added by the GeneRacer kit. A ribonuclease protection assay was performed using the RPAII ribonuclease protection assay kit (Ambion) according to the protocol of the manufacturer. Primers used to generate the probe for RPA were as follows: CYLD, GTCTAGCGAGAACAGATTCCAC (forward) and ATCTCTAAACCTTCCTTTTCCA (reverse). For Northern blot hybridization, total RNA was electrophoresed on a 1.2% agarose gel, transferred to a Hybond-N membrane (Amersham Biosciences-GE) by the capillary method. After prehybridization with QuikHyb (Stratagene), the membrane was hybridized with a Cyld-specific radioactive probe amplified using the primers GATTCCTTTTAGCAGAGCAG (forward) and AATTGTACTTTCAACACTTGC (reverse) and exposed to film overnight. To generate cDNA, reverse transcription was performed using M-MuLV reverse transcriptase, RNase inhibitor, random primers 9 (for qPCR) or oligo(dT) (for cloning), and dNTPs (New England BioLabs). cDNA was analyzed for mRNA expression levels using SYBR Green and TaqMan probe-based gene expression analysis with the following custom, full-length, specific CYLD primer/probe:

GCTCAGTGACGTGCTAGCT (forward) and GCGTGCCCCTGAAAGTTC (reverse), Probe (FAM)-CTGGAACTGGAAGATGAA (Applied Biosystems). IL6, TNF, IFNβ, IRAK2 probes obtained from Life Technologies. A Gapdh-specific TaqMan probe (catalog no. 4352339) was used to normalize mRNA expression.

Protein lysis and western blot analysis

To prepare whole- cell lysates, cells were lysed on ice with a cytoplasmic lysis buffer (50 mM Tris (pH 8), 150 mM NaCl, 2 mM EDTA, 1% Triton X-100, 1mM sodium vanadate, and 10mM NaF) supplemented with Halt protease inhibitor mixture (Thermo Fisher Scientific) for 10 min. Lysates were centrifuged for 10minat 13,000rpm at 4°C. Cleared lysates were mixed with Laemmli sample buffer and boiled for 10 min. Protein lysates were resolved on a 4–12% gradient Bis-Tris SDS gel (NuPAGE,Invitrogen) and transferred to a nitrocellulose membrane. After incubation with protein-specific antibodies, chemiluminescence was detected using ECL substrate (Thermo Fisher Scientific).

Lentiviral knockdown and overexpression

shRNA plasmids in the pLKO.1 vector were purchased from Open Biosystems (Thermo Scientific). A GFP-targeting shRNA hairpin was used as a control (Addgene, catalog no.12273). The Cyld-targeting shRNA vector was clone ID TRCN0000030991. The Irak2-targeted shRNA vector was clone ID TRCN0000022502. The CYLD overexpression construct was cloned from cDNA into a pLEX lentiviral expression vector. Lentiviral particles were generated by transfecting the shRNA expression construct (pLKO.1 construct) with the packaging constructs psPAX2 (lentivirus pack-aging) and pMD2.G (VSV G) into HEK293 cells using X-tremeGENE9 DNA

transfection reagent (Roche). Supernatants were collected 48 and 72 hours after transfection, pooled, and filtered using a 45 μm filter. BMDM and RAW264.7 cells were transduced by incubation with lentiviral supernatant for 24 h. Infected clones were selected by culturing with 3 μg/ml (BMDM) or 5 μg/ml (RAW) puromycin for 48–72 h.

siRNA transfection

Following peritoneal lavage, macrophages were plated and allowed to adhere for 4 hours prior to transfection. Peritoneal macrophages were transfected with 100 nM siRNA using the N-TER nanoparticle siRNA transfection system (Sigma). Cells were transfected for 24 hours before cell death assays were initiated. Gene-specific and control siRNA duplexes were obtained from Integrated DNA Technologies with the following sequences: siCYLD,GGUUUAGAGAUAAUGAUUGGAAAGA; negative control, CGUUAAUCGCGUAUAAUACGCGUAT.

Chromatin immunoprecipitation

To prepare chromatin, $1x10^7$ peritoneal macrophages from MOLF and B6 were stimulated with LPS for 2 hours. Cells were cross-linked with 1% formaldehyde for 10 min at room temperature. The reaction was stopped by adding glycine to a final concentration of 0.125 M and incubating for 5 min. After washing twice with cold PBS, cells were resuspended and centrifuged at 2000 rpm for 5 min at 4°C. Cells were rinsed once with 1 ml of PBS with protease inhibitors and then resuspended in cold lysis buffer (5 mM PIPES (pH 8), 85 mM KCl, and 0.5% Nonidet P-40) and incubated for 10 min on ice. After centrifugation at 5000 rpm for 5 min at 4°C to pellet the nuclei and discard the supernatant, the nuclei were resuspended in nucleus lysis buffer (50mM Tris-Cl (pH 8.1), 10 mM EDTA, and 1% SDS) with protease inhibitors and incubated on ice for 10 min.

Samples were then diluted with ChIP dilution buffer (1% Triton X-100, 2 mM EDTA, 150 mM NaCl, and 20 mM Tris-HCl (pH 8.1)) and protease inhibitors. Chromatin was sonicated with a Branson 350 sonifier. After sonication, samples were microfuged at 14,000 rpm for 10 min at 4°C, and supernatants were kept. Lysates were pre-cleared with agarose beads for 1–2 hours. After microfugation to remove agarose, a small fraction of supernatant was kept for input DNA control. Agarose-anti-RNA Pol II antibody N-20 (catalog no. sc-899X) complex was added to the sample, diluting the SDS to 0.1% using ChIP dilution buffer, and incubated overnight at 4°C. The following day, samples were washed for 30 min in wash buffer 1 (0.1% SDS, 1% Triton X-100, 2 mM EDTA, 20mM Tris-Cl (pH 8), and 150mM NaCl), for 30 min in wash buffer 2 (identical to wash buffer 1 but with 500 mM NaCl), and for 30 min in radioimmune precipitation assay buffer (50 mM HEPES (pH 7.6), 1mM EDTA, 0.7% sodium deoxycholate, 1% Nonidet P-40, and 0.5 M LiCl). The three wash steps were repeated. Samples were washed twice with 1 ml of cold Tris-EDTA (pH 7.6). Next, 100 µl of 1% SDS and 0.1 M $NaHCO_3$ were added to the ChIP sample and input control and incubated for 30 min at room temperature. Solutions were then incubated for 9hours at 65°C, purified with a QIAquick spin kit (Qiagen), treated with RNase mixture, and the DNA amounts in the input and immunoprecipitation were quantified using Nanodrop 2000 (Thermo Scientific). Quantitative PCR was performed using SYBR Green (as described above) using primers in the Cyld promoter with the following sequences: (-700): AGGTAGAGGGTGGAAAGC (forward) and CTCTTTCTGTCCTCAGATGG (reverse); (-300): CCCACCCTAGTTTTGACAGC (forward) and GCCAGTGTCATGTCACCATT (reverse); (TSS): CGGATCTCTGAATACGATTGG

(forward) and CAGCCGAACCTGCTACCTG (reverse); (+300): ACGAGCTTCTGACGTCAACC (forward) and CCCTGTGGTGCAGGAGTC (reverse); and (+700): TTATGGTCAGCCTTGGAGGA (forward) and GCAGCTGACCCAGATGAACT (reverse).

CHAPTER 3: TOLL-LIKE RECEPTORS ACTIVATE NECROPTOSIS IN C57BL/6 MACROPHAGES

A portion of this research was originally published in The Journal of Biological Chemistry. Stephen A. Schworer, Irina I. Smirnova, Irina Kurbatova, Uliana Bagina, Maria Churova, Trent Fowler, Ananda L. Roy, Alexei Degterev, and Alexander Poltorak. Toll-like receptor-mediated down-regulation of the deubiquitinase Cylindromatosis (CYLD) protects macrophages from necroptosis in wild-derived mice. The Journal of Biological Chemistry. 2014; 289:14422-14433. © The American Society for Biochemistry and Molecular Biology (246)**.**

Caspase inhibition leads to RIP1 kinase-dependent cell death in macrophages stimulated with TLR agonists

Macrophages are phagocytes that express numerous innate immune receptors to activate the immune response when a host is exposed to a pathogen (13). While the primary function of macrophages involves phagocytosis and the activation of gene expression programs to produce pro-inflammatory cytokines (247, 248), TLR stimulation can also induce programmed cell death in these cells (249). When NF-κB signaling is inhibited, LPS stimulation results in macrophages apoptosis, whereas when caspases are inhibited macrophages die with a necrotic phenotype characterized by a requirement for RIP1 and the loss of mitochondrial transmembrane potential (249). Necrotic cell death has also been observed in other cell types when caspases are inhibited (138), which is enhanced if death receptor agonists such as CD95L or TNF are present (116, 140).

With the goal of establishing conditions for a forward genetic screen to compare macrophages from classical inbred strains and wild-derived inbred strains, thioglycollate-elicited peritoneal macrophages from C57BL/6 were subjected to treatment with different doses the pan-caspase inhibitor ZVAD with and without stimulation with the death receptor agonist TNF. Stimulation with 50 μM and 25 μM ZVAD was sufficient to cause cell death in peritoneal macrophages (147) that was further induced by the addition of TNF (Figure 5A). Cell death did not occur when macrophages were exposed to a lower concentration of ZVAD (12.5 μM) without the addition of TNF, and while the addition of TNF increased cell death it did not reach the level of statistical significance.

Because caspase inhibition predisposes macrophages to cell death with necrotic characteristics (249), we hypothesized that these cells were dying by the RIP1 kinase-

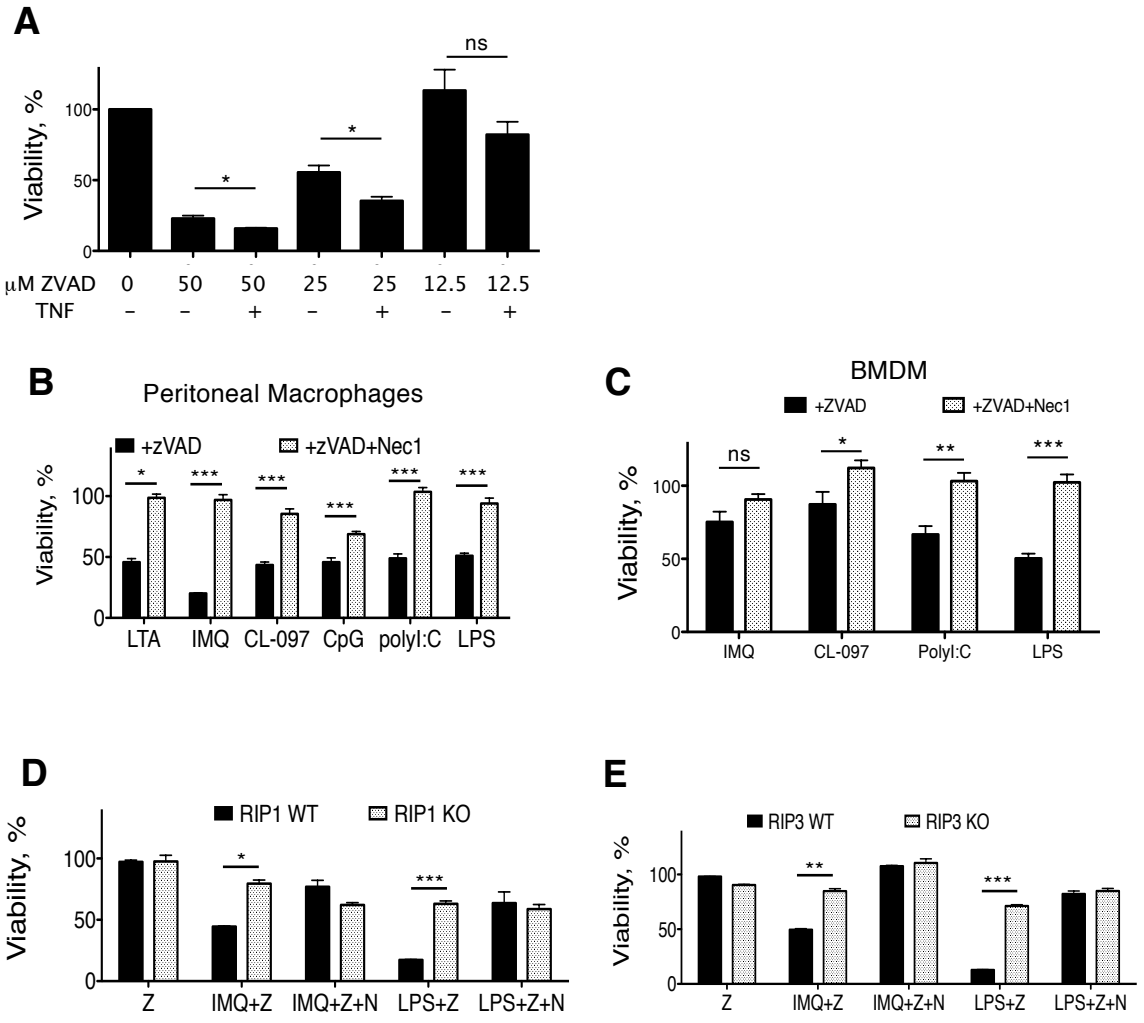

Figure 5. **Caspase inhibition results RIP1 kinase-dependent cell death in macrophages stimulated with TLR agonists.** (A) Peritoneal macrophages from C57BL/6 stimulated with ZVAD+/-50 ng/ml human TNF for 18 hr. (B) B6 peritoneal macrophages stimulated for 18 hours with lipoteichoic acid (LTA) (2 μg/ml), IMQ (5 μg/ml), CL-097 (1 μg/ml), CpG (200 nM), polyI:C (10 μg/ml), or LPS (100 ng/ml) in the presence of ZVAD (12.5 μM) with or without the RIP1 kinase inhibitor Nec-1 (30 μM). (C) B6 BMDM stimulated for 18 hours with IMQ (5 μg/ml), CL-097 (1 μg/ml), polyI:C (10 μg/ml), or LPS (100 ng/ml) in the presence of ZVAD (25 μM) with or without the RIP1 kinase inhibitor Nec-1 (30 μM). Immortalized macrophage cell lines lacking RIP1 (D) or RIP3 (E) were stimulated with TLR agonists in the presence of ZVAD (Z) (100 or 50 μM, respectively) with or without Nec-1 (N). Cell viability was measured by ATP level using the CellTiter-Glo assay (Promega). Values are a percentage of viable treated cells relative to cells in medium with vehicle (DMSO), shown as mean +/- S.E. Data presented from two (A,E) or three (C,D) pooled experiments or a representative of five independent experiments (B). Statistical significance was determined by two-tailed Student's *t* test. *, $p < 0.05$; **, $p < 0.001$; ***, $p < 0.0001$; *ns*, not significant.

dependent cell death mechanism known as necroptosis (or programmed necrosis) (116). To investigate whether TLR stimulation in the presence of ZVAD causes necroptosis (250), we stimulated peritoneal macrophages (Figure 5B) or bone marrow-derived macrophages (BMDM) (Figure 5C) with various TLR agonists and ZVAD at the dose that does not cause cell death on its own (12.5 μM) and attempted to inhibit cell death using the specific RIP1 kinase inhibitor Necrostatin-1 (Nec-1) (145, 146). Stimulation of TLR2 with *S. aureus* lipoteichoic acid (LTA), TLR7 with the imidazoquinoline compounds imiquimod and CL-097 (29), TLR9 with CpG oligodeoxynucleotides, TLR3 with polyinosinic:polycytidylic acid (poly I:C) (28), and TLR4 with lipopolysaccharide (LPS) in the presence of ZVAD resulted in cell death in peritoneal macrophages that was significantly inhibited by Nec-1 (Figure 5B). In BMDM with caspase inhibition, stimulation with TLR7 agonists induced necroptosis to a lesser extent than stimulation with poly I:C or LPS (Figure 5C). Stimulation with TLR agonists without ZVAD did not induce cell death. These data along with studies performed in other laboratories concurrently with our work demonstrate that TLR stimulation during caspase inhibition causes RIP1 kinase-mediated necroptosis (137, 251).

To more thoroughly establish that TLR-induced cell death is signaling through the RIP1/RIP3 axis, we used macrophage cell lines containing independent genetic deletion of each these molecules. Because *Ripk1*$^{-/-}$ mice are not viable due to failure to thrive shortly after birth (182), a fetal liver-derived macrophage cell line was used to assess whether genetic deletion of RIP1 prevents TLR-induced necroptosis. When compared with wild-type fetal liver-derived macrophages, RIP1 deficient cells were resistant to cell death induced by imiquimod or LPS (Figure 5D). RIP1 kinase activity executes

necroptosis through activation of RIP3 (148–150). Next, we demonstrated that cell death activated by imiquimod or LPS with caspase inhibition is prevented in RIP3-deficient immortalized BMDMs (Figure 5E). Together, these data establish that TLR stimulation of macrophages in the presence of caspase inhibition with ZVAD causes cell death that is prevented by RIP1 kinase inhibition with Nec-1 and genetic deletion of RIP1 or RIP3.

TLR-induced necroptosis has a differential requirement for TNF-R1 based on MyD88 or TRIF adapter usage

TLR signaling proceeds through two distinct adapter proteins, MyD88 and TRIF, that govern the downstream molecules that are recruited to the signaling receptor complex (33, 46, 47). To demonstrate that necroptosis activated by imidazoquinoline compounds requires activation of TLR7, peritoneal macrophages from *Tlr7*$^{-/-}$ mice were activated with imiquimod or CL-097 in the presence of ZVAD and were compared to activation with LPS and ZVAD. Cell death induced by TLR7 agonists but not LPS was prevented in *Tlr7*$^{-/-}$ macrophages, demonstrating that necroptosis is activated by signaling through this receptor (Figure 6A). Furthermore, when *Myd88*$^{-/-}$ macrophages were activated in the presence of ZVAD, cell death was completely prevented in imiquimod stimulation but only partially prevented in LPS stimulation (Figure 6B). This result is easily explained by the fact that TLR4 activation can occur using both adapters, MyD88 and TRIF (46) whereas TLR7 only engages MyD88 (29).

MyD88-dependent TLR signaling engages the IRAK protein family to form the Myddosome to activate downstream events such as NF-κB and MAPK activation (35, 38, 39). TRIF-dependent TLR signaling recruits RIP1 through its RHIM domain to activate

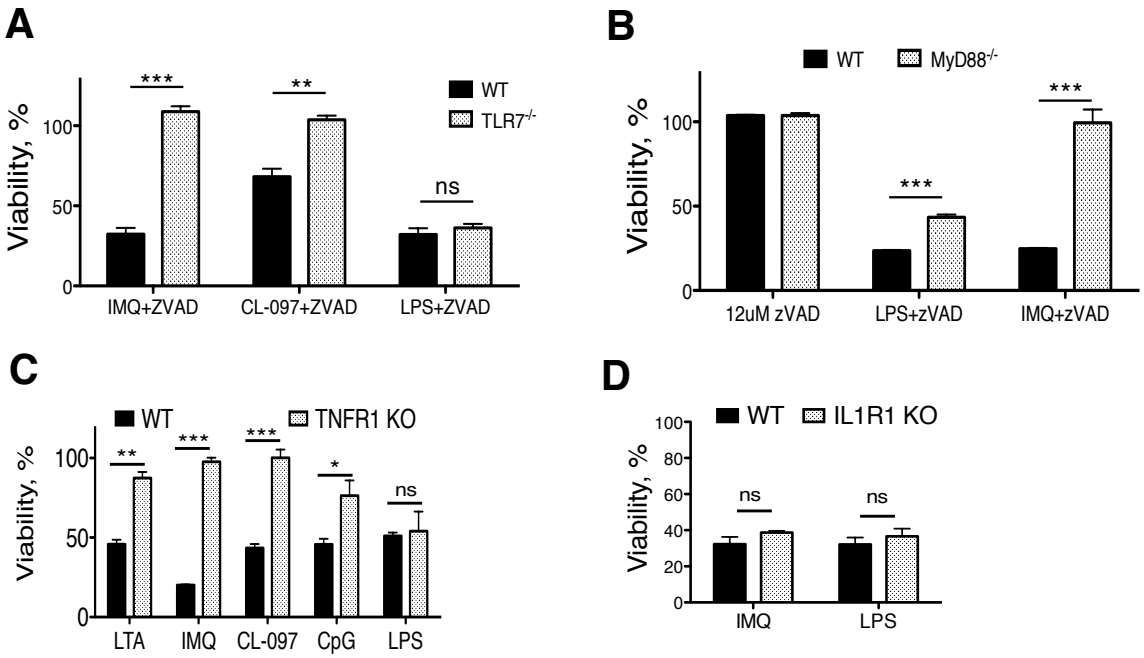

Figure 6. **TLR-induced necroptosis has a differential requirement for TNF-R1 based on MyD88 or TRIF adapter usage.** Peritoneal macrophages from C57BL/6 (WT), TLR7$^{-/-}$ (A), MyD88$^{-/-}$ (B), TNFR1$^{-/-}$ (C), or IL1R1$^{-/-}$ (D) stimulated with stimulated for 18 hours with lipoteichoic acid (LTA) (2 μg/ml), IMQ (5 μg/ml), CL-097 (1 μg/ml), CpG (200 nM), polyI:C (10 μg/ml), or LPS (100 ng/ml) in the presence of ZVAD (12.5 μM) with or without the RIP1 kinase inhibitor Nec-1 (30 μM). Cell viability was measured by ATP levels using the CellTiter-Glo assay (Promega). Values are a percentage of viable treated cells relative to cells in medium with vehicle (DMSO), shown as mean +/- S.E. from two (A,B) or three (C,D) independent experiments. Statistical significance was determined by two-tailed Student's *t* test. *, $p < 0.05$; **, $p < 0.001$; ***, $p < 0.0001$; *ns*, not significant.

NF-κB and MAPK (51, 132). The mechanism of TLR-induced necroptosis activated through these two sets of TLR adapters could occur through intrinsic signaling mechanisms or requires autocrine TNF production and signaling through TNF-R1 as was suggested for LPS-mediated apoptosis (252). Peritoneal macrophages deficient in TNF-R1 were stimulated in the presence of caspase inhibition with MyD88-dependent TLR agonists (LTA, imiquimod, CL-097, CpG) or LPS (which can engage MyD88 or TRIF). For all MyD88-dependent TLRs but not for TLR4, TNF-R1$^{-/-}$ peritoneal macrophages were protected from cell death (Figure 6C). This result in conjunction with a recent independent report using TNF-deficient macrophages suggest that for MyD88-dependent TLRs, which lack the capacity to directly recruit RIP1 to the Myddosome, autocrine TNF production and activation of TNF receptor signaling is required for necroptosis while TLRs that can signal through TRIF do not require TNF-R1 for this process (137). Deficiency in other cytokine receptors, such as IL1R1, did not prevent cell death by imiquimod or LPS (Figure 6D). Importantly, these data establish that necroptosis occurs downstream of TLR signaling and that autocrine activation of TNF-R1 signaling is required to execute this cell death pathway for MyD88-dependent TLRs but not TLRs that can engage TRIF.

CHAPTER 4: GENETIC DIVERSITY OF WILD-DERIVED STRAINS CONTRIBUTES TO DIFFERENTIAL SUSCEPTIBILITY TO TLR-INDUCED NECROPTOSIS

A portion of this research was originally published in The Journal of Biological Chemistry. Stephen A. Schworer, Irina I. Smirnova, Irina Kurbatova, Uliana Bagina, Maria Churova, Trent Fowler, Ananda L. Roy, Alexei Degterev, and Alexander Poltorak. Toll-like receptor-mediated down-regulation of the deubiquitinase Cylindromatosis (CYLD) protects macrophages from necroptosis in wild-derived mice. The Journal of Biological Chemistry. 2014; 289:14422-14433. *© The American Society for Biochemistry and Molecular Biology.*

Macrophage susceptibility to TLR-induced necroptosis varies based on mouse genetic background

The genetic composition of inbred mouse strains established through sequencing efforts (237, 239) and SNP analysis (236) identified the composition of the classical inbred mouse strain to be derived from an uneven contribution from four *Mus musculus* sub-species: *M. m. castaneus*, *M. m. domesticus*, *M. m. molossinus*, and *M. m. musculus*, with a majority of the C57BL/6 genome derived from *M. m. domesticus* (237). The wild-derived inbred mouse strains offer a model system with substantial genetic diversity from classical inbred strains in that the majority of the genome is of *M. m. molossinus* origin (237, 239) and the SNP frequency is approximately 1 in every 250-300 base pairs (236). The Poltorak laboratory has used wild-derived mice to investigate TLR signaling pathways through a forward genetic approach with the underlying hypothesis that genetic diversity underlies phenotypic diversity in these mouse strains. The aim of the laboratory is to capitalize on phenotypic diversity by using forward genetic analysis to identify individual genes or interactions between multiple genes that underlie a given trait.

To interrogate whether susceptibility to necroptosis induced by TLR ligation varies between mouse strains, peritoneal macrophages from a 19 strains representing wild-derived and classical inbred strains (indicated at the top of the graph) and the major *Mus musculus* sub-species contributor (or species in the case of *Mus spretus*) to genetic makeup (indicated at the bottom of the graph) were stimulated with the TLR7 agonist imiquimod in the presence of caspase inhibition with ZVAD (Figure 7A). Within groups of wild-derived and classical inbred strains there is a spread of susceptibility. Overall,

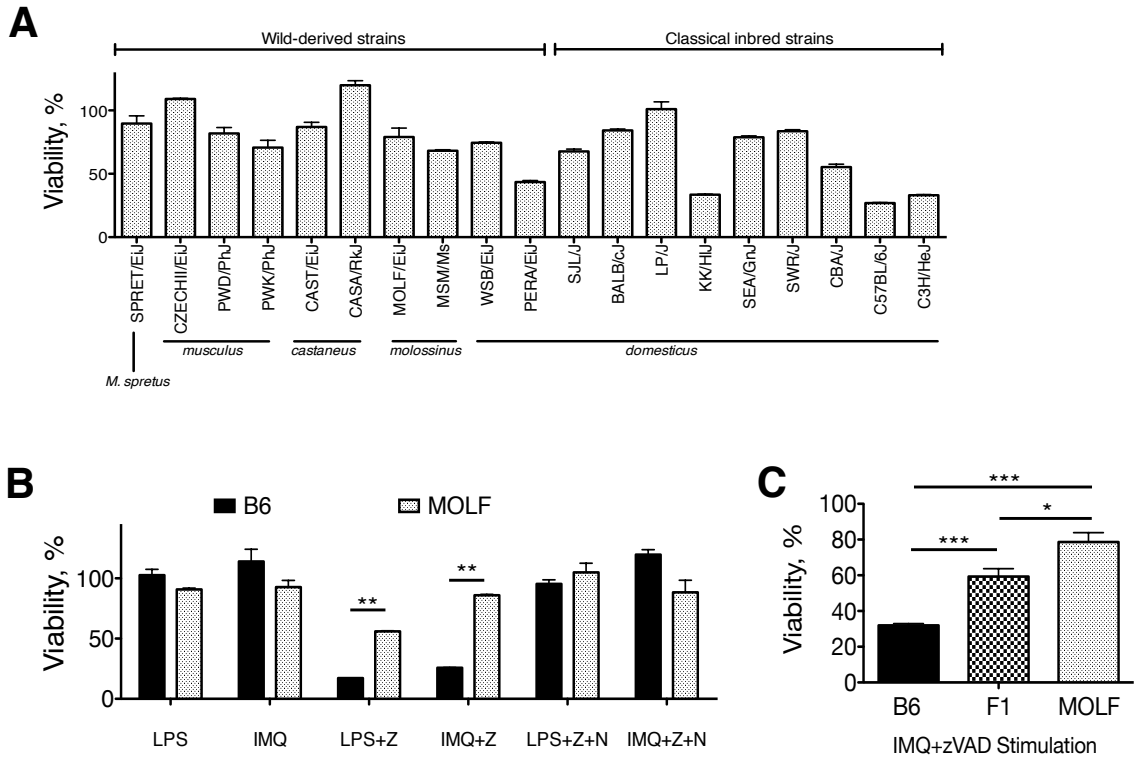

Figure 7. **Susceptibility to TLR-induced necroptosis varies based on mouse genetic background.** (A) Thioglycollate-elicited peritoneal macrophages were collected from *Mus spretus* and *Mus musculus* species were stimulated with IMQ (5 μg/ml) and ZVAD (12.5 μM) for 18 hours. Mice are grouped by whether they are considered to be wild-derived inbred mouse strains or classical inbred mouse strains (top) and by the *Mus musculus* sub-species that comprises the majority of the mouse genetic background (bottom). (B) B6 and MOLF peritoneal macrophages stimulated for 18 hours with LPS (100 ng/ml) or IMQ (5 μg/ml) with and without ZVAD (Z) (12.5 μM) and Nec-1 (N) (30 μM). (C) B6, F1 (B6xMOLF), and MOLF peritoneal macrophages stimulated with IMQ and ZVAD. Cell viability for A-C measured relative to cells kept in medium with vehicle (DMSO) using ATP measurement with the CellTiter-Glo assay. Shown are means for biological triplicates in a representative experiment. Error bars are mean +/- S.E. Data are representative of one (A) or at least three independent experiments (B,C). Statistical significance was determined by two-tailed Student's *t* test. *, $p < 0.05$; **, $p < 0.001$; ***, $p < 0.0001$.

more members of the wild-derived strains that we tested were resistant to necroptosis with PERA/EiJ as the exception. PERA/EiJ show a high level of subspecies introgression from CBA, potentially explaining why they are an outlier (237). Interestingly, classical inbred strains also demonstrate remarkable diversity in susceptibility to this form of cell death. SJL/J, LP/J, BALB/cJ, SEA/GnJ, and SWR/J are as resistant as most wild-derived strains. However, two of the most often used strains of classical inbred mice, C57BL/6 and C3H/HeJ, are highly susceptible to cell death.

Previous work in the Poltorak laboratory focused primarily on the strains comprising the *M. m. molossinus* subspecies as a representative of wild-derived strains. The work capitalized on phenotypic diversity the TLR signaling pathways in MOLF macrophages particularly measured by cytokine responses (e.g. hyper-IL-6 response to LTA (242) and hypo-responsiveness to CpG DNA (253, 254). In this study, the aim is to broaden the scope of the responses assayed in MOLF macrophages to include their resistance to necrotic cell death induced by TLR ligands in the presence of caspase inhibition. To more fully characterize to the resistance to cell death in peritoneal macrophages between our two strains of interest, B6 and MOLF cell viability was compared after stimulation with LPS or IMQ alone, with each agonist with ZVAD, and further with the RIP1 kinase inhibitor Nec-1. There was little or no change in cell viability after stimulation with LPS or imiquimod alone. However, while B6 peritoneal macrophages were susceptible to both agonists in the presence of ZVAD, MOLF macrophages were partially resistant to LPS and ZVAD and completely resistant to IMQ and ZVAD (Figure 7B). Importantly, the cell death occurring in either strain was abrogated upon the addition of Nec-1, strongly suggesting that this death is RIP1 kinase dependent necroptosis. To determine the

inheritance pattern of this trait (whether this trait was recessive, dominant, or co-dominant), F1 (B6xMOLF) peritoneal macrophages were stimulated with imiquimod in the presence of ZVAD, compared with both parental strains for cell viability, and determined to harbor a co-dominant phenotype (Figure 7C). Taken together, susceptibility to TLR-induced necroptosis varies based on genetic background. The wild-derived strain MOLF are resistant to caspase-independent cell death induced by IMQ or LPS, and this trait has an intermediate phenotype in F1 macrophages. These data suggest resistance to TLR-induced necroptosis is a heritable trait that can be subjected to forward genetic analysis.

Forward genetic analysis of TLR-induced necroptosis in N2 peritoneal macrophages links to resistance alleles on MOLF Chromosomes 1 and 8

To determine the genes that underlie the phenotypic difference between MOLF and B6 peritoneal macrophages in resistance to necroptosis, we constructed a panel of 67 N2 (B6x(B6xMOLF)) mice to screen through stimulation with imiquimod and ZVAD. As hypothesized, the genetic diversity in the N2 mice generates a panel of peritoneal macrophages with a broad range of phenotypic response (Figure 8A). Following genotyping of N2 mice using microsatellite markers (at least three per chromosome throughout the genome), QTL analysis (making the correlation between phenotype and genotype at a given locus to produce a LOD score) was performed. This N2 peritoneal macrophage panel revealed two regions of linkage with statistical significance: a 5.1 Mb region on Chromosome 8, LOD = 6.7 as well as a 26.7 Mb region on Chromosome 1, LOD = 3.39 (Figure 8B).

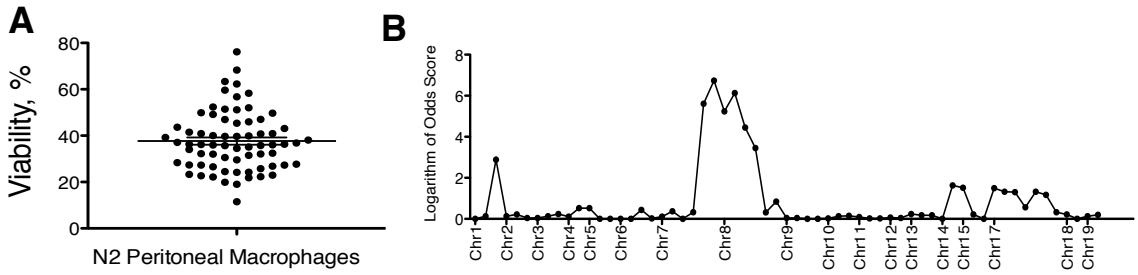

Figure 8. **Forward genetic analysis of IMQ-induced necroptosis maps resistance to loci on Chromosome 1 and Chromosome 8.** (A) Viability of peritoneal macrophages from 67 N2 (B6xF1) mice stimulated with IMQ (5 μg/ml) and ZVAD (12.5 μM) for 18 hours. Cell viability of treated cells compared to cells in media with vehicle (DMSO). Each circle represents an individual mouse. (B) Logarithm of odds score for samples in (A) calculated using QTXb software. LOD > 3 considered significant.

Because of its higher linkage score, the locus on Chromosome 8 was investigated for its contribution to resistance to cell death in MOLF macrophages. Sorting the viability of each sample based on the genotype at the microsatellite marker located at the point of the highest LOD score (*D8Mit51*) demonstrated that heterozygous mice containing a single MOLF allele to be significantly associated with resistance to imiquimod-induced necroptosis (Figure 9A). This 5.1 Mb region on Chromosome 8 contains two genes known to have function in the immune system: *Nod2* and *Cyld*, adjacent genes separated by 8.5 kilobases. NOD2, a pattern recognition receptor that senses bacterial muramyl dipeptide (255), has also been suggested to function in the context of autophagy, inflammasome activation, and the antiviral response (256–259). Because NOD2 is functional in B6 (255), we hypothesized that a loss of this protein or its function would be the most likely mechanism for MOLF to harbor a difference in *Nod2*, which would underlie resistance to necroptosis. Thus, *Nod2*$^{-/-}$ peritoneal macrophages were tested for susceptibility to necroptosis activated by imiquimod or LPS. However, no difference in viability was observed between the wild-type and *Nod2*-deficient macrophages, suggesting that *Nod2* was not the gene underlying this phenotype (Figure 9B).

Next, TNF production was measured to rule out the possibility that a difference in signal strength from autocrine TNF contributes to the susceptibility variation between B6 and MOLF because necroptosis activated by the MyD88-dependent TLR7 requires autocrine signaling through TNF-R1 (Chapter 3). TNF protein release by B6 and MOLF peritoneal macrophages was measured after 8 hours of imiquimod stimulation in the presence or absence of ZVAD and Nec-1 (Figure 9C). No significant difference was found in TNF

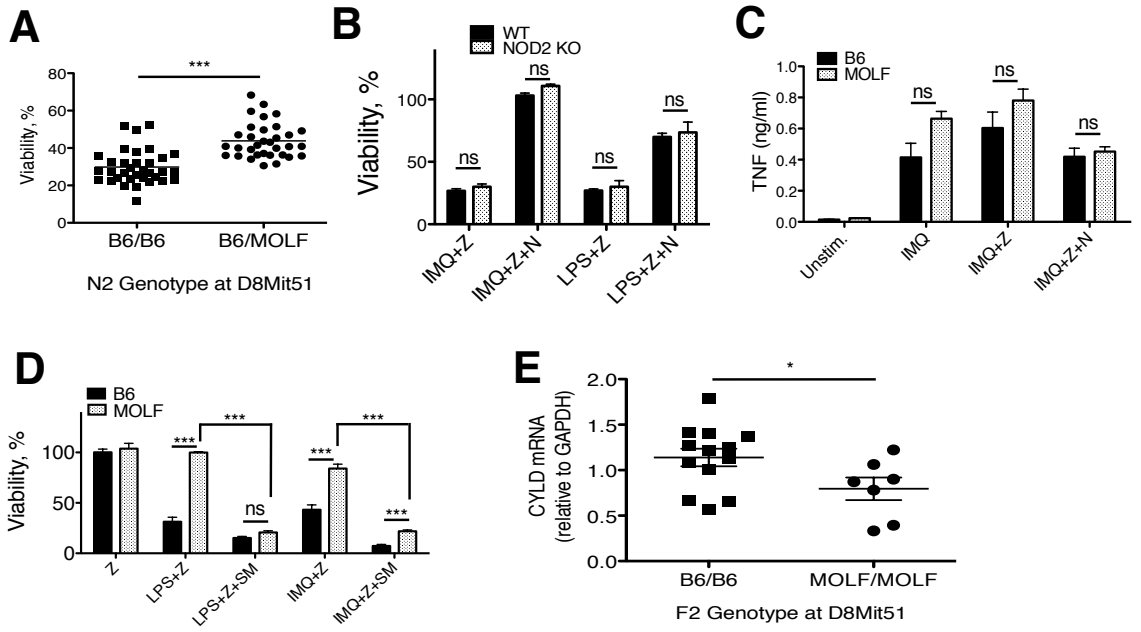

Figure 9. **Resistance to necroptosis in MOLF peritoneal macrophages is linked to *Cyld*.** (A) Viability of peritoneal macrophages from 67 N2 mice after stimulation with IMQ+ZVAD grouped by genotype at D8Mit51 (microsatellite marker within the peak of highest linkage). (B) NOD2$^{-/-}$ and B6 (WT) peritoneal macrophages were stimulated for 18 hours with IMQ (5 μg/ml) or LPS (100 ng/ml) and ZVAD (Z) (12.5 μM) +/- Nec-1 (N) (30 μM). Viability was measured by CellTiter-Glo ATP assay. (C) B6 and MOLF peritoneal macrophages stimulated for 8 h with IMQ (5 μg/ml), IMQ+ZVAD (12.5 μM), or IMQ+ZVAD+Nec-1 (30 μM). TNF production in supernatants was measured by ELISA. (D) B6 and MOLF peritoneal macrophages stimulated for 18 h with LPS (100 ng/ml) or IMQ (5 μg/ml) in the presence or absence of the SM164 (SM) (100 nM), ZVAD (12.5 μM), and Nec-1 (30 μM). (E) Peritoneal macrophages from 20 F2 mice were stimulated for 4 hours with LPS (100 ng/ml). CYLD mRNA levels were measured by qPCR. Samples from each mouse were sorted by genotype at D8Mit51. Error bars are mean +/- S.E. (B and D) or S.D. (C). Data from two (D) or three (B and C) independent experiments were pooled, with statistical significance determined by two-tailed Student's *t* test. *, $p < 0.05$; ***, $p < 0.0001$; ns, not significant.

production between B6 and MOLF cells, suggesting an intrinsic signaling defect directed toward cell death rather than altered TNF production.

The second candidate gene within the locus linked MOLF resistance on Chromosome 8 was the deubiquitinase CYLD. The importance of this DUB to drive TNF-R1-mediated necroptosis through its activity on RIP1 has recently been demonstrated (92). To investigate whether alteration of the ubiquitin status of RIP1 may be an important difference between B6 and MOLF peritoneal macrophages, the Smac-mimetic (IAP antagonist) SM-164 was used (260). Smac-mimetics target cIAPs, the E3 ubiquitin ligases responsible for lysine 63-linked ubiquitin ligation to RIP1, for autoubiquitination and degradation (69, 261). cIAP antagonism or depletion sensitizes many cell types to death by necroptosis (136, 155, 262). If a difference in the ubiquitination status of RIP1 underlies the phenotypic difference between B6 and MOLF, treatment with SM-164, which would reduce RIP1 ubiquitination (bypassing any CYLD-related defect in MOLF), and lead to an equalization of the susceptibility to TLR-induced necroptosis. When macrophages were stimulation during caspase inhibition with LPS or imiquimod, SM-164 significantly reduced viability in MOLF, suggesting that a reduction in ubiquitination status of a cIAP target, such as RIP1, allows for susceptibility in MOLF. Importantly, in LPS and ZVAD-treated macrophages, SM-164 eliminated the difference between the strains and in imiquimod and ZVAD-treated cells, SM-164 reduced the difference between the strains (Figure 9D). These data suggest that differential ubiquitination of a target of cIAPs such as RIP1 may underlie the difference in susceptibility.

Because SM-164 treatment reduced the difference in susceptibility between B6 and MOLF macrophages the likelihood that a difference *Cyld,* the only ubiquitin-modifying

enzyme within the region of interest on Chromosome 8, contributes to this phenotype became more likely. Expression differences between B6 and MOLF macrophages have been found to underlie multiple previously mapped traits (242, 254). Because CYLD promotes necroptosis (92), reduced expression of this protein in MOLF macrophages could explain the resistance of these cells to TLR-induced necroptosis. To determine if CYLD expression levels vary based on the genotype at *D8Mit51,* a panel of 20 F2 peritoneal macrophages was generated and levels of CYLD were measured by qPCR. Interestingly, MOLF homozygotes at the CYLD locus (*D8Mit51*) expressed significantly less *Cyld* transcript after LPS stimulation suggesting that there is a *cis*-acting change within the *Cyld* locus that confers lower expression of this gene (Figure 9E). While these data are circumstantial, genetic analysis and implication of the ubiquitination of RIP1 through the use of SM-164 both implicate *Cyld* as the gene on Chromosome 8 underlying MOLF resistance to necroptosis.

The secondary locus linked to resistance to TLR-induced necroptosis was on Chromosome 1. By sorting mice based on genotype at the microsatellite marker of highest linkage, it was revealed that the mice heterozygous for the MOLF allele at *D1Mit102* were significantly resistant to necroptosis when compared to B6 homozygotes (Figure 10A). While this locus is too large to assemble a short list of gene candidates, 196 protein-coding genes are located within the region of interest (see Appendix 1 for list of genes). Because of the identification of *Cyld* as the primary candidate gene for the locus on chromosome 8, genes that may interact with CYLD expression were examined. Of note, miR181-b1 is adjacent to the linked region.

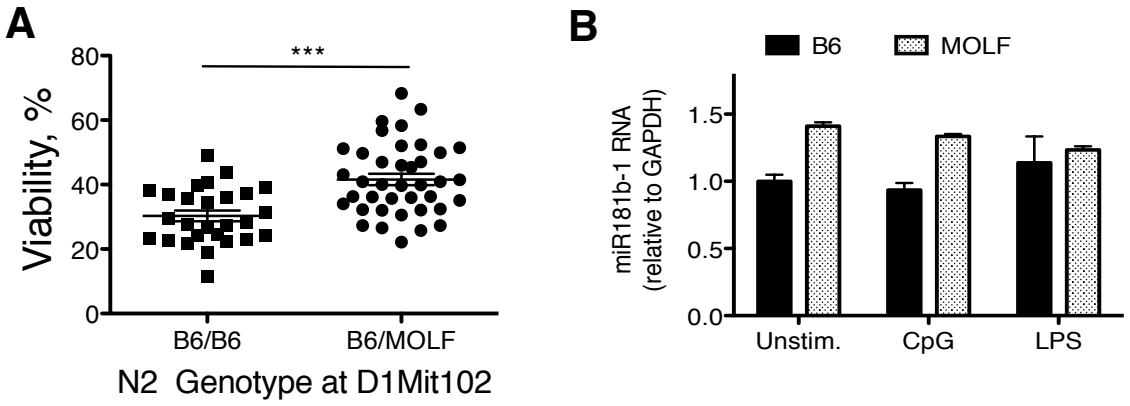

Figure 10. **Resistance to necroptosis in MOLF peritoneal macrophages is linked to a locus on Chromosome 1.** (A) Viability of peritoneal macrophages from 67 N2 mice after stimulation with IMQ+ZVAD grouped by genotype at D1Mit102 (microsatellite marker within the peak of highest linkage). Statistical significance determined by Student's *t* test. ***. $p < 0.0001$. (B) B6 and MOLF peritoneal macrophages stimulated with CpG (200nM) or LPS (100 ng/ml) for 4 hours. miR181b-1 levels measured using TaqMan quantitative PCR. Error bars are mean +/- S.E.

Because this miRNA is implicated in the negative regulation of CYLD expression (102), its expression levels were assessed by qPCR. However, no significant differences in expression at baseline or after TLR stimulation were noted (Figure 10B).

MOLF BMDMs are resistant to necroptosis activated by low doses of LPS

Bone marrow-derived macrophages (BMDM) are an important experimental system for the study of TLR signaling and cell death and have been shown to undergo necroptosis (137). To investigate whether MOLF resistance to TLR-induced necroptosis occurred in BMDM, these cells were stimulated with LPS in the presence of ZVAD. TLR7 agonists were not pursued because this signaling pathway was not a potent activator of cell death in BMDM (Figure 5C). At doses of LPS used in peritoneal macrophages (100 ng/ml), there was no difference in viability between B6 and MOLF BMDM (Figure 11A). However, when the LPS dose was lowered to 10 ng/ml, MOLF BMDM became resistant to LPS-mediated necroptosis in comparison to B6. A number of factors could underlie the difference in susceptibility to lower dose LPS-mediated necroptosis including factors related to TLR4 localization by CD14 (26), MyD88 recruitment through TIRAP (35), as well as other as-yet unidentified proteins specifically regulating necroptotic cell death. To approach this question in an unbiased manner, a forward genetic approach was used uncover loci linked to this trait. Using a panel of 69 F2 mice, a wide spread of BMDM viability following activation with LPS and ZVAD (Figure 11B). Of concern in this panel, the unstimulated samples were substantially lower in viability than in other experiments, perhaps because of the need for a survival signal to

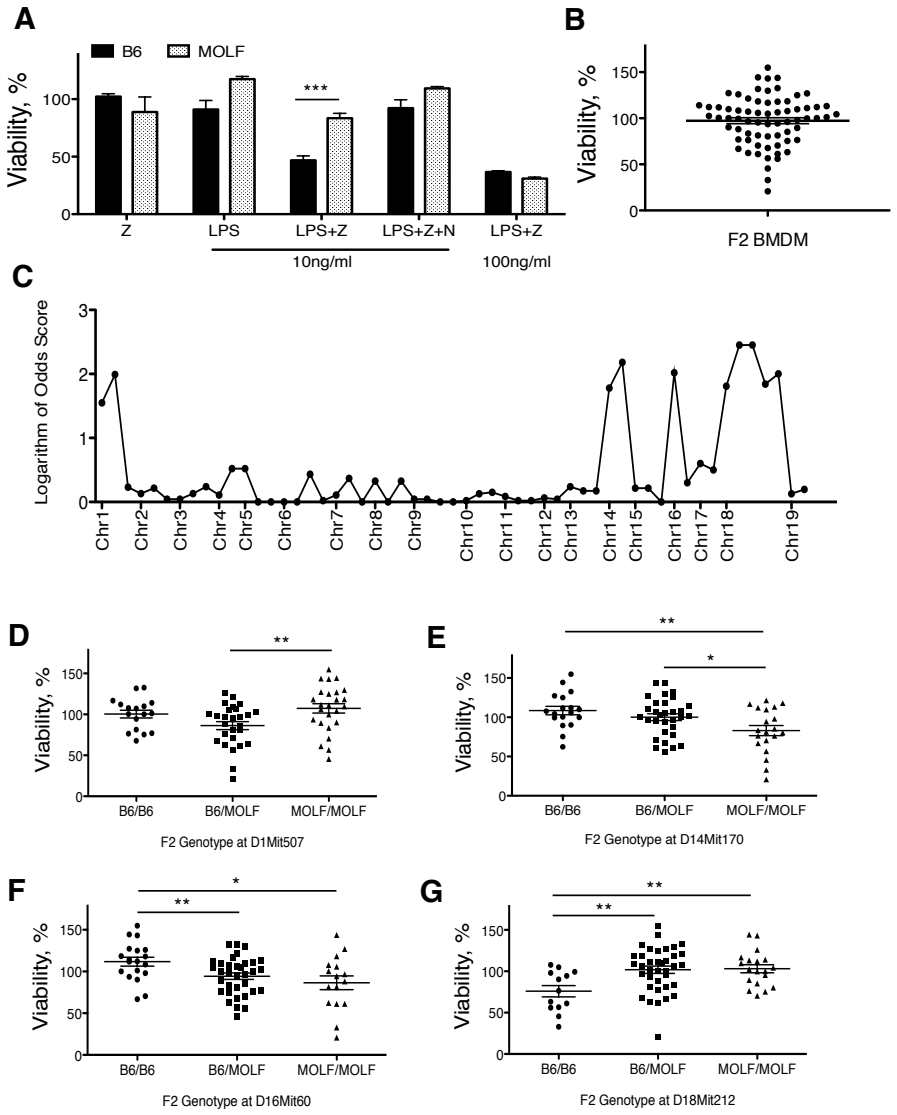

Figure 11. **MOLF BMDM are resistant to low dose LPS-induced necroptosis and linkage analysis of this trait suggests four linked loci.** (A) B6 and MOLF BMDM stimulated for 18 hours with LPS (10 ng/ml or 100 ng/ml) with and without ZVAD (Z) (25 μM) and Nec-1 (N) (30 μM). Cell viability was measured by ATP level using the CellTiter-Glo assay (Promega). Values are a percentage of viable treated cells relative to cells in medium with vehicle (DMSO), shown as mean +/- S.E. Data presented from three pooled experiments. (B) Viability of BMDM from 69 F2 mice stimulated with LPS (10 ng/ml) and ZVAD (25 μM) for 18 hours. Cell viability of treated cells compared to cells left in media with vehicle (DMSO). Each circle represents an individual mouse. (C) Logarithm of odds score for samples in (A) calculated using j/QTL software. LOD > 3 considered significant. (D-G) Viability of BMDM from 69 F2 mice (from panels B,C) stimulated with LPS+ZVAD grouped by genotype at microsatellite markers within the peak of highest linkage for each locus. Statistical significance determined by Student's *t* test. *, $p < 0.05$; **, $p < 0.001$.

keep BMDM alive in RPMI alone for the overnight stimulation. This feature caused the ratios between treated and untreated samples to skew to levels over 100%. However, because the lower viability in unstimulated BMDM was present in all samples, the data seem to be consistent within the experiment and thus amenable to genetic analysis.

Following microsatellite mapping and QTL analysis of 69 F2 mice, four suggestive but not statistically significant loci were linked to this trait (Figure 11C). To interrogate the allelic effect within each peak, mice were sorted based on the genotype at the microsatellite marker of highest linkage and viability of the F2 BMDM were compared (Figure 11D-G). A region on Chromosome 1 (28 Mb) containing 296 protein-coding genes was linked to increased survival in F2 mice homozygous for the MOLF allele at this locus over heterozygous mice but not over homozygous B6. Interestingly, this region does not overlap with the linked region in peritoneal macrophages. Two loci – one 36.1 Mb locus on Chromosome 14 containing 84 protein coding genes (see Appendix 2 for list of genes) and a second on Chromosome 16 of 81 Mb containing 536 protein coding genes showed that the MOLF allele was conferring susceptibility to necroptosis. Because the overall MOLF signaling network is likely somewhat different than B6 (as is true for TLR signaling and the expression of *Irak1bp1*in MOLF macrophages (242)), it is likely that the MOLF necroptotic signaling network contains genes that promote *more* cell death as well as those that cause resistance. While this signaling network balances to an overall resistance phenotype in the parental MOLF mouse, an F2 recombinant mouse may express certain genes that promote necroptosis in MOLF that are normally compensated for by other MOLF genes absent in that particular F2 mouse. Finally, the locus with highest linkage (LOD=2.45) is located on Chromosome 18 (13.4 Mb, 68

protein coding genes, see appendix 3 for a list of genes). Within this locus, there are no genes currently implicated in necroptosis or, as mentioned above, in dose-dependent TLR4 signaling. The question remains whether this phenotype is related to the ability for MOLF BMDM to traffic TLR4 to the appropriate compartment to engage TRIF signaling (26) or whether a defect exists in the intrinsic necroptosis machinery in MOLF BMDM (as is true for peritoneal macrophages, see Chapter 5). The ability to isolate TRIF-dependent signaling events from TLR4 in MOLF cells is somewhat limited due to a functional defect in TLR3 (253). Alternatively, mapping TLR4-TRIF-mediated responses independently from necroptosis could provide a reasonable alternative approach to identifying the mechanism underlying the difference in necroptosis susceptibility between B6 and MOLF BMDM, specifically whether it is true for TRIF-mediated TLR signaling globally or is specific to necroptosis.

CHAPTER 5: CYLD DOWN-REGULATION CONFERS PROTECTION FROM NECROPTOSIS IN MOLF PERITONEAL MACROPHAGES

The aim of this chapter is to investigate the locus on Chromosome 8 in which the presence of a MOLF allele was linked to resistance to TLR-induced necroptosis. The data examine 1) whether CYLD contributes to TLR-induced necroptosis in peritoneal macrophages and BMDM; 2) how CYLD is differentially regulated in MOLF peritoneal macrophages; 3) preliminary examination of the *Cyld* promoter through sequencing reveals a deletion in one CA repeat but whether this mutation is causative for the phenotype is not clear; 4) because experimental constrains prevented add-back of CYLD into peritoneal macrophages, analysis of CYLD role in necroptosis in B6 and MOLF BMDM.

A portion of this research was originally published in The Journal of Biological Chemistry. Stephen A. Schworer, Irina I. Smirnova, Irina Kurbatova, Uliana Bagina, Maria Churova, Trent Fowler, Ananda L. Roy, Alexei Degterev, and Alexander Poltorak. Toll-like receptor-mediated down-regulation of the deubiquitinase Cylindromatosis (CYLD) protects macrophages from necroptosis in wild-derived mice. The Journal of Biological Chemistry. 2014; 289:14422-14433. © The American Society for Biochemistry and Molecular Biology.

CYLD promotes TLR-induced necroptosis in macrophages

Forward genetic analysis discussed in Chapter 4 showed that resistance to TLR-induced necroptosis in N2 peritoneal macrophages mapped to a locus containing the gene encoding the deubiquitinase CYLD. While CYLD has been shown to promote cell death by apoptosis (76) and necroptosis (92, 147), these reports describe activation of cells either with ZVAD alone (which produces an autocrine TNF signal (191)) or via death receptor ligation. Deubiquitination of RIP1 can be accomplished by CYLD and promote necroptosis in fibroblasts (92, 94) and negatively regulate NF-κB signaling in germ cells (89). The question remains whether CYLD is required for necroptosis when it is driven by TLRs. While the signaling mechanisms of death receptors and TLRs share many characteristics whether CYLD truly functions in each of these pathways is debated based on studies in different knockout models (85–87). The knockout mice generated by Sun, *et al.* displayed a critical role for CYLD in negative regulation of RANK signaling (90), type I interferon productions through TBK1 and IKKε (91), and TAK1 activation in the liver (88). However, knockout mice generated by Jain, *et al.* demonstrated a role for CYLD as a negative regulator of TLR signaling in BMDM (86), which was not observed in the knockdown mice generated by Sun, *et al.*

Small interfering RNA transfection to silence CYLD in peritoneal macrophages was used to establish the contribution of CYLD to TLR-induced necroptosis. Following treatment with Dicer-substrate siRNA targeting CYLD or a negative control, B6 peritoneal macrophages were stimulated with LPS or imiquimod in the presence of ZVAD. Compared to negative control siRNA, macrophages transfected with CYLD-targeted siRNA demonstrated a statistically significant protection from cell death from

both stimuli (Figure 12A). When the efficiency of knockdown was assessed by western blot, densitometry revealed that 63% of CYLD protein remained in peritoneal macrophages, which are notoriously difficult to transfect (Figure 12B). Further assessment of knockdown efficiency by qPCR showed approximately 75% knockdown efficiency on the RNA level (Figure 12C). In B6 peritoneal macrophages, which exhibited a partial CYLD knockdown, a statistically significant protection from TLR-induced necroptosis was observed, establishing that CYLD has a role in driving this process.

Because B6 peritoneal macrophages are difficult to efficiency transfect, RAW264.7 macrophages, a cell type that is susceptible to TLR-induced necroptosis (251), were used as a model for over-expression of CYLD to show its sufficiency to promote necroptosis. RAW264.7 macrophages were transduced with lentivirus expressing CYLD or with empty vector-containing lentivirus and activated in the presence of ZVAD with LPS or imiquimod. Stimulation of CYLD-overexpressing cells with either agonist induced a statistically significant increase in cell death that was inhibited by the RIP1 kinase inhibitor Nec-1 (Figure 12D). These data establish that overexpression of CYLD is sufficient to increase TLR-induced necroptosis. While CYLD has been shown to drive cell death in the absence of stimuli when caspases are inhibited (92), the two-fold increase in expression as measured by qPCR in this system was not sufficient to drive cell death without TLR-mediated activation (Figure 12E).

While these experiments implicate CYLD in TLR-induced necroptosis, the possibility still existed that autocrine TNF production and activation of TNF-R1 signaling was occurring following activation with LPS and that CYLD was only important for

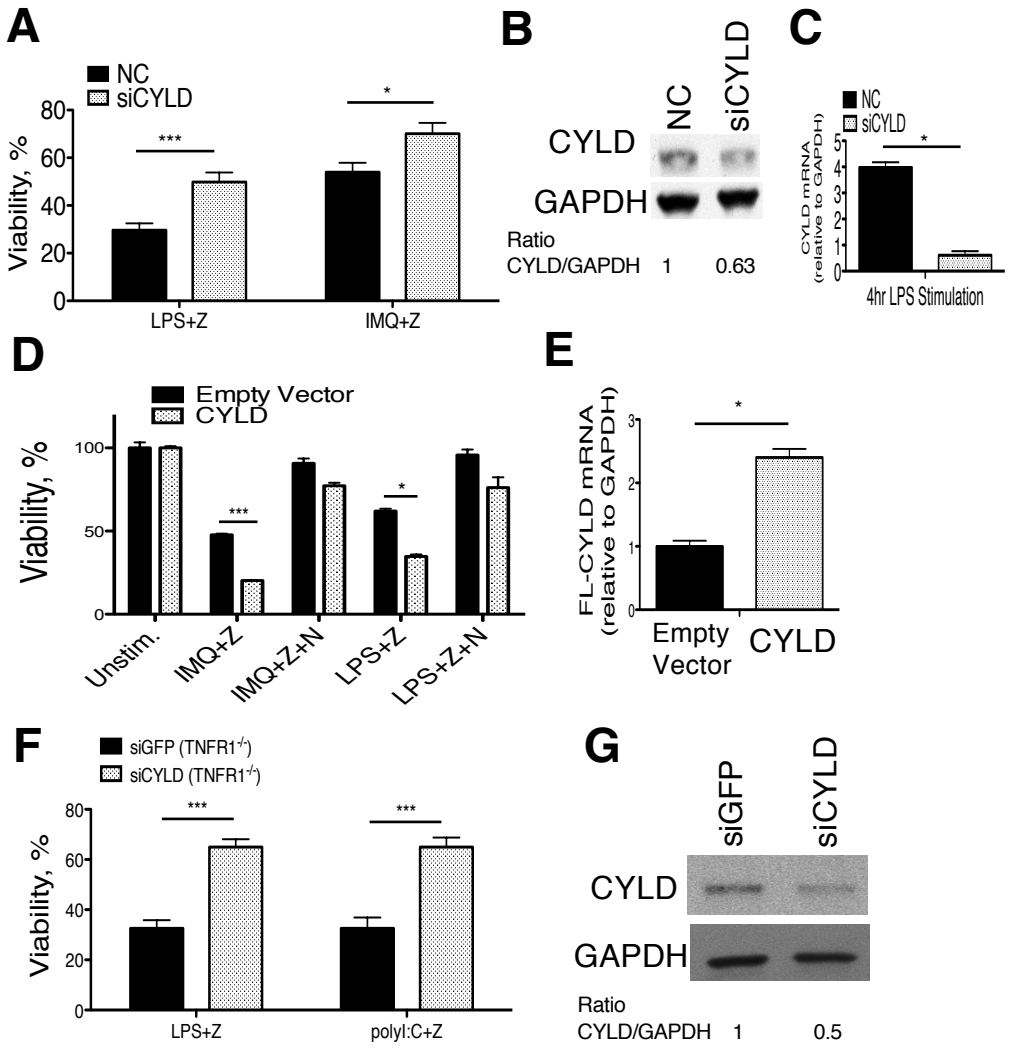

Figure 12. **CYLD promotes TLR-induced necroptosis.** (A) CYLD siRNA and control (NC) siRNA were transfected into peritoneal macrophages, followed by stimulation with LPS or IMQ and ZVAD (Z). Knockdown efficiency was assessed by western blotting for CYLD relative to GAPDH in unstimulated cells (B) and by qPCR after 4 hours of LPS stimulation (C). (D) RAW264.7 macrophages were infected with lentivirus containing full-length (FL) CYLD or an empty vector and stimulated with IMQ or LPS and ZVAD (50 μM) +/- Nec-1 (N) (30 μM). (E) Over-expression level of FL-CYLD measured by qPCR relative to empty vector. (F) $TNFR^{-/-}$ BMDM infected with lentivirus containing short hairpin RNA targeting GFP or CYLD stimulated with LPS (100 ng/ml) or polyI:C (200 μg/ml) with ZVAD (25 μM). (G) Western blotting for CYLD protein expression for samples in (F). For all experiments, cell viability was measured at 18 hours relative to cells kept in medium with vehicle (DMSO). Data shown are the mean +/- S.E. pooled from six (A) two (D), or three (F) pooled, independent experiments. Statistical significance was determined by two-tailed Student's *t* test. *, $p < 0.05$; ***, $p < 0.0001$.

protection from death through this mechanism. To address this question, TNF-R1-deficient BMDM were infected with lentivirus expressing shRNA targeting GFP or CYLD and stimulated with TLR agonists capable of activating intrinsic cell-death through TRIF; LPS targeting TLR4, which may produce TNF-R1 autocrine signaling (Figure 6C), and poly(I:C) targeting TLR3, which does not utilize TNF-R1 autocrine signaling (137). Knockdown of CYLD protected from necroptosis activated by LPS or poly(I:C) even in the absence of TNF-R1 autocrine signaling (Figure 12F) with a knockdown efficiency of 50% at the protein level (Figure 12G). These data establish that CYLD is required for activation of TLR-induced necroptosis through TRIF-mediated TLR signaling in addition to TNF-R1-mediated necroptosis.

TLR stimulation causes acute down-regulation of CYLD in MOLF peritoneal macrophages

With the above data establishing a role for CYLD in TLR-induced necroptosis, the regulation of CYLD in MOLF peritoneal macrophages was investigated with the goal of elucidating how CYLD may be differentially regulated in MOLF macrophages to permit resistance to this form of cell death. Sequencing of cDNA revealed no mutations between B6 and MOLF in either the protein-coding region, 5' UTR, or 3'UTR of *Cyld*. Because of the lack of coding mutations, an expression difference governed by a *cis*-acting mutation is the next most likely explanation for mapping to the *Cyld* locus. Notably, other forward genetic analyses using MOLF macrophages in the Poltorak laboratory have revealed that *cis*-acting mutations driving differences in expression underlie other traits related to TLR signaling (43, 242, 254). Furthermore, analysis of F2 peritoneal macrophages for CYLD

mRNA expression was suggestive of a *cis*-acting effect of the *Cyld* locus on expression of this mRNA (Figure 9E).

Expression of CYLD is regulated by down-regulation of the full-length isoform in cancers (80, 81) and alternative splicing in mice (105, 263). This splice variant lacks exons 7 and 8 ($CYLD^{ex7/8}$), which contain critical domains for CYLD to interact with NEMO, TRAF2, and TRAF6. To address whether alternative splicing of CYLD is occurring in MOLF macrophages, mRNA species were identified using 5'RACE in unstimulated and LPS stimulated peritoneal macrophages. Sequencing of PCR products revealed that B6 macrophages expressed both the full-length and the splice isoforms ($CYLD^{ex7/8}$) of CYLD in unstimulated and stimulated cells (Figure 13A). However, MOLF macrophages expressed only the full-length isoform in unstimulated cells and appeared to switch to the $CYLD^{ex7/8}$ splice isoform following LPS stimulation. While a mechanism of regulation in which MOLF macrophages preferentially expressed the $CYLD^{ex7/8}$ protein following LPS stimulation would be quite interesting, attempts to identify the splice variant on the protein level demonstrated that only the full-length isoform of CYLD is expressed in macrophages.

It is possible that alternative splicing "away" from the full-length isoform of CYLD could explain a mechanism for differential CYLD regulation between the strains. The first goal of the study was to establish that CYLD was indeed down-regulated in MOLF macrophages following TLR stimulation. While CYLD expression is decreased in a number of cancers through modification of histones (97, 264) and activation of repressing transcription factors (99, 101), stimulus-dependent down-regulation of this gene is less well characterized. A study in 293EBNA cells demonstrated that following TNF

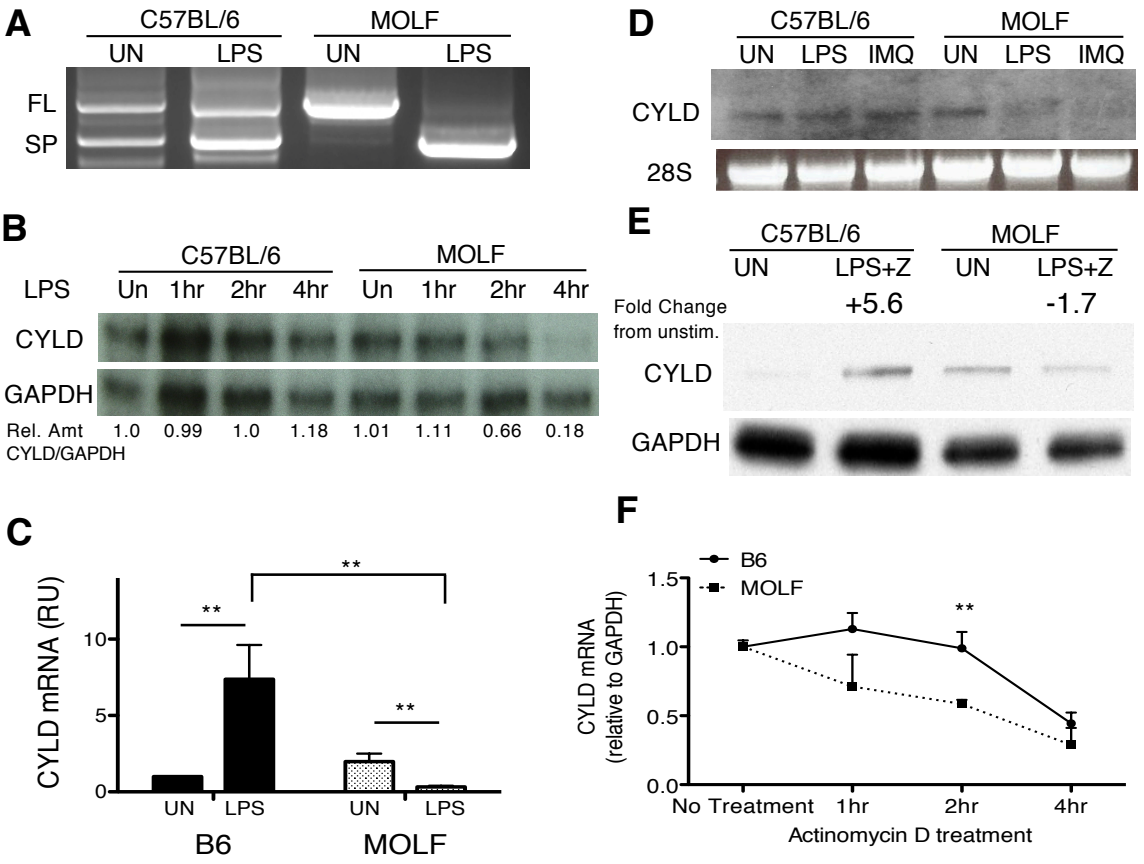

Figure 13. **CYLD is down-regulated by TLR stimulation in MOLF peritoneal macrophages.** (A-E) RNA extracted from B6 and MOLF peritoneal macrophages. (A) CYLD-specific PCR and sequencing of clones obtained from 5' rapid amplification of cDNA ends shows full-length (FL) and splice (SP) CYLD isoforms in unstimulated (UN) or 4 hour LPS-stimulated (100 ng/ml) cells. (B) Ribonuclease protection assay using CYLD-specific (top row) and GAPDH-specific (bottom row) probes on RNA samples from macrophages stimulated for 1, 2, and 4 hours with LPS (100 ng/ml). Shown is the relative amount (Rel Amt) of CYLD/GAPDH in each sample as determined by densitometry. (C) Quantitative RT-PCR was performed using a full-length, CYLD-specific TaqMan probe after LPS stimulation (4 hours). Values are presented as relative units (RU) normalized to GAPDH. (D) Northern blot on RNA samples of macrophages stimulated for 4 hours with LPS (100 ng/ml) or IMQ (5 μg/ml) using a CYLD-specific probe. 28 S rRNA ethidium bromide staining was the loading control. (E) B6 and MOLF peritoneal macrophages unstimulated or stimulated with LPS with ZVAD (LPS+Z) for 6 hours. Lysates were analyzed by Western blot analysis for CYLD protein levels with GAPDH as a loading control. Densitometry measured the fold change of the CYLD/GAPDH ratio relative to unstimulated levels within each mouse strain. (F) Samples were stimulated with LPS for 90 minutes followed by treatment with Actinomycin D for 0 (No treatment), 1, 2, or 4 hours. CYLD mRNA levels measured by qPCR as in (C). Data shown are representative of at least two independent experiments (A,B,D,E) or mean +/- S.E. from four pooled experiments (C,F). Statistical significance was determined by two-tailed Student's *t* test. **, $p < 0.001$.

priming, Sendai virus infection caused down-regulation of CYLD protein after 24 hours (104). However, numerous studies demonstrated that activation of NF-κB (95) or serum response factor (96) leads to increased CYLD expression and suggest this regulation is cell type and stimulus dependent (90).

In this study, RNA expression in LPS stimulated peritoneal macrophages from B6 and MOLF mice was measured by multiple assays. First, to specifically assess the expression of CYLD mRNA without PCR amplification, a ribonuclease protection assay using a full-length CYLD-specific probe was used to measure CYLD RNA following a time course of stimulation with LPS. Relative to GAPDH expression, B6 macrophage levels of CYLD remained unchanged or very slightly up-regulated (Figure 13B). In MOLF macrophages, expression of CYLD decreased by one-third after two hours of stimulation and by over 80% after four hours. To more quantitatively assess CYLD expression, an exon 7/8-spanning TaqMan probe was used for quantitative real-time PCR. Remarkably, MOLF peritoneal macrophages significantly down-regulated CYLD whereas B6 up-regulated expression of this mRNA following four hours of LPS stimulation (Figure 13C). Furthermore, northern blot analysis demonstrated that in addition to LPS, imiquimod was also capable of down-regulating CYLD mRNA expression in MOLF macrophages (Figure 13D). Collectively, these assays demonstrate that CYLD mRNA levels are decreased in MOLF peritoneal macrophages following TLR stimulation while B6 modestly up-regulate this mRNA.

While the above data establish that MOLF macrophages down-regulate CYLD mRNA expression following LPS stimulation, measurement of protein levels is critical to suggesting a functional effect. Accordingly, protein lysates from peritoneal macrophages

stimulated for six hours with LPS in the presence of ZVAD were subjected to SDS-PAGE and western blotting (Figure 13E). Stimulation of these cells in the presence of ZVAD was necessary because LPS-stimulation alone leads to CYLD cleavage by caspase-8 (92), which would prevent specific analysis of protein expression changes caused by a change in transcriptional activation. While B6 showed increased CYLD levels by over five-fold following LPS and ZVAD stimulation, MOLF show nearly two-fold less CYLD protein in stimulated cells. These data establish that, in addition to a role for caspase-8-mediated cleavage in the negative regulation of CYLD to prevent necroptosis (92), MOLF macrophages employ regulation of CYLD at the transcriptional level, reflected in deceased RNA and protein expression of the full-length isoform of CYLD.

To more thoroughly assess how CYLD may be regulated, additional experiments were performed to assess how CYLD mRNA may be regulated. Although no polymorphisms were detected in the *Cyld* 3'UTR between B6 and MOLF, CYLD mRNA transcript stability was assessed because of the possibility of a differentially regulated miRNA. Multiple reports describe miRNAs that target CYLD, including miR-181b-1 (102), which was similarly expression between the strains (Figure 10B) and miR-19 (103). Additionally, up-regulation of miR-181c, a miRNA located near the region linked to resistance to necroptosis on Chromosome 8, has been demonstrated to promote cell death in astrocytes likely through targeting of XIAP (265). However, whether CYLD could be a target of this miRNA is unknown. To address CYLD transcript stability in peritoneal macrophages, cells were stimulated for 90 minutes with LPS followed by addition of the actinomycin D to inhibit further transcription. CYLD mRNA levels were

assessed with the full-length CYLD-specific probe by qPCR. While CYLD mRNA levels decreased somewhat more rapidly in MOLF macrophages especially at the two hour time point, the levels of CYLD in B6 and MOLF appeared similar at four hours following actinomycin D treatment (Figure 13F). These data suggest a minor difference in stability of CYLD transcript between the strains. While definitive evidence for or against CYLD stability is not presented, the lack of a clear result prompted the investigation of activity at the *Cyld* promoter using chromosome immunoprecipitation (see below). Furthermore, it is not clear whether the activity of miR-181c contributes to CYLD regulation or necroptosis, as the previously identified target related to cell death is XIAP (265). The role of XIAP in preventing necroptosis is not well-studied but a recent reports suggests that down-regulation of XIAP leads to heightened susceptibility to caspase-mediated apoptosis in BMDM without an increase in susceptibility to necroptosis (262). Together, the data presented here, in addition to these published reports suggest that while miR-181c is a potential contributor to cell death, *if* it is differentially regulated between B6 and MOLF macrophages, it is not an obvious contributor to necroptotic cell death and is not a likely modifier of CYLD.

MOLF *Cyld* promoter has a single CA deletion with no detectable functional impact

To more fully characterize the *Cyld* promoter, sequencing analysis was performed. Sequencing of the *Cyld* promoter in MOLF revealed a single CA deletion within 2 Kb of the transcription start site and no mutations in splice sites or other portions of the introns between exons 6-7 and 8-9, which flank the $CYLD^{ex7/8}$ splice variant. The

A

```
b6.seq          TTAAACACACACACACACACACACACACACACACACACACACACACACACACACACACCCCT
molf.seq        TTAAACACACACACACACACACACACACACACACACACACACACACACACACACAC---CCCT
published.seq   TTAAACACACACACACACACACACACACACACACACACACACACACACACACACACCCCT
                ********************************************************  ****

b6.seq          CCTTCTCAGTATTAATCACCTTCTCCCATAATTAGTAGTTAAAATGTCAAAGGAGAAGGA
molf.seq        CCTTCTCAGTATTAATCACCTTCTCCCATAATTAGTAGTTAAAATGTCAAAGGAGAAGGA
published.seq   CCTTCTCAGTATTAATCACCTTCTCCCATAATTAGTAGTTAAAATGTCAAAGGAGAAGGA
                ************************************************************
```

B

```
b6.seq          TTAAACACACACACACACACACACACACACACACACACACACACACACACACACCCCT 179
molf.seq        TTAAACACACACACACACACACACACACACACACACACACACACACACACACAC---CCCT 149
human.seq       TTAAAAACACACACACACACACACACACACACACACACCCCT------------CCTC 89
                ***** ********************************** *              **

b6.seq          CCTTCTCAGTATTAATCACCTTCTCCCATAATTAGTAGTTAAAATGTCAAAGGAGAAGGA 239
molf.seq        CCTTCTCAGTATTAATCACCTTCTCCCATAATTAGTAGTTAAAATGTCAAAGGAGAAGGA 209
human.seq       CTTTCTCAGTGTTAATCACCTTCTCCTATAATTAGCACTTAAAATGTCAAAGGAGAAGAA 149
                * ******** ***************** ******** * ********************** *

b6.seq          ATTAATTAAGAGAACTATCCAGTGAAGCAAGTCATGTGCTGCCAGGCTCTGGGGCTGATT 299
molf.seq        ATTAATTAAGAGAACTATCCAGTGAAGCAAGTCATGTGCTGCCAGGCTCTGGGGCTGATT 269
human.seq       ATTAATTAACAGGAGTATCCAGTGCAGCAAG--------------GCTCTAGGACTGATT 195
                ********* ** * ********* ******             ***** ** ******

b6.seq          ATAAAAAGAGTTTCTTTAAATATTTTGAACACTTTTGGGAGTCAGAATCCTTCCGTCTAA 359
molf.seq        ATAAAAAGAGTTTCTTTAAATATTTTGAACACTTTTGGGAGTCAGAATCCTTCCGTCTAA 329
human.seq       ATAAAAAGCACTTCCTTAAATATTTTGAGTGCTTTTGGGAATCAGAAGCCTCCCTTCTAA 255
                ********   *** ************   ********** ****** *** ** *****
```

C

Mouse Strain	IMQ+zVAD Viability	#CA Repeats at -980
B6	Susceptible	25
MOLF	Resistant	24
MSM	Resistant	23
CZECH II	Resistant	24
CAST	Resistant	18
SPRET	Resistant	7
CBA	Susceptible	13
SEA	Resistant	13
BALB/c	Resistant	13
LP	Resistant	13
KK	Susceptible	13
SWR	Resistant	18

D

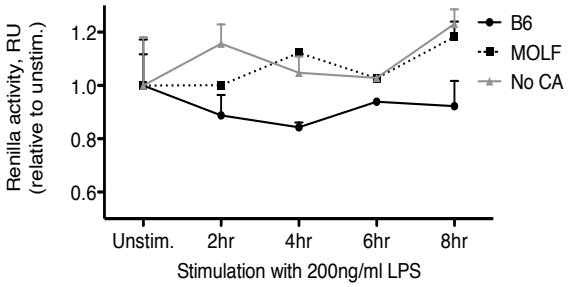

Figure 14. **MOLF *Cyld* promoter has a single CA-deletion but no functional impact is detected.** (A) Sequence alignment of B6 and MOLF genomic DNA aligned with published sequence. The only MOLF polymorphism within 2kb of the TSS is highlighted (980 base pairs upstream of TSS). (B) B6, MOLF, and human alignment of the *Cyld* promoter region shown in (A). (C) Number of CA repeats in the *Cyld* promoter region in classical inbred and wild-derived strains. Resistance or susceptibility from Figure 7A. (D) RAW264.7 macrophages stably transfected with pGL3-containing promoter constructs from B6, MOLF, and one lacking the CA-repeat region. Cells were transfected, selected with Hygromycin B, and stimulated for the indicated times with LPS (200 ng/ml). Renilla activity measured by luminometer and graphed relative to unstimulated value for each construct.

deletion of one CA repeat in MOLF occurred from a series of 25 CA repeats 980 base pairs upstream of the transcription start site (Figure 14A). Additionally, in the corresponding region of the human CYLD promoter, the CA repeat is a series of only 16 repeats (Figure 14B), suggesting that if a CA deletion underlies this phenotype, the MOLF loss of a CA repeat may more closely resemble the human *Cyld* promoter in this region. In other contexts, the deletion of a small number of CA repeats can cause a marked reduction in transcription of MMP9 (266), IL-10 (267), and IFN-γ (267). However, when this CA repeat region in MOLF was compared to other mouse strains, there was not a strong correlation between the number of CA repeats and the susceptibility to necroptosis (Figure 14C).

To determine whether this CA deletion can impact the promoter activity as measured by its ability to drive luciferase activity, the area of the promoter beginning with the CA repeat and extending to the TSS was cloned into the PGL4.76 vector with this promoter region driving luciferase activity. The B6 and MOLF sequences as well as a sequence lacking a CA repeat were each cloned and transfected into cells. Because the cellular environment may differentially affect this promoter, the *Cyld* promoter constructs were transfected into RAW 264.7 macrophages and stimulated with LPS to best approximate the environment of peritoneal macrophages. However, there was no appreciable effect of LPS stimulation on the promoter activity driven by any of the three constructs (Figure 14D).

Transcriptional regulation of the *Cyld* locus may be altered in MOLF by differences in RNA polymerase II pausing, stalling or elongation.

Because there was only a small difference in CYLD mRNA stability and no obvious mutation in a transcription factor within the *Cyld* promoter, recruitment of RNA polymerase II (RNA Pol II) to the promoter of *Cyld* was assessed to determine whether activity at this promoter might explain the difference in CYLD expression levels. Gene expression can be regulated by the recruitment of RNA Pol II and the pre-initiation complex as well as by promoter-proximal pausing and elongation rate (268). RNA Pol II forms a pre-initiation complex at the TSS after binding to promoters. Initiation of transcription begins, followed by a pausing step after transcription of 20-60 base pairs (269). Pol II pausing is induced by its binding of two factors: negative elongation factor (NELF) and DRB-sensitivity-inducing factor (DSIF). Pausing has been shown to be a stable complex, allowing for additional levels of regulation prior to the elongation step of transcription (270). The functions of RNA Pol II pausing likely include recruitment of nucleosome remodeling enzymes to open promoters, maintain the basal expression of genes through protecting promoters from nucleosomes, setting up transcription conditions for rapid synchronous activation of a gene network, and serving as a check point for coupling elongation and RNA processing (269, 271, 272).

To determine RNA Pol II recruitment to the *Cyld* locus in B6 and MOLF peritoneal macrophages, chromatin immunoprecipitation was performed on LPS-stimulated cells using an antibody directed at RNA Pol II. Although no significant differences in RNA Pol II accumulation were detected at the proximal (-300 base pairs) or distal (-700 base pairs) promoter region, an increase in RNA Pol II recruitment was

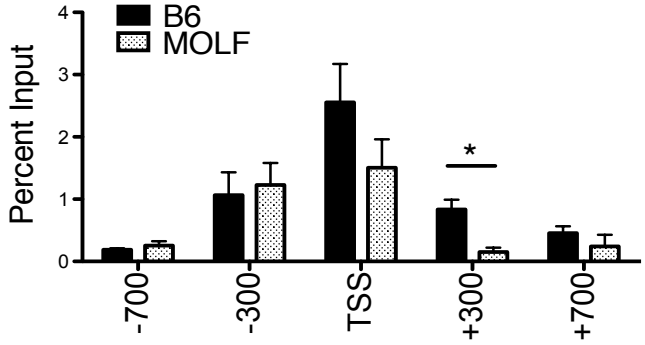

Figure 15. **Reduced RNA Pol II recruitment to *Cyld* promoter-proximal region in MOLF.** B6 and MOLF LPS-stimulated peritoneal macrophages were cross-linked and lysed, and DNA was sheared by sonication. RNA polymerase II ChIP was performed. Quantitative real-time PCR was performed at locations in the *Cyld* promoter indicated in reference to the TSS. Shown is the mean +/- S.E. of a representative experiments from two independent experiments. Statistical significance was determined by Student's *t* test. *, $p < 0.05$.

noted in B6 macrophages at the TSS and a statistically significant difference was found at +300 downstream of the TSS (Figure 15). As described above, RNA Pol II pausing occurs within the regions that were shown to have more RNA Pol II recruitment in B6 peritoneal macrophages (TSS through +300 base pairs). Interestingly, B6 peritoneal macrophages recruit more RNA Pol II to the regions associated with polymerase pausing, suggesting that this step in transcription may be differentially regulated between B6 and MOLF to cause the expression change in CYLD. Furthermore, if this is the case, a *cis*-acting element likely underlies this defect because the trait was genetically mapped to this locus. If a *cis*-acting polymorphism underlying the difference exists, it must be present outside of the 2 kb of promoter upstream of *Cyld* and 1 kb downstream of the TSS that has currently been sequenced. To more completely understand whether a *cis*-acting element in MOLF confers resistance to necroptosis and TLR-stimulated acute down-regulation of CYLD, congenic mice containing the MOLF allele at this locus on the B6 background are currently being generated.

CYLD expression and susceptibility to necroptosis are restored in MOLF BMDM

To formally demonstrate that the loss of CYLD activity caused resistance to TLR-induced necroptosis in MOLF peritoneal macrophages, an attempt to add-back this gene in MOLF cells was made. Unfortunately, peritoneal macrophages were unable to be efficiently transfected or transduced with lentivirus to re-express CYLD into MOLF cells due to the short time of survival of these cells *ex vivo* and their poor transfectability. Unfortunately, the Poltorak laboratory does not have access to an immortalized MOLF peritoneal macrophage cell line. The next best option was to characterize CYLD

expression in MOLF BMDM. However, the susceptibility to necroptosis induced by 100 ng/ml LPS or imiquimod in the presence of ZVAD was equal in B6 and MOLF (Figure 16A). To determine whether CYLD expression correlated with the susceptibility to necroptosis, BMDM from each strain were stimulated with LPS and mRNA was quantified using qPCR. Interestingly, expression of the full-length isoform of CYLD in MOLF mirrored that of B6, with both strains up-regulated CYLD expression following LPS stimulation (Figure 16B). Comparing the data between the two types of macrophages can be reconciled because the mechanism of regulation in MOLF peritoneal macrophages (such as RNA Pol II pausing) may be overcome by an M-CSF-driven signal in BMDM differentiation (273), which would allow for up-regulation of CYLD and thus susceptibility to necroptosis.

The concept of the "loss" of a phenotype in MOLF BMDM has been observed previously in our laboratory in the case of MRC1 expression and response to CpG ODN (254). In peritoneal macrophages, MOLF do not express MRC1 due to a mutation in the promoter region, rendering them unable to express this gene and respond to TLR9 ligation by CpG. However, in BMDM the M-CSF signal from differentiation media is sufficient to up-regulate MRC1 expression and permit CpG-driven responses. The difference in the origin of BMDM and peritoneal macrophages (one week of *in vitro* culture versus *ex vivo,* respectively) leads to differences in functionality of the cells and likely their gene expression profiles (274). Additionally, a preliminary characterization of MOLF compared to B6 peritoneal macrophages demonstrated that MOLF express a lower level of F4/80 staining in comparison to B6, which could indicate a less mature monocytic state (275, 276). However, substantially more work needs to be performed to

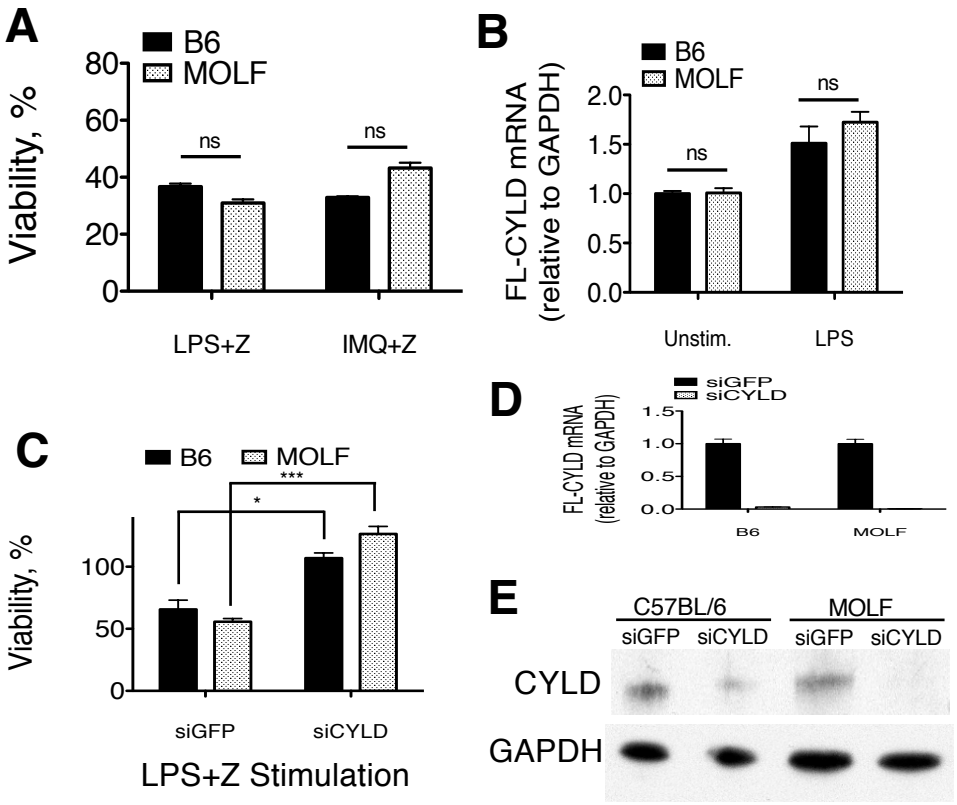

Figure 16. **CYLD expression and susceptibility to necroptosis are restored in MOLF BMDM.** (A) B6 and MOLF BMDM stimulated with LPS (100 ng/ml) or IMQ (5 μg/ml) and ZVAD (Z) (25 μM) for 18 hours. (B) Quantitative real-time PCR performed on cDNA reverse-transcribed from total RNA from unstimulated and LPS-stimulated B6 and MOLF BMDM. The full-length (FL) CYLD/ GAPDH ratio is presented as relative amounts in comparison to B6 unstimulated cells. (C) BMDM infected with lentivirus containing siGFP or siCYLD hairpin stimulated with LPS (100 ng/ml) and zVAD (25 μM) for 18 hours. (D) Relative expression of FL-CYLD as measured by qPCR in B6 and MOLF BMDM stimulated for 4 hours with LPS. (E) CYLD protein expression in B6 and MOLF BMDM measured by Western blot analysis in unstimulated cells. GAPDH was used as a loading control. A and C, cell viability was measured relative to cells in medium with vehicle (DMSO). Data are mean +/- S.E. from one representative experiment of three independent experiments. Statistical significance was determined by Student's t test. *, $p < 0.05$; ***, $p < 0.0001$; ns, not significant.

characterize these cells including staining for other markers such as Ly6C, Ly6G, Cd11b, and Cd11c.

The data on cell viability suggest that the MOLF signaling network is fully capable of activating TLR-induced necroptosis if CYLD is expressed at the same level as B6. To further demonstrate this point, knockdown was performed using transduction of shRNA-containing lentiviruses targeting CYLD or GFP. For B6 and MOLF BMDM, control hairpins targeting GFP left BMDM susceptible to LPS-mediated cell death in the presence of ZVAD, whereas knockdown of CYLD protected cells from death (Figure 16C). The knockdown efficiency was over 95% at the RNA level and was also quite efficient, particularly in the case of MOLF BMDM at the protein level (Figure 16D). While N2 mapping in peritoneal macrophages revealed resistance to TLR-induced necroptosis that was linked to a *Cyld*-containing locus on Chromosome 8, MOLF BMDM stimulated under the same conditions were susceptible to RIP1 kinase-dependent cell death in the presence of ZVAD. These data implicate *Cyld* as the gene underlying MOLF resistance in peritoneal macrophages, albeit circumstantially, because in MOLF BMDM, which are susceptible to necroptosis, CYLD is expressed at the same level as B6. Conversely, in peritoneal macrophages acute TLR-induced down-regulation of CYLD occurs in MOLF cells, rendering them resistant to necroptosis (Figure 17).

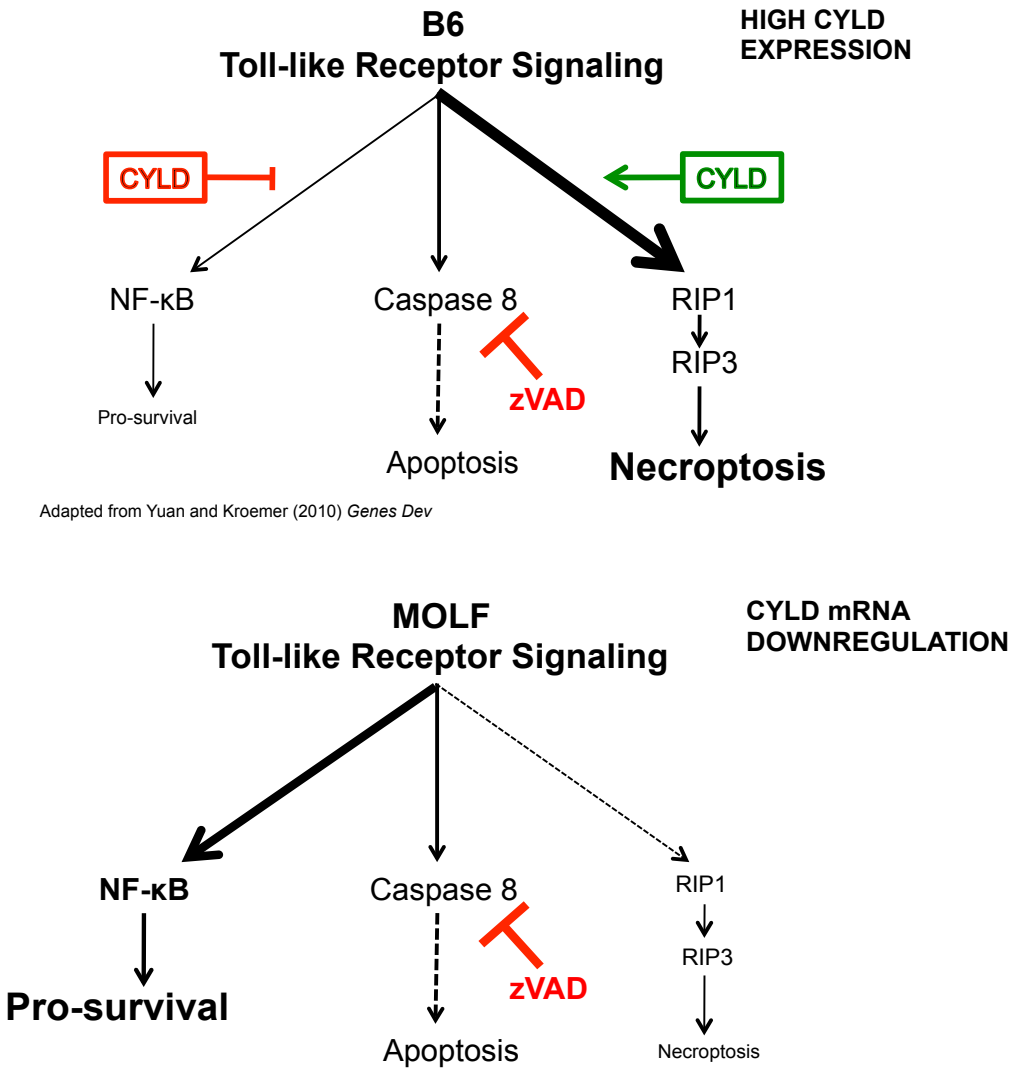

Figure 17. **Schematic of the impact of CYLD regulation on pro-survival and necroptotic signaling.** Stimulation of TLRs in B6 and MOLF peritoneal macrophages can activate pro-survival signals or cell death. When caspases are inhibited with ZVAD, it predisposes cells a binary choice: survival or death by RIP1 kinase dependent necroptosis. In B6 peritoneal macrophages, CYLD is expressed at high levels and promotes necroptosis while negatively regulating pro-survival signals. In MOLF peritoneal macrophages, TLR signaling down-regulates CYLD protein levels are reduces the pro-death signal downstream of TLRs. Adapted from Yuan and Kroemer (2010) *Genes Dev* (277).

CHAPTER 6: RIP1 KINASE-DEPENDENT CYTOKINE PRODUCTION

Multiple recent reports have identified a role for RIP1 kinase activity to drive cytokine production in addition to executing necroptosis (191, 194). In vitro studies in various cell types and agonists previously demonstrated that the scaffolding function of RIP1 important, though not absolutely required, for pro-inflammatory signaling through TNF-R1 and TLRs (51, 124, 182). However, RIP1 kinase activity activates necroptosis when caspases are inhibited during cell stimulation. One explanation for the lack of contribution of the kinase activity to pro-inflammatory cytokine production and cell death *in vitro* is its negative regulation by caspases (144, 278). When caspases are inhibited by the pan-caspase inhibitor ZVAD, RIP1 kinase may be 'released' to exert its effects on cellular signaling pathways. Studies by multiple groups, including our collaborators in the Degterev laboratory, have identified that RIP1 kinase activity contributes to cytokine production in whole mouse *in vivo* modes, suggesting that the molecular components of this signaling pathway warrant elucidation.

Necrostatin-1 treatment does not impact pro-inflammatory cytokine production in macrophages with activate caspases

As mentioned above, previous reports showed that a kinase inactive RIP1 mutant does not impact cytokine production in RIP1 dependent signaling pathways. To examine whether treatment with the RIP1 kinase inhibitor Nec-1 has the same effect, B6 and MOLF BMDM were stimulated with TLR agonists and treated with Nec-1. Production of TNF and IL-6 induced by LPS, LTA, or imiquimod was not affected by RIP1 kinase inhibition (Figure 18), in agreement with previous studies (132).

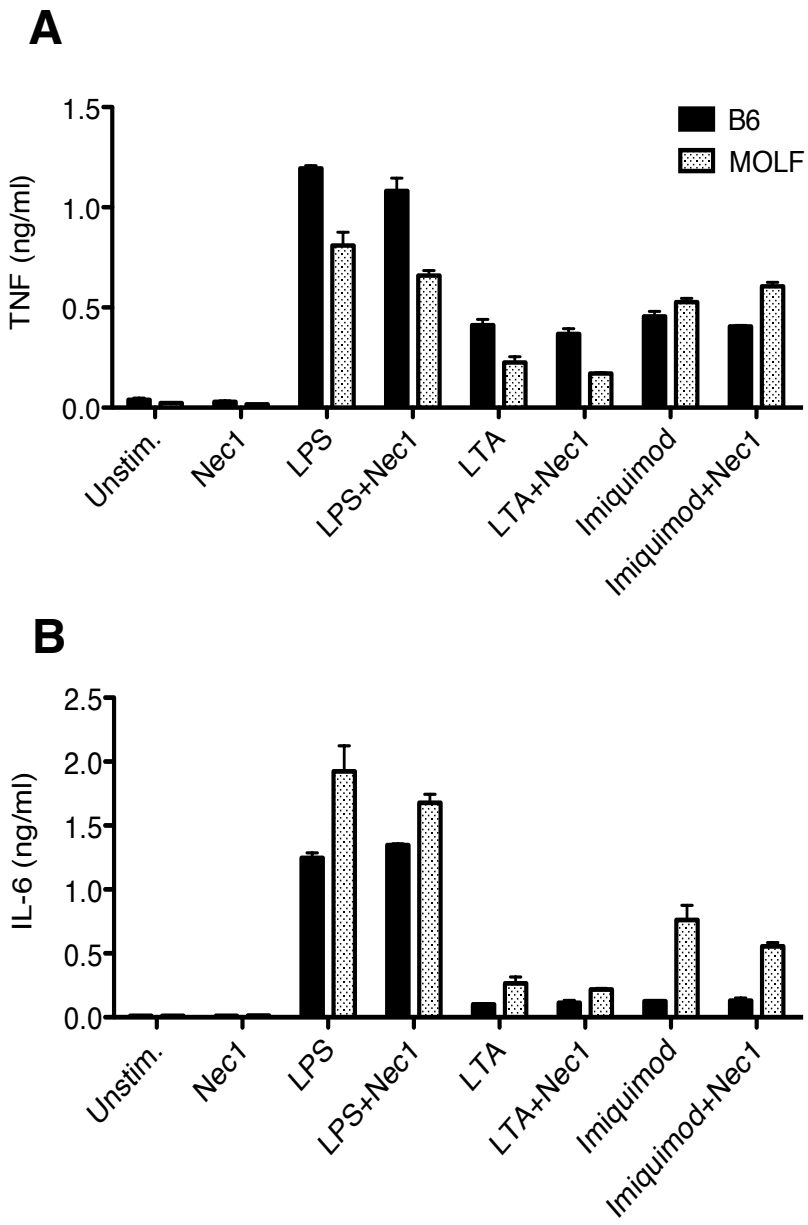

Figure 18. **Necrostatin-1 treatment does not affect cytokine production in BMDM.** B6 and MOLF BMDM were stimulated with or without Nec-1 (30 μM) for 6 hours. Agonists used were LPS (100 ng/ml), LTA 2 μg/ml, and imiquimod (5 μg/ml). TNF (A) and IL-6 (B) levels in the supernatant measured by ELISA. Data are mean +/- S.D. from one representative experiment of at least three independent experiments.

RIP1 kinase activity contributes to cytokine production in *Casp8*$^{-/-}$*Ripk3*$^{-/-}$ macrophages

To investigate whether RIP1 kinase-dependent pro-inflammatory signaling occurs in an environment without caspase-inhibition, *Casp8*$^{-/-}$ immortalized macrophages were obtained, which also lacked RIP3 to exclude a contribution of this molecule and its pro-death effects. Compared to wild-type cells, *Casp8*$^{-/-}$*Ripk3*$^{-/-}$ macrophages produce less TNF after LPS stimulation (Figure 19A). Additionally, while Nec-1 treatment had no effect on TNF production in wild-type macrophages, it caused a significant decrease in TNF production in *Casp8*$^{-/-}$*Ripk3*$^{-/-}$ cells after 4 hours of LPS stimulation and a strong trend toward significance at 6 hours. (Figure 19B). Additionally, IL-6 production was affected similarly, though with statistical significance at 6 hours (Figure 19C). Finally, Though interferon beta production was reduced by Nec-1 but did not reach statistical significance (Figure 19D). Together, these data establish that RIP1 kinase contributes to TNF, IL-6 and potentially type I interferon production in conditions without caspase-8 activity is absent in a RIP3 independent manner. Whether RIP1 requires RIP3 for pro-inflammatory cytokine production is not clear as different models have suggested RIP1 acts independently from RIP3 to produce IL-1α (279), that RIP1 and RIP3 contribute to TNF production in the absence of IAPs (193), and that RIP1, RIP3, and MLKL contribute to inflammasome activation (196). Thus, the necessity for RIP1, RIP3, and MLKL in pro-inflammatory cytokine production through the 'necroptosis' pathway involving RIP1 kinase activity likely differs based on stimulus and cell type.

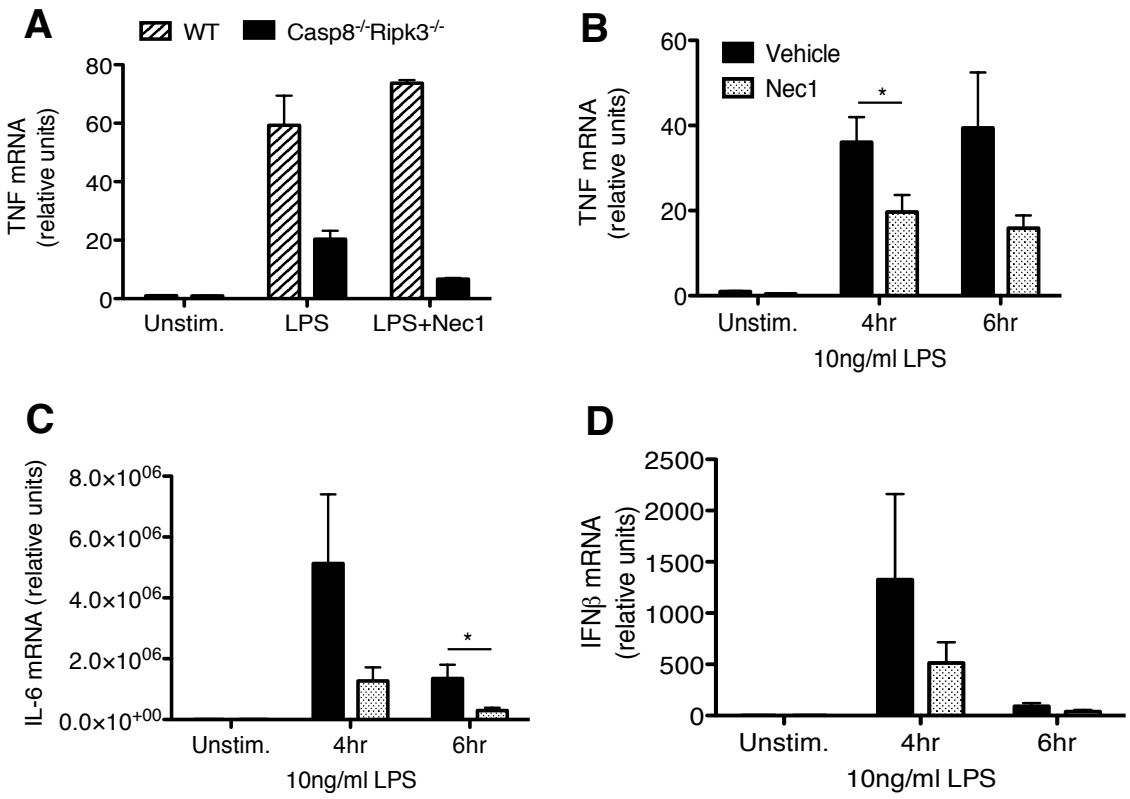

Figure 19. **RIP1 kinase activity contributes to cytokine production in *Casp8$^{-/-}$Ripk3$^{-/-}$* macrophages.** (A) Wild-type (B6) and *Casp8$^{-/-}$Ripk3$^{-/-}$* (DKO) immortalized macrophages were stimulated with LPS (10 ng/ml) for four hours with and without Nec-1 (30 μM). TNF mRNA was measured by qPCR. Relative amounts normalized to GAPDH and presented as fold-increase over unstimulated. (B-D) *Casp8$^{-/-}$Ripk3$^{-/-}$* (DKO) macrophages stimulated for the indicated times with LPS (10 ng/ml) with or without Nec-1 (30 μM). TNF (B), IL-6 (C), or IFNβ (D) mRNA measured by qPCR. Relative amounts normalized to GAPDH and presented as fold-increase over unstimulated. Data are mean +/- S.E. from one (A), three (C,D), or four (B) pooled independent experiments. Statistical significance was determined by Student's t test. *, $p < 0.05$.

ZVAD treatment leads to a RIP1 kinase-dependent increase in TNF and IFNβ, which is augmented in MOLF over B6

After demonstrating that RIP1 kinase activity contributes to pro-inflammatory cytokine output in caspase-8-deficient conditions in an immortalized cell line, primary cells were tested for their response to LPS stimulation in the presence of chemical inhibition of caspases with ZVAD. To attempt to recapitulate a state in which caspases are less active in the cell to release RIP1 from caspase-8-mediated inhibition, cells were pre-treated with inhibitors for 30 minutes prior to stimulation with LPS and left in the inhibitors through the duration of stimulation. B6 and MOLF BMDM were assessed for the contribution of RIP1 kinase dependent signaling to TNF, IL-6, CCL3, CXCL2, and IFNβ mRNA production after four hours of LPS stimulation. Though ZVAD treatment alone did not induce detectable levels of cytokines, stimulation with LPS and ZVAD produced a drastic increase in all of the above cytokines with the exception of IL-6 (Figure 20A-E). This increase was likely RIP1 kinase dependent as it was inhibited by Nec-1. However, as noted previously, Nec-1 had no effect on LPS stimulation without ZVAD. Furthermore Though B6 levels were certainly augmented with ZVAD, the levels of cytokines produced in MOLF were elevated far higher than their B6 counterparts, a similar trend was observed when protein levels in cell-free supernatant were assessed by ELISA for TNF and IFNβ after six hours of stimulation (Figure 20F-G). The ELISA data are critical because of the confounding factor of cell death in these assays. Unlike other work performed in dendritic cells (196), TLR stimulation of BMDM in the presence of ZVAD induces cell death even at four hours (Figure 20H). Though MOLF and B6 appear to be similarly resistant to death at this timepoint, it is possible that cell death may have

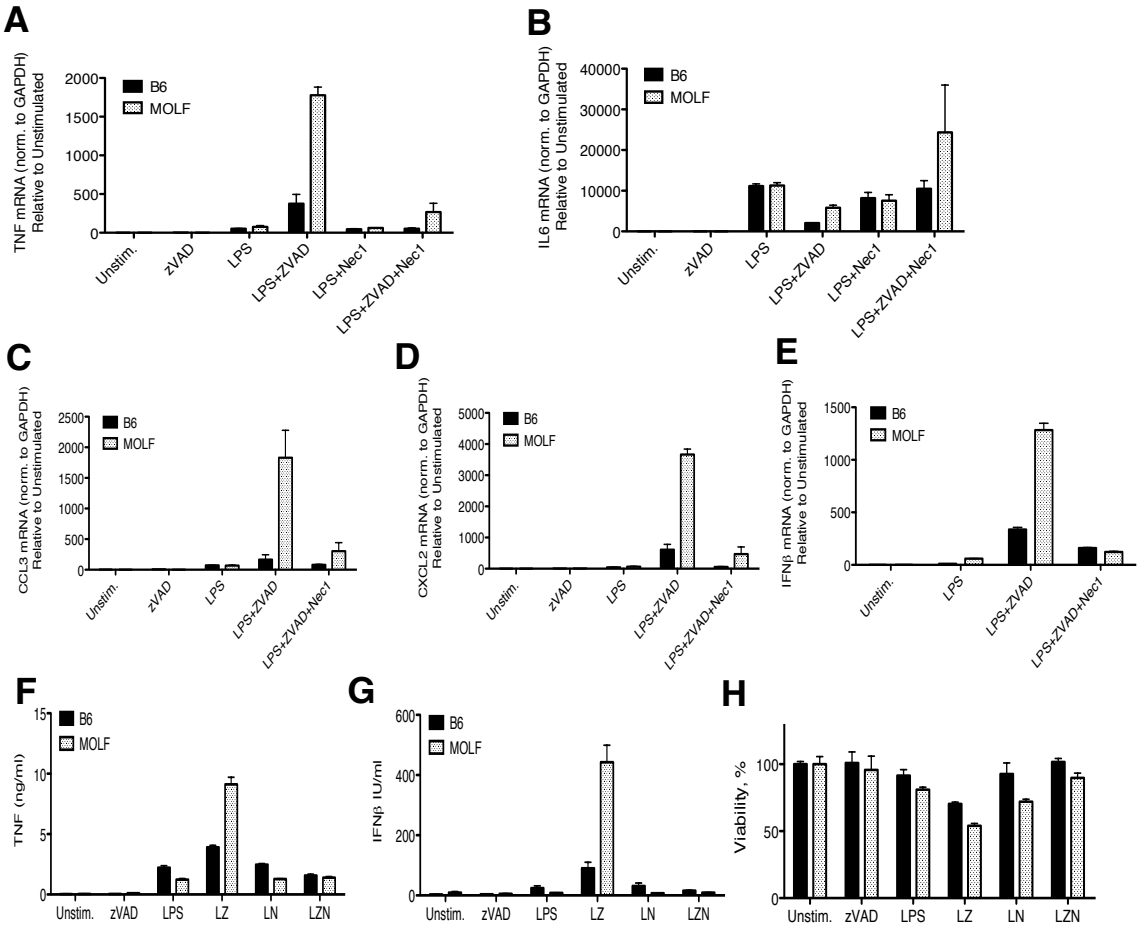

Figure 20. **ZVAD treatment induces RIP1 kinase-dependent cytokine and type I interferon production to a greater degree in MOLF than B6.** B6 and MOLF BMDM were stimulated with LPS (10 ng/ml) with the indicated inhibitors (50 μM ZVAD, 30 μM Nec-1) or vehicle control for 4 hours following a 30 minute pre-treatment of cells with inhibitors alone. Expression of mRNA for TNF (A), IL-6 (B), CCL3 (C), CXCL2 (D), and IFNβ (E) was measured by qPCR. Each sample was normalized to GAPDH expression and the fold-increase of the ratio in stimulated samples over the ratio in unstimulated samples is presented. Levels of TNF (F) or IFNβ (G) in the supernatants of cells treated as above for 6 hours were measured by ELISA. Viability of cells stimulated for 6 hours (F,G) was measured by ATP levels using the CellTiter-Glo assay. Values are a percentage of viable treated cells relative to cells in medium with vehicle (DMSO). Data are mean +/- S.E. (A-E,H) or S.D. (F,G) from one representative experiment of three (A,E), two (B,F-H), or one (C,D) independent experiments.

skewed the results in quantitative PCR that is normalized to expression of GAPDH. Therefore, the ELISA data help to establish that a hyper-production of cytokines is occurring in MOLF even in the presence of cell death. MyD88-dependent TLR2 and TLR7 did not induce elevated cytokine production with ZVAD, suggesting that TRIF-dependent signaling was required, though this has not yet been explicitly tested.

MOLF RIP1 kinase response requires p38 activity whereas both mouse strains require TAK1

Previous studies explored only the pathways activated through the scaffolding function of RIP1. In the case of caspase inhibition-induced RIP1 kinase activity driven transcription through TLR4, the specific signaling pathway leading to augmented cytokine production and release is unknown. First, the use of chemical inhibitors was used to investigate the importance of specific MAPKs. The MOLF macrophage response to TLR agonists hyper-activates the p38 MAPK pathway (43). To test whether p38 activation contributes to cytokine production by MOLF or B6 BMDM, the p38 inhibitor VX-702 was delivered to cells 30 minutes prior to stimulation. Though p38 inhibition had no effect on B6 TNF mRNA production and increased IFNβ mRNA production. However, in MOLF BMDM VX-702 treatment significantly deceased mRNAs from both TNF and IFNβ, suggesting a role for p38 in MOLF but not B6 RIP1 kinase-mediated signaling (Figure 21A-D). To investigate a MAP3K that is involved in activating multiple arms of the MAPK and IKK signaling pathways, TAK1 was inhibited using (5Z)-7-Oxozeaenol (5z7). TAK1 is known to promote RIP1 kinase dependent cell death (280–282) and may be an interaction target for pro-inflammatory signaling activation by RIP1

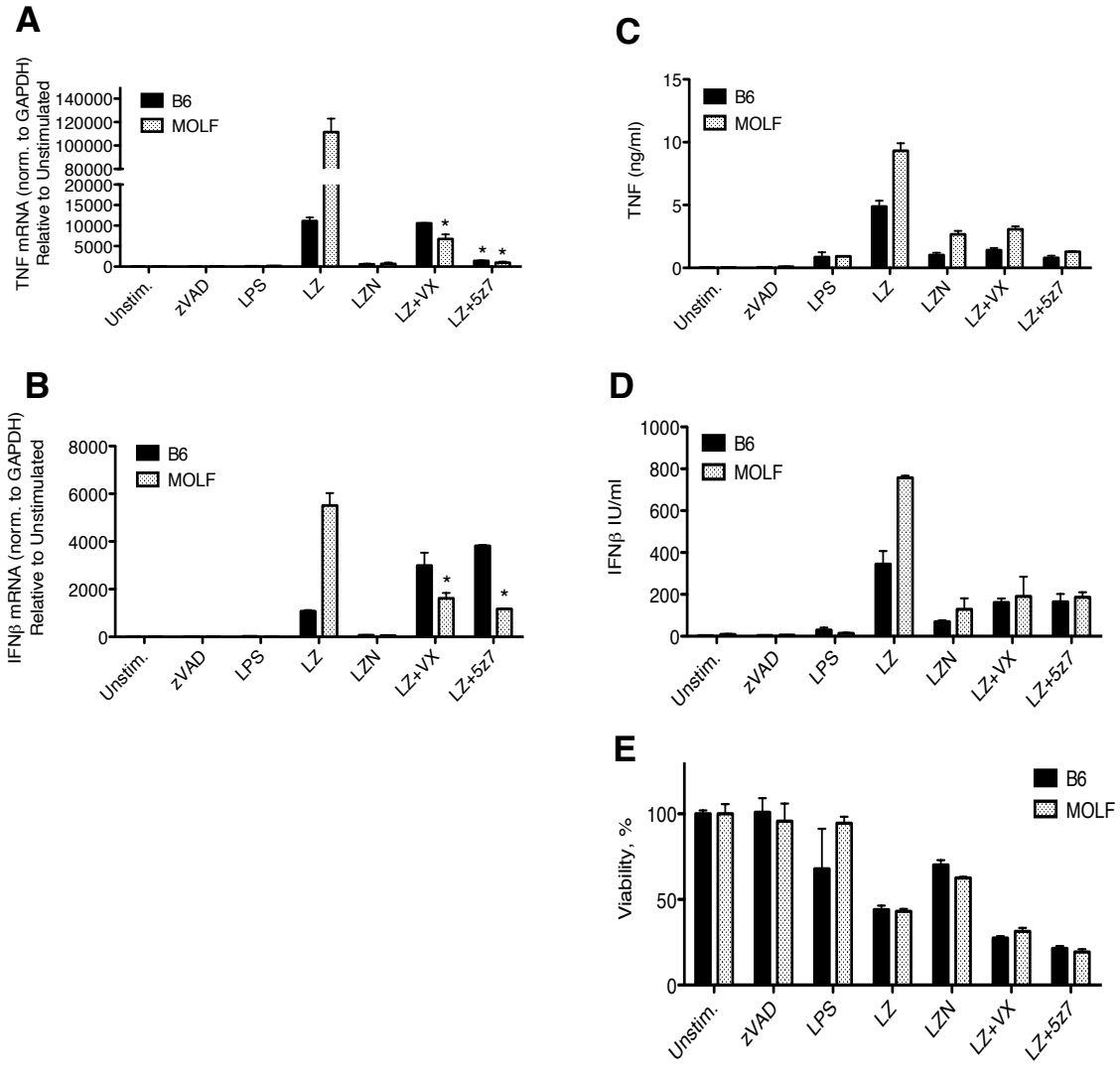

Figure 21. **Chemical inhibition of p38 reduces RIP1 kinase-dependent cytokine production in MOLF BMDM while TAK1 inhibition prevents RIP1 kinase-dependent cytokine production in B6 and MOLF.** B6 and MOLF BMDM were stimulated with LPS (10 ng/ml) with the indicated inhibitors (50 μM ZVAD, 30 μM Nec-1) or vehicle control for 4 hours following a 30 minute pre-treatment of cells with inhibitors alone. VX-702 (VX, 10 μM) and (5Z)-7-Oxozeaenol (5z7, 250 nM) were used to inhibit p38 MAPK and TAK1, respectively. Expression of mRNA for TNF (A) and IFNβ (B) was measured by qPCR. Each sample was normalized to GAPDH expression and the fold-increase of the ratio in stimulated samples over the ratio in unstimulated samples is presented. Levels of TNF (C) or IFNβ (D) in the supernatants of cells treated as above for 8 hours were measured by ELISA. Viability of cells stimulated for 8 hours (C,D) was measured by ATP. Values are a percentage of viable treated cells relative to cells in medium with vehicle (DMSO). Data are mean +/- S.E. (A,B,E) or S.D. (C,D) from one representative experiment of two independent experiments. Statistical significance was determined by Student's t test. *, $p < 0.05$ comparing a given point with the LPS+ZVAD-treated point within a given mouse strain.

kinase activity. Interestingly, TAK1 inhibition significantly decreased LPS with ZVAD-induced TNF production by both strains and had a statistically significant impact on IFNβ in MOLF (Figure 21A,B).

Similarly to stimulations with LPS and ZVAD without inhibitors, activation of BMDM with LPS, ZVAD, and either VX-702 or 5z7 induces cell death. Though LPS and ZVAD alone may not induce sufficient cell death to interfere with cytokine accumulation by eight hours (Figure 21E), adding addition inhibitors increased the amount of cell death in both strains and may have confounded the ELISA results (Figure 21C-D). However, through data analyzing RNA, important roles for p38 and TAK1 are evident in MOLF and in both strains, respectively.

ZVAD induces sustained RIP1 kinase dependent MAPK activation that is hyper-activated in MOLF.

To examine the intracellular signaling events that coincide with ZVAD-induced hyper-production of cytokines, protein analysis using SDS-PAGE and western blotting was performed using specific antibodies for the phosphorylated forms of MAPK and TBK1. Because p38 inhibition had a striking effect on MOLF cytokine production, its activation status as assessed by phosphorylation was assessed. LPS stimulation alone and with Nec-1 leads to a tapering of p38 MAPK phosphorylation at one hour that is even weaker at two hours in both strains (Figure 22A). Although B6 BMDM also show this similar pattern in LPS-treated cells with ZVAD while MOLF BMDM sustain p38 phosphorylation through four hours. Next, JNK and ERK phosphorylation were assessed in parallel to p38 (Figure 22B). In B6 and MOLF, JNK is sustained through four hours,

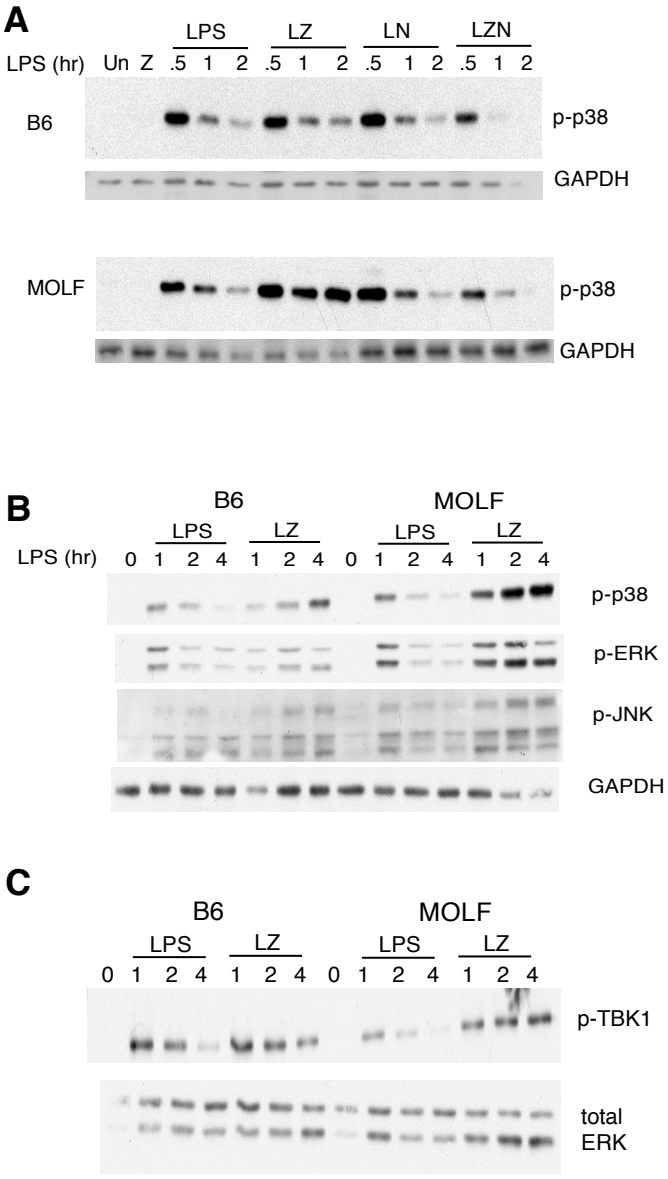

Figure 22. **ZVAD treatment induces RIP1 kinase-dependent MAPK phosphorylation, which is hyperactivated in MOLF.** B6 and MOLF BMDM were pre-treated with inhibitors (ZVAD+/-Nec1) for 30 minutes prior to activation with LPS (10 ng/ml) for the indicated times. Cytoplasmic lysis was performed and proteins separated by SDS-PAGE. (A) Western blotting performed for phospho-p38 after stimulation with ZVAD alone (Z) (50 μM) or with LPS treated with ZVAD and/or Nec-1 (30 μM). GAPDH used for loading control. (B) Western blotting performed for phospho-p38, phospho-ERK, phospho-JNK after stimulation with LPS with or without ZVAD. GAPDH used as loading control. (C) Western blotting performed for phospho-TBK1 after stimulation with LPS with or without ZVAD. Total ERK used as loading control. Films representative of at least two independent experiments.

while ERK phosphorylation seems to be sustained only in MOLF. The activation of JNK in a RIP1 kinase dependent fashion by TLRs is reminiscent of a study performed in L929 fibroblasts with ZVAD stimulation showing that JNK activation is important in RIP1 kinase-mediated TNF production (191). Further analysis of the MAPK pathway activation will be required as TAK1 has the capacity to activate p38, ERK, and JNK either directly through MAP2K (p38 and JNK) or indirectly through activation of IKK causing Tpl2 to signal (for ERK) (61). Finally, in concordance with IFNβ production, both MOLF and B6 sustain phosphorylation of TBK1, an IKK-related kinase that leads IRF3 dimerization and translocation into the nucleus (Figure 22C).

IRAK2 knockdown reduces MOLF TNF production but has a minor impact on p38 phosphorylation

As mentioned above, the MOLF hyper-responsiveness to TLR agonists has been mapped to a high level of p38 activation that is mediated by a pro-inflammatory isoform of IRAK2 (43). Because RIP1 kinase-mediated signaling showed sustained MAPK activation and increased cytokine levels, the role of IRAK2 was investigated using a lentiviral knockdown in BMDM. In control (siGFP) lentivirus infected cells, LPS with ZVAD produced a substantial increase in TNF production that was abrogated with Nec-1 in B6 and substantially reduced by Nec-1 in MOLF (Figure 23A). IRAK2 knockdown (levels measured in Figure 23B) had a statistically significant but modest effect on TNF production by B6 while it dramatically reduced MOLF TNF production. These data suggest that IRAK2 may be complementing RIP1 kinase dependent signaling in MOLF

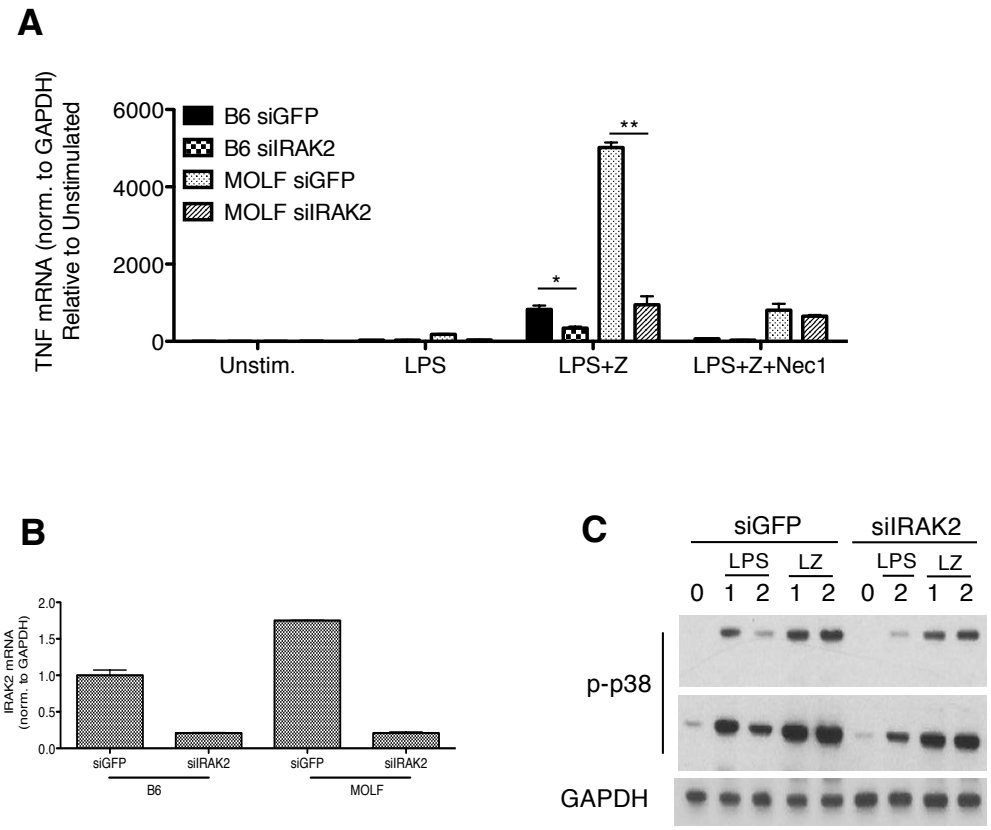

Figure 23. **IRAK2 knockdown substantially reduces MOLF TNF production but has a modest effect on p38 phosphorylation.** B6 and MOLF BMDM were transduced with lentivirus containing shRNA targeting GFP (siGFP) or IRAK2 (siIRAK2) and stimulated with LPS (10 ng/ml) in the presence of ZVAD (50 μM) with or without Nec-1 (30 μM) after 30 minute pre-treatment with inhibitors (A) TNF mRNA production measured by qPCR after 4 hours LPS stimulation. (B) Efficiency of IRAK2 knockdown in unstimulated cells was assessed by qPCR, presented relative to B6 siGFP. (C) MOLF BMDM cytoplasmic lysates collected and separated by SDS-PAGE. Western blotting for phospho-p38 performed in short (top panel) and long (middle panel) exposures. GAPDH used as loading control. Images representative of two independent experiments. Statistical significance was determined by two-tailed Student's *t* test. *, $p < 0.05$; **, $p < 0.001$.

cells to assist in the high production of TNF and potentially other pro-inflammatory cytokines. To examine whether IRAK2 also reduced the heighted and sustained p38 phosphorylation in MOLF, lysates from LPS stimulation with and without ZVAD from MOLF BMDM infected with lentivirus targeted GFP or IRAK2 were subjected to SDS-PAGE and western blotting for phospho-p38. In contrast to the substantial decrease in TNF production with IRAK2 knockdown in MOLF, the level of p38 was slightly decreased but still hyper-activated and sustained in comparison to siGFP (Figure 23C). These data suggest that IRAK2 does play a role in controlling or enhancing RIP1 kinase-dependent pro-inflammatory cytokine production but that other factors are also critical, at least in the maintaining the activation of MAPK. One potential interacting protein that could bridge IRAK family members and RIP1 is FADD. FADD has been shown to interact with IRAK1 and negatively regulate signaling (283), however, in conditions where RIP1 is not inhibited by caspases FADD may form a bridge between IRAK2 and RIP1 that allows for synergy between these to kinases (Figure 24).

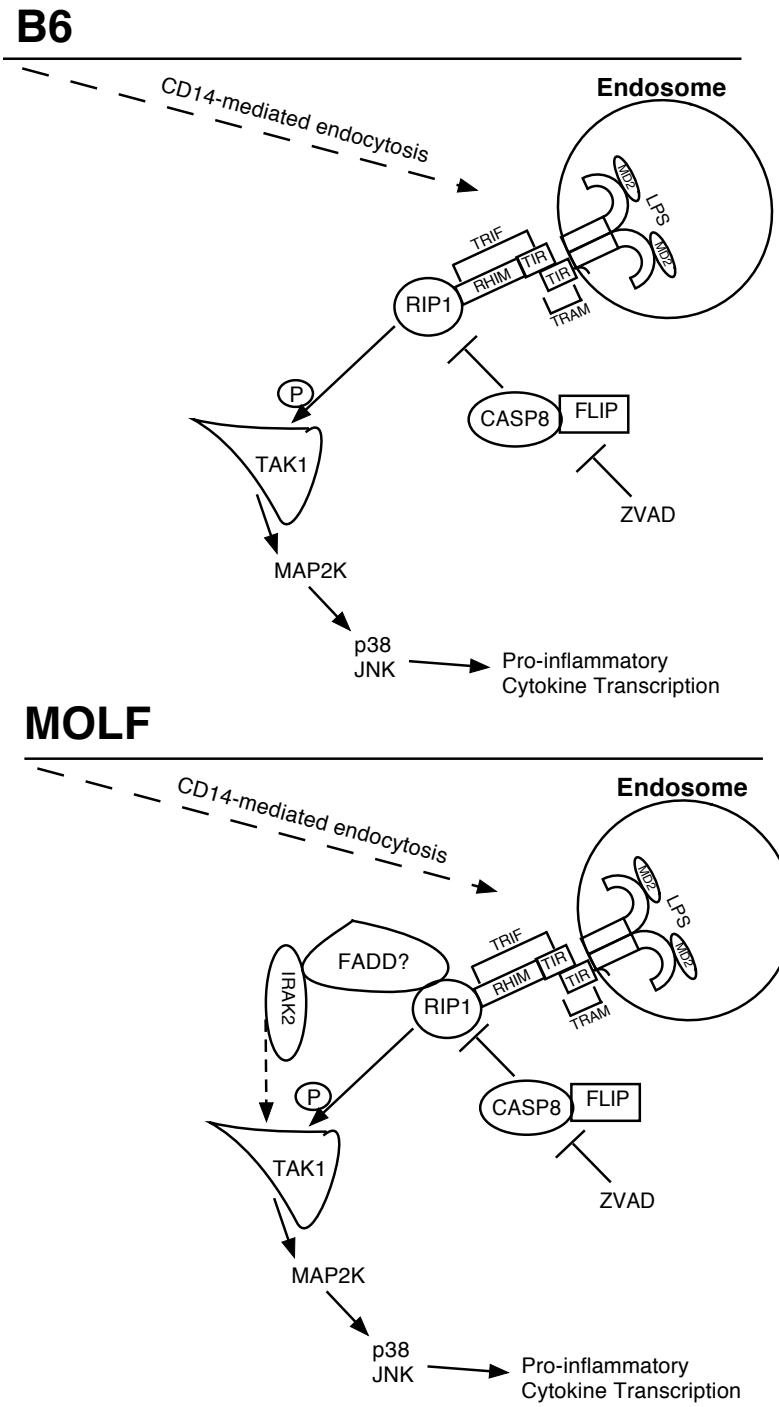

Figure 24. **Proposed model for B6 and MOLF RIP1 kinase dependent pro-inflammatory signaling cascade.** In B6 and MOLF BMDM, treated with ZVAD induces cytokine production and MAPK activation dependent on RIP1 kinase activity (inhibited by Nec-1). In both strains, ZVAD augments cytokine production, which is heightening in MOLF. IRAK2 knockdown reduces pro-inflammatory cytokines in MOLF but has a minor effect in B6. A possible interaction point for IRAK2 is through FADD, which has been shown to bind both RIP1 and IRAK family members (283).

CHAPTER 7: FORWARD GENETIC ANALYSIS OF TLR SIGNALING IN BMDM

Through mapping in peritoneal macrophages, the Poltorak laboratory has discovered a number of novel mechanisms by which TLR signaling is regulated (43, 242). Mapping using wild-derived mouse macrophages has identified that MOLF peritoneal macrophages produce high IL-6 following LTA stimulation (242), are hypo-responsive to CpG DNA activation with regard to all cytokines (254), and o not respond fully to TLR3 stimulation (253). While peritoneal macrophages serve as a standard model for the study of macrophage responses in vitro, a number of experimental drawbacks limit the study of these cells (Chapter 5). Peritoneal macrophages are difficult to transfect with plasmid DNA or to infect with retrovirus or lentivirus, thus making overexpression and knockdown of genes difficult. A widely used experimental *in vitro* macrophage system in which genes are more reliably overexpressed and knocked down is bone marrow-derived macrophages (BMDM). BMDM are derived from mouse bone marrow through one-week incubation in M-CSF-conditioned media. In the experience of the Poltorak laboratory, MOLF peritoneal macrophages and BMDM share many phenotypes but differ in others (242, 254). To accomplish the first mapping panel in F2 BMDM (B6xMOLF to generate F1, which were intercrossed) from 69 mice were screened. Through the collaboration with the Poltorak laboratory at Petrozavodsk State University, genome-wide scan microsatellite marker genotype was completed.

A locus on Chromosome 10 contributes to high IL-6 production in MOLF BMDM

MOLF peritoneal macrophages and BMDM display a more rapid and robust IL-6 production at mRNA and protein level than B6 (43, 242). LTA stimulation also led to a specific hyper-activation of p38 and NF-κB but not ERK or JNK. Forward genetic analysis mapped the hyper-IL-6 production trait to *Irak2*, an important serine/threonine kinase in TLR/IL1R signaling (39, 42). Knockdown of MOLF IRAK2 had a significantly greater impact on IL-6 production, p38 activation, and NF-κB activation in MOLF macrophages than in B6 macrophages. In MOLF, a mutation in the promoter of the inhibitory isoform IRAK2c diminishes expression of this protein (43). Without expression of IRAK2c, the ratio of the pro-inflammatory IRAK2a isoform is increased in MOLF and permits hyper-response.

While IRAK2 is an important component in hyper-IL-6 production in MOLF, other genes contribute to this phenotype. A congenic B6 mouse containing the MOLF *Irak2* gene (the *Why1* mouse) produces high IL-6 in response to LTA. However, the *Why1* locus was not sufficient to recapitulate the hyper-p38 activation in parental MOLF cells (284), strongly suggesting that other genes are involved in MOLF hyper-IL-6 production, NF-κB activation, and p38 activation in response to LTA and potentially other TLR agonists. Furthermore, forward genetic analysis by James Conner revealed additional loci that confer high IL-6 production in response to LTA in MOLF peritoneal macrophages that did not reach significance on Chromosome 9 and Chromosome 10 (284).

Because previous forward genetic analysis was performed in peritoneal macrophages, BMDM were analyzed to confirm the existence of the IL-6 hyper-response phenotype to multiple TLR agonists. To examine the IL-6 response of BMDM to agonists in addition

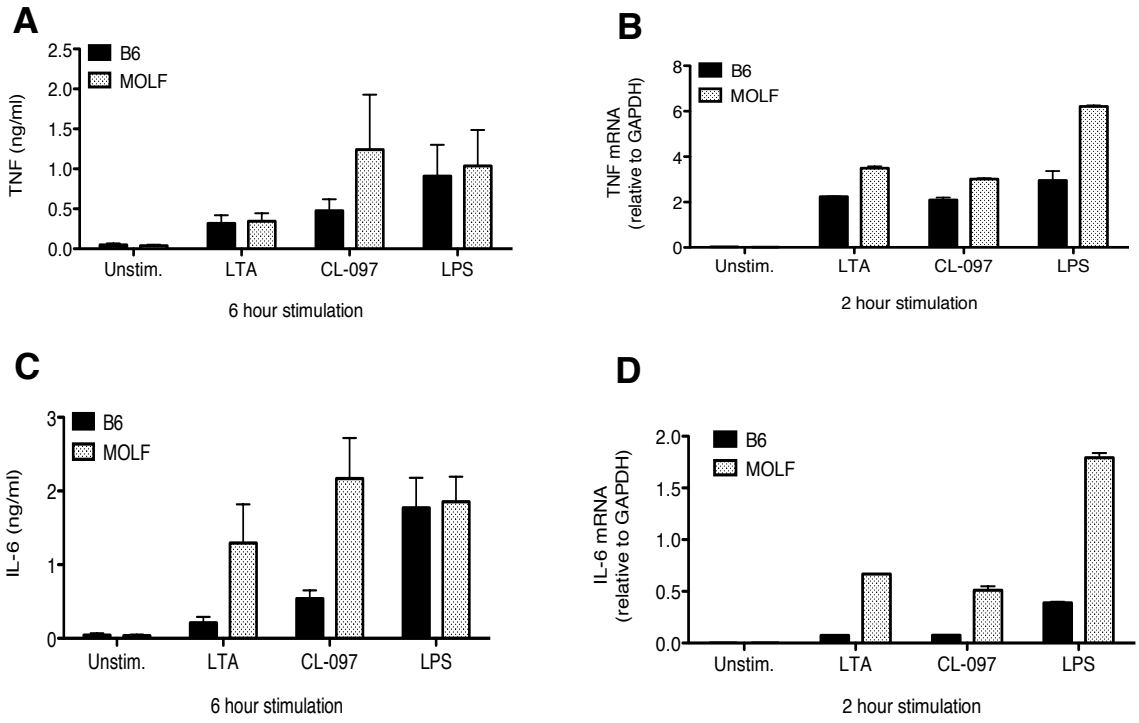

Figure 25. **MOLF BMDM hyper-IL-6 production in response to TLR2 and TLR7 agonists.** BMDM from B6 and MOLF were stimulated for the indicated times with LTA (2 μg/ml), CL-097 (1 μg/ml), or LPS (100 ng/ml). TNF was measured by ELISA (A) and qPCR (B). IL-6 was measured by ELISA (C) and qPCR (D). Data are pooled from four independent experiments (A, C) or are representative of at least three independent experiments (B, D).

to LTA, cells were stimulated with LTA, CL-097 (a TLR7 agonist), and LPS. While TNF levels were similar between B6 and MOLF BMDM in response to these agonists as measured by ELISA and qPCR (Figure 25A,B), MOLF showed a hyper-response to LTA and CL-097 by both ELISA and qPCR but LPS protein secretion was similar (Figure 25C,D). To investigate genes that are involved in IL-6 production, BMDM from a panel of 69 F2 mice were collected and stimulated for six hours with CpG or LTA (Figure 26A). Interestingly, IL-6 production by LTA or CpG showed a statistically significant correlation (Figure 26B). This analysis suggests that although LTA and CpG stimulate TLRs found in different cellular compartments, the response of these BMDM are similar, suggesting a common component underlies a substantial portion of the difference between B6 and MOLF responses.

Next, following genotyping of the F2 panel using microsatellite markers, QTL analysis was performed to identify genomic regions linked to IL-6 production in BMDM stimulated with LTA or CpG. The only significant region of linkage was located on Chromosome 10, within a 13 Mb region between *D10Mit52* and *D10Mit88*, which contains 107 protein-coding genes (see Appendix 4 for gene list). When mice were sorted based on genotyped at a marker within the region of highest linkage (*D10Mit40*), the MOLF allele conferred high IL-6 production (Figure 26C). Notably, this locus previously identified as a secondary locus in restriction of *Legionella pneumophila* intracellular growth in MOLF macrophages (285). Linkage to IL-6 production at this locus was significant, with logarithm of odds scores of 6.2 and 4.6 for LTA and CpG, respectively. While mice with a homozygous MOLF allele demonstrated significantly greater IL-6 production than homozygous B6, heterozygous mice were intermediate responders in

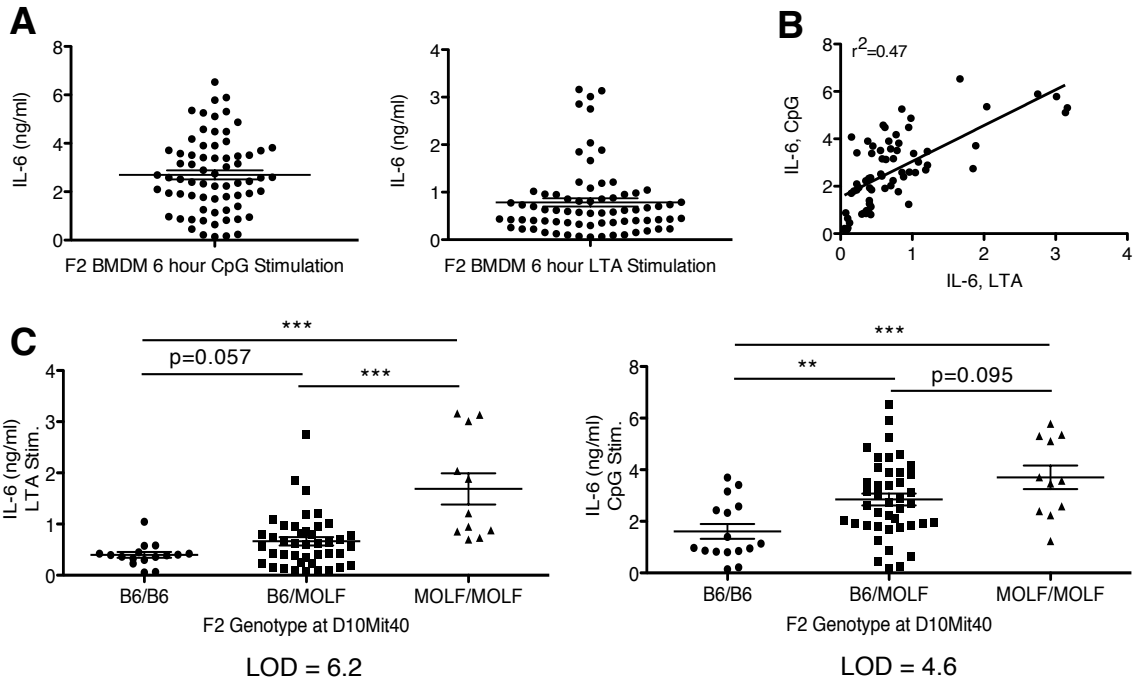

Figure 26. **High IL-6 production by MOLF BMDM in response to LTA or CpG stimulation is linked to a region on Chromosome 10.** (A) IL-6 secretion measured by ELISA from supernatants of BMDM from 69 F2 mice stimulated with CpG (200 nM) or LTA (2 μg/ml for 6 hours. Each circle represents an individual mouse. (B) Correlation of IL-6 production for LTA vs. CpG. (C) IL-6 ELISA of supernatants from BMDM from 69 F2 mice after stimulation with CpG or LTA for 6 hours grouped by genotype at D10Mit40 (microsatellite marker within the peak of highest linkage). Statistical significance was determined by Student's t test. **, $p < 0.001$.***, $p < 0.0001$.

LTA stimulation and covered a broad range in CpG stimulation. Because CpG hypo-responsiveness has been identified in MOLF macrophages, including BMDM, it is likely that other genes are contributing to the wide distribution of IL-6 production in F2 mice (254).

Low production of CXCL1 in MOLF BMDM maps to a locus on Chromosome 13

In contrast to the hyper-production of IL-6 when MOLF peritoneal macrophages stimulated with LTA, these cells are hypo-responsive to the TLR9 agonist CpG as measured by cytokine production. With IL-6 production as a read-out, this trait was mapped to a mutation in the promoter for the mannose receptor *Mrc1* that renders the protein not expressed in peritoneal macrophages (254). However, in BMDM Mrc1 is up-regulated and MOLF are able to respond to CpG through production of some cytokines, such as IL-6 whereas the response as measured by MAPK activation and production of other cytokines and chemokines such as TNF, CXCL1, CXCL2, and G-CSF (276). Because Mrc1 is up-regulated in BMDM, previous mapping data cannot explain the residual defect in BMDM signaling. To investigate the expression of CXCL1 and CXCL2 in BMDM, cells were stimulated with CpG and chemokine secretion was measured by ELISA after six hours. While CXCL1 production was low in MOLF and F1 BMDM when compared to B6 after CpG stimulation, production of CXCL2 was not different in CpG stimulation or in stimulation with other TLR agonists such as CL-097 and LPS (Figure 27A, B). To investigate whether the low production of CXCL1 was restricted to CpG stimulation, B6 and MOLF BMDM were stimulated with a panel of TLR agonists: CpG, LTA, CL-097, and LPS. In contrast to CXCL2, MOLF production of

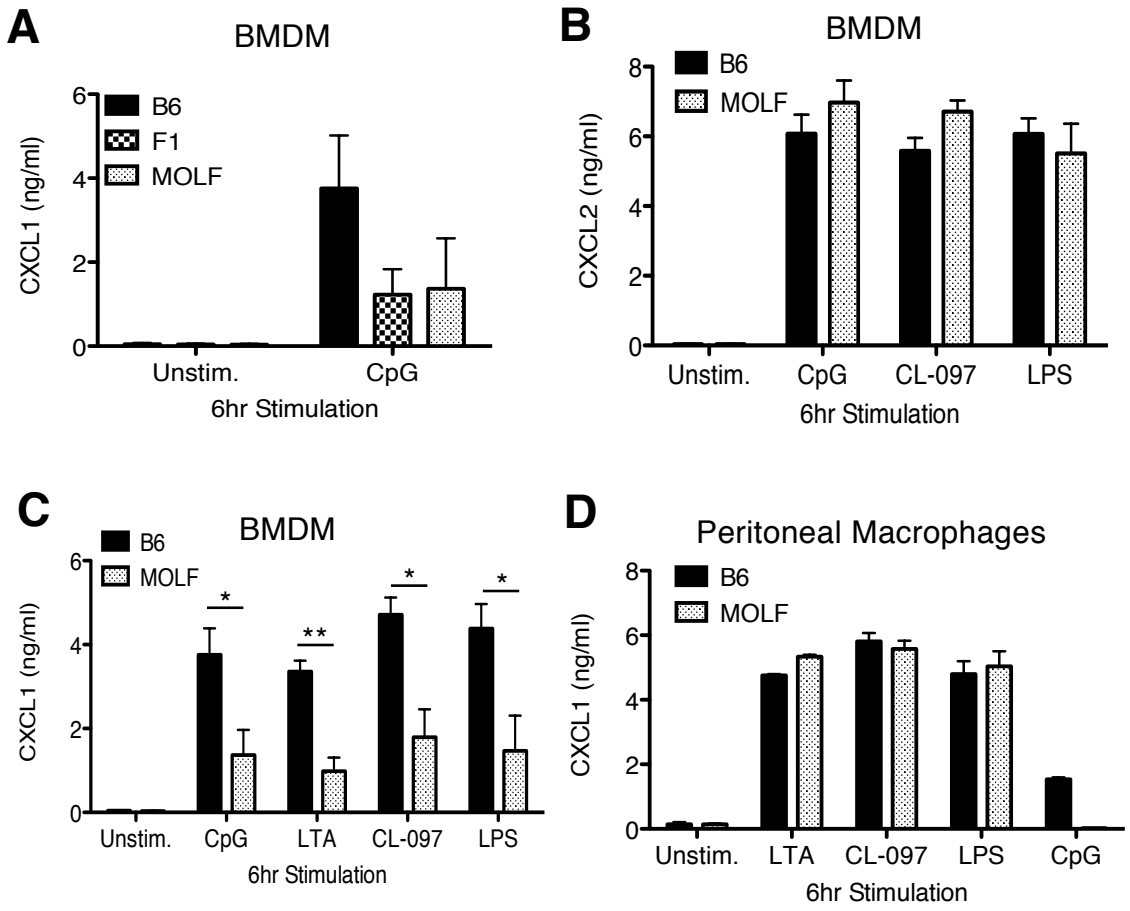

Figure 27. **MOLF BMDM produce low levels of CXCL1 in response to multiple TLR agonists.** (A) B6, F1, and MOLF BMDM stimulated with CpG (200 nM) for six hours. CXCL1 secretion measured by ELISA. (B) B6 and MOLF BMDM stimulated for six hours with CpG (200 nM), CL-097 (1 μg/ml), or LPS (100 ng/ml). CXCL2 secretion measured by ELISA. (C,D) B6 and MOLF BMDM (C) or peritoneal macrophages (D) stimulated for six hours with CpG, LTA (2 μg/ml), CL-097, or LPS in the doses indicated in (B). CXCL1 secretion measured by ELISA. Statistical significance (C) was determined by Student's *t* test for data from three independent experiments. *, $p < 0.05$; **, $p < 0.001$.

CXCL1 was lower than B6 following stimulation with each of the agonists (Figure 27C), suggesting a global defect in CXCL1 production. When peritoneal macrophages were assessed with the same TLRs, however, only CpG demonstrated a hypo-response (Figure 27D). These data suggest that there is a defect in CXCL1 production triggered by TLR signaling in BMDM that is not present in peritoneal macrophages. However, it is possible that molecules such as IRAK2 compensate for the low CXCL1 production in peritoneal macrophages, and the isolation of the gene underlying this trait may reveal a defect in its production in all tissues.

To identify genes that underlie low CXCL1 production, BMDM from 69 F2 mice were stimulated with CpG, LPS, or LTA for six hours followed by genotyping with microsatellite markers and quantitative trait linkage analysis with j/QTL (Figure 28A). In regard to CXCL1 production, there was an extremely strong correlation for each of the agonists, suggesting that the hypothesis that low CXCL1 production is common to multiple TLR signaling pathways (Figure 28B). Linkage analysis mapped this trait to a 8.6 Mb locus on Chromosome 13 containing 69 protein-coding genes (see Appendix 5 for gene list) with strongly correlated LOD scores: 10.02, 12.5, and 9.46 for CpG, LPS, and LTA stimulations, respectively. Importantly, there was no linkage to the *Cxcl1* locus itself, making a *cis*-acting defect in this gene unlikely. Through sorting CXCL1 responses based on genotype at the marker giving the highest linkage (*D13Mit24*), we determined this trait is dominant in MOLF (Figure 28C). The MOLF allele is dominant and correlates with low CXCL1 response to LPS, LTA, and CpG. This pattern of inheritance and resulting phenotype leads us to hypothesize that the gene of interest is an inhibitory molecule expressed in MOLF and not in B6. Thus, the heterozygous mice, containing one

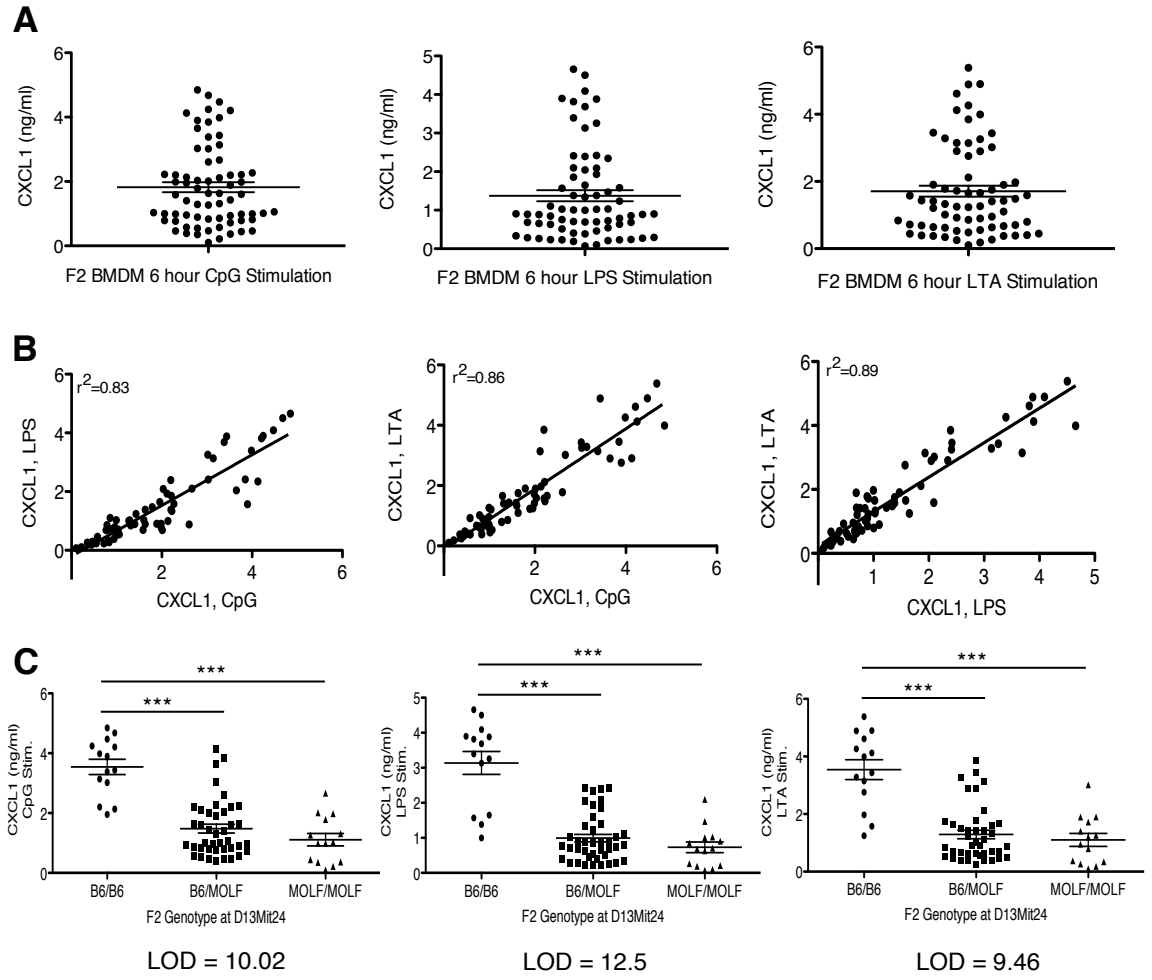

Figure 28. **Low production of CXCL1 in MOLF BMDM is linked to a 10 Mb region on Chromosome 13.** (A) CXCL1 secretion measured by ELISA from supernatants of BMDM from 69 F2 mice stimulated with CpG (200 nM), LPS (100 ng/ml), or LTA (2 μg/ml for 6 hours. Each circle represents an individual mouse. (B) Correlation of CXCL1 production for each agonist, CpG vs. LPS, CpG vs. LTA, and LPS vs. LTA. (C) CXCL1 ELISA of supernatants from BMDM from 69 F2 mice after stimulation with CpG, LPS, or LTA for 6 hours grouped by genotype at D13Mit24 (microsatellite marker within the peak of highest linkage). Statistical significance was determined by Student's t test. ***, $p < 0.0001$.

copy of the inhibitory molecule would be low responders while mice homozygous for the B6 allele, lacking the inhibitory molecule, are high responders.

CHAPTER 8: DISCUSSION

The primary goal of this thesis is to use the wild-derived mouse model system to uncover novel regulators necroptosis and cytokine production in macrophages activated though TLRs. Evolution leading to the sub-speciation of wild-derived mice produced a model with a great deal of genetic and phenotypic variation, both of which we exploit to investigate TLR signaling pathways using forward genetic analysis. In this section, the MOLF phenotypes of resistance to necroptosis, acute stimulus-dependent CYLD down-regulation, and heightened RIP1 kinase dependent cytokine production are discussed. Furthermore, the future directions of this work related to isolation of gene candidates through generation of congenic mice and expanded expression analysis using next generation sequences are presented.

MOLF resistance to necroptosis: Work beyond macrophages

Regulators of necroptosis

The major signaling molecules involved in necroptosis that are activated downstream of numerous signals are becoming well-established (134, 199). All triggers of necroptosis lead to activation of MLKL by RIP3, which requires RIP1 kinase activity in many, but not all instances (159, 163, 203). Some proteins that regulate TNF-R1 driven necroptosis, such as cIAP1/2 and CYLD are identified, but whether they are important regulators in all pathways leading to necroptosis or just to TNF-R1-dependent necroptosis is not yet clear. The work described in the preceding chapters aimed to use a forward genetic approach to identify proteins that regulate TLR-induced necroptosis. As is true with TNF-R1-mediated necroptosis, RIP1 kinase activity and RIP3 are required

for the TLR-driven activation of necroptosis in macrophages (Figure 5) (137, 251). Interestingly, while TLR2, TLR3, TLR4, TLR7, and TLR9 induced cell death, the MyD88-dependent TLRs required TNF-R1 to execute necroptosis, indicating an autocrine feedback loop was necessary (Figure 6), which is further supported by data showing the same phenotype in *Tnf*$^{-/-}$ macrophages (137). TRIF-dependent TLR3 and TLR4 were able to kill macrophages without TNF-R1 (Figure 6). Though not explicitly demonstrated by this work, others clearly established that direct necroptosis activation by TLR3 and TLR4 occurs through TRIF, which can recruit RIP1 and RIP3 through homotypic interactions in RHIM domains (137).

After establishing the core machinery of necroptosis is shared between TNF-R1 and TRIF-dependent TLRs, the next question was to assess whether regulatory proteins identified as important for TNF-R1 also affected TLR signaling. Because of the many shared molecules in these pathways, it would not be surprising that many regulatory mechanisms are identical, however, certain events such as RIP1 ubiquitination to activate pro-inflammatory cytokine production are mediated by different E3 ubiquitin ligases: cIAP1/2 for TNF-R1 signaling and Pellino1 for TLR3 signaling (133, 286). However, when caspases are inhibited, cIAPs prevent necroptosis driven through the Ripoptosome, TLR3, TLR4, and TNF-R1 (Figure 9) (76, 136, 155). Similarly, caspase inhibition is required for induction of necroptosis by TNF-R1 and TLRs. Finally, this study identified CYLD as a gene candidate underlying MOLF macrophage resistance to TLR-induced necroptosis. As was true for cIAPs and caspase-8, CYLD was known to act as a regulator of necroptosis downstream of TNF (92, 147). Mapping using imiquimod was the initial study that identified CYLD, which again implicates it in a TNF-R1-mediated process as

imiquimod uses MyD88 and autocrine TNF to activate necroptosis. However, further study using TNF-R1-deficient macrophages implicated CYLD in TRIF-dependent necroptosis activated through TLR3 and TLR4 as well.

Examination of these data together with other published works clearly implicates RIP1 ubiquitination as a critical regulatory step for necroptosis. Deubiquitination of RIP1 serves to either allow for pro-death complex formation (76, 92, 136, 155) or promote optimal kinase activity (94). However, what constitutes the formation of this pro-death complex in TLRs is not clear because no distinct complex I to complex II-like transition has been identified. Moreover, reports examination necrosome formation upon TLR3 ligation show direct recruitment of the pro-death complex to TLR3 (136). Thus, for TLR signaling whether the ubiquitinated RIP1 binds to pro-survival factors (or factors that prevent recruitment of RIP3) or ubiquitinated RIP1 prevents its kinase activity from driving necroptosis is not clear. Finally, because RIP1-independent forms of necroptosis seem to be important in viral infections (148, 203) and perhaps other pathological conditions, the regulators of RIP3-MLKL need to be elucidated. Considering that RIP3 appears to be more necroptosis-specific than RIP1, it is possible that the complex ubiquitin modifications likely conferring different functions have not evolved to affect RIP3. It appears that RIP3 is cleaved similarly to RIP1 (287), but other regulatory mechanisms await elucidation.

Resistance to necroptosis in MOLF – can it be used to understand necroptosis in disease models?

Unlike C57BL/6 macrophages, MOLF macrophages are resistant to TLR-induced necroptosis. While MOLF peritoneal cells show resistance to all TLR agonists, BMDM resistance is a less broad phenotype, only observed with low dose LPS stimulation. Forward genetic analysis identified resistance loci on MOLF Chromosomes 1 and 8 in peritoneal macrophages and Chromosomes 1 and 18 in BMDM. Though only Chromosome 8 was narrowed to a small enough region to identify a gene candidate (*Cyld*), presumably at least two additional MOLF alleles contribute to protection from necroptosis. Additional recombination events and more complete study of each locus will be necessary to identify these genes.

Presently in the case of the Chromosome 8 locus and in the future when genes on Chromosomes 1 and 18 are identified, how can resistance alleles be used to learn about necroptosis regulation? Though investigation of TNF-induced death or other mouse sepsis models would be of interest, other models such as acute kidney injury by ischemia-reperfusion injury are of interest to the laboratory. While the MOLF model possesses many benefits as demonstrated throughout this thesis, its capacity for *in vivo* analysis of necroptosis induced by any mechanism would be challenging. Besides being poor breeders, MOLF mice are resistant to death induced by LPS, TNF, and FAS ligation (coincident work in the Poltorak laboratory performed by Daniel Ram and Berri Jacque). It would be a challenge to isolate the effects of the genes of interest because of polymorphic nature of the MOLF mouse genome relative to B6 and the complexity of the *in vivo* phenotype. Additionally, without knockout mice bred on the MOLF background,

in depth study in genetic models is a challenge. As an alternative, the generation of congenic mice harboring MOLF resistance alleles will be pursued. According to the Jackson Lab criteria, mice are considered congenic following 10 generations of backcrossing, however N5-N9 generations are useful in experimental scenarios. The laboratory has had success with this mechanism in the past, creating B6.MOLF-*Why1*$^{M/M}$ to study the effects of MOLF IRAK2 on a B6 genetic background (43).

B6.MOLF-*Cyld*$^{M/M}$ mice are currently being generated. After determining whether the MOLF allele is sufficient to confer resistance to necroptosis *in vitro*, The B6.MOLF-*Cyld*$^{M/M}$ congenic could be a useful model to interrogate the implications of resistance to necroptosis applies *in vivo*. *Cyld*$^{-/-}$ mice have not been interrogated for resistance to necroptosis at a whole organism level, and spontaneous inflammation in these mice would certainly complicate any study related to necroptosis-specific processes (85). Because MOLF respond to stimuli by *cis*-acting down-regulation of CYLD, this model could be a more useful for the study of necroptosis induced in shock or ischemia-reperfusion injury models. A simple model for proof-of-principle would be to apply the experimental setup used by He, *et al.* in which LPS and ZVAD are injected into the peritoneal cavity and measurement of macrophage loss and cytokine release is performed (251). Though this experiment is somewhat artificial, it would indicate whether the MOLF *Cyld* allele is sufficient to prevent macrophage loss in the *in vivo* setting. If there is success with the B6.MOLF-*Cyld* mouse in this simple model, some of the pathological scenarios such as acute kidney injury by ischemia-reperfusion described in the introduction could be applied to this mouse.

Feasibility of congenic mouse generation

Though the idea of generating B6 congenic mice containing MOLF alleles for all linked traits is quite appealing, some drawbacks exist. The major question is how often a MOLF allele on a B6 background will be sufficient to confer a measurable change in phenotype, both *in vitro* and *in vivo*. The benefits of working on the B6 background are obvious: numerous tools such as an abundance of readily available knockout and transgenic mice, the capacity for bone marrow chimeras with these knockout/transgenic mice, and previously characterized conditions for diverse disease models in pathology and infection. Furthermore, the capacity to isolate a single MOLF allele allows conclusions to be drawn specifically on its effects. However, a number of substantial drawbacks to congenic mouse generation exist as well. The major problem with isolating MOLF alleles on the B6 background is the loss of the MOLF gene network (242). Because there is a great deal of polymorphism in the MOLF strain, certain gene-gene interactions are necessary for a given phenotypic response. This fact is perhaps most clearly illustrated by recent work in the laboratory concerning the response to the TLR9 agonist CpG DNA (254). Forward genetic analysis identified that the mannose receptor *Mrc1* is required for MOLF macrophages to respond to CpG. However, MRC1-deficient B6 mice are not different than their wild-type counterparts in CpG sensing and cytokine response. The necessity for MRC1 in MOLF macrophages reveals that additional genes are required to generate a network in which MRC1 is critical to the CpG uptake and response pathway. Therefore, generating a congenic mouse with the MOLF *Mrc1* allele would be a useless endeavor. Overall, the goals of congenic mouse generation are: 1) to use evolutionarily selected polymorphism in MOLF to determine the biological

significance of specific domains and residues on a given protein and 2) to discover MOLF genes that more closely resemble their human homologs such as *Irak1bp1* and *Irak2* (43, 44, 242).

One application where work described in this thesis is already being applied to congenic mice is for the altered MOLF cytokine responses described in Chapter 7. Work performed with Joseph Sarhan (and now carried forward as his thesis project) created B6 mice containing the region on MOLF Chromosome 13 linked to low CXCL1 production (termed B6.MOLF-*Lcx* for '**L**ow **CX**CL1'). These mice retained the low CXCL1 phenotype in response to all TLR agonists *in vitro* with heterozygosity for the MOLF allele in the N3, N4, N5, and N6 generations. Furthermore, this phenotype has been expanded to demonstrate low CXCL1 production in serum following LPS injection and *in vitro* in response to bacterial infection. Though the causative gene on this locus has yet to be identified, this project, which progressed in less than one year, demonstrates the capacity for rapid generation of congenic mice with a penetrant phenotype that can be used to investigate numerous biological questions. How often this MOLF allele will be sufficient to confer phenotypes in this manner and how to select phenotypes that lend themselves to successful backcrosses with penetrant phenotypes will be an interesting direction for future research using MOLF mice.

A novel mechanism of *Cyld* regulation

Genetic mapping identified *Cyld* as a likely candidate gene underlying MOLF resistance to necroptosis. Analysis of CYLD expression by 5' RACE showed a stimulus-dependent loss of the full-length isoform and gain of alternatively spliced $CYLD^{ex7/8}$

isoform in MOLF peritoneal macrophages, while B6 expressed both isoforms in unstimulated and stimulated cells (Figure 13A). Because the $CYLD^{ex7/8}$ alternatively spliced isoform is not expressed at the protein level in peritoneal macrophages, further analysis focused on the loss of the full-length isoform in MOLF macrophages. While this differential regulation was established at the RNA level, a causative polymorphism was not detected. The only mutation within the coding sequence, 3' UTR, and 2 kb upstream of the transcription start site was a deletion of CA at -980 bp from the TSS (Figure 14). Additionally, though not all introns were sequenced, those surrounding the alternative splice site between exons 6-7, 7-8, and 8-9 had no polymorphisms. However, there was a statistically significant change in RNA polymerase II recruitment in a promoter proximal region (+300 bp), suggesting that a difference in RNA polymerase II pausing, stalling, or elongation rate could underlie the difference in expression. The essential element moving forward will be to identify the genetic polymorphism between the two strains that exerts a *cis*-acting effect, however, identifying the mechanism of regulation would be insightful and may assist in identifying the lesion. Currently, there are two major models for CYLD regulation: 1) a transcription change causing by differences in pausing or an enhancer activity and 2) alternative splicing difference that favors the $CYLD^{ex7/8}$ isoform in MOLF.

Transcriptional repressors of CYLD have been identified including SNAIL and LEF1 but no mutations in these transcription factor binding sites exist in MOLF (99, 101). However, transcriptional changes can be caused by various DNA elements including enhancers. Enhancers can exert effects on genes as far as 900 Kb away and can act to recruit transcription factors, cause chromatin de-condensation, and directly interact with the RNA Pol II complex (288, 289). Enhancers can be identified through DNaseI

hypersensitivity sites and characteristic histone modifications such as H3K4me1 and H3K27ac (288, 290). Additionally, RNA Pol II pausing is known to be regulated by factors discussed above such as DSIF and NELF but other unidentified factors may act through unknown mechanisms (269).

Alternative splicing may also underlie the differential regulation at the *Cyld* locus. Pre-mRNA splicing is governed by *cis*-acting elements such as GU,AG pairs in the intronic sequence or exonic/intronic splicing enhancers or silencers which are normally located within 300 nucleotides of the splice site (291). As mentioned above, MOLF do not have polymorphisms in the regions surrounding the CYLD$^{ex7/8}$ splice sites. Control of alternative splicing by *cis*-acting factors can occur by promoter-driven mechanisms or differences in RNA Pol II elongate rate (291). Histone modifications in the promoter proximal region and throughout the mRNA can indicate splicing (292). An increase in H3K36me3, H3K4me3, and H3K27me2 on nucleosomes strongly indicates the presence of an exon. Furthermore, a high amount of H3K36me3 modifications are suggestive of a constitutively spliced exon whereas low levels mark alternatively spliced exons. Secondly, elongation rate of RNA polymerase II is correlated with alternative splicing (291, 293). In general, a slow elongate rate allows assembly of spliceosomes at weak splice sites to favor alternative splicing, which fits with the current data observed at the *Cyld* locus. Further analysis of the MOLF *Cyld* locus will be performed in B6.MOLF-*Cyld* congenic mice. This model will allow for the isolation of *cis*-acting changes without other effects of the MOLF genetic background.

A role for RIP1 kinase activity in pro-inflammatory cytokine production

The function of RIP1 kinase activity as a pathological signal in models of inflammatory disease is beginning to come into focus (194, 199, 213). Because most *in vitro* work has focused on RIP1 as a scaffold protein, the molecular mechanisms of how its kinase activity contributes to pro-inflammatory signaling are not adequately studied. In this thesis, an *in vitro* system in bone marrow-derived macrophages is established to study the molecular mechanisms by which RIP1 kinase exerts its effects on pro-inflammatory signaling cascades downstream of TLRs. Previous reports have established that RIP1 kinase activity is not activate in cultured fibroblasts or macrophages (51, 124, 132). To circumvent this issue, BMDM were treated with the pan-caspase inhibitor ZVAD, which led to an increase in pro-inflammatory cytokine production that was inhibited by Necrostatin-1. While ZVAD treatment led to an increase in TNF, CCL3, CXCL2, and IFNβ but not IL-6 in B6 and MOLF macrophages, though the MOLF response was more robust. Studies using chemical inhibitors identified a role for p38 in the high responses of MOLF and TAK1 was important for the RIP1 kinase dependent response in both strains. Additionally, IRAK2 may be an important contributor to the hyper-production of pro-inflammatory cytokines by MOLF in a RIP1 kinase dependent fashion, however whether this occurs through inducing p38 activation is not entirely clear. Overall, the data establish a model in which TLR signaling in the presence of ZVAD introduced a RIP1 kinase-dependent arm to the production of pro-inflammatory cytokines.

While these initial studies suggest that RIP1 kinase activity contributes to pro-inflammatory signaling, many questions remain, particularly regarding the ubiquitin

status of RIP1, the specific mechanism by which RIP1 interacts with the MAPK pathway, the specific set of genes that are regulated, and the genes underlying the difference between B6 and MOLF responses. As discussed above, RIP1 ubiquitination is an important and diverse method of modification to regulate this protein (69). In canonical TNF-R1 or TLR signaling, K63 and linear polyubiquitination of RIP1 is critical for its capacity to promote signaling. However, this mechanism is entirely dependent on how other proteins interact with polyubiquitin chains. How the ubiquitination of RIP1 relates to the activity of its kinase is not as clear. During necroptosis deubiquitination of RIP1 is an important positive regulatory step (76, 92, 136, 155). One study suggests that TNF production during hematopoiesis is promoted by the absence of IAPs in a RIP1 and RIP3 dependent fashion, suggesting that deubiquitinated RIP1 is the more important form in this pathway (193).

Secondly, though the experiments discussed above begin to address how RIP1 kinase enters the MAPK signaling pathway, further work is necessary. Data with chemical inhibition of TAK1 suggests that RIP1 kinase is upstream of this MAP3K, however no data presented within this work demonstrates an interaction between these two proteins. Investigation of a role for TAK1 in apoptosis and necroptosis revealed a role for TAK1 in a feed-forward loop to induce cell death that is augmented when caspases are inhibited, suggesting that a direct interaction and contribution to the pro-inflammatory aspect of this pathway is possible (281). Furthermore, experimental assessment of the involvement of RIP3 in production of TNF and IFNβ needs to be addressed, as these could be distinct signaling pathways.

In addition to elucidation of the core signaling pathway, exploration of differences between B6 and MOLF macrophages in RIP1 kinase action on gene expression and forward genetic analysis to elucidate genes that cause these differences will help to construct a thorough model of this pathway. In primary cells, IL-6 is not regulated by ZVAD and Nec-1 following LPS activation while other pro-inflammatory cytokines including TNF, CCL3, and CXCL2 show RIP1 kinase-dependent changes in expression. RNAseq in B6 and MOLF BMDM stimulated with LPS with and without ZVAD and Nec-1 will help to elucidate the full range of gene expression changes. In the same line of questioning, B6 and MOLF responses to LPS with and without ZVAD will be used in forward genetic analysis to find genes that contribute to RIP1 kinase signaling in each strain and perhaps to uncover the full set of genes that promotes hyper-p38 activation in MOLF.

Use of ZVAD and Nec-1 in the BMDM model system

The rationale for investigating RIP1 kinase-mediated signaling by necroptosis and pro-inflammatory signaling *in vitro* using ZVAD is to model an *in vivo* signaling mechanism. While published reports show that RIP1 kinase-inactive knock-in mice are protected form TNF-mediated lethality, whether this pathway promotes cell death or a 'cytokine storm' to cause death is complex (151, 194). Additional studies will need to establish the whether RIP1 kinase activity contributes to cytokine production following non-lethal LPS injection or models of bacterial or viral infection.

However, until we are able to identify an improved model, ZVAD is used to activate RIP1 kinase dependent signaling *in vitro*. From data presented here and

elsewhere, it appears that caspase-8 and FLIP are the two specific molecules that prevent RIP1 kinase activity from acting *in vitro* (144, 196). ZVAD itself has drawbacks in that it has off-target effects by inhibiting caspases aside from caspase-8, inhibiting cathepsins, and causing ER stress at high doses (172, 294, 295). As an alternative approach, lentiviral knockdown of caspase-8 in B6 and MOLF BMDM could be performed.

Nearly all of the data presented within this work relies on Necrostatin-1 to inhibit RIP1 kinase activity and mark its necessity in a given signaling process. The challenge of depleting RIP1 was revealed through recent reports discussed thoroughly above, in which the genetic deletion of *Ripk1* leads to embryonic lethality caused by RIP3 or caspase-8 (183, 188, 190). Though the kinase activity is not required to prevent aberrant activation of death pathways (190), expression of RIP1 as a scaffold, bound to Nec-1 or as a kinase-inactive protein, promotes homeostasis within these pro-inflammatory, pro-death pathways (151, 152, 188). In the model presented in this thesis, RIP1 deletion or efficient knockdown may remove this negative regulatory pathway and promote RIP3-dependent death, obscuring the study of RIP1 kinase-driven pro-inflammatory pathways. Taken together, utilization of the ZVAD, Nec-1 model for study of a wild-derived mouse strain provides a system to attempt to elucidate the molecular mechanisms by which TLRs activate RIP1 kinase activity.

Necroptosis: relevance to human disease

Though this work largely addresses signaling pathways involved in necroptosis activation and RIP1 kinase activity, the clinically relevant extension of necroptosis research lies in the identification of human disease processes in which this cell death

pathway drives pathogenesis. Recently developed genetic mouse models of RIP1 kinase inactive knock-in, RIP3-deficiency, and MLKL deficiency have shed significant light on the impact of necroptosis in certain disease models, as discussed in Chapter 1. Additionally, a few observational studies in human tissue samples have implicated necroptosis and its associated proteins (RIP1 kinase activity, RIP3, and MLKL) in human disease. The ileum of Crohn's disease patients is characterized by low caspase-8 and high RIP3 and MLKL expression (222, 226). Additionally, this inflamed tissue exhibits Paneth cell loss that could be explained to be activation of necroptosis. Additionally, in humans with drug-induced liver injury, biopsies identified the presence of phosphorylated MLKL through use of a phospho-specific antibody (165). Because MLKL phosphorylation is only known to occur via RIP3 kinase activity (163), a connection between this form of liver injury and necroptosis can be drawn. These studies are limited in that they rely heavily on detection of increased RIP3 and MLKL expression or phosphorylated MLKL detection, though the latter serves as a biomarker for RIP3 kinase activity. Future studies should assess markers of necroptosis more broadly in human tissues, examining the presence of phosphorylated MLKL and phosphorylated RIP1 with specific antibodies (165) and establishing the expression of RIP3 and MLKL proteins. Based on mouse models, clinical specimens from patients with diagnoses of pancreatitis, septic shock, stroke, or myocardial infarction would serve as appropriate starting points for these studies. Because these conditions are multi-factorial and arise from a diversity of etiologies, the presence or absence of necroptosis-associated proteins in these tissues must be assessed thoroughly through a variety of patient populations.

The next important question for the assessment of the relevance of necroptosis to human disease is the inquiry of its contribution to the causation of disease. Is necroptosis activation in itself sufficient to drive disease? Does it amplify inflammatory cytokine responses such as in the TNF injection modeled in *Ripk3*-deficient mice (213)? Is it an incidental finding that may contribute to observed morphological characteristics but lacks a role in disease pathogenesis? In mouse models of TNF-induced shock it is clear that necroptosis is required for driving the disease through the use of *Ripk3*$^{-/-}$, *Mlkl*$^{-/-}$, *and Ripk1*-kinase inactive knock-in animals (151, 185, 194, 213, 296). In humans, the development of therapeutics and clinical trials of RIP1 and RIP3 kinase inhibitors (137, 198, 297) and MLKL inhibitors (159) may be the most specific tools for examination of the significance of necroptosis. Though each of these proteins may perform functions independent from necroptosis, those roles for RIP3 and MLKL have yet to be elucidated. Clinical trials examining the effect of these inhibitors on diseases such as inflammatory bowel disease, a chronic inflammatory conditions promoted by pro-inflammatory cytokine production including TNF (226), is a rational starting point because of its known association with necroptosis in mouse models and in observational human studies. Additionally, the investigation of necroptosis blockade in septic shock is grounded in mouse models. Though previous attempts at TNF blockade or LPS neutralization in clinical trials for septic shock were unsuccessful (298, 299), patients were not selected based on the likelihood for therapeutic success, *e.g.* patients treated with TNF neutralizing drugs did not have TNF levels measured prior to initiation of therapy (212). Perhaps necroptosis blockade will prove to be a more successful target for septic shock in that it would allow an initial cytokine response but prevent the subsequent tissue damage

and worsening of disease caused by cell death within tissues and DAMP release during necroptosis (300).

APPENDIX 1

Genes within Chromosome 1 linked region (between *D1Mit495* and *D1Mit210*)

cM	Symbol	Name
56.89	Il10	interleukin 10
58.18	Myog	myogenin
65.05	Ncf2	neutrophil cytosolic factor 2
57.24	Cdk18	cyclin-dependent kinase 18
60.73	Ptprc	protein tyrosine phosphatase, receptor type, C
57.91	Ren1	renin 1 structural
63.84	Pdc	phosducin
57.94	Snrpe	small nuclear ribonucleoprotein E
58.24	Syt2	synaptotagmin II
65.3	Lamc1	laminin, gamma 1
61.62	Cfh	complement component factor h
65.43	Glul	glutamate-ammonia ligase (glutamine synthetase)
63.84	Ptgs2	prostaglandin-endoperoxide synthase 2
58.15	Adora1	adenosine A1 receptor
65.26	Lamc2	laminin, gamma 2
57.91	Sox13	SRY (sex determining region Y)-box 13
57.95	Atp2b4	ATPase, Ca++ transporting, plasma membrane 4
56.89	C4bp	complement component 4 binding protein
59.23	Csrp1	cysteine and glycine-rich protein 1
57.42	Cntn2	contactin 2
55.8	Lct	lactase
59.32	Tnnt2	troponin T2, cardiac
57.42	Nfasc	neurofascin
56.89	Daf2	decay accelerating factor 2
56.89	Cd55	CD55 antigen
59.28	Tnni1	troponin I, skeletal, slow 1
62.54	Trove2	TROVE domain family, member 2
65.37	Dhx9	DEAH (Asp-Glu-Ala-His) box polypeptide 9
58.1	Btg2	B cell translocation gene 2, anti-proliferative
59.61	Kif21b	kinesin family member 21B
56.43	Cxcr4	chemokine (C-X-C motif) receptor 4
62.56	Rgs2	regulator of G-protein signaling 2
64.15	Rnf2	ring finger protein 2
63.51	Pla2g4a	phospholipase A2, group IVA (cytosolic, calcium-dependent)
55.8	Map3k19	mitogen-activated protein kinase kinase kinase 19
65.43	Rgs16	regulator of G-protein signaling 16
59.35	Pkp1	plakophilin 1
58.09	Fmod	fibromodulin
56.9	Dyrk3	dual-specificity tyrosine-(Y)-phosphorylation regulated kinase 3

57.24	Elk4	ELK4, member of ETS oncogene family
56.89	Pigr	polymeric immunoglobulin receptor
56.89	Zp3r	zona pellucida 3 receptor
57.69	Lrrn2	leucine rich repeat protein 2, neuronal
57.14	Ctse	cathepsin E
64.85	Rgl1	ral guanine nucleotide dissociation stimulator,-like 1
56.89	Pfkfb2	6-phosphofructo-2-kinase/fructose-2,6-biphosphatase 2
57.75	Mdm4	transformed mouse 3T3 cell double minute 4
58.24	Ptprv	protein tyrosine phosphatase, receptor type, V
65.41	Rgs8	regulator of G-protein signaling 8
56.9	Eif2d	eukaryotic translation initiation factor 2D
59.3	Lad1	ladinin
56.93	Srgap2	SLIT-ROBO Rho GTPase activating protein 2
59.55	Cacna1s	calcium channel, voltage-dependent, L type, alpha 1S subunit
59.8	Kif14	kinesin family member 14
65.43	Rnasel	ribonuclease L (2', 5'-oligoisoadenylate synthetase-dependent)
58.42	Elf3	E74-like factor 3
55.8	Mcm6	minichromosome maintenance deficient 6
61.57	F13b	coagulation factor XIII, beta subunit
60.82	Lhx9	LIM homeobox protein 9
56.89	Mapkapk2	MAP kinase-activated protein kinase 2
61.62	Kcnt2	potassium channel, subfamily T, member 2
58.21	4933406M09Rik	RIKEN cDNA 4933406M09 gene
59.44	Igfn1	immunoglobulin-like and fibronectin type III domain containing 1
59.93	Zfp281	zinc finger protein 281
58.24	Ptpn7	protein tyrosine phosphatase, non-receptor type 7
60.87	Crb1	crumbs homolog 1 (Drosophila)
58.25	Gpr37l1	G protein-coupled receptor 37-like 1
59.61	Mroh3	maestro heat-like repeat family member 3
57.24	Dstyk	dual serine/threonine and tyrosine protein kinase
57.18	5430435G22Rik	RIKEN cDNA 5430435G22 gene
57.19	Pm20d1	peptidase M20 domain containing 1
57.91	Etnk2	ethanolamine kinase 2
65.15	Nmnat2	nicotinamide nucleotide adenylyltransferase 2
57.8	Ppp1r15b	protein phosphatase 1, regulatory (inhibitor) subunit 15b
61.36	Zbtb41	zinc finger and BTB domain containing 41 homolog
57.18	Slc26a9	solute carrier family 26, member 9
57.2	Slc41a1	solute carrier family 41, member 1
55.8	Rab3gap1	RAB3 GTPase activating protein subunit 1
60.84	Dennd1b	DENN/MADD domain containing 1B
60.82	Atp6v1g3	ATPase, H+ transporting, lysosomal V1 subunit G3
56.89	Il19	interleukin 19
58.79	Nav1	neuron navigator 1

57.91	Plekha6	pleckstrin homology domain containing, family A member 6
55.8	R3hdm1	R3H domain containing 1
57.91	Kiss1	KiSS-1 metastasis-suppressor
55.8	Acmsd	amino carboxymuconate semialdehyde decarboxylase
63.84	BC003331	cDNA sequence BC003331
57.21	Rab29	RAB29, member RAS oncogene family
58.23	Klhl12	kelch-like 12
62.56	Rgs13	regulator of G-protein signaling 13
65.43	Teddm1	transmembrane epididymal protein 1
65.07	Smg7	Smg-7 homolog, nonsense mediated mRNA decay factor
59.54	Ascl5	achaete-scute complex homolog 5 (Drosophila)
57.75	Pik3c2b	phosphoinositide-3-kinase, class 2, beta polypeptide
63.84	Hmcn1	hemicentin 1
65.43	Rgsl1	regulator of G-protein signaling like 1
65.97	Zfp648	zinc finger protein 648
59.61	Gpr25	G protein-coupled receptor 25
	Gm1627	predicted gene 1627
63.24	Brinp3	bone morphogenetic protein/retinoic acid inducible neural specific 3
58.24	Lgr6	leucine-rich repeat-containing G protein-coupled receptor 6
62.52	Cdc73	cell division cycle 73, Paf1/RNA polymerase II complex component
58.43	Rnpep	arginyl aminopeptidase (aminopeptidase B)
65.43	5830403L16Rik	RIKEN cDNA 5830403L16 gene
57.22	Nucks1	nuclear casein kinase and cyclin-dependent kinase substrate 1
58.24	Rabif	RAB interacting factor
64.21	Fam129a	family with sequence similarity 129, member A
61.62	Cfhr1	complement factor H-related 1
64.77	Colgalt2	collagen beta(1-O)galactosyltransferase 2
58.58	Shisa4	shisa homolog 4 (Xenopus laevis)
56.89	Il24	interleukin 24
58.51	Lmod1	leiomodin 1 (smooth muscle)
56.89	AA986860	expressed sequence AA986860
64.06	Ivns1abp	influenza virus NS1A binding protein
57.95	Lax1	lymphocyte transmembrane adaptor 1
55.8	Dars	aspartyl-tRNA synthetase
56.89	Yod1	YOD1 OTU deubiquitinating enzyme 1 homologue (S. cerevisiae)
57.24	Klhdc8a	kelch domain containing 8A
57.24	Mfsd4	major facilitator superfamily domain containing 4
56.55	Thsd7b	thrombospondin, type I, domain containing 7B
61.62	Cfhr2	complement factor H-related 2
58.15	Chil1	chitinase-like 1
59.26	Phlda3	pleckstrin homology-like domain, family A, member 3

62.56	Rgs1	regulator of G-protein signaling 1
58.15	Mybph	myosin binding protein H
60.82	Nek7	NIMA (never in mitosis gene a)-related expressed kinase 7
56.91	Rassf5	Ras association (RalGDS/AF-6) domain family member 5
62.99	Rgs18	regulator of G-protein signaling 18
56.89	Il20	interleukin 20
56.93	Ikbke	inhibitor of kappaB kinase epsilon
59.51	Tmem9	transmembrane protein 9
64.34	Edem3	ER degradation enhancer, mannosidase alpha-like 3
58.24	Ube2t	ubiquitin-conjugating enzyme E2T (putative)
		protein tyrosine phosphatase, receptor type, f polypeptide (PTPRF),
58.18	Ppfia4	interacting protein (liprin), alpha 4
57.24	Tmcc2	transmembrane and coiled-coil domains 2
64.12	Trmt1l	tRNA methyltransferase 1 like
64.43	1700025G04Rik	RIKEN cDNA 1700025G04 gene
60.82	2310009B15Rik	RIKEN cDNA 2310009B15 gene
58.24	4931440L10Rik	RIKEN cDNA 4931440L10 gene
57.24	Rbbp5	retinoblastoma binding protein 5
58.6	Ipo9	importin 9
65.36	Shcbp1l	Shc SH2-domain binding protein 1-like
58.21	Cyb5r1	cytochrome b5 reductase 1
56.99	Fam72a	family with sequence similarity 72, member A
55.8	Ccnt2	cyclin T2
63.91	3110040M04Rik	RIKEN cDNA 3110040M04 gene
57.42	Tmem81	transmembrane protein 81
57.24	Slc45a3	solute carrier family 45, member 3
57.24	Lemd1	LEM domain containing 1
		calmodulin regulated spectrin-associated protein family,
59.61	Camsap2	member 2
		asp (abnormal spindle)-like, microcephaly associated
61.45	Aspm	(Drosophila)
58.48	Timm17a	translocase of inner mitochondrial membrane 17a
59.98	Nr5a2	nuclear receptor subfamily 5, group A, member 2
57.09	Avpr1b	arginine vasopressin receptor 1B
		UDP-Gal:betaGlcNAc beta 1,3-galactosyltransferase,
62.52	B3galt2	polypeptide 2
56.89	Fcamr	Fc receptor, IgA, IgM, high affinity
63.84	Prg4	proteoglycan 4
64.75	Tsen15	tRNA splicing endonuclease 15 homolog (S. cerevisiae)
64.08	Swt1	SWT1 RNA endoribonuclease homolog (S. cerevisiae)
58.2	Tmem183a	transmembrane protein 183A
62.54	Uchl5	ubiquitin carboxyl-terminal esterase L5
65.02	Arpc5	actin related protein 2/3 complex, subunit 5
55.8	Ubxn4	UBX domain protein 4
59.73	Ddx59	DEAD (Asp-Glu-Ala-Asp) box polypeptide 59

57.91	Golt1a	golgi transport 1 homolog A (S. cerevisiae)
58.24	Arl8a	ADP-ribosylation factor-like 8A
58.24	Ppp1r12b	protein phosphatase 1, regulatory (inhibitor) subunit 12B
56.89	Faim3	Fas apoptotic inhibitory molecule 3
62.53	Glrx2	glutaredoxin 2 (thioltransferase)
57.94	Zc3h11a	zinc finger CCCH type containing 11A
55.8	Zranb3	zinc finger, RAN-binding domain containing 3
65.01	Apobec4	apolipoprotein B mRNA editing enzyme, catalytic polypeptide-like 4 (putative)
58.12	Chit1	chitinase 1 (chitotriosidase)
55.77	Tmem163	transmembrane protein 163
58.22	Adipor1	adiponectin receptor 1
65.38	Npl	N-acetylneuraminate pyruvate lyase
57.24	Nuak2	NUAK family, SNF1-like kinase, 2
59.61	5730559C18Rik	RIKEN cDNA 5730559C18 gene
58.24	Kdm5b	lysine (K)-specific demethylase 5B
63.84	Tpr	translocated promoter region, nuclear basket protein
58.1	Gm19497	predicted gene, 19497
57.95	Gm17678	predicted gene, 17678
58.02	Prelp	proline arginine-rich end leucine-rich repeat
58.02	Optc	opticin
59.12	Gm4793	predicted gene 4793
61.62	Cfhr3	complement factor H-related 3
63.32	Gm9931	predicted gene 9931
	Gm10537	predicted gene 10537
62.66	Rgs21	regulator of G-protein signalling 21
61.62	Gm4788	predicted gene 4788
65.43	Gm5531	predicted gene 5531
	Gm8947	predicted gene 8947
57.24	Gm10188	predicted gene 10188
57.94	Zbed6	zinc finger, BED domain containing 6
	Gm26616	predicted gene, 26616
	Gm28040	predicted gene, 28040

APPENDIX 2

Genes within Chromosome 14 linked region (between *D14Mit263* and end of Chr 14)

cM	Symbol	Name
65.99	Pcca	propionyl-Coenzyme A carboxylase, alpha polypeptide
64.72	Rap2a	RAS related protein 2a
51.67	Irg1	immunoresponsive gene 1
65.28	Dock9	dedicator of cytokinesis 9
65.97	Zic2	zinc finger protein of the cerebellum 2
62.6	Dnajc3	DnaJ (Hsp40) homolog, subfamily C, member 3
65.86	Gpr18	G protein-coupled receptor 18
66.18	Fgf14	fibroblast growth factor 14
45.8	Pcdh9	protocadherin 9
59.43	Gpc5	glypican 5
49.27	Pibf1	progesterone immunomodulatory binding factor 1
48.25	Dach1	dachshund 1 (Drosophila)
50.9	Klf12	Kruppel-like factor 12
56.16	Trim52	tripartite motif-containing 52
55.64	Ndfip2	Nedd4 family interacting protein 2
61.74	Tgds	TDP-glucose 4,6-dehydratase
49.22	Mzt1	mitotic spindle organizing protein 1
49.23	Bora	bora, aurora kinase A activator
64.44	Mbnl2	muscleblind-like 2
50.9	Tbc1d4	TBC1 domain family, member 4
64.86	Farp1	FERM, RhoGEF (Arhgef) and pleckstrin domain protein 1 (chondrocyte-derived)
65.86	Gpr183	G protein-coupled receptor 183
51.71	Cln5	ceroid-lipofuscinosis, neuronal 5
62.24	Abcc4	ATP-binding cassette, sub-family C (CFTR/MRP), member 4
66.1	Itgbl1	integrin, beta-like 1
66.04	Nalcn	sodium leak channel, non-selective
51.79	Mycbp2	MYC binding protein 2
61.92	Sox21	SRY (sex determining region Y)-box 21
64.95	Stk24	serine/threonine kinase 24
63.63	Oxgr1	oxoglutarate (alpha-ketoglutarate) receptor 1
66.04	Ggact	gamma-glutamylamine cyclotransferase
57.2	Slitrk6	SLIT and NTRK-like family, member 6
56.78	Slitrk1	SLIT and NTRK-like family, member 1
57.86	Slitrk5	SLIT and NTRK-like family, member 5
51.55	Kctd12	potassium channel tetramerisation domain containing 12
50.9	Prr30	proline rich 30
61.78	Gpr180	G protein-coupled receptor 180
46.92	Klhl1	kelch-like 1
52.75	Slain1	SLAIN motif family, member 1
65.86	Timm8a2	translocase of inner mitochondrial membrane 8A2

56.16	Spry2	sprouty homolog 2 (Drosophila)
50.9	Lmo7	LIM domain only 7
50.9	Uchl3	ubiquitin carboxyl-terminal esterase L3 (ubiquitin thiolesterase)
62.55	Cldn10	claudin 10
50.9	Commd6	COMM domain containing 6
65.86	Tm9sf2	transmembrane 9 superfamily member 2
65.78	Ubac2	ubiquitin associated domain containing 2
64.81	Ipo5	importin 5
55.36	Rbm26	RNA binding motif protein 26
60.34	Gpc6	glypican 6
49.43	Klf5	Kruppel-like factor 5
51.73	Fbxl3	F-box and leucine-rich repeat protein 3
62.67	Hs6st3	heparan sulfate 6-O-sulfotransferase 3
65.26	Slc15a1	solute carrier family 15 (oligopeptide transporter), member 1
52.51	Scel	sciellin
65.96	Zic5	zinc finger protein of the cerebellum 5
62.61	Uggt2	UDP-glucose glycoprotein glucosyltransferase 2
46.92	4921530L21Rik	RIKEN cDNA 4921530L21 gene
62.56	Dzip1	DAZ interacting protein 1
65.86	Clybl	citrate lyase beta like
54.24	Rnf219	ring finger protein 219
49.25	Dis3	DIS3 mitotic control homolog (S. cerevisiae)
66.04	Tmtc4	transmembrane and tetratricopeptide repeat containing 4
61.6	Dct	dopachrome tautomerase
53.05	Ednrb	endothelin receptor type B
54.21	Pou4f1	POU domain, class 4, transcription factor 1
61.96	Gm9376	predicted gene 9376
56.16	Gm6234	predicted gene 6234
44.68	Gm10110	predicted gene 10110
65.97	Gm10837	predicted gene 10837
50.9	Gm9922	predicted gene 9922
56.16	Gm9328	predicted gene 9328
56.16	Gm9327	predicted gene 9327
56.16	Gm6219	predicted gene 6219
56.16	Gm9324	predicted gene 9324
56.16	Gm9325	predicted gene 9325
56.16	Gm9326	predicted gene 9326
57.2	Gm6280	predicted gene 6280
56.16	Gm4666	predicted gene 4666
56.16	Gm6232	predicted gene 6232
56.16	Gm4663	predicted gene 4663
56.16	Gm4664	predicted gene 4664
64.76	Gm17613	predicted gene, 17613
66.19	Gm17615	predicted gene, 17615

APPENDIX 3

Genes within Chromosome 18 linked region (between *D18Mit186* and *D18Mit144*)

cM	Symbol	Name
52.38	Atp5a1	ATP synthase, H+ transporting, mitochondrial F1 complex, alpha subunit 1
45.24	Dcc	deleted in colorectal carcinoma
51.06	Smad7	SMAD family member 7
50.7	Myo5b	myosin VB
51.42	Smad2	SMAD family member 2
52.13	St8sia5	ST8 alpha-N-acetyl-neuraminide alpha-2,8-sialyltransferase 5
54.11	Sall3	sal-like 3 (Drosophila)
49.51	Smad4	SMAD family member 4
52.07	Pias2	protein inhibitor of activated STAT 2
50.76	Acaa2	acetyl-Coenzyme A acyltransferase 2 (mitochondrial 3-oxoacyl-Coenzyme A thiolase)
50.7	Mbd1	methyl-CpG binding domain protein 1
50.96	BC031181	cDNA sequence BC031181
57.53	Fam69c	family with sequence similarity 69, member C
50.21	Mro	maestro
51.06	Ctif	CBP80/20-dependent translation initiation factor
57.53	Zfp407	zinc finger protein 407
53.28	Adnp2	ADNP homeobox 2
52.38	Haus1	HAUS augmin-like complex, subunit 1
49.29	Mex3c	mex3 homolog C (C. elegans)
57.53	Cndp1	carnosine dipeptidase 1 (metallopeptidase M20 family)
50.96	Rpl17	ribosomal protein L17
52.38	8030462N17Rik	RIKEN cDNA 8030462N17 gene
57.53	Zadh2	zinc binding alcohol dehydrogenase, domain containing 2
51.1	Zbtb7c	zinc finger and BTB domain containing 7C
50.31	Mapk4	mitogen-activated protein kinase 4
52.28	Rnf165	ring finger protein 165
57.39	Zfp516	zinc finger protein 516
52.02	Katnal2	katanin p60 subunit A-like 2
51.98	Hdhd2	haloacid dehalogenase-like hydrolase domain containing 2
52.67	Setbp1	SET binding protein 1
53.22	Pard6g	par-6 family cell polarity regulator gamma
49.83	Elac1	elaC homolog 1 (E. coli)
57.53	Tshz1	teashirt zinc finger family member 1
53.34	Txnl4a	thioredoxin-like 4A
52.53	Slc14a2	solute carrier family 14 (urea transporter), member 2
52.49	Slc14a1	solute carrier family 14 (urea transporter), member 1
57.53	Fbxo15	F-box protein 15
53.9	Atp9b	ATPase, class II, type 9B

57.53	Cyb5a	cytochrome b5 type A (microsomal)
56.26	Zfp236	zinc finger protein 236
53.48	Ctdp1	CTD (carboxy-terminal domain, RNA polymerase II, polypeptide A) phosphatase, subunit 1
51.98	Ier3ip1	immediate early response 3 interacting protein 1
53.35	Hsbp1l1	heat shock factor binding protein 1-like 1
52.2	Loxhd1	lipoxygenase homology domains 1
53.33	Rbfa	ribosome binding factor A
52.38	Epg5	ectopic P-granules autophagy protein 5 homolog (C. elegans)
50.7	Cxxc1	CXXC finger 1 (PHD domain)
52.38	Pstpip2	proline-serine-threonine phosphatase-interacting protein 2
55.78	Galr1	galanin receptor 1
50.94	Lipg	lipase, endothelial
57.53	Cndp2	CNDP dipeptidase 2 (metallopeptidase M20 family)
50.67	Ska1	spindle and kinetochore associated complex subunit 1
53.37	Pqlc1	PQ loop repeat containing 1
50.97	Dym	dymeclin
57.53	Timm21	tranlocase of inner mitochondrial membrane 21
50.7	Ccdc11	coiled-coil domain containing 11
55.84	Mbp	myelin basic protein
53.66	Nfatc1	nuclear factor of activated T cells, cytoplasmic, calcineurin dependent 1
49.95	Me2	malic enzyme 2, NAD(+)-dependent, mitochondrial
50.49	Gm9925	predicted gene 9925
	Gm10265	predicted gene 10265
51.93	Skor2	SKI family transcriptional corepressor 2
52.13	Gm7276	predicted gene 7276
52.43	Siglec15	sialic acid binding Ig-like lectin 15
53.4	Kcng2	potassium voltage-gated channel, subfamily G, member 2
53.34	Gm16286	predicted gene 16286
57.53	Gm17266	predicted gene, 17266
	Gm21886	predicted gene, 21886

APPENDIX 4

Genes within Chromosome 10 linked region (between *D10Mit52* and *D10Mit88*)

cM	Symbol	Name
27.11	Pln	phospholamban
24.87	Sim1	single-minded homolog 1 (Drosophila)
25.5	Lilrb4	leukocyte immunoglobulin-like receptor, subfamily B, member 4
23.01	Cd24a	CD24a antigen
18.85	Frk	fyn-related kinase
20.02	Lama4	laminin, alpha 4
23.14	Aim1	absent in melanoma 1
22.89	Nr2e1	nuclear receptor subfamily 2, group E, member 1
26.64	Nus1	nuclear undecaprenyl pyrophosphate synthase 1 homolog (S. cerevisiae)
23.24	Atg5	autophagy related 5
22.42	Smpd2	sphingomyelin phosphodiesterase 2, neutral
18.85	Tspyl1	testis-specific protein, Y-encoded-like 1
19.13	Amd2	S-adenosylmethionine decarboxylase 2
27.4	Man1a	mannosidase 1, alpha
18.85	Tspyl4	TSPY-like 4
23.27	Prep	prolyl endopeptidase
19.44	Hdac2	histone deacetylase 2
20.51	Fyn	Fyn proto-oncogene
28.64	Gja1	gap junction protein, alpha 1
24.87	Grik2	glutamate receptor, ionotropic, kainate 2 (beta 2)
19.49	Marcks	myristoylated alanine rich protein kinase C substrate
26.18	Ros1	Ros1 proto-oncogene
23.24	Prdm1	PR domain containing 1, with ZNF domain
25.5	Gp49a	glycoprotein 49 A
21.85	Amd1	S-adenosylmethionine decarboxylase 1
18.85	Col10a1	collagen, type X, alpha 1
18.84	Rsph4a	radial spoke head 4 homolog A (Chlamydomonas)
22.38	Zbtb24	zinc finger and BTB domain containing 24
21.37	BC021785	cDNA sequence BC021785
22.02	Mettl24	methyltransferase like 24
23.12	Rtn4ip1	reticulon 4 interacting protein 1
25.66	Gprc6a	G protein-coupled receptor, family C, group 6, member A
23.65	Hace1	HECT domain and ankyrin repeat containing, E3 ubiquitin protein ligase 1
26.16	Vgll2	vestigial like 2 homolog (Drosophila)
22.88	Lace1	lactation elevated 1
19.31	Hs3st5	heparan sulfate (glucosamine) 3-O-sulfotransferase 5
18.85	Nt5dc1	5'-nucleotidase domain containing 1
28.45	Tbc1d32	TBC1 domain family, member 32

18.85	Fam26f	family with sequence similarity 26, member F
18.85	Dse	dermatan sulfate epimerase
25.74	Rfx6	regulatory factor X, 6
22.41	Mical1	microtubule associated monooxygenase, calponin and LIM domain containing 1
22.89	Ostm1	osteopetrosis associated transmembrane protein 1
18.82	Sult3a1	sulfotransferase family 3A, member 1
23.35	Popdc3	popeye domain containing 3
22.08	Gpr6	G protein-coupled receptor 6
22.77	Sesn1	sestrin 1
22.89	Sec63	SEC63-like (S. cerevisiae)
23.11	Qrsl1	glutaminyl-tRNA synthase (glutamine-hydrolyzing)-like 1
25.62	Fam162b	family with sequence similarity 162, member B
22.0	Ddo	D-aspartate oxidase
21.43	AI317395	expressed sequence AI317395
22.08	Fig4	FIG4 homolog (S. cerevisiae)
20.86	Traf3ip2	TRAF3 interacting protein 2
18.85	Fam26e	family with sequence similarity 26, member E
22.89	Sobp	sine oculis-binding protein homolog (Drosophila)
26.54	Gopc	golgi associated PDZ and coiled-coil motif containing
26.79	Slc35f1	solute carrier family 35, member F1
24.87	Ascc3	activating signal cointegrator 1 complex subunit 3
21.94	Cdk19	cyclin-dependent kinase 19
22.07	Wasf1	WAS protein family, member 1
23.0	Bend3	BEN domain containing 3
22.89	Scml4	sex comb on midleg-like 4 (Drosophila)
19.98	Rfpl4b	ret finger protein-like 4B
22.23	Ak9	adenylate kinase 9
23.5	Lin28b	lin-28 homolog B (C. elegans)
21.04	Rev3l	REV3-like, catalytic subunit of DNA polymerase zeta RAD54 like (S. cerevisiae)
23.47	Bves	blood vessel epicardial substance
22.46	Cd164	CD164 antigen
22.89	Snx3	sorting nexin 3
22.79	Foxo3	forkhead box O3
20.14	Fam229b	family with sequence similarity 229, member B
21.76	Rpf2	ribosome production factor 2 homolog (S. cerevisiae)
21.79	Gtf3c6	general transcription factor IIIC, polypeptide 6, alpha
22.77	Armc2	armadillo repeat containing 2
	5430427G11Rik	RIKEN cDNA 5430427G11 gene
28.5	Msl3l2	male-specific lethal 3-like 2 (Drosophila)
22.9	9030612E09Rik	RIKEN cDNA 9030612E09 gene
27.24	Asf1a	anti-silencing function 1A histone chaperone
18.85	Rwdd1	RWD domain containing 1
26.6	Nepn	nephrocan
26.41	Dcbld1	discoidin, CUB and LCCL domain containing 1

23.01	1700021F05Rik	RIKEN cDNA 1700021F05 gene
22.69	Cep57l1	centrosomal protein 57-like 1
21.99	Slc22a16	solute carrier family 22 (organic cation transporter), member 16
25.83	4933411G06Rik	RIKEN cDNA 4933411G06 gene
22.91	Pdss2	prenyl (solanesyl) diphosphate synthase, subunit 2
27.21	Mcm9	minichromosome maintenance complex component 9
22.06	Cdc40	cell division cycle 40
20.16	Tube1	epsilon-tubulin 1
21.31	2010001E11Rik	RIKEN cDNA 2010001E11 gene
21.48	Slc16a10	solute carrier family 16 (monocarboxylic acid transporters), member 10
18.85	Zufsp	zinc finger with UFM1-specific peptidase domain
22.43	Ppil6	peptidylprolyl isomerase (cyclophilin)-like 6
27.26	Fam184a	family with sequence similarity 184, member A
22.48	Ccdc162	coiled-coil domain containing 162
18.85	Fam26d	family with sequence similarity 26, member D
20.19	Wisp3	WNT1 inducible signaling pathway protein 3
22.61	Gm6976	predicted gene 6976
18.85	Trappc3l	trafficking protein particle complex 3 like
18.76	Gm4794	predicted gene 4794
27.09	Cep85l	centrosomal protein 85-like
21.35	G630090E17Rik	RIKEN cDNA G630090E17 gene
	Gm5079	predicted gene 5079
	Gm3577	predicted gene 3577
18.85	Gm17567	predicted gene, 17567
	Gm26741	predicted gene, 26741

APPENDIX 5

Genes within Chromosome 13 linked region (between *D13Mit310* and *D13Mit143*)

cM	Symbol	Name
35.55	Srd5a1	steroid 5 alpha-reductase 1
34.54	Zfp58	zinc finger protein 58
35.55	Adcy2	adenylate cyclase 2
34.54	Ptdss1	phosphatidylserine synthase 1
35.55	Med10	mediator complex subunit 10
35.55	Nsun2	NOL1/NOP2/Sun domain family member 2
34.7	Zfp65	zinc finger protein 65
38.43	Irx1	Iroquois related homeobox 1 (Drosophila)
39.23	Irx2	Iroquois related homeobox 2 (Drosophila)
34.74	Zfp85	zinc finger protein 85
34.4	Olfr466	olfactory receptor 466
34.62	A530054K11Rik	RIKEN cDNA A530054K11 gene
34.8	Zfp273	zinc finger protein 273
34.54	Zfp759	zinc finger protein 759
34.54	Zfp708	zinc finger protein 708
34.85	BC048507	cDNA sequence BC048507
34.54	Zfp458	zinc finger protein 458
34.54	Zfp456	zinc finger protein 456
34.54	Zfp459	zinc finger protein 459
34.54	Zfp874b	zinc finger protein 874b
34.54	Zfp874a	zinc finger protein 874a
34.66	Zfp738	zinc finger protein 738
34.54	Zfp595	zinc finger protein 595
34.54	Zfp455	zinc finger protein 455
34.54	Zfp457	zinc finger protein 457
34.54	Rsl1	regulator of sex limited protein 1
34.52	2410141K09Rik	RIKEN cDNA 2410141K09 gene
35.55	Ube2ql1	ubiquitin-conjugating enzyme E2Q family-like 1
34.54	Zfp712	zinc finger protein 712
34.59	AA987161	expressed sequence AA987161
35.97	Adamts16	a disintegrin-like and metallopeptidase (reprolysin type) with thrombospondin type 1 motif, 16
35.54	Mtrr	5-methyltetrahydrofolate-homocysteine methyltransferase reductase
35.97	Ice1	interactor of little elongation complex ELL subunit 1
34.53	Zfp640	zinc finger protein 640
35.55	Papd7	PAP associated domain containing 7
34.21	Prss47	protease, serine 47
35.97	8030423J24Rik	RIKEN cDNA 8030423J24 gene
34.45	Nlrp4f	NLR family, pyrin domain containing 4F
34.47	Zfp369	zinc finger protein 369

34.54	Zfp87	zinc finger protein 87
34.54	Zfp953	zinc finger protein 953
34.21	Spata31d1c	spermatogenesis associated 31 subfamily D, member 1C
34.54	Mterfd1	MTERF domain containing 1
34.54	Uqcrb	ubiquinol-cytochrome c reductase binding protein
35.55	1700001L19Rik	RIKEN cDNA 1700001L19 gene
34.77	Zfp493	zinc finger protein 493
39.64	Irx4	Iroquois related homeobox 4 (Drosophila)
34.21	Hiatl1	hippocampus abundant transcript-like 1
34.54	Zfp748	zinc finger protein 748
35.55	Fastkd3	FAST kinase domains 3
34.54	Zfp429	zinc finger protein 429
39.09	Gm19659	predicted gene, 19659
34.54	Gm10767	predicted gene 10767
34.47	Gm10775	predicted gene 10775
34.51	Gm10324	predicted gene 10324
34.48	Gm10139	predicted gene 10139
34.82	Gm10037	predicted gene 10037
34.51	Gm10772	predicted gene 10772
34.54	Gm10323	predicted gene 10323
	Gm3844	predicted gene 3844
34.33	Gm3785	predicted gene 3785
	Gm3772	predicted gene 3772
34.93	Gm7969	predicted gene 7969
34.54	Gm17404	predicted gene, 17404
34.54	Gm17449	predicted gene, 17449
	Rslcan18	regulator of sex-limitation candidate 18
	Gm26965	predicted gene, 26965
	Gm28041	predicted gene, 28041
	Gm28044	predicted gene, 28044

REFERENCES

1. Medzhitov, R. 2008. Origin and physiological roles of inflammation. *Nature* 454: 428–35.

2. Medzhitov, R. 2010. Inflammation 2010: New Adventures of an Old Flame. *Cell* 140: 771–776.

3. Tracey, K. J. 2007. Physiology and immunology of the cholinergic antiinflammatory pathway. *J Clin Invest* 117: 289–296.

4. Rock, K. L., E. Latz, F. Ontiveros, and H. Kono. 2010. The sterile inflammatory response. *Annu. Rev. Immunol.* 28: 321–42.

5. Nathan, C. 2002. Points of control in inflammation. *Nature* 420: 846–852.

6. Kaczmarek, A., P. Vandenabeele, and D. Krysko. 2013. Necroptosis: The Release of Damage-Associated Molecular Patterns and Its Physiological Relevance. *Immunity* 38: 209–223.

7. Cohen, J. 2002. The immunopathogenesis of sepsis. *Nature* 420: 885–891.

8. Croft, M., C. a Benedict, and C. F. Ware. 2013. Clinical targeting of the TNF and TNFR superfamilies. *Nat. Rev. Drug Discov.* 12: 147–68.

9. Green, D. R., T. Ferguson, L. Zitvogel, and G. Kroemer. 2009. Immunogenic and tolerogenic cell death. *Nat. Rev. Immunol.* 9: 353–63.

10. Wallach, D., T.-B. Kang, and A. Kovalenko. 2014. Concepts of tissue injury and cell death in inflammation: a historical perspective. *Nat. Rev. Immunol.* 14: 51–59.

11. Matzinger, P. 1994. Tolerance, Danger, and the Extended Family. *Annu. Rev. Immunol.* 12: 991–1045.

12. Lamkanfi, M., and V. M. Dixit. 2010. Manipulation of Host Cell Death Pathways during Microbial Infections. *Cell Host Microbe* 8: 44–54.

13. Takeuchi, O., and S. Akira. 2010. Pattern Recognition Receptors and Inflammation. *Cell* 140: 805–820.

14. Davis, B. K., H. Wen, and J. P.-Y. Ting. 2011. The Inflammasome NLRs in Immunity, Inflammation, and Associated Diseases. *Annu. Rev. Immunol.* 29: 707–735.

15. Cai, X., Y.-H. Chiu, and Z. J. Chen. 2014. The cGAS-cGAMP-STING Pathway of Cytosolic DNA Sensing and Signaling. *Mol. Cell* 54: 289–296.

16. Kayagaki, N., M. T. Wong, I. B. Stowe, S. R. Ramani, L. C. Gonzalez, S. Akashi-Takamura, K. Miyake, J. Zhang, W. P. Lee, A. Muszynski, L. S. Forsberg, R. W. Carlson, and V. M. Dixit. 2013. Noncanonical Inflammasome Activation by Intracellular LPS Independent of TLR4. *Science (80-.).* 1246: 1246–1249.

17. Hagar, J. a, D. a Powell, Y. Aachoui, R. K. Ernst, and E. A. Miao. 2013. Cytoplasmic LPS activates caspase-11: implications in TLR4-independent endotoxic shock. *Science* 341: 1250–3.

18. Beutler, B., and E. T. Rietschel. 2003. Innate immune sensing and its roots: the story of endotoxin. *Nat. Rev. Immunol.* 3: 169–76.

19. Tan, Y., and J. C. Kagan. 2014. A Cross-Disciplinary Perspective on the Innate Immune Responses to Bacterial Lipopolysaccharide. *Mol. Cell* 54: 212–223.

20. Janeway, C. A. 1989. Approaching the Asymptote? Evolution and Revolution in Immunology. *Cold Spring Harb. Symp. Quant. Biol.* 54: 1–13.

21. Poltorak, A., X. He, I. Smirnova, M.-Y. Liu, C. Van Huffel, X. Du, D. Birdwell, E. Alejos, M. Silva, C. Galanos, M. Freudenberg, P. Ricciardi-Castagnoli, B. Layton, and B. Beutler. 1998. Defective LPS Signaling in C3H/HeJ and C57BL/10ScCr Mice: Mutations in Tlr4 Gene. *Science (80-.).* 282: 2085–2088.

22. Lemaitre, B., E. Nicolas, L. Michaut, J. M. Reichhart, and J. a Hoffmann. 1996. The dorsoventral regulatory gene cassette spätzle/Toll/cactus controls the potent antifungal response in Drosophila adults. *Cell* 86: 973–83.

23. Medzhitov, R., P. Preston-Hurlburt, E. Kopp, a Stadlen, C. Chen, S. Ghosh, and C. A. Janeway. 1998. MyD88 is an adaptor protein in the hToll/IL-1 receptor family signaling pathways. *Mol. Cell* 2: 253–8.

24. Kang, J. Y., and J.-O. Lee. 2011. Structural Biology of the Toll-Like Receptor Family. *Annu. Rev. Biochem.* 80: 917–941.

25. Moresco, E. M. Y., D. LaVine, and B. Beutler. 2011. Toll-like receptors. *Curr. Biol.* 21: R488–93.

26. Zanoni, I., R. Ostuni, L. R. Marek, S. Barresi, R. Barbalat, G. M. Barton, F. Granucci, and J. C. Kagan. 2011. CD14 controls the LPS-induced endocytosis of Toll-like receptor 4. *Cell* 147: 868–80.

27. Blasius, A. L., and B. Beutler. 2010. Intracellular Toll-like Receptors. *Immunity* 32: 305–315.

28. Alexopoulou, L., A. C. Holt, R. Medzhitov, and R. A. Flavell. 2001. Recognition of double-stranded RNA and activation of NF-[kappa]B by Toll-like receptor 3. *Nature* 413: 732–738.

29. Hemmi, H., T. Kaisho, O. Takeuchi, S. Sato, H. Sanjo, K. Hoshino, T. Horiuchi, H. Tomizawa, K. Takeda, and S. Akira. 2002. Small anti-viral compounds activate immune cells via the TLR7 MyD88-dependent signaling pathway. *Nat. Immunol.* 3: 196–200.

30. Colak, E., A. Leslie, K. Zausmer, E. Khatamzas, A. V Kubarenko, T. Pichulik, S. N. Klimosch, A. Mayer, O. Siggs, A. Hector, R. Fischer, B. Klesser, A. Rautanen, M. Frank, A. V. S. Hill, B. Manoury, B. Beutler, D. Hartl, A. Simmons, and A. N. R. Weber. 2014. RNA and Imidazoquinolines Are Sensed by Distinct TLR7/8 Ectodomain Sites Resulting in Functionally Disparate Signaling Events. *J. Immunol.* .

31. Yarovinsky, F. 2014. Innate immunity to Toxoplasma gondii infection. *Nat. Rev. Immunol.* 14: 109–21.

32. O'Neill, L. A. J., and A. G. Bowie. 2007. The family of five: TIR-domain-containing adaptors in Toll-like receptor signalling. *Nat Rev Immunol* 7: 353–364.

33. Kawai, T., O. Adachi, T. Ogawa, K. Takeda, and S. Akira. 1999. Unresponsiveness of MyD88-deficient mice to endotoxin. *Immunity* 11: 115–22.

34. Horng, T., G. M. Barton, R. A. Flavell, and R. Medzhitov. 2002. The adaptor molecule TIRAP provides signalling specificity for Toll-like receptors. *Nature* 420: 329–333.

35. Bonham, K. S., M. H. Orzalli, K. Hayashi, A. I. Wolf, C. Glanemann, W. Weninger, A. Iwasaki, D. M. Knipe, and J. C. Kagan. 2014. A Promiscuous Lipid-Binding Protein Diversifies the Subcellular Sites of Toll-like Receptor Signal Transduction. *Cell* 156: 705–716.

36. Fitzgerald, K. A., E. M. Palsson-McDermott, A. G. Bowie, C. A. Jefferies, A. S. Mansell, G. Brady, E. Brint, A. Dunne, P. Gray, M. T. Harte, D. McMurray, D. E. Smith, J. E. Sims, T. A. Bird, and L. A. J. O'Neill. 2001. Mal (MyD88-adapter-like) is required for Toll-like receptor-4 signal transduction. *Nature* 413: 78–83.

37. Kagan, J. C., and R. Medzhitov. 2006. Phosphoinositide-Mediated Adaptor Recruitment Controls Toll-like Receptor Signaling. *Cell* 125: 943–955.

38. Lin, S.-C., Y.-C. Lo, and H. Wu. 2010. Helical assembly in the MyD88-IRAK4-IRAK2 complex in TLR/IL-1R signalling. *Nature* 465: 885–890.

39. Muzio, M., J. Ni, P. Feng, and V. M. Dixit. 1997. IRAK (Pelle) Family Member IRAK-2 and MyD88 as Proximal Mediators of IL-1 Signaling. *Science (80-.).* 278: 1612–1615.

40. Li, S., A. Strelow, E. J. Fontana, and H. Wesche. 2002. IRAK-4: A novel member of the IRAK family with the properties of an IRAK-kinase. *Proc. Natl. Acad. Sci. U. S. A.* 99: 5567–5572.

41. Wu, H. 2013. Higher-order assemblies in a new paradigm of signal transduction. *Cell* 153: 287–92.

42. Kawagoe, T., S. Sato, K. Matsushita, H. Kato, K. Matsui, Y. Kumagai, T. Saitoh, T. Kawai, O. Takeuchi, and S. Akira. 2008. Sequential control of Toll-like receptor-dependent responses by IRAK1 and IRAK2. *Nat Immunol* 9: 684–691.

43. Conner, J. R., I. I. Smirnova, and A. Poltorak. 2009. A mutation in Irak2c identifies IRAK-2 as a central component of the TLR regulatory network of wild-derived mice. *J. Exp. Med.* 206: 1615–1631.

44. Flannery, S. M., S. E. Keating, J. Szymak, and A. G. Bowie. 2011. Human Interleukin-1 Receptor-associated Kinase-2 Is Essential for Toll-like Receptor-mediated Transcriptional and Post-transcriptional Regulation of Tumor Necrosis Factor alpha. *J. Biol. Chem.* 286: 23688–23697.

45. Kawai, T., and S. Akira. 2010. The role of pattern-recognition receptors in innate immunity: update on Toll-like receptors. *Nat Immunol* 11: 373–384.

46. Hoebe, K., X. Du, P. Georgel, E. Janssen, K. Tabeta, S. O. Kim, J. Goode, P. Lin, N. Mann, S. Mudd, K. Crozat, S. Sovath, J. Han, and B. Beutler. 2003. Identification of Lps2 as a key transducer of MyD88-independent TIR signalling. *Nature* 424: 743–8.

47. Yamamoto, M., S. Sato, H. Hemmi, K. Hoshino, T. Kaisho, H. Sanjo, O. Takeuchi, M. Sugiyama, M. Okabe, K. Takeda, and S. Akira. 2003. Role of Adaptor TRIF in the MyD88-Independent Toll-Like Receptor Signaling Pathway. *Science (80-.).* 301: 640–643.

48. Yamamoto, M., S. Sato, H. Hemmi, S. Uematsu, K. Hoshino, T. Kaisho, O. Takeuchi, K. Takeda, and S. Akira. 2003. TRAM is specifically involved in the Toll-like receptor 4-mediated MyD88-independent signaling pathway. *Nat. Immunol.* 4: 1144–50.

49. Kagan, J. C., T. Su, T. Horng, A. Chow, S. Akira, and R. Medzhitov. 2008. TRAM couples endocytosis of Toll-like receptor 4 to the induction of interferon-[beta]. *Nat Immunol* 9: 361–368.

50. Fitzgerald, K. A., D. C. Rowe, B. J. Barnes, D. R. Caffrey, A. Visintin, E. Latz, B. Monks, P. M. Pitha, and D. T. Golenbock. 2003. LPS-TLR4 signaling to IRF-3/7 and NF-kappaB involves the toll adapters TRAM and TRIF. *J. Exp. Med.* 198: 1043–55.

51. Meylan, E., K. Burns, K. Hofmann, V. Blancheteau, F. Martinon, M. A. Kelliher, and J. Tschopp. 2004. RIP1 is an essential mediator of Toll-like receptor 3-induced NF-[kappa]B activation. *Nat Immunol* 5: 503–507.

52. Jiang, Z., P. Georgel, X. Du, L. Shamel, S. Sovath, S. Mudd, M. Huber, C. Kalis, S. Keck, C. Galanos, M. Freudenberg, and B. Beutler. 2005. CD14 is required for MyD88-independent LPS signaling. *Nat. Immunol.* 6: 565–70.

53. Oganesyan, G., S. K. Saha, B. Guo, J. Q. He, A. Shahangian, B. Zarnegar, A. Perry, and G. Cheng. 2006. Critical role of TRAF3 in the Toll-like receptor-dependent and -independent antiviral response. *Nature* 439: 208–11.

54. Häcker, H., V. Redecke, B. Blagoev, I. Kratchmarova, L.-C. Hsu, G. G. Wang, M. P. Kamps, E. Raz, H. Wagner, G. Häcker, M. Mann, and M. Karin. 2006. Specificity in Toll-like receptor signalling through distinct effector functions of TRAF3 and TRAF6. *Nature* 439: 204–7.

55. Napetschnig, J., and H. Wu. 2013. Molecular Basis of NF-κB Signaling. *Annu. Rev. Biophys.* 42: 443–68.

56. Li, J., T. McQuade, A. Siemer, J. Napetschnig, K. Moriwaki, Y.-S. Hsiao, E. Damko, D. M. Moquin, T. Walz, A. McDermott, F. K.-M. Chan, and H. Wu. 2012. The RIP1/RIP3 Necrosome Forms a Functional Amyloid Signaling Complex Required for Programmed Necrosis. *Cell* 150: 339–350.

57. Gilmore, T. D. 2006. Introduction to NF-kappaB: players, pathways, perspectives. *Oncogene* 25: 6680–4.

58. Kawai, T., and S. Akira. 2007. Signaling to NF-kappaB by Toll-like receptors. *Trends Mol. Med.* 13: 460–9.

59. Hayden, M. S., and S. Ghosh. 2008. Shared Principles in NF-kB Signaling. *Cell* 132: 344–362.

60. Kyriakis, J. M., and J. Avruch. 2012. Mammalian MAPK signal transduction pathways activated by stress and inflammation: a 10-year update. *Physiol. Rev.* 92: 689–737.

61. Arthur, J. S. C., and S. C. Ley. 2013. Mitogen-activated protein kinases in innate immunity. *Nat. Rev. Immunol.* 13: 679–692.

62. Park, J. M., F. R. Greten, A. Wong, R. J. Westrick, J. S. C. Arthur, K. Otsu, A. Hoffmann, M. Montminy, and M. Karin. 2005. Signaling Pathways and Genes that Inhibit Pathogen-Induced Macrophage Apoptosis- CREB and NF-[kappa]B as Key Regulators. *Immunity* 23: 319–329.

63. Smale, S. T. 2014. Transcriptional regulation in the immune system: a status report. *Trends Immunol.* 35: 190–194.

64. Sabio, G., and R. J. Davis. 2014. TNF and MAP kinase signalling pathways. *Semin. Immunol.* 26: 237–245.

65. Smale, S. T. 2012. Transcriptional regulation in the innate immune system. *Curr. Opin. Immunol.* 24: 51–57.

66. Natoli, G., S. Saccani, D. Bosisio, and I. Marazzi. 2005. Interactions of NF-[kappa]B with chromatin: the art of being at the right place at the right time. *Nat Immunol* 6: 439–445.

67. Anderson, P. 2008. Post-transcriptional control of cytokine production. *Nat Immunol* 9: 353–359.

68. Hao, S., and D. Baltimore. 2009. The stability of mRNA influences the temporal order of the induction of genes encoding inflammatory molecules. *Nat Immunol* 10: 281–288.

69. Wertz, I. E., and V. M. Dixit. 2010. Regulation of death receptor signaling by the ubiquitin system. *Cell Death Differ* 17: 14–24.

70. Iwai, K. 2012. Diverse ubiquitin signaling in NF-kB activation. *Trends Cell Biol.* 22: 355–364.

71. Harhaj, E. W., and V. M. Dixit. 2011. Deubiquitinases in the regulation of NF-κB signaling. *Cell Res.* 21: 22–39.

72. Zinngrebe, J., A. Montinaro, N. Peltzer, and H. Walczak. 2014. Ubiquitin in the immune system. *EMBO Rep.* 15: 28–45.

73. Sun, S.-C. 2008. Deubiquitylation and regulation of the immune response. *Nat Rev Immunol* 8: 501–511.

74. Ye, Y., G. Blaser, M. H. Horrocks, M. J. Ruedas-Rama, S. Ibrahim, A. a Zhukov, A. Orte, D. Klenerman, S. E. Jackson, and D. Komander. 2012. Ubiquitin chain conformation regulates recognition and activity of interacting proteins. *Nature* 492: 266–70.

75. Newton, K., M. L. Matsumoto, I. E. Wertz, D. S. Kirkpatrick, J. R. Lill, J. Tan, D. Dugger, N. Gordon, S. S. Sidhu, F. a Fellouse, L. Komuves, D. M. French, R. E. Ferrando, C. Lam, D. Compaan, C. Yu, I. Bosanac, S. G. Hymowitz, R. F. Kelley, and V. M. Dixit. 2008. Ubiquitin chain editing revealed by polyubiquitin linkage-specific antibodies. *Cell* 134: 668–78.

76. Wang, L., F. Du, and X. Wang. 2008. TNF-[alpha] Induces Two Distinct Caspase-8 Activation Pathways. *Cell* 133: 693–703.

77. Bignell, G. R., W. Warren, S. Seal, M. Takahashi, E. Rapley, R. Barfoot, H. Green, C. Brown, P. J. Biggs, S. R. Lakhani, C. Jones, J. Hansen, E. Blair, B. Hofmann, R. Siebert, G. Turner, D. G. Evans, C. Schrander-Stumpel, F. A. Beemer, A. van den Ouweland, D. Halley, B. Delpech, M. G. Cleveland, I. Leigh, J. Leisti, S. Rasmussen, M. R. Wallace, C. Fenske, P. Banerjee, N. Oiso, R. Chaggar, S. Merrett, N. Leonard, M. Huber, D. Hohl, P. Chapman, J. Burn, S. Swift, A. Smith, A. Ashworth, and M. R. Stratton. 2000. Identification of the familial cylindromatosis tumour-suppressor gene. *Nat Genet* 25: 160–165.

78. Bowen, S., M. Gill, D. a Lee, G. Fisher, R. G. Geronemus, M. E. Vazquez, and J. T. Celebi. 2005. Mutations in the CYLD gene in Brooke-Spiegler syndrome, familial cylindromatosis, and multiple familial trichoepithelioma: lack of genotype-phenotype correlation. *J. Invest. Dermatol.* 124: 919–20.

79. Blake, P. W., and J. R. Toro. 2009. Update of cylindromatosis gene (CYLD) mutations in Brooke-Spiegler syndrome: novel insights into the role of deubiquitination in cell signaling. *Hum. Mutat.* 30: 1025–1036.

80. Sun, S.-C. 2010. CYLD: a tumor suppressor deubiquitinase regulating NF-[kappa]B activation and diverse biological processes. *Cell Death Differ* 17: 25–34.

81. Massoumi, R. 2010. Ubiquitin chain cleavage: CYLD at work. *Trends Biochem. Sci.* 35: 392–399.

82. Trompouki, E., E. Hatzivassiliou, T. Tsichritzis, H. Farmer, A. Ashworth, and G. Mosialos. 2003. CYLD is a deubiquitinating enzyme that negatively regulates NF-[kappa]B activation by TNFR family members. *Nature* 424: 793–796.

83. Brummelkamp, T. R., S. M. B. Nijman, A. M. G. Dirac, and R. Bernards. 2003. Loss of the cylindromatosis tumour suppressor inhibits apoptosis by activating NF-[kappa]B. *Nature* 424: 797–801.

84. Kovalenko, A., C. Chable-Bessia, G. Cantarella, A. Israel, D. Wallach, and G. Courtois. 2003. The tumour suppressor CYLD negatively regulates NF-[kappa]B signalling by deubiquitination. *Nature* 424: 801–805.

85. Reiley, W. W., M. Zhang, W. Jin, M. Losiewicz, K. B. Donohue, C. C. Norbury, and S.-C. Sun. 2006. Regulation of T cell development by the deubiquitinating enzyme CYLD. *Nat Immunol* 7: 411–417.

86. Zhang, J., B. Stirling, S. T. Temmerman, C. A. Ma, I. J. Fuss, J. M. J. Derry, and A. Jain. 2006. Impaired regulation of NF-kB and increased susceptibility to colitis-associated tumorigenesis in CYLD-deficient mice. *J. Clin. Invest.* 116: 3042–3049.

87. Massoumi, R., K. Chmielarska, K. Hennecke, A. Pfeifer, and R. Fassler. 2006. Cyld Inhibits Tumor Cell Proliferation by Blocking Bcl-3-Dependent NF-[kappa]B Signaling. *Cell* 125: 665–677.

88. Reiley, W. W., W. Jin, A. J. Lee, A. Wright, X. Wu, E. F. Tewalt, T. O. Leonard, C. C. Norbury, L. Fitzpatrick, M. Zhang, and S.-C. Sun. 2007. Deubiquitinating enzyme CYLD negatively regulates the ubiquitin-dependent kinase Tak1 and prevents abnormal T cell responses. *J. Exp. Med.* 204: 1475–1485.

89. Wright, A., W. W. Reiley, M. Chang, W. Jin, A. J. Lee, M. Zhang, and S.-C. Sun. 2007. Regulation of Early Wave of Germ Cell Apoptosis and Spermatogenesis by Deubiquitinating Enzyme CYLD. *Dev. Cell* 13: 705–716.

90. Jin, W., M. Chang, E. M. Paul, G. Babu, A. J. Lee, W. W. Reiley, A. Wright, M. Zhang, J. You, and S.-C. Sun. 2008. Deubiquitinating enzyme CYLD negatively regulates RANK signaling and osteoclastogenesis in mice. *J. Clin. Invest.* 118: 1858–1866.

91. Zhang, M., X. Wu, A. J. Lee, W. Jin, M. Chang, A. Wright, T. Imaizumi, and S.-C. Sun. 2008. Regulation of IkappaB Kinase-related Kinases and Antiviral Responses by Tumor Suppressor CYLD. *J. Biol. Chem.* 283: 18621–18626.

92. O'Donnell, M. A., E. Perez-Jimenez, A. Oberst, A. Ng, R. Massoumi, R. Xavier, D. R. Green, and A. T. Ting. 2011. Caspase 8 inhibits programmed necrosis by processing CYLD. *Nat Cell Biol* 13: 1437–1442.

93. Font-Burgada, J., E. Seki, and M. Karin. 2012. CYLD and HCC: When Being Too Sensitive to Your Dirty Neighbors Results in Self-Destruction. *Cancer Cell* 21: 711–712.

94. Moquin, D. M., T. McQuade, and F. K.-M. Chan. 2013. CYLD Deubiquitinates RIP1 in the TNFα-Induced Necrosome to Facilitate Kinase Activation and Programmed Necrosis. *PLoS One* 8: e76841.

95. Jono, H., J. H. Lim, L.-F. Chen, H. Xu, E. Trompouki, Z. K. Pan, G. Mosialos, and J.-D. Li. 2004. NF-kB Is Essential for Induction of CYLD, the Negative Regulator of NF-kB. *J. Biol. Chem.* 279: 36171–36174.

96. Liang, G., K. Ahlqvist, R. Pannem, G. Posern, and R. Massoumi. 2011. Serum response factor controls CYLD expression via MAPK signaling pathway. *PLoS One* 6: e19613.

97. Wang, L., R. A. Baiocchi, S. Pal, G. Mosialos, M. Caligiuri, and S. Sif. 2005. The BRG1- and hBRM-Associated Factor BAF57 Induces Apoptosis by Stimulating Expression of the Cylindromatosis Tumor Suppressor Gene. *Mol. Cell. Biol.* 25: 7953–7965.

98. Espinosa, L., S. Cathelin, T. D'Altri, T. Trimarchi, A. Statnikov, J. Guiu, V. Rodilla, J. Inglés-Esteve, J. Nomdedeu, B. Bellosillo, C. Besses, O. Abdel-Wahab, N. Kucine, S.-C. Sun, G. Song, C. C. Mullighan, R. L. Levine, K. Rajewsky, I. Aifantis, and A. Bigas. 2010. The Notch/Hes1 pathway sustains NF-κB activation through CYLD repression in T cell leukemia. *Cancer Cell* 18: 268–81.

99. Liu, P., B. Xu, W. Shen, H. Zhu, W. Wu, Y. Fu, H. Chen, H. Dong, Y. Zhu, K. Miao, W. Xu, and J. Li. 2012. Dysregulation of TNF[alpha]-induced necroptotic signaling in chronic lymphocytic leukemia: suppression of CYLD gene by LEF1. *Leukemia* 26: 1293–1300.

100. Kuphal, S., G. Shaw-Hallgren, M. Eberl, S. Karrer, F. Aberger, A. K. Bosserhoff, and R. Massoumi. 2011. GLI1-dependent transcriptional repression of CYLD in basal cell carcinoma. *Oncogene* 30: 4523–4530.

101. Massoumi, R., S. Kuphal, C. Hellerbrand, B. Haas, P. Wild, T. Spruss, A. Pfeifer, R. Fässler, and A. K. Bosserhoff. 2009. Down-regulation of CYLD expression by Snail promotes tumor progression in malignant melanoma. *J. Exp. Med.* 206: 221–32.

102. Iliopoulos, D., S. A. Jaeger, H. A. Hirsch, M. L. Bulyk, and K. Struhl. 2010. STAT3 Activation of miR-21 and miR-181b-1 via PTEN and CYLD Are Part of the Epigenetic Switch Linking Inflammation to Cancer. *Mol. Cell* 39: 493–506.

103. Ye, H., X. Liu, M. Lv, Y. Wu, S. Kuang, J. Gong, P. Yuan, Z. Zhong, Q. Li, H. Jia, J. Sun, Z. Chen, and A.-Y. Guo. 2012. MicroRNA and transcription factor co-regulatory network analysis reveals miR-19 inhibits CYLD in T-cell acute lymphoblastic leukemia. *Nucleic Acids Res.* 40: 5201–14.

104. Friedman, C. S., M. A. O'Donnell, D. Legarda-Addison, A. Ng, W. B. Cardenas, J. S. Yount, T. M. Moran, C. F. Basler, A. Komuro, C. M. Horvath, R. Xavier, and A. T. Ting. 2008. The tumour suppressor CYLD is a negative regulator of RIG-I-mediated antiviral response. *EMBO Rep* 9: 930–936.

105. Hovelmeyer, N., F. T. Wunderlich, R. Massoumi, C. G. Jakobsen, J. Song, M. A. Worns, C. Merkwirth, A. Kovalenko, M. Aumailley, D. Strand, J. C. Bruning, P. R. Galle, D. Wallach, R. Fassler, and A. Waisman. 2007. Regulation of B cell homeostasis and activation by the tumor suppressor gene CYLD. *J. Exp. Med.* 204: 2615–2627.

106. Reiley, W. W., M. Zhang, X. Wu, E. Granger, and S.-C. Sun. 2005. Regulation of the Deubiquitinating Enzyme CYLD by IkB Kinase Gamma-Dependent Phosphorylation. *Mol. Cell. Biol.* 25: 3886–3895.

107. Hutti, J. E., R. R. Shen, D. W. Abbott, A. Y. Zhou, K. M. Sprott, J. M. Asara, W. C. Hahn, and L. C. Cantley. 2009. Phosphorylation of the Tumor Suppressor CYLD by the Breast Cancer Oncogene IKK[var epsilon] Promotes Cell Transformation. *Mol. Cell* 34: 461–472.

108. An, J., D. Mo, H. Liu, M. S. Veena, E. S. Srivatsan, R. Massoumi, and M. B. Rettig. 2008. Inactivation of the CYLD Deubiquitinase by HPV E6 Mediates Hypoxia-Induced NF-kB Activation. *Cancer Cell* 14: 394–407.

109. Kerr, J. F. R., A. H. Wyllie, and A. R. Currie. 1972. Apoptosis: A basic biological phenomenon with wide-ranging implications in tissue kinetics. *Br. J. Cancer* 26.

110. Kroemer, G., L. Galluzzi, P. Vandenabeele, J. Abrams, E. S. Alnemri, E. H. Baehrecke, M. V Blagosklonny, W. S. El-Deiry, P. Golstein, D. R. Green, M. Hengartner, R. A. Knight, S. Kumar, S. A. Lipton, W. Malorni, G. Nunez, M. E. Peter, J. Tschopp, J. Yuan, M. Piacentini, B. Zhivotovsky, and G. Melino. 2009. Classification of cell death: recommendations of the Nomenclature Committee on Cell Death 2009. *Cell Death Differ* 16: 3–11.

111. Galluzzi, L., I. Vitale, J. M. Abrams, E. S. Alnemri, E. H. Baehrecke, M. V Blagosklonny, T. M. Dawson, V. L. Dawson, W. S. El-Deiry, S. Fulda, E. Gottlieb, D. R. Green, M. O. Hengartner, O. Kepp, R. A. Knight, S. Kumar, S. A. Lipton, X. Lu, F. Madeo, W. Malorni, P. Mehlen, G. Nunez, M. E. Peter, M. Piacentini, D. C. Rubinsztein, Y. Shi, H. U. Simon, P. Vandenabeele, E. White, J. Yuan, B. Zhivotovsky, G. Melino, and G. Kroemer. 2011. Molecular definitions of cell death subroutines: recommendations of the Nomenclature Committee on Cell Death 2012. *Cell Death Differ* .

112. Salvesen, G. S., and S. J. Riedl. 2008. Caspase mechanisms. *Adv. Exp. Med. Biol.* 615: 13–23.

113. Duprez, L., E. Wirawan, T. Vanden Berghe, and P. Vandenabeele. 2009. Major cell death pathways at a glance. *Microbes Infect.* 11: 1050–1062.

114. Youle, R. J., and A. Strasser. 2008. The BCL-2 protein family: opposing activities that mediate cell death. *Nat. Rev. Mol. Cell Biol.* 9: 47–59.

115. Berghe, T. Vanden, A. Linkermann, S. Jouan-Lanhouet, H. Walczak, and P. Vandenabeele. 2014. Regulated necrosis: the expanding network of non-apoptotic cell death pathways. *Nat. Rev. Mol. Cell Biol.* 15: 135–147.

116. Vandenabeele, P., L. Galluzzi, T. Vanden Berghe, and G. Kroemer. 2010. Molecular mechanisms of necroptosis: an ordered cellular explosion. *Nat Rev Mol Cell Biol* 11: 700–714.

117. Miao, E. A., J. V Rajan, and A. Aderem. 2011. Caspase-1-induced pyroptotic cell death. *Immunol. Rev.* 243: 206–14.

118. Lu, A., V. G. Magupalli, J. Ruan, Q. Yin, M. K. Atianand, M. R. Vos, G. F. Schröder, K. A. Fitzgerald, H. Wu, and E. H. Egelman. 2014. Unified Polymerization Mechanism for the Assembly of ASC-Dependent Inflammasomes. *Cell* 156: 1193–1206.

119. Cai, X., J. Chen, H. Xu, S. Liu, Q.-X. Jiang, R. Halfmann, and Z. J. Chen. 2014. Prion-like Polymerization Underlies Signal Transduction in Antiviral Immune Defense and Inflammasome Activation. *Cell* 156: 1207–1222.

120. Kayagaki, N., S. Warming, M. Lamkanfi, L. Vande Walle, S. Louie, J. Dong, K. Newton, Y. Qu, J. Liu, S. Heldens, J. Zhang, W. P. Lee, M. Roose-Girma, and V. M. Dixit. 2011. Non-canonical inflammasome activation targets caspase-11. *Nature* advance on.

121. Aachoui, Y., I. a Leaf, J. a Hagar, M. F. Fontana, C. G. Campos, D. E. Zak, M. H. Tan, P. a Cotter, R. E. Vance, A. Aderem, and E. A. Miao. 2013. Caspase-11 protects against bacteria that escape the vacuole. *Science* 339: 975–8.

122. Zhang, D., J. Lin, and J. Han. 2010. Receptor-interacting protein (RIP) kinase family. *Cell Mol Immunol* 7: 243–249.

123. Ofengeim, D., and J. Yuan. 2013. Regulation of RIP1 kinase signalling at the crossroads of inflammation and cell death. *Nat. Rev. Mol. Cell Biol.* 14: 727–736.

124. Lee, T. H., J. Shank, N. Cusson, and M. A. Kelliher. 2004. The Kinase Activity of Rip1 Is Not Required for Tumor Necrosis Factor-alpha-induced IkB Kinase or p38 MAP Kinase Activation or for the Ubiquitination of Rip1 by Traf2. *J. Biol. Chem.* 279: 33185–33191.

125. Haas, T. L., C. H. Emmerich, B. Gerlach, A. C. Schmukle, S. M. Cordier, E. Rieser, R. Feltham, J. E. Vince, U. Warnken, T. Wenger, R. Koschny, D. Komander, J. Silke, and H. Walczak. 2009. Recruitment of the Linear Ubiquitin Chain Assembly Complex Stabilizes the TNF-R1 Signaling Complex and Is Required for TNF-Mediated Gene Induction. *Mol. Cell* 36: 831–844.

126. Walczak, H. 2011. TNF and ubiquitin at the crossroads of gene activation, cell death, inflammation, and cancer. *Immunol. Rev.* 244: 9–28.

127. O'Donnell, M., and A. T. Ting. 2012. NFκB and ubiquitination: partners in disarming RIPK1-mediated cell death. *Immunol. Res.* 1–13.

128. Darding, M., and P. Meier. 2012. IAPs: Guardians of RIPK1. *Cell Death Differ* 19: 58–66.

129. Micheau, O., and J. Tschopp. 2003. Induction of TNF receptor I-mediated apoptosis via two sequential signaling complexes. *Cell* 114: 181–90.

130. Komander, D., F. Reyes-Turcu, J. D. F. Licchesi, P. Odenwaelder, K. D. Wilkinson, and D. Barford. 2009. Molecular discrimination of structurally equivalent Lys 63-linked and linear polyubiquitin chains. *EMBO Rep* 10: 466–473.

131. Bertrand, M. J. M., and P. Vandenabeele. 2011. The Ripoptosome: Death Decision in the Cytosol. *Mol. Cell* 43: 323–325.

132. Cusson-Hermance, N., S. Khurana, T. H. Lee, K. A. Fitzgerald, and M. A. Kelliher. 2005. Rip1 mediates the Trif-dependent toll-like receptor 3- and 4-induced NF-{kappa}B activation but does not contribute to interferon regulatory factor 3 activation. *J. Biol. Chem.* 280: 36560–6.

133. Chang, M., W. Jin, and S.-C. Sun. 2009. Peli1 facilitates TRIF-dependent Toll-like receptor signaling and proinflammatory cytokine production. *Nat. Immunol.* 10: 1089–95.

134. Christofferson, D. E., Y. Li, and J. Yuan. 2014. Control of Life-or-Death Decisions by RIP1 Kinase. *Annu. Rev. Physiol.* 76: 129–50.

135. Walczak, H. 2013. Death receptor-ligand systems in cancer, cell death, and inflammation. *Cold Spring Harb. Perspect. Biol.* 5: a008698.

136. Feoktistova, M., P. Geserick, B. Kellert, D. P. Dimitrova, C. Langlais, M. Hupe, K. Cain, M. MacFarlane, G. Hacker, and M. Leverkus. 2011. cIAPs Block Ripoptosome Formation, a RIP1/Caspase-8 Containing Intracellular Cell Death Complex Differentially Regulated by cFLIP Isoforms. *Mol. Cell* 43: 449–63.

137. Kaiser, W. J., H. Sridharan, C. Huang, P. Mandal, J. W. Upton, P. J. Gough, C. a Sehon, R. W. Marquis, J. Bertin, and E. S. Mocarski. 2013. Toll-like Receptor 3-mediated necrosis via TRIF, RIP3 and MLKL. *J. Biol. Chem.* 288: 31268–79.

138. Vercammen, D., R. Beyaert, G. Denecker, V. Goossens, G. Van Loo, W. Declercq, J. Grooten, W. Fiers, and P. Vandenabeele. 1998. Inhibition of Caspases Increases the Sensitivity of L929 Cells to Necrosis Mediated by Tumor Necrosis Factor. *J. Exp. Med.* 187: 1477–1485.

139. Vercammen, D., G. Brouckaert, G. Denecker, M. Van de Craen, W. Declercq, W. Fiers, and P. Vandenabeele. 1998. Dual signaling of the Fas receptor: initiation of both apoptotic and necrotic cell death pathways. *J. Exp. Med.* 188: 919–30.

140. Holler, N., R. Zaru, O. Micheau, M. Thome, A. Attinger, S. Valitutti, J.-L. Bodmer, P. Schneider, B. Seed, and J. Tschopp. 2000. Fas triggers an alternative, caspase-8-independent cell death pathway using the kinase RIP as effector molecule. *Nat Immunol* 1: 489–495.

141. Matsumura, H., Y. Shimizu, Y. Ohsawa, a Kawahara, Y. Uchiyama, and S. Nagata. 2000. Necrotic death pathway in Fas receptor signaling. *J. Cell Biol.* 151: 1247–56.

142. Chan, F. K.-M., J. Shisler, J. G. Bixby, M. Felices, L. Zheng, M. Appel, J. Orenstein, B. Moss, and M. J. Lenardo. 2003. A role for tumor necrosis factor receptor-2

and receptor-interacting protein in programmed necrosis and antiviral responses. *J. Biol. Chem.* 278: 51613–21.

143. Pop, C., A. Oberst, M. Drag, B. J. Van¬†Raam, S. J. Riedl, D. R. Green, and G. S. Salvesen. 2011. FLIPL induces caspase 8 activity in the absence of interdomain caspase 8 cleavage and alters substrate specificity. *Biochem. J.* 433: 447–457.

144. Oberst, A., C. P. Dillon, R. Weinlich, L. L. McCormick, P. Fitzgerald, C. Pop, R. Hakem, G. S. Salvesen, and D. R. Green. 2011. Catalytic activity of the caspase-8-FLIPL complex inhibits RIPK3-dependent necrosis. *Nature* 471: 363–367.

145. Degterev, A., Z. Huang, M. Boyce, Y. Li, P. Jagtap, N. Mizushima, G. D. Cuny, T. J. Mitchison, M. A. Moskowitz, and J. Yuan. 2005. Chemical inhibitor of nonapoptotic cell death with therapeutic potential for ischemic brain injury. *Nat Chem Biol* 1: 112–119.

146. Degterev, A., J. Hitomi, M. Germscheid, I. L. Ch'en, O. Korkina, X. Teng, D. Abbott, G. D. Cuny, C. Yuan, G. Wagner, S. M. Hedrick, S. A. Gerber, A. Lugovskoy, and J. Yuan. 2008. Identification of RIP1 kinase as a specific cellular target of necrostatins. *Nat Chem Biol* 4: 313–321.

147. Hitomi, J., D. E. Christofferson, A. Ng, J. Yao, A. Degterev, R. J. Xavier, and J. Yuan. 2008. Identification of a Molecular Signaling Network that Regulates a Cellular Necrotic Cell Death Pathway. *Cell* 135: 1311–1323.

148. Cho, Y., S. Challa, D. M. Moquin, R. Genga, T. D. Ray, M. Guildford, and F. K.-M. Chan. 2009. Phosphorylation-Driven Assembly of the RIP1-RIP3 Complex Regulates Programmed Necrosis and Virus-Induced Inflammation. *Cell* 137: 1112–1123.

149. He, S., L. Wang, L. Miao, T. Wang, F. Du, L. Zhao, and X. Wang. 2009. Receptor Interacting Protein Kinase-3 Determines Cellular Necrotic Response to TNF-[alpha]. *Cell* 137: 1100–1111.

150. Zhang, D.-W., J. Shao, J. Lin, N. Zhang, B.-J. Lu, S.-C. Lin, M.-Q. Dong, and J. Han. 2009. RIP3, an Energy Metabolism Regulator That Switches TNF-Induced Cell Death from Apoptosis to Necrosis. *Science (80-.).* 325: 332–336.

151. Newton, K., D. L. Dugger, K. E. Wickliffe, N. Kapoor, M. Cristina de-Almagro, D. Vucic, L. Komuves, R. E. Ferrando, D. M. French, J. Webster, M. Roose-Girma, S. Warming, and V. M. Dixit. 2014. Activity of Protein Kinase RIPK3 Determines whether Cells Die by Necroptosis or Apoptosis. *Science* 343: 1357–1360.

152. Orozco, S., N. Yatim, M. R. Werner, H. Tran, S. Y. Gunja, S. W. Tait, M. L. Albert, D. R. Green, and A. Oberst. 2014. RIPK1 both positively and negatively regulates RIPK3 oligomerization and necroptosis. *Cell Death Differ.* 1–11.

153. Wu, X.-N., Z.-H. Yang, X.-K. Wang, Y. Zhang, H. Wan, Y. Song, X. Chen, J. Shao, and J. Han. 2014. Distinct roles of RIP1-RIP3 hetero- and RIP3-RIP3 homo-interaction in mediating necroptosis. *Cell Death Differ.* 1–12.

154. Cook, W. D., D. M. Moujalled, T. J. Ralph, P. Lock, S. N. Young, J. M. Murphy, and D. L. Vaux. 2014. RIPK1- and RIPK3-induced cell death mode is determined by target availability. *Cell Death Differ.* 1–13.

155. Tenev, T., K. Bianchi, M. Darding, M. Broemer, C. Langlais, F. Wallberg, A. Zachariou, J. Lopez, M. MacFarlane, K. Cain, and P. Meier. 2011. The Ripoptosome, a Signaling Platform that Assembles in Response to Genotoxic Stress and Loss of IAPs. *Mol. Cell* 43: 432–448.

156. Wallach, D., A. Kovalenko, and T.-B. Kang. 2011. Necrosome -induced inflammation: must cells die for it? *Trends Immunol.* 32: 505–509.

157. Dillon, C. P., A. Oberst, R. Weinlich, L. J. Janke, T.-B. Kang, T. Ben-Moshe, T. W. Mak, D. Wallach, and D. R. Green. 2012. Survival function of the FADD-CASPASE-8-cFLIP(L) complex. *Cell Rep.* 1: 401–7.

158. Oberst, A., and D. R. Green. 2011. It cuts both ways: reconciling the dual roles of caspase 8 in cell death and survival. *Nat Rev Mol Cell Biol* 12: 757–763.

159. Sun, L., H. Wang, Z. Wang, S. He, S. Chen, D. Liao, L. Wang, J. Yan, W. Liu, X. Lei, and X. Wang. 2012. Mixed Lineage Kinase Domain-like Protein Mediates Necrosis Signaling Downstream of RIP3 Kinase. *Cell* 148: 213–227.

160. Zhao, J., S. Jitkaew, Z. Cai, S. Choksi, Q. Li, J. Luo, and Z.-G. Liu. 2012. Mixed lineage kinase domain-like is a key receptor interacting protein 3 downstream component of TNF-induced necrosis. *Proc. Natl. Acad. Sci. U. S. A.* 109: 5322–7.

161. Wang, Z., H. Jiang, S. Chen, F. Du, and X. Wang. 2012. The Mitochondrial Phosphatase PGAM5 Functions at the Convergence Point of Multiple Necrotic Death Pathways. *Cell* 148: 228–243.

162. Tait, S. W. G., A. Oberst, G. Quarato, S. Milasta, M. Haller, R. Wang, M. Karvela, G. Ichim, N. Yatim, M. L. Albert, G. Kidd, R. Wakefield, S. Frase, S. Krautwald, A. Linkermann, and D. R. Green. 2013. Widespread mitochondrial depletion via mitophagy does not compromise necroptosis. *Cell Rep.* 5: 878–85.

163. Murphy, J. M., P. E. Czabotar, J. M. Hildebrand, I. S. Lucet, J.-G. Zhang, S. Alvarez-Diaz, R. Lewis, N. Lalaoui, D. Metcalf, A. I. Webb, S. N. Young, L. N. Varghese, G. M. Tannahill, E. C. Hatchell, I. J. Majewski, T. Okamoto, R. C. J. Dobson, D. J. Hilton, J. J. Babon, N. A. Nicola, A. Strasser, J. Silke, and W. S. Alexander. 2013. The Pseudokinase MLKL Mediates Necroptosis via a Molecular Switch Mechanism. *Immunity* 39: 443–453.

164. Green, D. R. 2013. Pseudokiller, Qu'est-ce que C'est? *Immunity* 39: 421–422.

165. Wang, H., L. Sun, L. Su, J. Rizo, L. Liu, L.-F. Wang, F.-S. Wang, and X. Wang. 2014. Mixed Lineage Kinase Domain-like Protein MLKL Causes Necrotic Membrane Disruption upon Phosphorylation by RIP3. *Mol. Cell* 54: 133–146.

166. Chen, X., W. Li, J. Ren, D. Huang, W.-T. He, Y. Song, C. Yang, W. Li, X. Zheng, P. Chen, and J. Han. 2013. Translocation of mixed lineage kinase domain-like protein to plasma membrane leads to necrotic cell death. *Cell Res.* 1: 1–17.

167. Cai, Z., S. Jitkaew, J. Zhao, H.-C. Chiang, S. Choksi, J. Liu, Y. Ward, L.-G. Wu, and Z.-G. Liu. 2013. Plasma membrane translocation of trimerized MLKL protein is required for TNF-induced necroptosis. *Nat. Cell Biol.* 15: 1–13.

168. Dondelinger, Y., W. Declercq, S. Montessuit, R. Roelandt, A. Goncalves, I. Bruggeman, P. Hulpiau, K. Weber, C. A. Sehon, R. W. Marquis, J. Bertin, P. J. Gough, S. Savvides, J.-C. Martinou, M. J. M. Bertrand, and P. Vandenabeele. 2014. MLKL Compromises Plasma Membrane Integrity by Binding to Phosphatidylinositol Phosphates. *Cell Rep.* 1–11.

169. Fuentes-Prior, P., and G. S. Salvesen. 2004. The protein structures that shape caspase activity, specificity, activation and inhibition. *Biochem. J.* 384: 201–32.

170. Ekert, P. G., J. Silke, and D. L. Vaux. 1999. Caspase inhibitors. *Cell Death Differ.* 6: 1081–6.

171. Upton, J. W., and F. K.-M. Chan. 2014. Staying Alive: Cell Death in Antiviral Immunity. *Mol. Cell* 54: 273–280.

172. Schotte, P., W. Declercq, V. Hu, P. Vandenabeele, and R. Beyaert. 1999. Non-specific effects of methyl ketone peptide inhibitors of caspases. *FEBS Lett.* 442: 117–121.

173. Biton, S., and A. Ashkenazi. 2011. NEMO and RIP1 Control Cell Fate in Response to Extensive DNA Damage via TNF-[alpha] Feedforward Signaling. *Cell* 145: 92–103.

174. Degterev, A., J. L. Maki, and J. Yuan. 2013. Activity and specificity of necrostatin-1, small-molecule inhibitor of RIP1 kinase. *Cell Death Differ.* 20: 366.

175. Xie, T., W. Peng, Y. Liu, C. Yan, J. L. Maki, A. Degterev, J. Yuan, and Y. Shi. 2013. Structural basis of RIP1 inhibition by necrostatins. *Structure* 21: 493–9.

176. Takahashi, N., L. Duprez, S. Grootjans, a Cauwels, W. Nerinckx, J. B. DuHadaway, V. Goossens, R. Roelandt, F. Van Hauwermeiren, C. Libert, W. Declercq, N. Callewaert, G. C. Prendergast, A. Degterev, J. Yuan, and P. Vandenabeele. 2012. Necrostatin-1

analogues: critical issues on the specificity, activity and in vivo use in experimental disease models. *Cell Death Dis.* 3: e437.

177. Varfolomeev, E., M. Schuchmann, V. Luria, N. Chiannilkulchai, J. S. Beckmann, I. L. Mett, D. Rebrikov, V. M. Brodianski, O. C. Kemper, O. Kollet, T. Lapidot, D. Soffer, T. Sobe, K. B. Avraham, T. Goncharov, H. Holtmann, P. Lonai, and D. Wallach. 1998. Targeted disruption of the mouse Caspase 8 gene ablates cell death induction by the TNF receptors, Fas/Apo1, and DR3 and is lethal prenatally. *Immunity* 9: 267–76.

178. Zhang, J., D. Cado, A. Chen, N. H. Kabra, and A. Winoto. 1998. Fas-mediated apoptosis and activation-induced T-cell proliferation are defective in mice lacking FADD/Mort1. *Nature* 392: 296–300.

179. Yeh, W. 1998. FADD: Essential for Embryo Development and Signaling from Some, But Not All, Inducers of Apoptosis. *Science (80-.).* 279: 1954–1958.

180. Yeh, W. C., a Itie, a J. Elia, M. Ng, H. B. Shu, A. Wakeham, C. Mirtsos, N. Suzuki, M. Bonnard, D. V Goeddel, and T. W. Mak. 2000. Requirement for Casper (c-FLIP) in regulation of death receptor-induced apoptosis and embryonic development. *Immunity* 12: 633–42.

181. Kang, T.-B., T. Ben-Moshe, E. E. Varfolomeev, Y. Pewzner-Jung, N. Yogev, a. Jurewicz, a. Waisman, O. Brenner, R. Haffner, E. Gustafsson, P. Ramakrishnan, T. Lapidot, and D. Wallach. 2004. Caspase-8 Serves Both Apoptotic and Nonapoptotic Roles. *J. Immunol.* 173: 2976–2984.

182. Kelliher, M. A., S. Grimm, Y. Ishida, F. Kuo, B. Z. Stanger, and P. Leder. 1998. The death domain kinase RIP mediates the TNF-induced NF-kappaB signal. *Immunity* 8: 297–303.

183. Rickard, J. A., J. A. O'Donnell, J. M. Evans, N. Lalaoui, A. R. Poh, T. Rogers, J. E. Vince, K. E. Lawlor, R. L. Ninnis, H. Anderton, C. Hall, S. K. Spall, T. J. Phesse, H. E. Abud, L. H. Cengia, J. Corbin, S. Mifsud, L. Di Rago, D. Metcalf, M. Ernst, G. Dewson, A. W. Roberts, W. S. Alexander, J. M. Murphy, P. G. Ekert, S. L. Masters, D. L. Vaux, B. A. Croker, M. Gerlic, and J. Silke. 2014. RIPK1 Regulates RIPK3-MLKL-Driven Systemic Inflammation and Emergency Hematopoiesis. *Cell* 157: 1175–1188.

184. Newton, K., X. Sun, and V. M. Dixit. 2004. Kinase RIP3 Is Dispensable for Normal NF-κBs , Signaling by the B-Cell and T-Cell Receptors , Tumor Necrosis Factor Receptor 1 , and Toll-Like Receptors 2 and 4. *Mol Cell Biol* 24: 1464–1469.

185. Wu, J., Z. Huang, J. Ren, Z. Zhang, P. He, Y. Li, J. Ma, W. Chen, Y. Zhang, X. Zhou, Z. Yang, S.-Q. Wu, L. Chen, and J. Han. 2013. Mlkl knockout mice demonstrate the indispensable role of Mlkl in necroptosis. *Cell Res.* 23: 994–1006.

186. Kaiser, W. J., J. W. Upton, A. B. Long, D. Livingston-Rosanoff, L. P. Daley-Bauer, R. Hakem, T. Caspary, and E. S. Mocarski. 2011. RIP3 mediates the embryonic lethality of caspase-8-deficient mice. *Nature* 471: 368–372.

187. Bidère, N., H. C. Su, and M. J. Lenardo. 2006. Genetic disorders of programmed cell death in the immune system. *Annu. Rev. Immunol.* 24: 321–52.

188. Dillon, C. P., R. Weinlich, D. A. Rodriguez, J. G. Cripps, G. Quarato, P. Gurung, K. C. Verbist, T. L. Brewer, F. Llambi, Y.-N. Gong, L. J. Janke, M. A. Kelliher, T.-D. Kanneganti, and D. R. Green. 2014. RIPK1 Blocks Early Postnatal Lethality Mediated by Caspase-8 and RIPK3. *Cell* 157: 1189–1202.

189. Zhang, H., X. Zhou, T. McQuade, J. Li, F. K.-M. Chan, and J. Zhang. 2011. Functional complementation between FADD and RIP1 in embryos and lymphocytes. *Nature* 471: 373–376.

190. Kaiser, W. J., L. P. Daley-Bauer, R. J. Thapa, P. Mandal, S. B. Berger, C. Huang, a. Sundararajan, H. Guo, L. Roback, S. H. Speck, J. Bertin, P. J. Gough, S. Balachandran, and E. S. Mocarski. 2014. RIP1 suppresses innate immune necrotic as well as apoptotic cell death during mammalian parturition. *Proc. Natl. Acad. Sci.* .

191. Christofferson, D. E., Y. Li, J. Hitomi, W. Zhou, C. Upperman, H. Zhu, S. A. Gerber, S. Gygi, and J. Yuan. 2012. A novel role for RIP1 kinase in mediating TNF[alpha] production. *Cell Death Dis* 3: e320.

192. McNamara, C. R., R. Ahuja, A. D. Osafo-Addo, D. Barrows, A. Kettenbach, I. Skidan, X. Teng, G. D. Cuny, S. Gerber, and A. Degterev. 2013. Akt Regulates TNFα synthesis downstream of RIP1 kinase activation during necroptosis. *PLoS One* 8: e56576.

193. Wong, W. W.-L., J. E. Vince, N. Lalaoui, K. E. Lawlor, D. Chau, A. Bankovacki, H. Anderton, D. Metcalf, L. O'Reilly, P. J. Jost, J. M. Murphy, W. S. Alexander, A. Strasser, D. L. Vaux, and J. Silke. 2014. cIAPs and XIAP regulate myelopoiesis through cytokine production in a RIPK1 and RIPK3 dependent manner. *Blood* 123: 2562–2572.

194. Berger, S. B., V. Kasparcova, S. Hoffman, B. Swift, L. Dare, M. Schaeffer, C. Capriotti, M. Cook, J. Finger, A. Hughes-Earle, P. a Harris, W. J. Kaiser, E. S. Mocarski, J. Bertin, and P. J. Gough. 2014. Cutting Edge: RIP1 Kinase Activity Is Dispensable for Normal Development but Is a Key Regulator of Inflammation in SHARPIN-Deficient Mice. *J. Immunol.* .

195. Rathinam, V. A. K., S. K. Vanaja, and K. A. Fitzgerald. 2012. Regulation of inflammasome signaling. *Nat Immunol* 13: 332–333.

196. Kang, T.-B., S.-H. Yang, B. Toth, A. Kovalenko, and D. Wallach. 2013. Caspase-8 Blocks Kinase RIPK3-Mediated Activation of the NLRP3 Inflammasome. *Immunity* 38: 27–40.

197. Vince, J. E., W. †Wei-L. Wong, I. Gentle, K. Lawlor, R. Allam, L. O'Reilly, K. Mason, O. Gross, S. Ma, G. Guarda, H. Anderton, R. Castillo, G. H‰cker, J. Silke, and J. Tschopp. 2012. Inhibitor of Apoptosis Proteins Limit RIP3 Kinase-Dependent Interleukin-1 Activation. *Immunity* 36: 215–227.

198. Weng, D., R. Marty-Roix, S. Ganesan, M. K. Proulx, G. I. Vladimer, W. J. Kaiser, E. S. Mocarski, K. Pouliot, F. K.-M. Chan, M. A. Kelliher, P. A. Harris, J. Bertin, P. J. Gough, D. M. Shayakhmetov, J. D. Goguen, K. A. Fitzgerald, N. Silverman, and E. Lien. 2014. Caspase-8 and RIP kinases regulate bacteria-induced innate immune responses and cell death. *Proc. Natl. Acad. Sci.* 1–6.

199. Linkermann, A., and D. R. Green. 2014. Necroptosis. *N. Engl. J. Med.* 370: 455–465.

200. Mocarski, E. S., J. W. Upton, and W. J. Kaiser. 2012. Viral infection and the evolution of caspase 8-regulated apoptotic and necrotic death pathways. *Nat Rev Immunol* 12: 79–88.

201. Kaiser, W. J., J. W. Upton, and E. S. Mocarski. 2013. Viral modulation of programmed necrosis. *Curr. Opin. Virol.* 3: 296–306.

202. Mocarski, E. S., W. J. Kaiser, D. Livingston-Rosanoff, J. W. Upton, and L. P. Daley-Bauer. 2014. True grit: programmed necrosis in antiviral host defense, inflammation, and immunogenicity. *J. Immunol.* 192: 2019–26.

203. Upton, J. W., W. J. Kaiser, and E. S. Mocarski. 2010. Virus Inhibition of RIP3-Dependent Necrosis. *Cell Host Microbe* 7: 302–313.

204. Upton, J. W., W. J. Kaiser, and E. S. Mocarski. 2012. DAI/ZBP1/DLM-1 Complexes with RIP3 to Mediate Virus-Induced Programmed Necrosis that Is Targeted by Murine Cytomegalovirus vIRA. *Cell Host Microbe* 11: 290–297.

205. Shen, H., and P. Vandenabeele. 2014. *Necrotic Cell Death*, (H.-M. Shen, and P. Vandenabeele, eds). Springer New York, New York, NY.

206. Han, J., C.-Q. Zhong, and D.-W. Zhang. 2011. Programmed necrosis: backup to and competitor with apoptosis in the immune system. *Nat Immunol* 12: 1143–1149.

207. Robinson, N., S. McComb, R. Mulligan, R. Dudani, L. Krishnan, and S. Sad. 2012. Type I interferon induces necroptosis in macrophages during infection with Salmonella enterica serovar Typhimurium. *Nat. Immunol.* 13: 954–62.

208. Thapa, R. J., S. Nogusa, P. Chen, J. L. Maki, A. Lerro, M. Andrake, G. F. Rall, A. Degterev, and S. Balachandran. 2013. Interferon-induced RIP1/RIP3-mediated necrosis requires PKR and is licensed by FADD and caspases. *Proc. Natl. Acad. Sci. U. S. A.* 1–10.

209. Autheman, D., M. Wyder, M. Popoff, K. D'Herde, S. Christen, and H. Posthaus. 2013. Clostridium perfringens beta-toxin induces necrostatin-inhibitable, calpain-dependent necrosis in primary porcine endothelial cells. *PLoS One* 8: e64644.

210. Roca, F. J., and L. Ramakrishnan. 2013. TNF Dually Mediates Resistance and Susceptibility to Mycobacteria via Mitochondrial Reactive Oxygen Species. *Cell* 153: 521–34.

211. Rittirsch, D., M. S. Huber-Lang, M. A. Flierl, and P. A. Ward. 2008. Immunodesign of experimental sepsis by cecal ligation and puncture. *Nat. Protoc.* 4: 31–36.

212. Deutschman, C. S., and K. J. Tracey. 2014. Sepsis: Current Dogma and New Perspectives. *Immunity* 40: 463–475.

213. Duprez, L., N. Takahashi, F. Van Hauwermeiren, B. Vandendriessche, V. Goossens, T. Vanden Berghe, W. Declercq, C. Libert, A. Cauwels, and P. Vandenabeele. 2011. RIP Kinase-Dependent Necrosis Drives Lethal Systemic Inflammatory Response Syndrome. *Immunity* 35: 908–918.

214. Linkermann, A., J. H. Bräsen, F. De Zen, R. Weinlich, R. A. Schwendener, D. R. Green, U. Kunzendorf, and S. Krautwald. 2012. Dichotomy between RIP1- and RIP3-mediated necroptosis in tumor necrosis factor-α-induced shock. *Mol. Med.* 18: 577–86.

215. Jang, H. R., and H. Rabb. 2009. The innate immune response in ischemic acute kidney injury. *Clin. Immunol.* 130: 41–50.

216. Yellon, D. M., and D. J. Hausenloy. 2007. Myocardial reperfusion injury. *N. Engl. J. Med.* 357: 1121–35.

217. Linkermann, A., J. H. Bräsen, M. Darding, M. K. Jin, A. B. Sanz, J.-O. Heller, F. De Zen, R. Weinlich, A. Ortiz, H. Walczak, J. M. Weinberg, D. R. Green, U. Kunzendorf, and S. Krautwald. 2013. Two independent pathways of regulated necrosis mediate ischemia-reperfusion injury. *Proc. Natl. Acad. Sci. U. S. A.* 110: 12024–9.

218. Oerlemans, M. I. F. J., J. Liu, F. Arslan, K. den Ouden, B. J. van Middelaar, P. a Doevendans, and J. P. G. Sluijter. 2012. Inhibition of RIP1-dependent necrosis prevents adverse cardiac remodeling after myocardial ischemia-reperfusion in vivo. *Basic Res. Cardiol.* 107: 270.

219. Linkermann, A., M. J. Hackl, U. Kunzendorf, H. Walczak, S. Krautwald, and A. M. Jevnikar. 2013. Necroptosis in immunity and ischemia-reperfusion injury. *Am. J. Transplant.* 13: 2797–804.

220. Lau, A., S. Wang, J. Jiang, A. Haig, A. Pavlosky, A. Linkermann, Z.-X. Zhang, and A. M. Jevnikar. 2013. RIPK3-mediated necroptosis promotes donor kidney inflammatory injury and reduces allograft survival. *Am. J. Transplant* 13: 2805–18.

221. Lin, J., H. Li, M. Yang, J. Ren, Z. Huang, F. Han, J. Huang, J. Ma, D. Zhang, Z. Zhang, J. Wu, D. Huang, M. Qiao, G. Jin, Q. Wu, Y. Huang, J. Du, and J. Han. 2013. A role of RIP3-mediated macrophage necrosis in atherosclerosis development. *Cell Rep.* 3: 200–10.

222. Gunther, C., E. Martini, N. Wittkopf, K. Amann, B. Weigmann, H. Neumann, M. J. Waldner, S. M. Hedrick, S. Tenzer, M. F. Neurath, and C. Becker. 2011. Caspase-8 regulates TNF-[alpha]-induced epithelial necroptosis and terminal ileitis. *Nature* 477: 335–339.

223. Welz, P.-S., A. Wullaert, K. Vlantis, V. Kondylis, V. Fernandez-Majada, M. Ermolaeva, P. Kirsch, A. Sterner-Kock, G. van Loo, and M. Pasparakis. 2011. FADD prevents RIP3-mediated epithelial cell necrosis and chronic intestinal inflammation. *Nature* 477: 330–334.

224. Bonnet, M., D. Preukschat, P.-S. Welz, G. van†Loo, M. Ermolaeva, W. Bloch, I. Haase, and M. Pasparakis. 2011. The Adaptor Protein FADD Protects Epidermal Keratinocytes from Necroptosis In†Vivo and Prevents Skin Inflammation. *Immunity* 35: 572–582.

225. Kovalenko, A., J.-C. Kim, T.-B. Kang, A. Rajput, K. Bogdanov, O. Dittrich-Breiholz, M. Kracht, O. Brenner, and D. Wallach. 2009. Caspase-8 deficiency in epidermal keratinocytes triggers an inflammatory skin disease. *J. Exp. Med.* 206: 2161–2177.

226. Pierdomenico, M., A. Negroni, L. Stronati, R. Vitali, E. Prete, J. Bertin, P. J. Gough, M. Aloi, and S. Cucchiara. 2013. Necroptosis Is Active in Children With Inflammatory Bowel Disease and Contributes to Heighten Intestinal Inflammation. *Am. J. Gastroenterol.* 1–9.

227. O'Donnell, M. A., and A. T. Ting. 2011. RIP1 comes back to life as a cell death regulator in TNFR1 signaling. *FEBS J.* 278: 877–87.

228. Moresco, E. M. Y., X. Li, and B. Beutler. 2013. Going forward with genetics: recent technological advances and forward genetics in mice. *Am. J. Pathol.* 182: 1462–73.

229. Ermann, J., and L. H. Glimcher. 2012. After GWAS: mice to the rescue? *Curr. Opin. Immunol.* 24: 564–70.

230. Beutler, B. 2009. TLRs and innate immunity. *Blood* 113: 1399–407.

231. Flint, J., W. Valdar, S. Shifman, and R. Mott. 2005. Strategies for mapping and cloning quantitative trait genes in rodents. *Nat. Rev. Genet.* 6: 271–86.

232. Beutler, B., X. Du, and Y. Xia. 2007. Precis on forward genetics in mice. *Nat. Immunol.* 8: 659–64.

233. Hunter, K. W., and N. P. S. Crawford. 2008. The future of mouse QTL mapping to diagnose disease in mice in the age of whole-genome association studies. *Annu. Rev. Genet.* 42: 131–41.

234. Peters, L. L., R. F. Robledo, C. J. Bult, G. a Churchill, B. J. Paigen, and K. L. Svenson. 2007. The mouse as a model for human biology: a resource guide for complex trait analysis. *Nat. Rev. Genet.* 8: 58–69.

235. Guénet, J. L., and F. Bonhomme. 2003. Wild mice: an ever-increasing contribution to a popular mammalian model. *Trends Genet.* 19: 24–31.

236. Frazer, K. A., E. Eskin, H. M. Kang, M. A. Bogue, D. A. Hinds, E. J. Beilharz, R. V Gupta, J. Montgomery, M. M. Morenzoni, G. B. Nilsen, C. L. Pethiyagoda, L. L. Stuve, F. M. Johnson, M. J. Daly, C. M. Wade, and D. R. Cox. 2007. A sequence-based variation map of 8.27 million SNPs in inbred mouse strains. *Nature* 448: 1050–1053.

237. Yang, H., J. R. Wang, J. P. Didion, R. J. Buus, T. A. Bell, C. E. Welsh, F. Bonhomme, A. H.-T. Yu, M. W. Nachman, J. Pialek, P. Tucker, P. Boursot, L. McMillan, G. A. Churchill, and F. P.-M. de Villena. 2011. Subspecific origin and haplotype diversity in the laboratory mouse. *Nat Genet* 43: 648–655.

238. Guenet, J.-L., A. Orth, and F. Bonhomme. 2012. *Chapter 1.1 – Origins and Phylogenetic Relationships of the Laboratory Mouse*, Second Edi. Elsevier ; :3–20.

239. Yang, H., T. A. Bell, G. A. Churchill, and F. Pardo-Manuel de Villena. 2007. On the subspecific origin of the laboratory mouse. *Nat Genet* 39: 1100–1107.

240. Khan, R., V. Sancho-Shimizu, C. Prendergast, M.-F. Roy, J.-C. Loredo-Osti, and D. Malo. 2012. Refinement of the genetics of the host response to Salmonella infection in MOLF/Ei: regulation of type 1 IFN and TRP3 pathways by Ity2. *Genes Immun.* 13: 175–83.

241. Sebastiani, G., L. Olien, S. Gauthier, E. Skamene, K. Morgan, P. Gros, and D. Malo. 1998. Mapping of genetic modulators of natural resistance to infection with Salmonella typhimurium in wild-derived mice. *Genomics* 47: 180–6.

242. Conner, J. R., I. I. Smirnova, and A. Poltorak. 2008. Forward genetic analysis of Toll-like receptor responses in wild-derived mice reveals a novel antiinflammatory role for IRAK1BP1. *J. Exp. Med.* 205: 305–314.

243. Conner, J. R., I. I. Smirnova, A. P. Moseman, and A. Poltorak. 2010. IRAK1BP1 inhibits inflammation by promoting nuclear translocation of NFkB p50. *Proc. Natl. Acad. Sci.* 107: 11477–11482.

244. Hardy, M. P., and L. A. J. O'Neill. 2004. The Murine Irak2 Gene Encodes Four Alternatively Spliced Isoforms, Two of Which Are Inhibitory. *J. Biol. Chem.* 279: 27699–27708.

245. Weischenfeldt, J., and B. Porse. 2008. Bone Marrow-Derived Macrophages (BMM): Isolation and Applications. *Cold Spring Harb. Protoc.* 3: 106.

246. Schworer, S. A., I. I. Smirnova, I. Kurbatova, U. Bagina, M. Churova, T. Fowler, A. L. Roy, A. Degterev, and A. Poltorak. 2014. Toll-like Receptor-Mediated Downregulation of the Deubiquitinase Cylindromatosis (CYLD) Protects Macrophages from Necroptosis in Wild-Derived Mice. *J. Biol. Chem.* 289: 14422–14433.

247. Beutler, B., D. Greenwald, J. D. Hulmes, M. Chang, Y.-C. E. Pan, J. Mathison, R. Ulevitch, and A. Cerami. 1985. Identity of tumor necrosis factor and the macrophage-secreted factor cachectin. *Nature* 316: 552–554.

248. Hirschfeld, M., J. J. Weis, V. Toshchakov, C. A. Salkowski, M. J. Cody, D. C. Ward, S. M. Michalek, and S. N. Vogel. 2001. Signaling by Toll-Like Receptor 2 and 4 Agonists Results in Differential Gene Expression in Murine Macrophages. *Infect. Immun.* 69: 1477–1482.

249. Ma, Y., V. Temkin, H. Liu, and R. M. Pope. 2005. NF-kB Protects Macrophages from Lipopolysaccharide-induced Cell Death. *J. Biol. Chem.* 280: 41827–41834.

250. Xu, Y., S. O. Kim, Y. Li, and J. Han. 2006. Autophagy Contributes to Caspase-independent Macrophage Cell Death. *J. Biol. Chem.* 281: 19179–19187.

251. He, S., Y. Liang, F. Shao, and X. Wang. 2011. Toll-like receptors activate programmed necrosis in macrophages through a receptor-interacting kinase-3-mediated pathway. *Proc. Natl. Acad. Sci.* 108: 20054–20059.

252. Xaus, J., A. F. Valledor, J. Lloberas, F. Lo, C. Bogdan, and A. Celada. 2000. LPS induces apoptosis in macrophages mostly through the autocrine production of TNF-alpha. *Blood* 95: 3823–3831.

253. Stephan, K., I. Smirnova, B. Jacque, and A. Poltorak. 2007. Genetic analysis of the innate immune responses in wild-derived inbred strains of mice. *Eur. J. Immunol.* 37: 212–223.

254. Moseman, A. P., E. A. Moseman, S. A. Schworer, I. Smirnova, T. Volkova, U. von Andrian, and A. Poltorak. 2013. Mannose Receptor 1 Mediates Cellular Uptake and Endosomal Delivery of CpG-Motif Containing Oligodeoxynucleotides. *J. Immunol.* 191: 5615–5624.

255. Kobayashi, K. S., M. Chamaillard, Y. Ogura, O. Henegariu, N. Inohara, G. Nunez, and R. A. Flavell. 2005. Nod2-Dependent Regulation of Innate and Adaptive Immunity in the Intestinal Tract. *Science* 307: 731–734.

256. Strober, W., and T. Watanabe. 2011. NOD2, an intracellular innate immune sensor involved in host defense and Crohn's disease. *Mucosal Immunol* 4: 484–495.

257. Pan, Q., J. Mathison, C. Fearns, V. V Kravchenko, J. Da Silva Correia, H. M. Hoffman, K. S. Kobayashi, J. Bertin, E. P. Grant, A. J. Coyle, F. S. Sutterwala, Y. Ogura, R. A. Flavell, and R. J. Ulevitch. 2007. MDP-induced interleukin-1beta processing requires Nod2 and CIAS1/NALP3. *J. Leukoc. Biol.* 82: 177–183.

258. Ferwerda, G., M. Kramer, D. de Jong, A. Piccini, L. A. Joosten, I. DevesaGiner, S. E. Girardin, G. J. Adema, J. W. M. van der Meer, B.-J. Kullberg, A. Rubartelli, and M. G. Netea. 2008. Engagement of NOD2 has a dual effect on proIL-1β mRNA transcription and secretion of bioactive IL-1β. *Eur. J. Immunol.* 38: 184–191.

259. Hsu, L.-C., S. R. Ali, S. McGillivray, P.-H. Tseng, S. Mariathasan, E. W. Humke, L. Eckmann, J. J. Powell, V. Nizet, V. M. Dixit, and M. Karin. 2008. A NOD2/NALP1 complex mediates caspase-1-dependent IL-1beta secretion in response to Bacillus anthracis infection and muramyl dipeptide. *Proc. Natl. Acad. Sci.* 105: 7803–7808.

260. Lu, J., L. Bai, H. Sun, Z. Nikolovska-Coleska, D. McEachern, S. Qiu, R. S. Miller, H. Yi, S. Shangary, Y. Sun, J. L. Meagher, J. A. Stuckey, and S. Wang. 2008. SM-164: A Novel, Bivalent Smac Mimetic That Induces Apoptosis and Tumor Regression by Concurrent Removal of the Blockade of cIAP-1/2 and XIAP. *Cancer Res.* 68: 9384–9393.

261. Varfolomeev, E., J. W. Blankenship, S. M. Wayson, A. V Fedorova, N. Kayagaki, P. Garg, K. Zobel, J. N. Dynek, L. O. Elliott, H. J. a Wallweber, J. a Flygare, W. J. Fairbrother, K. Deshayes, V. M. Dixit, and D. Vucic. 2007. IAP antagonists induce autoubiquitination of c-IAPs, NF-kappaB activation, and TNFalpha-dependent apoptosis. *Cell* 131: 669–81.

262. McComb, S., H. H. Cheung, R. G. Korneluk, S. Wang, L. Krishnan, and S. Sad. 2012. cIAP1 and cIAP2 limit macrophage necroptosis by inhibiting Rip1 and Rip3 activation. *Cell Death Differ.* 19: 1791–801.

263. Srokowski, C. C., J. Masri, N. Hovelmeyer, A. K. Krembel, C. Tertilt, D. Strand, K. Mahnke, R. Massoumi, A. Waisman, and H. Schild. 2009. Naturally occurring short splice variant of CYLD positively regulates dendritic cell function. *Blood* 113: 5891–5895.

264. Zhong, S., C. R. Fields, N. Su, Y. X. Pan, and K. D. Robertson. 2006. Pharmacologic inhibition of epigenetic modifications, coupled with gene expression

profiling, reveals novel targets of aberrant DNA methylation and histone deacetylation in lung cancer. *Oncogene* 26: 2621–2634.

265. Hutchison, E. R., E. M. Kawamoto, D. D. Taub, A. Lal, K. Abdelmohsen, Y. Zhang, W. H. Wood, E. Lehrmann, S. Camandola, K. G. Becker, M. Gorospe, and M. P. Mattson. 2013. Evidence for miR-181 involvement in neuroinflammatory responses of astrocytes. *Glia* 61: 1018–28.

266. Shimajiri, S., N. Arima, A. Tanimoto, Y. Murata, T. Hamada, K.-Y. Wang, and Y. Sasaguri. 1999. Shortened microsatellite d(CA)21 sequence down-regulates promoter activity of matrix metalloproteinase 9 gene. *FEBS Lett.* 455: 70–74.

267. Pravica, V., A. Asderakis, C. Perrey, A. Hajeer, P. J. Sinnott, and I. V Hutchinson. 1999. In vitro production of IFN-γ correlates with CA repeat polymorphism in the human IFN-γ gene. *Eur. J. Immunogenet.* 26: 1–3.

268. Fuda, N. J., and J. T. Lis. 2013. A new player in Pol II pausing. *EMBO J.* 32: 1796–8.

269. Adelman, K., and J. T. Lis. 2012. Promoter-proximal pausing of RNA polymerase II: emerging roles in metazoans. *Nat. Rev. Genet.* 13: 720–31.

270. Henriques, T., D. A. Gilchrist, S. Nechaev, M. Bern, G. W. Muse, A. Burkholder, D. C. Fargo, and K. Adelman. 2013. Stable Pausing by RNA Polymerase II Provides an Opportunity to Target and Integrate Regulatory Signals. *Mol. Cell* 52: 517–528.

271. Core, L. J., J. J. Waterfall, D. A. Gilchrist, D. C. Fargo, H. Kwak, K. Adelman, and J. T. Lis. 2012. Defining the status of RNA polymerase at promoters. *Cell Rep.* 2: 1025–35.

272. Gilchrist, D. A., G. Fromm, G. dos Santos, L. N. Pham, I. E. McDaniel, A. Burkholder, D. C. Fargo, and K. Adelman. 2012. Regulating the regulators: the pervasive effects of Pol II pausing on stimulus-responsive gene networks. *Genes Dev.* 26: 933–44.

273. Gobert Gosse, S., C. Bourgin, W. Q. Liu, C. Garbay, and G. Mouchiroud. 2005. M-CSF stimulated differentiation requires persistent MEK activity and MAPK phosphorylation independent of Grb2-Sos association and phosphatidylinositol 3-kinase activity. *Cell. Signal.* 17: 1352–62.

274. Wang, C., X. Yu, Q. Cao, Y. Wang, G. Zheng, T. K. Tan, H. Zhao, Y. Zhao, Y. Wang, and D. C. Harris. 2013. Characterization of murine macrophages from bone marrow, spleen and peritoneum. *BMC Immunol.* 14: 6.

275. Kool, M., V. Petrilli, T. De Smedt, a. Rolaz, H. Hammad, M. van Nimwegen, I. M. Bergen, R. Castillo, B. N. Lambrecht, and J. Tschopp. 2008. Cutting Edge: Alum

Adjuvant Stimulates Inflammatory Dendritic Cells through Activation of the NALP3 Inflammasome. *J. Immunol.* 181: 3755–3759.

276. Moseman, A. P. 2013. Forward Genetic Analysis of the CpG Hypo-response in Wild-derived MOLF/Ei Mice. 3554068.

277. Yuan, J., and G. Kroemer. 2010. Alternative cell death mechanisms in development and beyond. *Genes Dev.* 24: 2592–2602.

278. Lin, Y., A. Devin, Y. Rodriguez, and Z. Liu. 1999. Cleavage of the death domain kinase RIP by Caspase-8 prompts TNF-induced apoptosis. *Genes Dev.* 13: 2514–2526.

279. Lukens, J. R., P. Vogel, G. R. Johnson, M. A. Kelliher, Y. Iwakura, M. Lamkanfi, and T.-D. Kanneganti. 2013. RIP1-driven autoinflammation targets IL-1α independently of inflammasomes and RIP3. *Nature* 498: 224–7.

280. Lamothe, B., Y. Lai, M. Xie, M. D. Schneider, and B. G. Darnay. 2013. TAK1 Is Essential for Osteoclast Differentiation and Is an Important Modulator of Cell Death by Apoptosis and Necroptosis. *Mol. Cell. Biol.* 33: 582–595.

281. Morioka, S., P. Broglie, E. Omori, Y. Ikeda, G. Takaesu, K. Matsumoto, and J. Ninomiya-Tsuji. 2014. TAK1 kinase switches cell fate from apoptosis to necrosis following TNF stimulation. *J. Cell Biol.* 204: 607–623.

282. Dondelinger, Y., M. A. Aguileta, V. Goossens, C. Dubuisson, S. Grootjans, E. Dejardin, P. Vandenabeele, and M. J. M. Bertrand. 2013. RIPK3 contributes to TNFR1-mediated RIPK1 kinase-dependent apoptosis in conditions of cIAP1/2 depletion or TAK1 kinase inhibition. *Cell Death Differ.* 20: 1381–1392.

283. Zhande, R., S. M. Dauphinee, J. A. Thomas, M. Yamamoto, S. Akira, and A. Karsan. 2007. FADD Negatively Regulates Lipopolysaccharide Signaling by Impairing Interleukin-1 Receptor-Associated Kinase 1-MyD88 Interaction. *Mol. Cell. Biol.* 27: 7394–7404.

284. Conner, J. R. 2011. Forward Genetic Analysis of the Toll-Like Receptor Response in Wild-Derived Mice. 3372514.

285. Losick, V. P., K. Stephan, I. I. Smirnova, R. R. Isberg, and A. Poltorak. 2009. A hemidominant Naip5 allele in mouse strain MOLF/Ei-derived macrophages restricts Legionella pneumophila intracellular growth. *Infect. Immun.* 77: 196–204.

286. Bertrand, M. J. M., S. Milutinovic, K. M. Dickson, W. C. Ho, A. Boudreault, J. Durkin, J. W. Gillard, J. B. Jaquith, S. J. Morris, and P. A. Barker. 2008. cIAP1 and cIAP2 Facilitate Cancer Cell Survival by Functioning as E3 Ligases that Promote RIP1 Ubiquitination. *Mol. Cell* 30: 689–700.

287. Feng, S., Y. Yang, Y. Mei, L. Ma, D. Zhu, N. Hoti, M. Castanares, and M. Wu. 2007. Cleavage of RIP3 inactivates its caspase-independent apoptosis pathway by removal of kinase domain. *Cell. Signal.* 19: 2056–67.

288. Calo, E., and J. Wysocka. 2013. Modification of enhancer chromatin: what, how, and why? *Mol. Cell* 49: 825–37.

289. Heintzman, N. D., and B. Ren. 2009. Finding distal regulatory elements in the human genome. *Curr. Opin. Genet. Dev.* 19: 541–9.

290. Birnbaum, R. Y., E. J. Clowney, O. Agamy, M. J. Kim, J. Zhao, T. Yamanaka, Z. Pappalardo, S. L. Clarke, A. M. Wenger, L. Nguyen, F. Gurrieri, D. B. Everman, C. E. Schwartz, O. S. Birk, G. Bejerano, S. Lomvardas, and N. Ahituv. 2012. Coding exons function as tissue-specific enhancers of nearby genes. *Genome Res.* 22: 1059–68.

291. Braunschweig, U., S. Gueroussov, A. M. Plocik, B. Graveley, and B. Blencowe. 2013. Dynamic Integration of Splicing within Gene Regulatory Pathways. *Cell* 152: 1252–1269.

292. Luco, R. F., M. Allo, I. E. Schor, A. R. Kornblihtt, and T. Misteli. 2011. Epigenetics in alternative pre-mRNA splicing. *Cell* 144: 16–26.

293. Shukla, S., E. Kavak, M. Gregory, M. Imashimizu, B. Shutinoski, M. Kashlev, P. Oberdoerffer, R. Sandberg, and S. Oberdoerffer. 2011. CTCF-promoted RNA polymerase II pausing links DNA methylation to splicing. *Nature* 479: 74–9.

294. Callus, B. A., and D. L. Vaux. 2007. Caspase inhibitors: viral, cellular and chemical. *Cell Death Differ.* 14: 73–8.

295. Misaghi, S., G. A. Korbel, B. Kessler, E. Spooner, and H. L. Ploegh. 2005. z-VAD-fmk inhibits peptide:N-glycanase and may result in ER stress. *Cell Death Differ* 13: 163–165.

296. Polykratis, A., N. Hermance, M. Zelic, J. Roderick, C. Kim, T. H. Lee, F. K. M. Chan, M. Pasparakis, and M. A. Kelliher. 2014. RIPK1 kinase inactivate mice are viable and protected from TNF-induced necroptosis in vivo. *J. Immunol.* 1–5.

297. Harris, P. A., D. Bandyopadhyay, S. B. Berger, N. Campobasso, C. A. Capriotti, J. A. Cox, L. Dare, J. N. Finger, S. J. Ho, K. M. Kahler, R. Lehr, J. D. Lich, R. Nagilla, R. T. Nolte, M. T. Ouellette, C. S. Pao, M. C. Schae, A. Smallwood, H. H. Sun, B. A. Swift, R. D. Totoritis, P. Ward, R. W. Marquis, J. Bertin, and P. J. Gough. 2013. Discovery of Small Molecule RIP1 Kinase Inhibitors for the Treatment of Pathologies Associated with Necroptosis. *ACS Med. Chem. Lett.* 4: 1238–1243.

298. Opal, S. M., B. Francois, S. P. Larosa, D. C. Angus, R. Schein, M. Lynn, D. P. Rossignol, and J. L. Wheeler. 2013. Effect of Eritoran, an Antagonist of MD2-TLR4, on Mortality in Patients With Severe Sepsis. *JAMA* 309: 1154–1162.

299. Angus, D. C., and T. van der Poll. 2013. Severe Sepsis and Septic Shock. *N. Engl. J. Med.* 369: 840–851.

300. Galluzzi, L., and G. Kroemer. 2011. Necroptosis Turns TNF Lethal. *Immunity* 35: 849–851.